Click here

Efimov Universality in Exotic Strange and Charm Nuclei: A Low-energy Effective Theory Framework

A thesis
submitted for the degree of
Doctor of Philosophy

Ghanashyam Meher

Under the guidance of
Dr. Udit Raha

Department of Physics
Indian Institute of Technology Guwahati
Guwahati 781 039, Assam, India

Efimov Universality in Exotic Strange and Charm Nuclei: A Low-energy Effective Theory Framework

A thesis
submitted for the degree of
Doctor of Philosophy

Ghanashyam Meher
Roll No. 146121004

Under the guidance of
Dr. Udit Raha

Department of Physics
Indian Institute of Technology Guwahati
Guwahati 781 039, Assam, India

It's not that I'm so smart, it's just that I stay with problems longer.

- Albert Einstein

Dedicated to my Maa and Bapa

Declaration

The work in this thesis entitled "Efimov Universality in Exotic Strange and Charm Nuclei: A Low-energy Effective Theory Framework" has been carried out by me under the supervision of Dr. Udit Raha, Department of Physics, Indian Institute of Technology Guwahati. No part of this thesis has been submitted elsewhere for award of any other degree or qualification.

In keeping with general practice of reporting scientific observations, due acknowledgments have been made wherever the work described is based on the findings of other investigations.

Place: IIT Guwahati
Date: 12/01/2023

Ghanashyam Meher
Roll No. 146121004

भारतीय प्रौद्योगिकी संस्थान गुवाहाटी
Indian Institute of Technology Guwahati

Certificate

This is to certify that the research work contained in this thesis entitled "Efimov Universality in Exotic Strange and Charm Nuclei: A Low-energy Effective Theory Framework" by Mr. Ghanashyam Meher, a PhD student of the Department of Physics, IIT Guwahati was carried out under my supervision. This work is original and has not been submitted elsewhere for award of any degree.

Place: IIT Guwahati
Date: 12/01/2023

Dr. Udit Raha
Department of Physics,
IIT Guwahati.
Email: udit.raha@iitg.ac.in

भारतीय प्रौद्योगिकी संस्थान गुवाहाटी
Indian Institute of Technology Guwahati

Acknowledgements

I shall be ever indebted to my supervisor Dr. Udit Raha for introducing this interesting and challenging topic to me. His brilliant ideas and motivation always guided me to achieve my objectives during the thesis work. I have always admired his problem-solving abilities. If I ever get an opportunity to choose a supervisor for any future work I will always be looking forward to a person like him. Also, I am much obliged to Prof. Shung-Ichi Ando of Sunmoon University, Asan Korea, who during his brief visit to IIT Guwahati enlightened me on various conceptual issues that crucially helped me formulate the foundations of this thesis.

I express my sincere gratitude to my doctoral committee chairman, Prof. Bipul Bhuyan, and the other two committee members, Prof. Sitangshu Bikas Santra and Prof. Partha Sarathi Mandal, for reviewing my progress meticulously each year during my Ph.D., giving their valuable suggestions and feedback which helped me shape the present thesis work. Let me also take the opportunity to convey my heartfelt appreciation to the reviewers (Prof. Gautam Rupak and Prof. B. Ananthanarayan) of this thesis for patiently reading through all my presented works and helping me to improve the presentation through various constructive criticisms. I am most indebted to them.

I would like to thank all the faculty members of the Department of Physics who has helped me to understand the fundamental concepts of physics during my Ph.D. coursework. Special thanks go to all the Heads of the Department of Physics, Prof. Saurabh Basu, Prof. Poulose Poulose, Prof. Subhradip Ghosh, and Prof. Perumal Alagarsamy for providing a conducive environment for research and various other academic activities.

I would like to thank all my friends from IIT Guwahati and B. Sc. degree college who have always stood on my behalf and given me company in all my good and bad times. I would also like to thank my lab mates who helped me in troubleshooting various Fortran 90/95 and Mathematica codes. I especially thank my senior, Dr. Pulak Talukdar, for his constant encouragement and patience in hearing me regarding numerous academic, as well as non-academic issues.

My sincere thanks go to IIT Guwahati for providing me a scholarship for five years, grants to attend the conferences and other necessary resources to accomplish my research work.

My deepest gratitude goes to my Mother and Father for their affection and love without whom this long and arduous academic journey would not have been possible. I will forever be indebted to them for their love for me. The love and regard that I received from all my brothers and sisters, along with their constant belief in me have kept my spirits alive and motivation high during this entire journey.

Last but not the least, I thank the most divine Lord Shree Krishna for everything that I am today.

Abstract

The present thesis deals with the investigation of low-energy two- and three-body universality that could manifest in exotic strange and charm nuclei. To supplement the plethora of existing works based on potential models on such systems, the main objective of this thesis is to employ a model-independent effective field theory (EFT) framework as a modern systematic computational tool for understanding the underlying binding mechanism without reference to inherent (microscopic) short-distance details. In particular, pionless EFT or its variant, so-called the *Halo/Cluster* EFT, provides a versatile theoretical technique to specifically search for the feasibility of Efimov mechanism in halo-like nuclear clusters. Here we presented leading order EFT investigations of the putative S-wave bound hypernuclear cluster states, such as the iso-doublet mirror partners ($^{5}_{\Lambda\Lambda}$H, $^{5}_{\Lambda\Lambda}$He) in the ($J = 1/2$, $T = 1/2$) channel, as well as the $\Xi^{-}nn$ cluster in the ($J = 1/2$, $T = 3/2$) channel, in the strange sector. The mirror clusters are studied as 2Λ (double-Λ-hyperon) halo systems with a composite core, identified either as a triton (t) or helion (h). Whereas, the $\Xi^{-}nn$ system is studied as a $2n$-halo system with a Ξ-hyperon elementary core. Furthermore, in the charm sector, we studied the putative $2n$ halo-bound $D^{0}nn$ system in the ($J = 0$, $T = 3/2$) channel invoking an idealized zero-coupling-limit ansatz which excludes all effects of decay and coupled channels dynamics. The general EFT formalism involves the diagrammatic construction of a system of Faddeev-like three-body integral equations embodying the re-scattering dynamics in the momentum-space representation. Using momentum cut-off regulators in the integral equations which are significantly larger than the hard scale of the EFTs, the three-body contact interaction becomes cyclically singular indicating the onset of renormalization group (RG) limit cycles with discrete scale invariance. Thus, our results formally indicate the manifestly Efimovian nature of each of the cluster systems leading to ostensible Efimov states. However, the paucity of current empirical information to determine various free EFT parameters precludes definitive conclusions on the feasibility of such systems being realistically Efimov-bound. Nevertheless, despite phenomenological limitations, the thesis amply demonstrates the predictability of the EFT analyses by illuminating various remnant features of Efimov universality at a qualitative level. Constraining the cut-off dependence of double-Λ separation energy and the corresponding three-body scattering lengths of the ($^{5}_{\Lambda\Lambda}$H, $^{5}_{\Lambda\Lambda}$He) mirrors, predicting the Phillips-line correlation curves for the $^{5}_{\Lambda\Lambda}$H, $^{5}_{\Lambda\Lambda}$He and $\Xi^{-}nn$ systems, and finally, demonstrating the structural universality of the ground state of a plausible $D^{0}nn$ halo-bound cluster by determining its geometrical features (e.g., matter density form factors, mean square radii, etc.), were some of the predictable features emphasized in this thesis.

Contents

List of Figures

List of Tables

Chapter 1

Introduction

The physics at different scales yields different constituent particles and the fundamental forces between their constituent particles. For example, on the atomic scale, the constituent particles are atoms and the fundamental force is the electromagnetic force arising from the exchange of photons, which helps to bind the atoms and even form different molecules. Analogously, at the scale of the atomic nucleus, the constituent particles are nucleons that are bound by strong nuclear interactions arising due to various boson exchanges (e.g., meson-exchange at low-energies and the more fundamental gluon-exchange between quarks at high-energies). Hence, for a particular scale, we need a particular theory to describe the dynamics of pertinent systems. In high-energy physics, the strong nuclear interactions are ultimately governed by Quantum Chromodynamics (QCD), the fundamental theory of quarks and gluons. Quarks carry "color charges", which are generalizations of the electrical charge, and the forces between such "colored" particles are mediated by gluons. However, since at low-energies nucleons are in fact realized as bound composite systems of quarks and gluons, the emergence of nuclear forces amongst them must be a manifestation of certain long-distance phenomena arising from the residual interaction between "color-singlet" objects, akin to van der Waals forces between electrically neutral atoms and molecules. Consequently, determining the physics of nuclear structure and reactions requires complex many-body numerical calculations involving lots of adjustable parameters based on intricate model assumptions for nuclear forces. Nevertheless, there exists a simple tractable "unitary regime" where identical low-energy physical phenomena manifest in very different few-body systems (having different constituent particles and fundamental forces), with exactly the same few adjustable parameters which characterize their commensurate descriptions. For instance, low-energy[1] nucleon-nucleon reactions are

[1]Low-energy refers to pertinent energies close to the scattering threshold, namely, the regime when the de Broglie wavelengths $\lambda \sim \hbar/q$ of the relevant degrees of freedom with generic momentum q are much larger than the natural length scale R of the system. In low-energy atomic process where Coulomb interactions between polarized atoms are asymptotically ($r \to \infty$) dominated by van der Waals potential $V(r) \sim C_6/r^6$, R may be identified with the *van der Waals length* $R \sim \ell_{\rm vdW} = (MC_6/\hbar^2)^{1/4}$, where M is the atomic mass. Likewise in low-energy nuclear processes dominated by Yukawa-like meson-exchange inter-nucleon potentials $V(r) \sim e^{-m_M/r}$, R is often identified with the characteristic interaction or *effective range* $R \sim r_0 \sim 1/m_M$ of the interaction, where m_M is the mass of the exchanges boson.

described only in terms of two parameters, the S-wave *Fermi scattering length* a_0 and the corresponding effective range r_0. In such a scattering regime there exists a certain resonant limit in which the scattering length becomes much larger than any other length scales, including the effective range, whereby the underlying physics becomes invariant under re-scaling of all distances. This is a familiar situation in statistical mechanics where in the vicinity of a second-order phase transition correlation length diverges leading to fluctuations occurring in all length scales. Such a phenomenon associated with a large separation between the short-distance scale of the interaction and the long-distance scales relevant to the physical system is termed as *Low-energy Universality*. This happens, in particular, if the colliding particles (of mass m) interacting attractively are close to forming a two-body bound state with binding energy given by

$$-B_2 = \frac{-\hbar^2}{m a_0^2}\,. \tag{1.1}$$

The above universal formula holds in an ideal sense applicable in the so-called *scaling limit* for $r_0 \to 0$. In reality, however, non-universal effects are introduced by corrections suppressed by power of r_0/a_0, termed as *scaling violation*. Indeed, as the two-body center-of-mass energy $\mathscr{E}$ approaches the scattering threshold with $\mathscr{E} \to -B_2 \sim 0$, the scattering length a_0 diverges. This is reminiscent of the well-known BCS mechanism of S-wave superconductivity where the effective interaction between pairs of electrons becomes sufficiently attractive close to the critical temperature, forming bound quasi-particles called *Cooper pairs*. In this case the onset of the superconducting phase is associated with diverging coherence lengths (Cooper-pair size) $\xi_{\rm BCS} = \hbar v_f/(\pi\Delta)$, where v_f is the Fermi velocity of the electrons, as the superconducting energy gap vanishes $\Delta \sim 0$ for $T \sim T_c$.[2].

Predominantly, physical systems exist in their *natural paradigm* where the scattering length is of the same order as the interaction range. Only, in certain exceptional cases do we find systems in the *unnatural paradigm* where the scattering lengths become unnaturally large leading to the aforementioned universal scenarios. Illustrated in the Table (1.1) are some of the few examples from atomic and nuclear systems where the difference between the natural and unnatural paradigms are clearly manifest. For instance, in the case of low-energy ^{3}He$-^3$He atomic collision, both the scattering length and effective range are numerically of the same order, and hence such a binary system may be ascribed natural. In contrast, for processes like ^{4}He $-$ ^{4}He atomic collision and neutron-proton $(n-p)$ scattering, the respective scattering lengths are much larger than the corresponding interaction range. Such binary systems are qualified as unnatural or *fine-tuned* since their description requires certain non-perturbative re-shuffling of contributions between long and short-distance effects arising from the quantum-loop corrections. Standard explanation *via* potential models fail to provide a satisfactory explanation of the existence of anomalously shallow bound states which are often associated with such fine-tuned systems. For instance, even accepting that pion exchanges are responsible for generating non-perturbative interactions that lead to the formation of the real-bound state,

[2]Notable, however, is the fact that while bound states are manifestations of spatial correlations, the BCS phenomenon corresponds to correlations in momentum space on the Fermi surface

TABLE 1.1: The table illustrates typical examples of comparison between natural and unnatural paradigms in terms of the two-body interaction range R and the scattering length a_0 for different low-energy S-wave systems. Here we denote $a_{\rm Bohr} = 5.29 \times 10^{-11}$ m as the Bohr radius. In the context of atomic (nuclear) processes, the van der Waals length (effective range) $\ell_{\rm vdW}$ (r_0) is used to denote the interaction range.

Process	$^1S_0$ System	Interaction range R	Scattering length a_0	Nature
Atomic	^{3}He $-$ ^{3}He	$\ell_{\rm vdW} \approx 13.7\, a_{\rm Bohr}$	$-33\, a_{\rm Bohr}$	Natural
Atomic	^{4}He $-$ ^{4}He	$\ell_{\rm vdW} \approx 10.2\, a_{\rm Bohr}$	$189\, a_{\rm Bohr}$	Fine-tuned
Nuclear	$n-p$	$r_0 \approx 2.73$ fm	-23.7 fm	Fine-tuned

the *deuteron*, in the $n-p$ ($^3S_1$) scattering channel, or the virtual-bound state, the *di-neutron*, in the $n-n$ ($^1S_0$) scattering channel, it is quite non-trivial to accept the deuteron (di-neutron) is only bound (anti-bound) by $B_2 \approx 2.22$ MeV (1.78 MeV). A proper explanation of the dynamics of fine-tuned two-body systems requires a modification of the standard perturbative scaling properties of low-energy observables based on naive dimensional analysis. This is achieved in the context of *Pionless Effective Field Theory* ($\not\pi$EFT) [1–6], where a special counting scheme has been proposed that requires a leading order two-body contact interaction to be iterated to all orders. It has been realized that such a non-perturbative/strong-coupling scaling inherently stems from the critical tuning of the two-body coupling to a renormalization group (RG) trajectory that asymptotically approaches a *non-trivial ultraviolet (UV) fixed point*. On the other hand, the standard perturbative/weak-coupling scaling is interpreted as the RG flow of the coupling induced by a *trivial infrared fixed point* [8].

Universality in a three-body system is a far more fascinating one. A system of three particles interacting *via* short-range interactions, with at least two of the three particle pairs having large two-body S-wave scattering lengths, becomes *resonant* and exhibits remarkable universal properties. In 1970 Efimov pointed out that when the scattering length $|a_0|$ becomes sufficiently large compared to the range r_0 of the interacting potential, a sequence of three-body bound *trimer* states exist whose binding energies are roughly spaced geometrically in the interval between $\hbar^2/ma_0^2$ and $\hbar^2/mr_0^2$. Furthermore, by approaching the unitary/resonant limit of the two-body interactions with $a_0 \to \pm\infty$, an infinitely many arbitrarily shallow trimers emerge accumulating to the zero energy scattering threshold. This striking phenomenon is referred to as *Efimov effect* [9–11] and the three-body bound states are *Efimov trimers*. In particular, on approaching one of the unitary limits, the ratios of the successive trimer binding energies $B_3^{(n)}$ approach a certain *universal number* which only depends on mass ratios of the constituent particles and their gross quantum numbers, such as the total spin and isospin of the three-body system, while independent of the individual nature of the particles (whether they be atoms, nucleons or other elementary particles) and the form of their short-range interaction. Note, however, that the quantum statistics of each the constituent particle does play a crucial role. In the case of a system of three indistinguishable bosons, the following

result manifests [9–12]:

$$\frac{B_3^{(n)}}{B_3^{(n+1)}} \to e^{2\pi/s_0} = 515.03$$

where

$$B_3^{(n)} \to (e^{-2\pi/s_0})^n \frac{\hbar^2\kappa_*^2}{m} \quad \text{as } n \to \infty, \quad \text{with} \quad a_0 \to \pm\infty\,. \tag{1.2}$$

The parameter κ_* is approximately related to the wavenumber of the deepest (ground) trimer state, which becomes the exact wavenumber in the unitary limit. The universal ratio is not particularly unique to the three-boson system but is also found in other three-body bound nuclear systems, such as the triton and helion, and in exotic hypernuclei, such as the hypertriton. A salient feature inherent to the Efimov spectrum is the so-called *asymptotic discrete scaling-symmetry*, *viz.* invariance under the discrete subgroup of scale transformations:

$$\kappa_* \to \kappa_*\,, \quad a_0 \to \lambda_0^n a_0\,, \quad \mathbf{r} \to \lambda_0^n \mathbf{r}\,, \quad t \to \lambda_0^{2n} t\,, \quad E \to \lambda_0^{-2} E\,, \tag{1.3}$$

where $\lambda_0 = e^{\pi/s_0}$. Such scaling is characterized by the three-body parameter s_0, which in the case of the three-boson system is given by the transcendental number $s_0 \approx 1.00624....$ As described in Chapter 2, this parameter is obtained as one of the purely imaginary solutions $s = \pm i s_0$ to the transcendental equation:

$$1 - \frac{8}{\sqrt{3}s} \frac{\sin\left(\frac{\pi s}{6}\right)}{\cos\left(\frac{\pi s}{2}\right)} = 0\,, \tag{1.4}$$

which arises from the consistency requirement while extrapolating the three-body *hyperradial wavefunction* between the "end-points" of the boundary conditions in the limit of vanishing hyper-radius R. The emergence of the dynamical parameter s_0 is related to the breakdown of the *continuous scaling-symmetry* which the three-body system trivially exhibits in the scaling limit, *viz.* invariance under arbitrary scale transformations:

$$a_0 \to \lambda a_0\,, \quad \mathbf{r} \to \lambda \mathbf{r}\,, \quad t \to \lambda^2 t\,, \quad E \to \lambda^{-2} E\,, \tag{1.5}$$

where $\lambda > 0$ is arbitrary. The remnant discrete symmetry of the three-body system yields the characteristic scaling of the Efimov spectrum, which for the three-boson system is given by the factor $\lambda_0^2 = (22.7)^2 = 515.03$. Figure 1.1 illustrates the typical Efimov plot for the three-boson spectrum, where the trimer binding wavenumber $\kappa_T = \sqrt{mB_3/\hbar^2}$ is plotted as a function of the inverse S-wave scattering length $1/a_0$. Both the abscissa and ordinate are re-scaled to their $(1/4)^{\text{th}}$ power in order to accommodate up to the second excited trimer levels thereby reducing the discrete scaling factor in the figure to $\lambda_0^{1/4} = (22.7)^{1/4} = 2.18$. As detailed in Chapter 3, the energy eigenvalues are obtained by solving a homogeneous Faddeev-like integral equation in the momentum representation (so-called the *Skornyakov-Ter-Martirosyan* or STM equation [13, 14]) by introducing a sharp momentum UV cut-off regulator Λ_{reg}, that fixes the short-distance two-body interactions range $r_0 \sim 1/\Lambda_{\text{reg}}$. In the figure, we have arbitrarily chosen $\Lambda_{\text{reg}} = 1000\sqrt{m/\hbar^2}$, which allows us to display up to the

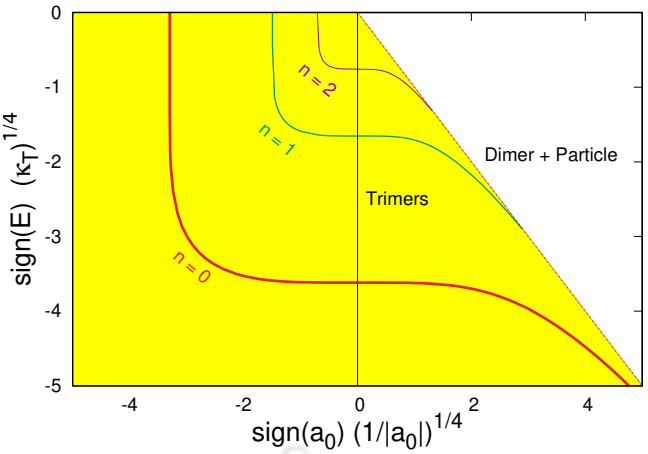

FIGURE 1.1: Efimov plot for a system of three indistinguishable bosons where the trimer binding wavenumber $\mathrm{sign}(E)\kappa_T = \mathrm{sign}(E)\sqrt{|E|}$ is plotted as a function of the inverse S-wave scattering length $1/a_0 = \mathrm{sign}(a_0)\sqrt{B_2}$, both in units of $\sqrt{m/\hbar^2}$. Furthermore, both are respectively re-scaled to their $(1/4)^{\text{th}}$ powers in order to accommodate the first three Efimov states. The plot has been obtained by numerically solving the STM equation [13, 14] (see Chapter 3 for details) using a sharp momentum UV cut-off $\Lambda_{\text{reg}} = 1000$ in units of $\sqrt{m/\hbar^2}$. The region shaded by yellow depicts the Efimov region with the three lowest trimer states displayed. This region is separated from the dimer-particle scattering region by the (2+1)-break-up threshold, represented by the inclined dotted red line.

second exited Efimov state. Increasing this cut-off progressively leads to the deepening of the Efimov levels with successive emergence of further shallower excited levels either from the *three-particle break-up threshold* ($E = 0$ axis in the figure) for $a_0 < 0$ or the *particle-dimer break-up threshold* (the inclined dotted axis in the figure) for $a_0 > 0$. For a detailed exposition of the nature of the Efimov spectrum, we refer the reader to the review works of Refs. [12, 15].

For large but finite values of the scattering length $|a_0| \neq \infty$ (i.e., slightly away from the unitary limit - represented by points on the ordinate axis of the Efimov plot), the Efimov spectrum not only depends on a_0 but also on the three-body parameter κ_*. In general, κ_* is a complicated function of the interaction range r_0, which in turn determines the deepest eigenvalue. Consequently, in the scaling limit as $r_0 \to 0$, $\kappa_* \sim 1/r_0 \to \infty$, the ground state becomes unbounded from below. Such an unphysical situation, termed as a *Thomas Collapse* [16], can be attributed to the restoration of continuous scaling-invariance in the scaling limit. In practice, however, due to non-zero interaction range in a physical system, such a pathology never arises. Moreover, the parametric dependence of the Efimov spectrum on κ_* generates a *logarithmic scaling-violations* which reduces the trivial continuous scaling-symmetry into a residual discrete-scaling subgroup. This is reflected in the asymptotic spectrum defined by Eq. (1.2), that consists of the zeros of a log-periodic of $\ln(\kappa_*)$:

$$\sin\left(\frac{1}{2}s_0 \ln\left[mB_3^{(n)}/(\hbar^2\kappa_*^2)\right]\right) = 0\,.$$

Consequently, low-energy three-body observables also exhibit a log-periodic dependence of the

form $f \sim s_0 \ln(|a_0|\kappa_*)$. Such a quasi-periodic dependence stems from a certain characteristic of Wilsonian RG, termed as an *UV limit cycle* [17], which basically represents a cyclic flow of the RG trajectory around a closed loop in the Hamiltonian space.[3] We refer the reader to Chapter 3 for a detailed description of the RG limit cycle nature of the three-boson system presented in the context of a pionless EFT at the leading order. This unusual type of RG arises in other branches of physics as well, such as in condensed matter (see e.g., Refs. [18–22]), or in the study of turbulence and complex systems (see e.g., Ref. [23]). Curiously enough, such a discrete scaling behavior bears a close resemblance to the well-known Russian *Matryoshka dolls*, as displayed in Fig. 1.2. They consist of an assembly of hollow wooden dolls of decreasing size nested one within the other such that the ratio of the sizes of successive dolls remains approximately constant. For instance, as shown in the figure, the discrete scaling factor λ_0, in this case, is given by

$$\lambda_0 = e^{2\pi/s_0^{(\mathrm{doll})}} \approx \frac{\mathrm{doll}^{(n)}}{\mathrm{doll}^{(n+1)}} \approx 1.5\,. \tag{1.6}$$

FIGURE 1.2: Demonstration of RG limit cycle: Discrete scaling behavior found in Russian nesting dolls with sizes of successive dolls decreasing by a constant factor, say, $\lambda_0 \sim 1.5$.

The physics of Efimov universality discussed thus far is manifested in a large number of physical systems and in a variety of different ways. In particular, *heteronuclear* three-body systems involving different kinds of bound particles exhibit an, even more, richer Efimov physics, although conditions can turn out to be quite restrictive. The following observed facts are in order:

[3] An RG limit cycle constitutes a family of Hamiltonians $\mathscr{H}_*(\theta)$ which goes around in a closed loop and can be parameterized by an angle $0 \leq \theta \leq 2\pi$ that describes a linear RG flow with $\ln(\Lambda_{\mathrm{reg}})$, where Λ_{reg} is the UV cut-off. This implies that the Hamiltonian repeats itself around the limit cycle whenever Λ_{reg} changes by a multiplicative factor λ_0. Thus, if the corresponding set of coupling constants of the theory $\mathbf{g} = \mathbf{g}(g_1, g_2, ...)$ at some initial scale Λ_0 is denoted by $\mathbf{g}(\Lambda_0) \equiv \mathbf{g}_*(\theta)$, then the general cut-off dependence of the set of couplings can be represented as [12]

$$\mathbf{g}(\Lambda_{\mathrm{reg}}) = \mathbf{g}_*\left[\theta + 2\pi \ln(\Lambda_{\mathrm{reg}}/\Lambda_0)/\ln(\lambda_0)\right] .$$

Here the set of couplings $\mathbf{g} = \mathbf{g}(g_1, g_2, ...)$ is invariant under the discrete symmetry transformation $\Lambda_{\mathrm{reg}} \to \lambda_0^{-n}\Lambda_{\mathrm{reg}}$ with λ_0 as the discrete scaling factor. This physically implies that on integrating out degrees of freedom between length scales between the scales Λ_{reg} and $\Lambda_{\mathrm{reg}}/\lambda_0^n$, the dynamics of a system is unchanged.

- For a three-particle system to exhibit Efimov effect, at least two pairs of constituent particles must interact resonantly with sufficiently large S-wave scattering lengths. Moreover, Efimov effect is always restricted to S-wave systems only. The reason it does not manifest in higher partial waves is that the centrifugal repulsion they generate easily suppresses Efimov attraction.

- Efimov effect is crucially restricted by the statistic of the individual particles. In the case of identical fermions, Pauli-blocked states often inhibit Efimov effect. Thus, in general, bosonic systems are more favorable for exhibiting Efimov effect.

- Mass-imbalanced systems are more likely to enhance Efimov effect.

- For systems with two identical particles which exhibit Efimov effect, based on the signs and magnitudes of the two-body subsystem scattering lengths, there are four possibilities of trimer configurations [24]: 1) *Borromean System*: All unbound/virtual-bound subsystems; 2) *All-bound System*: All subsystems are real-bound with large and positive scattering lengths; 3) *Samba System*: One unbound/virtual-bound subsystem, and the other two subsystems being real-bound with large and positive scattering lengths; 4) *Tango System*: One real-bound subsystem with large and positive scattering length, and the other subsystems being unbound/virtual-bound.

Thus, it is evident that the general formalism of Efimov physics applies to a vast spectrum of quantum systems that are of interest in molecular, atomic, nuclear, condensed matter, high-energy, and even in statistical physics. In the context of atomic systems, the implications of Efimov universality has been extensively investigated through the behavior of magnetically trapped ultra-cold alkali atoms near Feshbach resonances (see Ref. [15] for a comprehensive review). In the context of applications in nuclear systems, an extensive repository of literature exist where low-energy EFTs have been utilized over the past two decades in order to predict or investigate the properties of exotic bound cluster systems of nucleons, light or heavy mesons , and hyperons. A distinctive feature concerning *structural universality* arises in a special universal class of heteronuclear three-body systems called *Halo nuclei* [25–29].[4] In particular, it has been observed that Efimov effect is largely favored in halo nuclei that involve two neutrons as two of the three bound particles. These bound systems are termed as $2n$-halo nuclei, and the following reasons could be attributed in favor of their Efimovian nature:

- The interaction between two neutrons is naturally resonant with a large value of the ${}^1S_0$ scattering length, namely, $a_{nn} = -18.63$ fm [30], which is the basic requirement of Efimov attraction.

- Neutrons, unlike protons, being electrically neutral, do not have any Coulomb repulsion between themselves to compete with the Efimov attraction.

[4] They are so-called due to their characteristic diffuse structure with large radius having a few loosely held "valence" neutrons orbiting about their compact cores at considerably large distances.

- The presence of decay and coupled-channel dynamics tend to reduce Efimov attraction. In this respect, $2n$-halo systems in their maximal isospin state tend to be particle-stable against decay into other open channels, hence favoring Efimov effect.

Neutron-rich three-body halo-systems can thus be exploited to explore Efimov universality. With their core excitation energies typically much larger than the halo-neutron separation energies result in a characteristic scale separation that makes them amenable to a model-independent low-energy EFT description. A variant of the standard $\not\pi$EFT, so-called the *Halo/Cluster EFT* [7, 31] has been proposed that is tailor-made to tackle the multi-scale nature of the threshold dynamics of such halo nuclei (for a recent review see Ref. [32]). Such a framework provides a starting point in exploring the low-energy characteristic of various shallow-bound $2n$-halo systems, such as ^{6}He, ^{11}Li, ^{12}Be, ^{14}Be, ^{18}C, ^{20}C, etc.

The versatility of the *Halo/Cluster EFT* [7, 31] in exploiting the separation of scales provides an ideal platform for further investigation on exotic *clustering* mechanisms often found in strangeness and charm nuclear physics. In this regard, the physics of light kaonic/D-mesonic nuclei (such as $\bar{K}NN$ and DNN systems) and S-shell hypernucleus (single-Λ systems, such as ${}^{3}_{\Lambda}$H, ${}^{3}_{\Lambda}$He, ${}^{4}_{\Lambda}$H, ${}^{4}_{\Lambda}$He, etc., double-Λ systems such, as ${}^{3}_{\Lambda\Lambda}$n, ${}^{4}_{\Lambda\Lambda}$n, ${}^{4}_{\Lambda\Lambda}$H, ${}^{4}_{\Lambda\Lambda}$He, ${}^{5}_{\Lambda\Lambda}$H, ${}^{5}_{\Lambda\Lambda}$He, ${}^{6}_{\Lambda\Lambda}$He, etc., and other analogous systems of Σ, Ξ and Ω hyperons) are two areas that have attracted ever-increasing attention over the years, owing to their relevance in connection with *hot and dense* QCD matter. Such forms of matter do not prevail under ordinary laboratory conditions, but are likely to be generated copiously either within the "fireballs" of relativistic heavy-ion collision (RHIC) experiments (at facilities, such as BNL, J-PARC, KEK, GSI, INFN and LHC), or at the inner dense cores of neutron stars. Under these extreme conditions of temperature and pressure, nuclear matter is likely to exhibit properties that may be predicted through such universality-based EFT investigations. A huge gamut of past theoretical works exist on the development of phenomenological potential models of exotic bound states (see Ref. [33] for a recent review), but few have actually focused on the underlying binding mechanisms governing their formation. It is, thus, timely to supplement the multitude of the existing model results with systematic model-independent EFT predictions based on Efimov universality which is otherwise difficult to implement using *ad hoc* potential models. Rather than continuing the ultimately futile endeavor of figuring out *the exact* nuclear potential, one simply needs to construct effective potentials as a means of systematic expansion, thereby adding new operators to describe physics at subsequently higher energy scales. Thus, by using low-energy EFT this thesis seeks to explore the remnant universal features in the search and characterization of putative S-wave bound states, such as the $J = 1/2$ iso-doublet double-Λ hypernuclei (${}^{5}_{\Lambda\Lambda}$H, ${}^{5}_{\Lambda\Lambda}$He), the Ξ-hypernucleus $\Xi^{-}nn$ ($I = 3/2$, $J^{P} = 1/2^{+}$) and the D-meson nucleus $D^{0}nn$ ($J = 0, T = 3/2$).

Thesis Outline:

The thesis is organized with six following chapters to the present introductory chapter. In Chapters 2 and 3 we review the conceptual foundations on which the major works of this thesis, as presented in Chapters 4 through 6, are based on. Below we briefly summarise the contents of each chapter:

- **Chapter 2:** In this chapter, we review the standard quantum mechanics of two- and three-body scattering. In the two-body sector we discuss the asymptotic results of solving the time-independent Schrödinger equation. A formal operator approach to the two-body scattering problem is also presented which leads to a the well-known *Lippmann-Schwinger* relation for the two-body scattering T-matrix. Furthermore, we discuss a convenient separable form of the two-body potential with Gaussian regulators that not only yields the correct separable form of the T-matrix in the vicinity of bound states, the renormalization of the two-body interactions become analytically feasible. Going to the quantum mechanical description of three-body systems, we discuss the methodology of solving the so-called *low-energy Faddeev equation* in the position space using *hyperspherical representation* for a system of three indistinguishable bosons. Using suitable *adiabatic* boundary conditions solution leads to an attractive $1/R^2$ effective hyperspherical potential which manifests in the S-wave channel as Efimov effect. In this chapter, we also point out certain crucial differences in connection with solving a three-body Schrödinger equation, in contrast to solving the Faddeev equation [34]. It is to be noted that the purpose of this chapter is to establish the background quantum mechanical nature of the dynamics of few-body universality, only for the sake of pedagogical reasons. However, the bulk of the remaining chapters of the thesis primarily relies on pionless EFT, an effective perturbative (Feynman diagrammatic) technique of analysis, in contrast to a non-perturbative approach of solving quantum mechanical equations.

- **Chapter 3:** In this chapter, we present a detailed review of the basic framework of describing low-energy two- and three-body scattering in the framework of (non-relativistic) pionless EFT, developed in Refs. [1–6]. In particular, we choose a zero-range toy-model with indistinguishable bosons to demonstrate the prototypical quantitative (leading order) EFT analysis that is extensively relied upon at all stages of the works carried out in this thesis. In this EFT approach, dynamical pions are integrated out of the picture, and all low-energy interactions are represented by local vertices with phenomenologically fixed coupling, known as *low-energy constants*. In the two-body sector, universality implies the existence of shallow S-wave two-body bound states whenever the scattering length becomes very large compared to the effective range of the short-distance interactions. In such a fine-tuning scenario where the underlying dynamics are inherently non-perturbative, the scaling of two-body observables are based on an expansion around

a non-trivial fixed point. A novel power-counting scheme is thus employed which requires a leading order contact interaction to be resummed to all orders. Furthermore, with the introduction of auxiliary *dimeron* fields in the pionless EFT framework, it becomes convenient to naturally integrate (real or virtual) bound two-body subsystems into the formalism, especially while dealing with three-body universality. Going to the three-body sector, the re-scattering dynamics are described using the Faddeev-like coupled STM [13, 14] integral equation in momentum space. Universality in the three-body sector is exhibited whenever the STM equation becomes ill-defined in the asymptotic UV limit. A UV-regulator in the form of a sharp momentum cut-off is thus needed to be introduced to regularize the STM equations, and simultaneously a genuine three-body contact interaction is required to be promoted to the leading order to renormalize the artificial scale dependence of the integral equation. The resulting cut-off regulator dependence of the three-body coupling displays log-periodic cyclic singularities suggesting the onset of an RG limit cycle behavior with an inherent discrete scaling-invariance of the integral equations. This is a formal signature of Efimov effect and the quasi-cyclic singularities denote the successive formation of bound trimer states. The methodology discussed in this chapter lies at the heart of most of the works carried out in the thesis, as described in the following chapters.

- **Chapter 4:** In this chapter, the $J = 1/2$ iso-doublet double-Λ-hypernuclei, namely, ${}^{5}_{\Lambda\Lambda}\mathrm{H}$ and ${}^{5}_{\Lambda\Lambda}\mathrm{He}$, are examined as the three-body cluster states, $\Lambda\Lambda t$ ($t \equiv {}^{3}\mathrm{H}$ or triton) and $\Lambda\Lambda h$ ($h \equiv {}^{3}\mathrm{He}$ or helion), respectively, in a model-independent framework utilizing pionless Halo/Cluster effective theory. Both singlet and triplet states of the constituent ΛT ($T \equiv t, h$) subsystem are used in the elastic channel for the study of ${}^{4}_{\Lambda}\mathrm{H}{-}\Lambda$ and ${}^{4}_{\Lambda}\mathrm{He}{-}\Lambda$ scattering processes. Subsequently, upon normalization of our solutions to the integral equation with respect to a single pair of input data from an *ab initio* potential model analysis for each mirror hypernuclei, yields $B_{\Lambda\Lambda}$ which agrees fairly well with various erstwhile regulator independent potential models for our choice of the cutoff scale of $\Lambda_{\mathrm{reg}} \sim 200$ MeV. This is either consistent with pionless effective theory or with its slightly augmented version with a hard scale of $\Lambda_H \gtrsim 2m_\pi$, where low-energy Λ-Λ interactions dominated by $\pi\pi$ or σ-meson exchange. Finally, to demonstrate the predictability of our effective theory, we present preliminary estimates of the S-wave $\Lambda\Lambda T$ three-body scattering lengths and the Λ-separation energies using a range of currently accepted values of the double-Λ scattering length from a variety of existing phenomenological predictions that is constrained by the recent experimental data from relativistic heavy-ion collisions.

- **Chapter 5:** In this chapter, we study the $\Xi^{-}nn$ ($S = -2$, $T = 3/2$, $J^P = 1/2^+$) three-body system using low-energy effective field theory. Such a system is of astrophysical interest. A precise determination of neutron star equation-of-state of putative hyperonic cores relies on essential input from the $S = -2$ sector. In this obscure current scenario,

a pionless EFT analysis provides a systematic model-independent framework for assessing the feasibility of light three-particle-stable bound states, utilizing low-energy universality. Here we take recourse to simplistic speculation of the three-body system by eliminating the repulsive spin-singlet $\Xi^- n$ subsystem while retaining the predominantly attractive (possibly bound) spin-triplet $\Xi^- n$ and the virtual bound spin-singlet nn subsystems. In particular, a qualitative leading order EFT investigation by introducing a sharp momentum ultraviolet cut-off parameter $\Lambda_{\rm reg}$ into the coupled integral equations indicates a discrete scaling behavior akin to a renormalization group limit cycle, thereby suggesting the formal existence of Efimov states in the unitary limit, as $\Lambda_{\rm reg} \to \infty$. Our subsequent non-asymptotic analysis indicates that the three-body binding energy B_3 is sensitively dependent on the cut-off without the inclusion of three-body contact interactions. Furthermore, our analysis reproduces several values of the binding energy $B_3 \sim 3$ - 4 MeV, predicted in the context of existing potential models, with the regulator in the range $\Lambda_{\rm reg} \sim 350$ - 460 MeV. Finally, based on these model inputs for B_3, a ballpark estimate of the three-body scattering length in the range 2.6 - 4.9 fm, is naively constrained by our EFT analysis.

- **Chapter 6:** In this chapter, we present a demonstration of structural universality in $2n$-halo system by estimating the three-body matter density form factors and the associated mean square distances of the putative S-wave halo-bound Efimovian D^0nn system in $J = 0, T = 3/2$ channel. For this purpose, we present a detailed description of the effective quantum mechanical framework using Faddeev techniques in momentum representation, as previously developed in Refs. [24, 35–38]. Using Jacobi momentum representation we build a complete set of partial wave projected basis states in order to reconstruct the full three-body D^0nn wavefunction in terms of different re-arrangement subsystem channels. By projecting onto the chosen basis, a set of coupled Faddeev integral equations are derived that describe the re-scattering dynamics of the coupled spin and isospin subsystems. Using the so-called *spectator-representation* of the scattering amplitude (T-matrix) we establish a one-to-one correspondence with the analogous STM integral equations in the context of pionless EFT. In order to study the sensitivity of the results to the regulator variations, two different regularisation schemes are employed: Gaussian and sharp momentum cut-off regularization. Although both schemes yield almost identical results for large values of the cut-off, the results at small cut-off values display numerical instabilities, which is especially rather pronounced in the Gaussian scheme.

- **Chapter 7:** In this final chapter, we summarize all the works done in this thesis along with some concluding remarks. An outlook is finally presented for possible future extensions and the scope of the works done in the thesis.

- **Appendix A :** Derivation of the intermediate steps to obtain the hyper-radial solution, Eq. (2.118), in Chapter 2.

- **Appendix B :** One- and two-body non-relativistic propagators for $\Lambda\Lambda T$ ($T = {}^3$He or ^{3}H) system.
- **Appendix C :** A full derivation of STM equation of $\Xi^- nn$ system.

Chapter 2

Universality in Two- and Three-body Systems: A Quantum Mechanical Overview

It is known that at sufficiently low-energies most few-body physical systems with short-range interactions have wavefunctions so delocalized that many microscopic features of the interactions often become irrelevant with most properties being effectively described only in terms of a few parameters. The is the essence of *universal physics* in the sense that similar types of physics principles are applicable for many different systems, regardless of their microscopic details. In this chapter, we shall explore the basic non-relativistic quantum mechanical framework that was originally used in the investigation of two- and three-body universality in interacting systems that culminated in a remarkable discovery in 1970 by Vitaly Efimov, termed as *Efimov effect* [9–11], involving the quantum spectrum of a low-energy *nearly resonant* three-boson system. By the term "resonantly interacting" in quantum mechanics, we refer to attractive interactions that is barely strong enough to support a shallow two-body bound (or virtually bound) state. It is, thus, important to understand the dynamics of systems leading to the formation of two-body bound states, and especially study the implications of certain asymptotic two-body boundary conditions that lead to the formation of special three-body bound states termed as *Efimov states*.

The purpose of this chapter is to present a detailed review on the background physics needed to investigate two- and three-body universality. The content of this chapter draws inspiration from the reviews in Refs. [12, 39, 40]. This chapter is organized as follows. In Sec. 2.1 we review the well-known results of the two-body scattering problem in standard non-relativistic quantum mechanics. Here we especially study the general asymptotic results of the elastic scattering process where two particles are interacting *via* a static central potential. The corresponding solution to the time-independent Schrödinger equation in the center-of-mass frame is presented. Furthermore, a formal operator or integral equation approach to the

two-body scattering problem is presented which leads to a well-known operator relation for the two-body T-matrix. We close the section by discussing how universal features, such as S-wave two-body bound states, emerge by tuning certain low-energy parameters close to their asymptotic limits. A special emphasis is given to the idea of separable potentials with Gaussian regulators. In this case, not only the correct separable form of the T-matrix is reproduced near the two-body bound state pole, the renormalization of the two-body interactions becomes analytically feasible. Next, in Sec. 2.2 we review the quantum mechanical three-body problem with equal masses, employing a special Jacobi-coordinate system. We demonstrate that the Faddeev equation approach is a more preferred one (in comparison to three-body Schrödinger equation) in the investigation of two- and three-body S-wave universality by virtue of its asymptotic decoupling of the component binary subsystems. By imposing certain low-energy adiabatic approximations we end up with an integro-differential eigenvalue equation. Using appropriate short-distance asymptotic boundary conditions leads to the lowest eigenvalue channel becoming attractive with a characteristic inverse square potential intrinsic to the three-body system. Furthermore, under resonant conditions of the S-wave two-body subsystems, lead to a solution that exhibits logarithmic scaling violations through the dynamical generation of a three-body parameter. This implies the existence of Efimov-bound states. We finally conclude with a brief discussion on Efimov universality and the resulting nature of the three-body energy spectrum.

2.1 Quantum Mechanical Two-body Problem

We begin with an essential preliminary discussion on the general quantum mechanical formulation of a two-body potential scattering problem and its solution using Schrödinger equation. In particular, we discuss the relevance of the S-wave two-body scattering length a_0 and the effective interaction range r_0 as two crucial parameters governing the nature of low-energy universality of binary interacting systems, especially in the vicinity of shallow two-body bound states.

2.1.1 Two-body Potential Scattering

Let us consider an elastic scattering process (see Fig. 2.1) comprising of two particles of masses m_1 and m_2 incoming (outgoing) three-momenta $\mathbf{k}_1$ ($\mathbf{k}_1'$) and $\mathbf{k}_2$ ($\mathbf{k}_2'$), respectively, interacting *via* a central potential $V(r_{12})$ with total energy $\mathbb{E}$, where $r_{12} = |\mathbf{x}| = |\mathbf{r}_2 - \mathbf{r}_2|$ denotes the relative coordinate of the two particles. The non-relativistic Schrödinger equation in laboratory frame of reference (*lab.*-frame) is given by

$$\left[\frac{\mathbf{k}_1^2}{2m_1} + \frac{\mathbf{k}_2^2}{2m_2} + V(r_{12})\right] \Psi_{\rm lab}(\mathbf{r}_1, \mathbf{r}_2) = \mathbb{E}\Psi_{\rm lab}(\mathbf{r}_1, \mathbf{r}_2) \ . \tag{2.1}$$

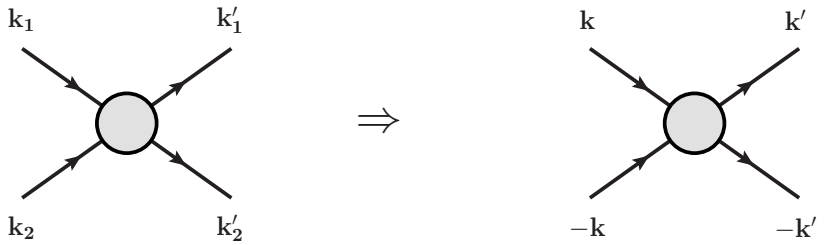

FIGURE 2.1: Two-body elastic scattering process in the laboratory and center-of mass frames.

where $\Psi_{\rm lab}(\mathbf{r}_1, \mathbf{r}_2)$ is the solution to the wavefunction in the *lab.*-frame. Henceforth, it will be convenient to express the solutions in the center-of-mass frame which may be viewed as a scattering of a single particle by a fixed potential. Thus, we introduce the *relative* incoming (outgoing) momentum vector $\mathbf{k} = \frac{m_2\mathbf{k}_1 - m_1\mathbf{k}_2}{m_1+m_2}$ ($\mathbf{k}' = \frac{m_2\mathbf{k}'_1 - m_1\mathbf{k}'_2}{m_1+m_2}$) between the two particles, and the *total lab.*-frame momentum of the two-body center-of-mass (CM) reference frame $\mathbf{P}_{\rm CM} = \mathbf{k}_1 + \mathbf{k}_2$. Since the overall center-of-mass momentum of the system does not play any role in the relative dynamics, it is best *eliminated* with the advantage that the two-body kinematics is effectively described as the one-body problem, with the corresponding Schrödinger equation written as[1]

$$\left[\frac{\mathbf{k}^2}{2\mu} + V(r_{12})\right]\psi(\mathbf{x}) = \left(\mathbb{E} - \frac{\mathbf{P}^2_{\rm CM}}{2(m_1+m_2)}\right)\psi(\mathbf{x})\ , \tag{2.2}$$

where $\mu = \frac{m_1 m_2}{m_1+m_2}$ is the reduced mass of two-body system and $\psi(\mathbf{r}_{12})$ is the solution to the wavefunction in the CM frame. For brevity, we henceforth prefer to drop the subscript "12" and regard $r \equiv r_{12}$. Now, the asymptotic ($r \to \infty$) scattering state solutions $\psi(\mathbf{x}) \to \psi^{(+)}_k(\mathbf{x})$ to the above equation are *improper* (non-normalizable) eigenvectors of the two-body (relative) Hamiltonian $h \equiv h_{\rm rel}$, and is expressed in standard collision theory by the following form at time $t = 0$:

$$\psi^{(+)}_k(\mathbf{x}) \equiv \langle \mathbf{x}|\mathbf{k}+\rangle \overset{r\to\infty}{\longrightarrow} (2\pi)^{-3/2}\left(e^{i\mathbf{k}\cdot\mathbf{x}} + f(k,\theta)\frac{e^{ikr}}{r}\right)\ . \tag{2.3}$$

Here, the first term $\phi_k(\mathbf{x}) \equiv \langle \mathbf{x}|\mathbf{k}\rangle = (2\pi)^{-3/2}e^{i\mathbf{k}\cdot\mathbf{x}}$ denotes the incoming plane wave and the second term denotes the scattered outgoing spherical wave. The terms $f(k,\theta)$ represents the scattering amplitude, with θ being the scattering angle, i.e., the angle between the direction

[1] We may regard the Hilbert space $\hbar_{\rm lab}$ of wavefunctions $\Psi_{\rm lab}(\mathbf{r}_1, \mathbf{r}_2) \equiv \Psi_{\rm lab}(\mathbf{R}_{\rm CM}, \mathbf{r}_{12})$ as spanned by the product wavefunctions of the form $\varphi(\mathbf{R}_{\rm CM})\psi(\mathbf{r}_{12})$, where $\mathbf{R}_{\rm CM} = \frac{m_1\mathbf{r}_1 + m_2\mathbf{r}_2}{m_1+m_2}$, and therefore be written as

$$\hbar_{\rm lab} = \hbar_{\rm CM} \otimes \hbar_{\rm rel}\ ,$$

where $\hbar_{\rm CM}$ and $\hbar_{\rm rel}$ are the respective Hilbert sub-spaces spanned by wavefunctions of the CM and relative coordinates. In this case, the total laboratory frame Hamiltonian of the binary system can be written as

$$h_{\rm lab} = \frac{\mathbf{P}^2_{\rm CM}}{2(m_1+m_2)} + \left[\frac{\mathbf{k}^2}{2\mu} + V(r_{12})\right] \equiv h_{\rm CM} + h_{\rm rel}.$$

of the incident ($\mathbf{k}$) and scattered waves ($\mathbf{k}'$). Using the following well-known partial wave expansions:

$$e^{ikr\cos\theta} \overset{r\to\infty}{\longrightarrow} \frac{1}{2ikr}\sum_{l=0}^{\infty}(2l+1)P_l(\cos\theta)\left[e^{ikr}-e^{-i(kr-l\pi)}\right] , \tag{2.4}$$

and

$$f(k,\theta) = \sum_{l=0}^{\infty}(2l+1)f_l(k)P_l(\cos\theta) , \tag{2.5}$$

where

$$\begin{aligned} f_l(k) &= \frac{e^{i2\delta_l(k)}-1}{2ik} = \frac{e^{i\delta_l(k)}\sin\delta_l(k)}{k} \\ &= \frac{k^{2l}}{k^{2l+1}\cot\delta_l(k) - ik^{2l+1}} . \end{aligned} \tag{2.6}$$

denotes the l^{th} partial wave amplitude, Eq. (2.3) can be expressed as [41]

$$\psi_k^{(+)}(\mathbf{x}) \overset{r\to\infty}{\longrightarrow} (2\pi)^{-3/2}\frac{1}{2ikr}\sum_{l=0}^{\infty}(2l+1)P_l(\cos\theta)\left[e^{i(kr+2\delta_l(k))}-e^{-i(kr-l\pi)}\right] . \tag{2.7}$$

Here, $P_l(\cos\theta)$ denotes the Legendre polynomial of degree $l = 0, 1, ..., \infty$, and $\delta_l(k)$ denotes the corresponding phase shift in the l^{th} partial wave. The term $k^{2l+1}\cot\delta_l(k)$ can be expanded using Taylor series in k^2, namely, the *effective-range expansion* [42–44]:

$$k^{2l+1}\cot\delta_l(k) = -\frac{1}{a_l} + \frac{r_l k^2}{2} + \mathcal{O}(k^4) . \tag{2.8}$$

In particular, for low-energy processes only the S-wave contributions become dominant, in which case the above equation boils down to

$$k\cot\delta_0(k) = -\frac{1}{a_0} + \frac{r_0 k^2}{2} + \mathcal{O}(k^4) , \tag{2.9}$$

where, as mentioned earlier, a_0 and r_0 denote the S-wave scattering length and effective-range of the interaction potential, respectively. In order to determine the scattering amplitude, one may resort to one of two genuinely alternative approaches: a differential approach and an integral approach. Here, we follow the latter approach which is closely related to an operator representation of an integral scattering equation, *vis-a-vis* the *Lippmann-Schwinger* (LS) equation. In practice, such an approach provides a model-independent quantum description of the general dynamics of scattering which connects more naturally to a field-theoretic description.

2.1.2 Integral approach: Lippmann-Schwinger equation

Let us express the solutions $\psi_\alpha(\mathbf{x}) \equiv \langle \mathbf{x}|\psi_\alpha\rangle$ to the time-independent Schrödinger equation for a generic two-body scattering process (which includes both scattering as well as possible two-body bound states) with total two-body energy $\mathscr{E}_\alpha$ in the operator form:

$$h|\psi_\alpha\rangle = \mathscr{E}_\alpha|\psi_\alpha\rangle\,, \tag{2.10}$$

where $h = h_0 + V$ is the full two-body Hamiltonian, h_0 is the free Hamiltonian, and V is a finite range local effective potential. Also, the free particle states $\phi_k(\mathbf{x}) \equiv \langle \mathbf{x}|\mathbf{k}\rangle$ satisfy the time-independent Schrödinger's equation in operator form:

$$h_0|\phi_k\rangle = \mathscr{E}_k^{(0)}|\phi_k\rangle\,, \tag{2.11}$$

where $\mathscr{E}_k^{(0)} = k^2/2\mu$ is the free two-body kinetic energy in the CM frame. In general, for the non-asymptotic region with non-zero potential, we use the index α is used to denote a particular set of quantum numbers for wave-packet states ψ_α, including those denoting bound states. However, for *purely* scattered wave-packet states $\psi_\alpha^{(+)}(\mathbf{x}) \equiv \langle \mathbf{x}|\psi_\alpha^{(+)}\rangle \sim \langle \mathbf{x}|\mathbf{k}+\rangle$ (i.e., which exclude bound states) with momentum sharply peaked about $\mathbf{k}$, their energies $\mathscr{E}_\alpha$ also become *sharp*, namely, $\mathscr{E}_\alpha \to \mathscr{E}_k^{(0)} = k^2/2\mu$. In this case the complete orthonormal set of eigenstates, ϕ_α of the free Hamiltonian can be related to the corresponding set of "scattered" eigenstates $\psi_\alpha^{(+)}$ (at $t = 0$) of the full two-body Hamiltonian *via* the isometric (non-unitary) operator, termed as the *Möller scattering operator*:[2]

$$|\psi_\alpha^{(+)}\rangle = \Omega_+|\phi_\alpha\rangle\,, \tag{2.12}$$

where

$$\Omega_+ = \sum_{j=\alpha,\beta,\ldots} |\psi_j^{(+)}\rangle\langle\phi_j| = \lim_{\varepsilon\to 0^+} \sum_{j=\alpha,\beta,\ldots} \frac{i\varepsilon}{\mathscr{E}_j + i\varepsilon - h}|\phi_j\rangle\langle\phi_j|\,, \tag{2.13}$$

[2]Technically speaking, the *proper* (normalizable) eigenvectors are assumed to be expandable in terms of the corresponding improper (non-normalizable) eigenvectors, namely,

$$|\psi_\alpha^+\rangle = \int \mathrm{d}^3\mathbf{p}\, f_\alpha(\mathbf{p})|\mathbf{p}+\rangle\,, \quad \text{and}$$
$$|\phi_\alpha\rangle = \int \mathrm{d}^3\mathbf{p}\, f_\alpha(\mathbf{p})|\mathbf{p}\rangle\,,$$

where $f_\alpha(\mathbf{p})$ is a regular function sharply localized about $\mathbf{p} = \mathbf{k}$. Further, it is demanded here that the corresponding time-dependent solutions $\psi_\alpha^{(+)}(\mathbf{x},t)$ develop from the free packet solutions $\phi_\alpha(\mathbf{x},t)$ in the infinite past ($t \to -\infty$). That the energies $\mathscr{E}_\alpha$ in this case is same as the energy $\mathscr{E}_k^{(0)}$, can be proved using the so-called *intertwining relation* for the Möller operators, $h\Omega_+ = \Omega_+ h_0$:

$$h|\psi_\alpha^{(+)}\rangle = h\Omega_+|\phi_\alpha\rangle = \Omega_+ h_0|\phi_\alpha\rangle = \Omega_+\frac{k^2}{2\mu}|\phi_\alpha\rangle = \mathscr{E}_k^{(0)}|\psi_\alpha^{(+)}\rangle\,.$$

and consequently,

$$|\psi_\alpha^{(+)}\rangle = \lim_{\varepsilon\to 0^+} \frac{i\varepsilon}{\mathscr{E}_\alpha + i\varepsilon - h}|\phi_\alpha\rangle\,. \tag{2.14}$$

Next we re-write the above equation in the form

$$\begin{aligned}|\psi_\alpha^{(+)}\rangle &= \lim_{\varepsilon\to 0^+} \frac{\mathscr{E}_\alpha - h_0 - V + V + i\varepsilon}{\mathscr{E}_\alpha + i\varepsilon - h}|\phi_\alpha\rangle\,,\\ &= |\phi_\alpha\rangle + g^{(+)}(\mathscr{E}_\alpha + i\varepsilon)V|\phi_\alpha\rangle\,,\end{aligned} \tag{2.15}$$

where $g^{(+)}$ is the full Green's function or the so-called *resolvent* function of the full Hamiltonian h, and given by

$$g^{(+)}(\mathscr{E}_\alpha + i\varepsilon) \equiv \lim_{\varepsilon\to 0^+} \frac{1}{\mathscr{E}_\alpha + i\varepsilon - h}\,, \tag{2.16}$$

or equivalently, in the operator form, $g(z) = 1/(z-h)$, with $z = \mathscr{E}_\alpha + i\varepsilon$. Likewise, we can define the free Green's function or resolvent of the free Hamiltonian h_0 as $g_0(z) = 1/(z-h_0)$. Now, using the operator identity, $\frac{1}{\mathscr{P}} - \frac{1}{\mathbb{Q}} = \frac{1}{\mathbb{Q}}(\mathbb{Q} - \mathscr{P})\frac{1}{\mathscr{P}}$, the two resolvents can be related as

$$g(z) = g_0(z) + g_0(z)Vg(z)\,. \tag{2.17}$$

Using this identity, we can further simplify the Eq. (2.15) as follows:

$$\begin{aligned}|\psi_\alpha^{(+)}\rangle &= |\phi_\alpha\rangle + \Big(g_0(z) + g_0(z)Vg(z)\Big)V|\phi_\alpha\rangle\\ &= |\phi_\alpha\rangle + g_0(z)V\Big(|\phi_\alpha\rangle + g(z)V|\phi_\alpha\rangle\Big)\\ |\psi_\alpha^{(+)}\rangle &= |\phi_\alpha\rangle + g_0(z)V|\psi_\alpha^{(+)}\rangle\,.\end{aligned} \tag{2.18}$$

The above equation is no other than the well-known LS equation. In configuration space, the LS equation is written as

$$\langle \mathbf{x}|\psi_\alpha^{(+)}\rangle = \langle \mathbf{x}|\phi_\alpha\rangle + \int \mathrm{d}^3\mathbf{x}'\,\langle \mathbf{x}|\frac{1}{\mathscr{E}_\alpha + i\varepsilon - h_0}|\mathbf{x}'\rangle\,\langle \mathbf{x}'|V|\psi_\alpha^{(+)}\rangle\,. \tag{2.19}$$

By inserting a complete set of states $|\mathbf{p}\rangle$ in the kernel of the above equation, we find

$$\langle \mathbf{x}|g_0(z)|\mathbf{x}'\rangle = \int \mathrm{d}^3\mathbf{p}\,\langle \mathbf{x}|g_0(z)|\mathbf{p}\rangle\,\langle \mathbf{p}|\mathbf{x}'\rangle = \frac{1}{(2\pi)^3}\int \mathrm{d}^3\mathbf{p}\,\frac{e^{i\mathbf{p}\cdot(\mathbf{x}-\mathbf{x}')}}{z - \mathscr{E}_p^{(0)}}\,. \tag{2.20}$$

using the fact that $h_0|\mathbf{p}\rangle = \mathscr{E}_p^{(0)}|\mathbf{p}\rangle = \frac{p^2}{2\mu}|\mathbf{p}\rangle$. Subsequently, employing complex contour integration to evaluate the Cauchy residue at the positive pole $k = +\sqrt{2\mu(\mathscr{E}_\alpha + i0)}$, we obtain the result for the free Green's function:

$$g_0(\mathbf{x},\mathbf{x}') = \langle \mathbf{x}|\frac{1}{\mathscr{E}_\alpha + i\varepsilon - h_0}|\mathbf{x}'\rangle = -\frac{\mu}{2\pi}\frac{e^{ik|\mathbf{x}-\mathbf{x}'|}}{|\mathbf{x}-\mathbf{x}'|}\,, \tag{2.21}$$

where $\mathscr{E}_\alpha = \mathscr{E}_k^{(0)} = \frac{k^2}{2\mu}$ is the two-body energy. With the local potential V satisfying the relation

$$\langle \mathbf{x}'|V|\psi_\alpha^{(+)}\rangle = V(\mathbf{x}')\,\langle \mathbf{x}'|\psi_\alpha^{(+)}\rangle\,, \tag{2.22}$$

the LS equation finally becomes

$$\langle \mathbf{x}|\psi_\alpha^{(+)}\rangle = \langle \mathbf{x}|\phi_\alpha\rangle - \frac{\mu}{2\pi}\int \mathrm{d}^3\mathbf{x}'\,\frac{e^{ik|\mathbf{x}-\mathbf{x}'|}}{|\mathbf{x}-\mathbf{x}'|}\,V(\mathbf{x}')\,\langle \mathbf{x}'|\psi_\alpha^{(+)}\rangle\,. \tag{2.23}$$

Having established the LS equation for two-body potential scattering, we now wish to determine the relationship between the scattering amplitude $f(k,\theta)$ and the local potential $V(r)$. To this end, let us consider the analogous LS equation satisfied by the improper eigenstates $\psi_k^{(+)}(\mathbf{x}) \equiv \langle \mathbf{x}|\mathbf{k}+\rangle$ with sharp momentum $\mathbf{k}$:

$$\langle \mathbf{x}|\mathbf{k}+\rangle = \langle \mathbf{x}|\mathbf{k}\rangle - \frac{\mu}{2\pi}\int \mathrm{d}^3\mathbf{x}'\,\frac{e^{ik|\mathbf{x}-\mathbf{x}'|}}{|\mathbf{x}-\mathbf{x}'|}\,V(\mathbf{x}')\,\langle \mathbf{x}'|\mathbf{k}+\rangle\,. \tag{2.24}$$

Let P be a far-way observation point with position vector $\mathbf{x}$, while $\mathbf{x}'$ be a point within the domain of influence of the local potential V located at the origin of reference O, as illustrated in Fig. 2.2. Also, let $r = |\mathbf{x}| \gg r' = |\mathbf{x}'|$, and α denotes the angle between the position vectors $\mathbf{x}$ and $\mathbf{x}'$. For elastic scattering, the scattered wave vector reaching the observation point is $\mathbf{k}' = \frac{k}{r}\mathbf{x}$. We can now expand $|\mathbf{x}-\mathbf{x}'|$ in powers of r'/r:

$$|\mathbf{x}-\mathbf{x}'| = \sqrt{\mathbf{x}^2 + \mathbf{x}'^2 - 2\mathbf{x}\cdot\mathbf{x}'} = r\left[1 - \frac{2\mathbf{x}\cdot\mathbf{x}'}{r^2} + \mathcal{O}\left(\frac{r'^2}{r^2}\right)\right]^{1/2} \approx r - \frac{\mathbf{x}\cdot\mathbf{x}'}{r}\,.$$

Consequently, for $r \to \infty$, we have

$$\frac{e^{ik|\mathbf{x}-\mathbf{x}'|}}{|\mathbf{x}-\mathbf{x}'|} \approx \frac{e^{ikr}e^{-i\mathbf{k}'\cdot\mathbf{x}'}}{r}\,,$$

such that the LS equation leads to the same asymptotic form as displayed in Eq. (2.3):

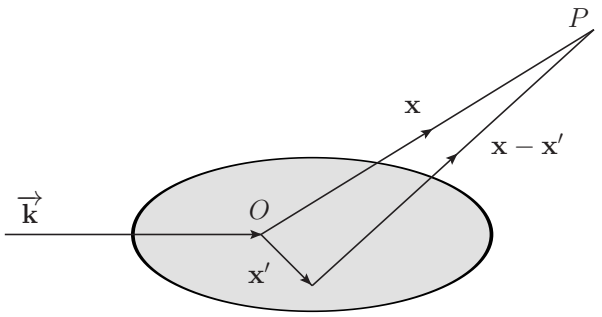

FIGURE 2.2: The incoming plane wave $\phi_k \equiv \langle \mathbf{x}|\mathbf{k}\rangle$ is scattered by a finite range local potential V located at O. P denotes the observation point where the wavefunction $\psi_k^{(+)} \equiv \langle \mathbf{x}|\mathbf{k}+\rangle$ is to be evaluated. The shaded region represents the domain within which the effect of potential could be felt.

$$\langle \mathbf{x}|\mathbf{k}+\rangle \overset{r\to\infty}{\longrightarrow} \langle \mathbf{x}|\mathbf{k}\rangle - \frac{\mu}{2\pi}\frac{e^{ikr}}{r}\int \mathrm{d}^3\mathbf{x}'\, e^{-i\mathbf{k}'\cdot\mathbf{x}'}V(\mathbf{x}')\,\langle \mathbf{x}'|\mathbf{k}+\rangle$$
$$= (2\pi)^{-3/2}\left(e^{i\mathbf{k}\cdot\mathbf{x}} + \frac{e^{ikr}}{r}f(\mathbf{k},\mathbf{k}')\right), \tag{2.25}$$

where

$$f(\mathbf{k},\mathbf{k}') = -\sqrt{2\pi}\mu\int \mathrm{d}^3\mathbf{x}'\, e^{-i\mathbf{k}'\cdot\mathbf{x}'}V(\mathbf{x}')\,\langle \mathbf{x}'|\mathbf{k}+\rangle$$
$$= -(2\pi)^2\mu\int \mathrm{d}^3\mathbf{x}'\,\langle \mathbf{k}'|\mathbf{x}'\rangle\, V(\mathbf{x}')\,\langle \mathbf{x}'|\mathbf{k}+\rangle\,. \tag{2.26}$$

Upon integration, we obtain the defining relation for the elastic scattering amplitude:

$$f(k,\theta) \equiv f(\mathbf{k},\mathbf{k}') = -(2\pi)^2\mu\langle \mathbf{k}'|V|\mathbf{k}+\rangle\,. \tag{2.27}$$

2.1.3 Two-body T-matrix

The two-body T-matrix operator t is related to the potential V by the correspondence:

$$V|\mathbf{k}+\rangle \equiv t|\mathbf{k}\rangle \tag{2.28}$$

Using the LS equation for the improper (momentum) eigenvectors [in analogy to Eq. (2.18)], namely,

$$|\mathbf{k}+\rangle = |\mathbf{k}\rangle + g_0(z)V|\mathbf{k}+\rangle\,, \tag{2.29}$$

then multiplying V on both side and using the transformation, Eq.(2.28), we obtain the corresponding LS equation for the two-body T-matrix operator:

$$t(z) = V + Vg_0(z)t(z)\,. \tag{2.30}$$

Comparing with Eq.(2.27), the scattering amplitude can be written in terms of the T-matrix:[3]

$$f(\mathbf{k},\mathbf{k}') = -(2\pi)^2\mu\langle \mathbf{k}'|t|\mathbf{k}\rangle\,. \tag{2.31}$$

[3]We point out in connection with literature dealing with effective field theory (EFT) approaches (see e.g., Ref. [12] and other references within), an alternate relation is often used, namely,

$$\mathcal{A}_2(\mathbf{k},\mathbf{k}') \equiv \frac{1}{(2\pi)^3}f(\mathbf{k},\mathbf{k}') = -\frac{\mu}{2\pi}\langle \mathbf{k}'|t|\mathbf{k}\rangle\,,$$

where $\mathcal{A}_2(\mathbf{k},\mathbf{k}')$ is the two-body Feynman scattering amplitude. This difference essentially stems from considering the unnormalized versions of the free and scattering eigenstates, i.e., by omitting the factor of $(2\pi)^{-3/2}$, e.g., $\phi_k \equiv \langle \mathbf{x}|\mathbf{k}\rangle \sim e^{i\mathbf{k}\cdot\mathbf{x}}$, and in the definition of asymptotic scattered wave

$$\psi_k^{(+)} \equiv \langle \mathbf{x}|\mathbf{k}+\rangle \overset{r\to\infty}{\longrightarrow} e^{i\mathbf{k}\cdot\mathbf{x}} + f(k,\theta)\frac{e^{ikr}}{r}\,.$$

2.1.4 Scattering length

The partial wave decomposition of the amplitude $f(\mathbf{k}, \mathbf{k}')$ is given by the well-known relation:

$$f(\mathbf{k}, \mathbf{k}') = \sum_{l=0}^{\infty} (2l+1) f_l(k) P_l(\cos\theta) \,. \tag{2.32}$$

The analogous expansion for the two-body T-matrix $t(\mathbf{k}, \mathbf{k}'; \mathscr{E}) \equiv -\langle \mathbf{k}'|t|\mathbf{k}\rangle$ is given by

$$t(\mathbf{k}, \mathbf{k}'; \mathscr{E}) = \sum_{l=0}^{\infty} (2l+1) t_l(k, k'; \mathscr{E}) P_l(\cos\theta) \,. \tag{2.33}$$

In particular, the *fully on-shell* T-matrix is obtained by evaluating the above expression at the *on-shell* point $k = k' = \sqrt{2\mu(\mathscr{E}_k + i0)}$. Using Eq. (2.6) for the partial wave amplitude $f_l(k)$, expressed in terms of the scattering phase shift, the corresponding on-shell partial wave T-matrix is obtained as

$$f_l(k) = \frac{1}{k \cot\delta_l(k) - ik} = -(2\pi)^2 \mu \, t_l(k; \mathscr{E}_k) \,. \tag{2.34}$$

In this context, the most important parameter in low-energy two-body scattering is the S-wave ($l = 0$) scattering length a_0. Mathematically, the scattering length can be defined as the low-energy limit of the S-wave elastic scattering amplitude:

$$a_0 = -\lim_{k\to 0} f_0(k) \,. \tag{2.35}$$

Likewise, the corresponding relation between the scattering length and the S-wave on-shell T-matrix is given as:[4]

$$a_0 = -\lim_{k\to 0} (2\pi)^2 \mu \, t_0(k; \mathscr{E}_k) \,. \tag{2.36}$$

Generically, in the context of S-wave two-body universality, the scattering length a_0 becomes much larger compared to the corresponding range r_0 of the potential V. In that case, the T-matrix develops simple poles at certain negative values of the two-body energy ($\mathscr{E} < 0$), associated with the formation of two-body threshold bound ($a_0 > 0$) or anti-bound/virtual ($a_0 < 0$) states. The binding energy is given by the universal formula:

$$\mathscr{E} = -B_2 \approx -\frac{\hbar^2}{2\mu a_0^2} \,. \tag{2.37}$$

[4]Here again, owing to the difference in the normalization of the free and scattering states by the factor $(2\pi)^{-3/2}$ in the context of EFT-related works (see e.g., Ref. [12] and other references within), the alternative relation that can be found is

$$a_0 = -\lim_{k\to 0} \frac{\mu}{2\pi} T(k; \mathscr{E}_k) \,.$$

In fact, the later part of this thesis dealing with our EFT analyses (Chapters 4-6) adopts this convention for reasons of consistency to similar EFT works.

The formula is universal in the sense that it is applicable near the two-body scattering threshold where it becomes *exact* in the limit $a_0 \to \pm\infty$. The corresponding radial part of the two-body CM frame wavefunction in proximity to the S-wave bound state (i.e., with imaginary momentum $k \to \pm i\kappa$) also has the universal form [12]:

$$\psi_{\rm dimer}(r) = \lim_{\kappa\to 0} \mp \frac{i}{2\pi\kappa r^2} \sin\left[\pm i\kappa r + \delta_0\right] \approx -\frac{1}{2\pi r} e^{-r/a_0} \,. \tag{2.38}$$

where $r \sim a_0 \gg r_0$ denotes the two-body separation with $\kappa \sim 1/a_0$ and $\delta(\kappa) \sim -\kappa a_0$. Such a limit, defining the maximal value of the total scattering cross-section saturating the upper bound from the $l = 0$ partial-wave unitarity, namely,[5]

$$\lim_{a_0\to\pm\infty} \sigma_{\rm tot}^{(l=0)} = \frac{4\pi \sin^2\delta_0(k)}{k^2} \xrightarrow{k\to 0} 4\pi a_0^2 \,, \tag{2.39}$$

is termed as the *resonant* or *unitary limit*. Otherwise, the above formulas receive parametrically small corrections suppressed by powers of r_0/a_0. The simplicity of these universal results tacitly assumes the related idealization $r_0 \to 0$, termed as the *scaling limit*. The fact that low-energy observables are dependent on the single parameter a_0 with the dimension of length is formally realized as a *continuous scaling-symmetry* under the following transformations in terms of an arbitrary scaling parameter $\lambda \in \mathbb{R}$:

$$a_0 \to \lambda a_0 \,, \quad E \to \lambda^{-2} E \,. \tag{2.40}$$

A general feature near the vicinity of two-body bound states is that the T-matrix elements $\langle \mathbf{k}'|t|\mathbf{k}\rangle$ becomes separable (factorizes into $\mathbf{k}'$ and $\mathbf{k}$), and consequently, the LS equation is exactly solvable. To facilitate a quantum mechanical model description it becomes useful to introduce a potential that is also separable. This is the context of the discussion in the following subsection.

2.1.5 Two-body T-matrix with Separable Potential

Here we review the quantum mechanical framework, developed originally in the Refs. [35–37, 46], and used in the study of two-body S-wave bound states for a single-channel (rank 1) attractive local potential which is separable. In the momentum space such a model potential can be represented as

$$\frac{1}{(2\pi)^3} \langle \mathbf{k}'|V^S|\mathbf{k}\rangle = V(\mathbf{k},\mathbf{k}') = C_0 \chi(k)\chi(k') + \cdots \,, \tag{2.41}$$

where $C_0 < 0$ is a two-body coupling constant, and the ellipses denote contributions from higher partial waves that do not concern us. The separable potential can also be expressed

[5] Note that the elastic unitary cross-section gets doubled for identical particles, i.e., $\sigma_{\rm tot}^{(l=0)} \to 8\pi a_0^2$.

in the form of a projection operator:

$$V^S \equiv C_0|\chi\rangle\langle\chi|\,, \tag{2.42}$$

where $\chi(p) = \langle \mathbf{p}|\chi\rangle$ and $\chi(p') = \langle\chi|\mathbf{p}'\rangle$ are the so-called *form factor* functions. Here we consider their choice as Gaussian regulators of the form:

$$\chi(k, \Lambda_{\rm reg}) = \exp\left(-\frac{k^2}{\Lambda_{\rm reg}^2}\right)\,. \tag{2.43}$$

These regulator functions suppress dynamical contributions arising from the high-momentum region, i.e., for $k, k' \geq \Lambda_{\rm reg}$, where $\Lambda_{\rm reg}$ is a large cut-off parameter defining the effective range of the potential $r_0 \sim 1/\Lambda_{\rm reg}$. In other words, taking $\Lambda_{\rm reg} \to \infty$ is equivalent to considering a zero-range potential.

Now, it is easy to show that for the separable potential V^S the two-body T-matrix is itself separable. To this end we consider the T-matrix in the operator form

$$\begin{aligned} t(z) &= V^S + V^S g_0(z) t(z) \\ &= C_0|\chi\rangle\langle\chi| + C_0|\chi\rangle\langle\chi|g_0(z)t(z)\,. \end{aligned}$$

Multiplying by $\langle\chi|g_0$ from the left, we have

$$\langle\chi|g_0(z)t(z) = C_0\langle\chi|g_0(z)|\chi\rangle\langle\chi| + C_0\langle\chi|g_0(z)|\chi\rangle\langle\chi|g_0(z)t(z)\,.$$

Solving for $\langle\chi|g_0 t$ we get,

$$\langle\chi|g_0(z)t(z) = \frac{\langle\chi|g_0(z)|\chi\rangle\langle\chi|}{C_0^{-1} - \langle\chi|g_0(z)|\chi\rangle}\,.$$

On inserting back into T-matrix operator equation, we obtain

$$t(z) = C_0|\chi\rangle\langle\chi| + \frac{C_0|\chi\rangle\langle\chi|g_0(z)|\chi\rangle\langle\chi|}{C_0^{-1} - \langle\chi|g_0(z)|\chi\rangle}\,,$$

which is equivalent to the separable form:

$$t(z) = |\chi\rangle\tau(z)\langle\chi|\,, \tag{2.44}$$

where

$$\tau(z) = \frac{1}{C_0^{-1} - \langle\chi|g_0(z)|\chi\rangle}\,. \tag{2.45}$$

Next, let us express the S-wave T-matrix $T(\mathbf{k},\mathbf{k}';\mathscr{E}) \equiv -\langle \mathbf{k}'|t|\mathbf{k}\rangle/(2\pi)^3$ *via* the LS equation in the momentum-space representation:

$$\begin{aligned}
T(\mathbf{k},\mathbf{k}';\mathscr{E}) &= V(\mathbf{k},\mathbf{k}') + \int \mathrm{d}^3\mathbf{p}\, \frac{V(\mathbf{k},\mathbf{p})}{\mathscr{E} - \frac{p^2}{2\mu} + i\varepsilon} T(\mathbf{p},\mathbf{k}';\mathscr{E}) \\
&= C_0\chi(k,\Lambda_{\rm reg})\,\chi(k',\Lambda_{\rm reg}) + C_0\chi(k,\Lambda_{\rm reg}) \int \mathrm{d}^3\mathbf{p}\, \frac{\chi(p,\Lambda_{\rm reg})}{\mathscr{E} - \frac{p^2}{2\mu} + i\varepsilon} T(\mathbf{p},\mathbf{k}';\mathscr{E}) \\
&= C_0\chi(k,\Lambda_{\rm reg})\,\chi(k',\Lambda_{\rm reg}) + C_0\chi(k,\Lambda_{\rm reg}) \int \mathrm{d}^3\mathbf{p}\, \frac{\chi(p)}{\mathscr{E} - \frac{p^2}{2\mu} + i\varepsilon} \\
&\quad \times \left[C_0\chi(p,\Lambda_{\rm reg})\,\chi(k',\Lambda_{\rm reg}) + C_0^2\chi(p,\Lambda_{\rm reg})\,\chi(k',\Lambda_{\rm reg}) \int \mathrm{d}^3\mathbf{p}'\, \frac{|\chi(p',\Lambda_{\rm reg})|^2}{\mathscr{E} - \frac{p'^2}{2\mu} + i\varepsilon} + \cdots \right] \\
&= C_0\chi(k,\Lambda_{\rm reg})\,\chi(k',\Lambda_{\rm reg}) \left[1 + C_0\mathscr{I}(\mathscr{E},\Lambda_{\rm reg}) + C_0^2\mathscr{I}^2(\mathscr{E},\Lambda_{\rm reg}) + \cdots \right] \\
&\equiv \chi(k,\Lambda_{\rm reg})\,\chi(k',\Lambda_{\rm reg}) \frac{1}{C_0^{-1} - \mathscr{I}(\mathscr{E},\Lambda_{\rm reg})}\,,
\end{aligned} \tag{2.46}$$

where

$$\mathscr{I}(\mathscr{E},\Lambda_{\rm reg}) = \int \mathrm{d}^3\mathbf{p}\, \frac{|\chi(p,\Lambda_{\rm reg})|^2}{\mathscr{E} - \frac{p^2}{2\mu} + i\varepsilon} = 8\pi\mu \int_0^\infty \mathrm{d}p\, p^2 \frac{\exp\left(-\frac{2p^2}{\Lambda_{\rm reg}^2}\right)}{2\mu\mathscr{E} - p^2 + i\varepsilon}\,. \tag{2.47}$$

Since we are concerned with two-body bound states where the total energy is negative ($\mathscr{E} < 0$), the $i\varepsilon$ prescription in the denominator of integral $\mathscr{I}$ becomes redundant. A straightforward evaluation of the integration leads to the following closed-form expression [46]:

$$\mathscr{I}(\mathscr{E},\Lambda_{\rm reg}) = -4\pi^2\mu \left[\frac{\Lambda_{\rm reg}}{\sqrt{2\pi}} - \sqrt{-2\mu\mathscr{E}}\, \exp\left(\frac{2(-2\mu\mathscr{E})}{\Lambda_{\rm reg}^2}\right) \mathrm{erfc}\left(\frac{\sqrt{2(-2\mu\mathscr{E})}}{\Lambda_{\rm reg}}\right) \right], \tag{2.48}$$

where

$$\mathrm{erfc}(x) = 1 - \frac{2}{\sqrt{\pi}} \int_0^x \mathrm{d}t\, \exp(-t^2) \tag{2.49}$$

denotes the complementary error function, which quickly goes to 1 for $x << 1$. Taking the zero-range limit, $\Lambda_{\rm reg} \to \infty$, the first term in the above expression yields an ultraviolet (UV) divergence. Since low-energy observables are expected to be independent of regulators, such terms are eliminated through proper renormalization as shown by the following:
With the binary S-wave system with large positive (negative) scattering length a_0 a two-body shallow bound (virtual) state with energy $\mathscr{E} = -B_2 = -\hbar^2/(2\mu a_0^2)$ is produced at leading order, as indicated by the pole of the T-matrix represented by the condition:

$$\frac{1}{C_0} = \mathscr{I}(\mathscr{E} = -B_2, \Lambda_{\rm reg})\,. \tag{2.50}$$

Utilizing the pole position we can fix the running of the two-body coupling $C_0 \to C_0(\Lambda_{\rm reg})$ in order to reproduce the scattering length a_0. In particular with $a_0\Lambda_{\rm reg} >> 1$, both the

exponential and error functions quickly approach 1, leading to a simpler expression [46]:

$$C_0(\Lambda_{\rm reg}) = \frac{a_0}{4\pi^2\mu}\left[1 - \frac{a_0\Lambda_{\rm reg}}{\sqrt{2\pi}}\right]^{-1} \tag{2.51}$$

Consequently, the leading order renormalized two-body T-matrix for negative energies ($\mathscr{E} < 0$) in the vicinity of S-wave bound state is given by

$$T(\mathbf{k},\mathbf{k}';\mathscr{E}) = \chi(k,\Lambda_{\rm reg})\,\chi(k',\Lambda_{\rm reg})\frac{1}{4\pi^2\mu}\left[\frac{1}{a_0}\,\exp\left(\frac{2}{a_0^2\Lambda_{\rm reg}^2}\right)\mathrm{erfc}\left(\frac{\sqrt{2}}{|a_0|\Lambda_{\rm reg}}\right)\right.$$
$$\left. - \sqrt{-2\mu\mathscr{E}}\,\exp\left(\frac{2(-2\mu\mathscr{E})}{\Lambda_{\rm reg}^2}\right)\mathrm{erfc}\left(\frac{\sqrt{2(-2\mu\mathscr{E})}}{\Lambda_{\rm reg}}\right)\right]^{-1}. \tag{2.52}$$

We note here that the cut-off scale ($\Lambda_{\rm reg}$) dependence of the Gaussian regulators (χ) ensures the approximate regulator independence of the T-matrix, as expressed *via* the RG invariance relation:

$$\lim_{\Lambda_{\rm reg}\to\infty}\frac{\Lambda_{\rm reg}}{[T(\Lambda_{\rm reg})]^2}\left[\frac{\mathrm{d}T(\Lambda_{\rm reg})}{\mathrm{d}\Lambda_{\rm reg}}\right] \approx 0\,, \tag{2.53}$$

given that the error due to the truncation of the T-matrix at the leading order is in general suppressed by powers of $1/(a_0\Lambda_{\rm reg})$.

2.2 Quantum Mechanical Three-body Problem

In this section, we discuss the general quantum mechanical framework for dealing with a low-energy three-body bound state problem. For this purpose a special coordinate system, namely, the *hyperspherical coordinate* system is used to study the dynamics of the three-body system. The hyperspherical coordinate system is based on the well-known *Jacobi coordinate* system, where the three-body system is studied as a combination of two-body subsystems interacting with the third spectator particle. Here, we shall especially discuss two important variants of the quantum mechanical formulation: firstly, *via* the standard Schrödinger equation approach, and secondly, *via* the Faddeev equation [34] which rectifies certain drawbacks with the former approach. The contents of this section are predominantly borrowed from the review work of Ref. [12], which must be referred to for further details. For reasons of simplicity, as done in Ref. [12], the major portion of the section deals with a *resonantly interacting* system of three *identical bosons*, i.e., with large S-wave two-particle scattering length tuned to the unitary limit where $a_0 \to 0$.

2.2.1 Jacobi coordinate system

The study of a three-body system is more efficiently facilitated using a Jacobi coordinate system rather than in the Cartesian system. The Jacobi system eliminates the overall motion of the three-body center-of-mass (CM), thereby reducing the total degrees of freedom to six, compared to nine in the Cartesian system. Here, the coordinates are defined in terms of two *separation vectors*: $\mathbf{r}_{jk}$ between a pair of particles j and k, and $\mathbf{r}_{i,jk}$ between a third *spectator* particle i and the two-body CM of the (jk)-pair. The corresponding diagrammatic representation of the Jacobi coordinate system is illustrated in Fig. 2.3. For three different masses m_i, m_j, and m_k the separation vectors are written as

$$\mathbf{r}_{jk} = \mathbf{r}_j - \mathbf{r}_k \ , \quad \mathbf{r}_{i,jk} = \mathbf{r}_i - \frac{m_k \mathbf{r}_j + m_j \mathbf{r}_k}{m_j + m_k} \ , \tag{2.54}$$

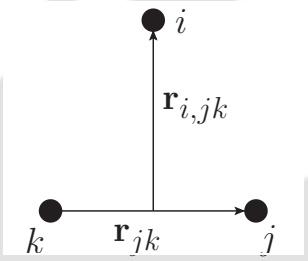

FIGURE 2.3: Jacobi coordinate system for a three-particle system with particle i as the spectator. The system is equally well described by the cyclic permutation of indices $(i, j, k) \equiv (1, 2, 3)$

where the system is equally well described by the cyclic permutation of indices $(i, j, k) \equiv (1, 2, 3)$. In particular, for equal masses $(m_1 = m_2 = m_3 = m)$, the separation vectors boil down to

$$\mathbf{r}_{jk} = \mathbf{r}_j - \mathbf{r}_k \ , \quad \mathbf{r}_{i,jk} = \mathbf{r}_i - \frac{\mathbf{r}_j + \mathbf{r}_k}{2} \ . \tag{2.55}$$

For simplicity of three-body kinematic, in this section we assume the particle to have equal masses. In order to specify the exact configuration of the three-body system two more quantities are needed to be introduced. The first one is the so-called *hyper-radius* (R), which is nothing but the rms separation of three particles, defined as

$$R^2 = \frac{r_{12}^2 + r_{23}^2 + r_{31}^2}{3} = \frac{r_{jk}^2}{2} + \frac{2}{3} r_{i,jk}^2 \, . \tag{2.56}$$

While a small value of hyper-radius means that all three particles are close together (compact configuration), a large value signifies any one particle being far away from to the other two. Since hyper-radius can be the same for several different three-body configurations, it becomes necessary to introduce another quantity known as the *Delves hyper-angle* $(0 \leq \alpha_i \leq \pi/2)$,

defined as

$$\alpha_i = \arctan\left(\frac{\sqrt{3}r_{jk}}{2r_{i,jk}}\right) . \tag{2.57}$$

The hyper-angle $\alpha_i \to 0$ when the spectator particle i is far away from the CM of the (jk)-pair, and $\alpha_i \to \frac{\pi}{2}$ when i is in close proximity to the CM of the (jk)-pair. The magnitudes of the separation vectors can now be expressed in terms of the hyper-radius and hyper-angle as

$$r_{jk} = \sqrt{2}R\sin\alpha_i, \quad \text{and} \quad r_{i,jk} = \sqrt{\frac{3}{2}}R\cos\alpha_i\,. \tag{2.58}$$

Using the expression for α_i and the Jacobi coordinates $\mathbf{r}_{jk}$ and $\mathbf{r}_{i,jk}$, the other hyper-angles can be determined:

$$\sin^2\alpha_j = \frac{1}{4}\sin^2\alpha_i + \frac{3}{4}\cos^2\alpha_i + \frac{\sqrt{3}}{2}\sin\alpha_i\cos\alpha_i\,(\hat{\mathbf{r}}_{jk}\cdot\hat{\mathbf{r}}_{i,jk})\ , \tag{2.59}$$

where for a fixed value $\alpha_i = \alpha_i^0$, the value of α_j has the following range:

$$\left|\frac{\pi}{3} - \alpha_i^0\right| < \alpha_j < \frac{\pi}{2} - \left|\frac{\pi}{6} - \alpha_i^0\right| . \tag{2.60}$$

It is notable that the the three hyper-angles α_1, α_2 and α_3, are not really independent, as one of them could be expressed in terms of the other two. In fact, the hyper-angles are related by the following identity:

$$\sin^2\alpha_1 + \sin^2\alpha_2 + \sin^2\alpha_3 = \frac{3}{2}\,. \tag{2.61}$$

Finally, the volume element in the hyperspherical coordinate system can be expressed as

$$\mathrm{d}^3\mathbf{r}_{jk}\,\mathrm{d}^3\mathbf{r}_{i,jk} = \frac{3\sqrt{3}}{4}R^5\sin^2(2\alpha_i)\,\mathrm{d}R\,\mathrm{d}\alpha_i\,\mathrm{d}\Omega_{jk}\,\mathrm{d}\Omega_{i,jk}\,, \tag{2.62}$$

with $\mathrm{d}\Omega_{jk}$ and $\mathrm{d}\Omega_{i,jk}$ being the differential solid angles associated with the directions of the separation vectors $\hat{\mathbf{r}}_{jk}$ and $\hat{\mathbf{r}}_{i,jk}$. In what follows, we shall denote $\Omega \equiv (\alpha_i, \Omega_{jk}, \Omega_{i,jk})$ as a five-dimensional system of hyperangular variables, collectively, such that for a fixed R the hyperangular integral of any arbitrary function $F(R,\Omega)$ is expressed as

$$\int_{\mathbb{R}^5}\mathrm{d}\Omega\,F(R,\Omega) = \int_0^{\frac{\pi}{2}}\mathrm{d}\alpha_i\,\sin^2(2\alpha_i)\int\mathrm{d}\Omega_{jk}\int\mathrm{d}\Omega_{i,jk}\,F(R,\Omega)\,. \tag{2.63}$$

2.2.2 Three-body Schrödinger equation

The time-independent Schrödinger equation in Cartesian representation with three equal mass ($m_1 = m_2 = m_3 = m$), interacting *via* a short-range potential $V(r_1, r_2, r_3)$ and total energy

E, is given by

$$\left[-\frac{\hbar^2}{2m}\sum_{i=1}^{3}\nabla_i^2 + V(r_1, r_2, r_3)\right]\Psi = E\Psi\,. \tag{2.64}$$

Using hyperspherical representation, the Schrödinger equation becomes

$$\left[T_R + T_{\alpha_i} + \frac{\Lambda_{i,jk}^2}{2mR^2} + V(R,\Omega)\right]\Psi = E\Psi\,, \tag{2.65}$$

where T_R is the hyper-radial kinetic energy operator,

$$T_R = -\frac{\hbar^2}{2m}\left[\frac{\partial^2}{\partial R^2} + \frac{5}{R}\frac{\partial}{\partial R}\right] = \frac{\hbar^2}{2m}R^{-5/2}\left[-\frac{\partial^2}{\partial R^2} + \frac{15}{4R^2}\right]R^{5/2}\,, \tag{2.66}$$

T_{α_i} is the hyperangular kinetic energy operator,

$$T_{\alpha_k} = -\frac{\hbar^2}{2mR^2}\left[\frac{\partial^2}{\partial\alpha_i^2} + 4\cot(2\alpha_i)\frac{\partial}{\partial\alpha_i}\right] = \frac{\hbar^2}{2mR^2}\frac{1}{\sin(2\alpha_i)}\left[-\frac{\partial^2}{\partial\alpha_i^2} - 4\right]\sin(2\alpha_i)\,, \tag{2.67}$$

and $\Lambda_{i,jk}^2$ is the generalized angular momentum operator,[6]

$$\Lambda_{i,jk}^2 = \frac{L_{jk}^2}{\sin^2\alpha_i} + \frac{L_{i,jk}^2}{\cos^2\alpha_i}\,, \tag{2.68}$$

where $\mathbf{L}_{jk}$ is the relative angular momentum between the (jk)-pair and $\mathbf{L}_{i,jk}$ is the angular momentum of particle i relative to the center-of-mass of the (jk)-pair. The potential here is assumed to be translation invariant depends on six independent variables, R and five other hyperangular variables Ω. The same goes for the wavefunction as well.

A possible solution $\Psi(R,\Omega)$ to the above Schrödinger equation is obtained *via* an *adiabatic* ansatz, namely, by expanding in a complete set of hyperangular wavefunctions $\Phi_n(R,\Omega)$ for fixed hyper-radius R:

$$\Psi(R,\Omega) = R^{-5/2}\sum_n f_n(R)\Phi_n(R,\Omega)\,, \tag{2.69}$$

where $\Phi_n(R,\Omega)$ are solutions to the differential equation

$$\left[T_{\alpha_i} + \frac{\Lambda_{i,jk}^2}{2mR^2} + V(R,\Omega)\right]\Phi_n(R,\Omega) = \mathscr{V}_n(R)\Phi_n(R,\Omega)\,, \tag{2.70}$$

satisfying the orthogonality condition

$$\int \mathrm{d}\Omega\,\Phi_n^*(R,\Omega)\Phi_m(R,\Omega) = \delta_{nm} \tag{2.71}$$

[6]For the purpose of a general discussion we introduce the angular momentum operator, but eventually, we shall specialize to the case of zero total angular momentum S-wave three-body systems.

The eigenvalues $\mathcal{V}_n(R)$ constitute the effective potentials for the respective channels (labeled by n) associated with the hyperspherical wave functions Φ_n, and are termed as the *hyperspherical potential*. Using Eqs. (2.65), (2.66), (2.69) and (2.70), the Schrödinger equation boils down to the form

$$\frac{\hbar^2}{2m}\sum_n\left[-\frac{\partial^2}{\partial R^2}+\frac{15}{4R^2}\right]f_n(R)\Phi_n(R,\Omega)+\sum_n\mathcal{V}_n(R)f_n(R)\Phi_n(R,\Omega) = E\sum_n f_n(R)\Phi_n(R,\Omega)\,, \tag{2.72}$$

which upon using the aforementioned orthogonality condition, yields a coupled set of eigenvalue equations for the hyper-radial function $f(R)$:

$$\left[\frac{\hbar^2}{2m}\left(-\frac{\partial^2}{\partial R^2}+\frac{15}{4R^2}\right)+\mathcal{V}_n(R)\right]f_n(R) + \sum_m\left(2U_{nm}(R)\frac{\partial}{\partial R}+W_{nm}(R)\right)f_m(R) = Ef_n(R), \tag{2.73}$$

where the coupling potential are given by

$$U_{nm}(R) = -\frac{\hbar^2}{2m}\int d\Omega\,\Phi_n^*(R,\Omega)\,\frac{\partial\Phi_m(R,\Omega)}{\partial R}\,,$$
$$W_{nm}(R) = -\frac{\hbar^2}{2m}\int d\Omega\,\Phi_n^*(R,\Omega)\,\frac{\partial^2\Phi_m(R,\Omega)}{\partial R^2}\,. \tag{2.74}$$

Notably, the off-diagonal potentials ($m \neq n$) fall off at large distances much more rapidly in comparison to the hyperspherical potential $\mathcal{V}_n$, say at least a factor of $1/R^2$ [47]. Since we are ultimately interested in the low-energy (or long-distance) behavior of the system, the off-diagonal potentials being small are neglected. This constitutes the so-called, *adiabatic hyperspherical approximation* [48], and leads a single uncoupled eigenvalue equation for the n^{th} channel:

$$\left[\frac{\hbar^2}{2m}\left(-\frac{\partial^2}{\partial R^2}+\frac{15}{4R^2}\right)+\mathcal{V}_n(R)+2U_{nn}(R)\frac{\partial}{\partial R}+W_{nn}(R)\right]f_n(R) = Ef_n(R)\,. \tag{2.75}$$

The problem with Schrödinger equation for a three-body system is that it does not take advantage of the $2+1$ configuration of the system in which a binary subsystem (often a bound state with two particles being very close together) is interacting with a well-separated third particle. In the case of the Faddeev equation [34], as demonstrated in the following subsection, it exploits the *asymptotic decoupling* of the component binary subsystems which makes the numerical solution easier in their asymptotic forms. For instance, each of the Faddeev components holds *only* bound states of the corresponding two-body subsystems. In this respect, the separation vector $\mathbf{r}_i$ represents the internal coordinate of the corresponding binary cluster, while the $\mathbf{r}_{i,jk}$ coordinate plays the role of a reaction coordinate for all the states below the three-body break-up threshold. This ensues a simple physical interpretation

of the coordinates, thereby suggesting a natural requirement for *discretizing* the corresponding degrees of freedom: the discrete analogs of the $\mathbf{r}_i$ coordinate should reproduce the bound spectrum of the i^{th} binary cluster, while the discrete+continuum analogs of the $\mathbf{r}_{i,jk}$ coordinate must describe the corresponding i-(jk) particle-dimer scattering states. The consideration of subsystem angular momenta is another concerning issue that complicates matters in the Schrödinger equation as compared to the Faddeev equation approach, where its neglect is a more legitimate approximation. In the latter approach, couplings between different higher-order subsystem angular momenta enter only at second order in the two-body potential, and hence, are suppressed at low-energies. Whereas in the former approach they appear at the first order, and hence, can not be neglected [47].

2.2.3 Faddeev Equation at Low-energies

In this chapter, we shall restrict ourselves to the coordinate space description of the (three-body) Faddeev equation [34] and the associated universality. The corresponding momentum space description of the Faddeev equation is presented in Chapter 6, which becomes particularly convenient in assessing the universal geometrical features of Efimov-like systems. The ensuing discussion is based on the treatment of Fedorov and Jensen presented in Ref. [49] (also, see Ref. [12]).

In the Faddeev equation we decompose the potential as a sum of three two-body components $V_i(r_{jk})$, each being a function of the separation distance r_{jk} of the (jk)-pair only, namely,

$$V(\mathbf{r_1}, \mathbf{r_2}, \mathbf{r_3}) = V_1(r_{23}) + V_2(r_{31}) + V_3(r_{12})\,, \tag{2.76}$$

with cyclic permutation of the indices $(i, j, k) \equiv (1, 2, 3)$ implies. The term $V_i(r_{jk})$ essentially represents the two-body interaction between the closely located (jk)-pair of particle, while the spectator particle i is non-interacting. More generally, a genuine three-body short-distances interaction potential $V_{3-\text{body}}$ could also be included leading to a slightly modified formalism, as discussed in the book by W. Glöckle [50]. Nevertheless, even though our definition of the full potential does not include an explicit three-body term, the two-body off-shell dynamics of low-energy universality that emerge from the asymptotic boundary conditions for wavefunctions implicitly replicate the effect of the missing three-body potential.

The Faddeev equations constitute a set of three coupled-channel equations signifying the three *re-arrangement channels* for describing the same three-body system in Jacobi coordinates (see Fig. 2.4). The corresponding three solutions constitute equivalent descriptions of the three-body system, referred to as the *Faddeev partitions*. The sum total of all the components determine the full solution to the time-independent three-body Schrödinger equation, as described in the previous subsection. Thus, the full solution is in the spectator representation (denoted by the superscript) is decomposed as [34]

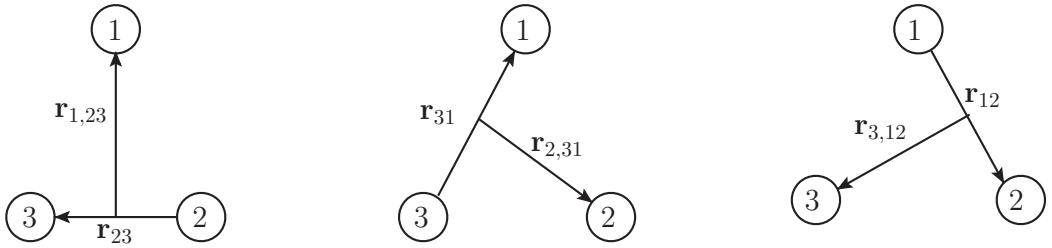

$Channel-1$ $Channel-2$ $Channel-3$

FIGURE 2.4: The three re-arrangement channels for a three-body bound system in Jacobi representation.

$$\Psi(\mathbf{r_1},\mathbf{r_2},\mathbf{r_3}) = \psi^{(1)}(\mathbf{r}_{23},\mathbf{r}_{1,23}) + \psi^{(2)}(\mathbf{r}_{31},\mathbf{r}_{2,31}) + \psi^{(3)}(\mathbf{r}_{12},\mathbf{r}_{3,12})\,, \tag{2.77}$$

with each component $(i = 1, 2, 3)$ satisfying

$$\left[-\frac{\hbar^2}{2m}\nabla^2_{\mathbf{r}_{jk}} - \frac{\hbar^2}{2m}\nabla^2_{\mathbf{r}_{i,jk}} + V_i(r_{jk}) - E\right]\psi^{(i)}(\mathbf{r}_{jk},\mathbf{r}_{i,jk}) = V_i(r_{jk})\sum_{j\neq i}\psi^{(j)}(\mathbf{r}_{ki},\mathbf{r}_{j,ki})\,, \tag{2.78}$$

or equivalently,

$$\left[T_R + T_{\alpha_i} + \frac{\Lambda_{i,jk}}{2mR^2} + V_i(r_{jk}) - E\right]\psi^{(i)} = V_i(r_{jk})(\psi^{(j)} + \psi^{(k)})\,, \quad i = 1,2,3\,. \tag{2.79}$$

Furthermore, the system of equations can equivalently be represented as a system of coupled-channel integral equations expressed in the following compact operator representation:

$$|\psi^{(i)}\rangle = G_0^{(i)}(E+i0)\,t_i(E)\sum_{i\neq j}|\psi^{(j)}\rangle\,, \tag{2.80}$$

where

$$G_0^{(i)}(E+i0) = \left[E + i0 - T_R - T_{\alpha_i} - \frac{\Lambda_{1,23}}{2mR^2}\right]^{-1}\,, \tag{2.81}$$

is the three-body free resolvent or Green's functions in the spectator representation of the two-body Lippmann-Schwinger equation (in the space of three-body kinematics) is

$$t_i(E+i0) = V_i + G_0^{(i)}(E+i0)\,V_i\,t_i(E+i0)\,. \tag{2.82}$$

For more details, we refer to the treatment presented in Chapter 6 of the thesis.

Next, we specialize to the case of an interacting system of three identical bosons with zero total spin, as well as subsystem orbital angular momentum ($\mathbf{L}_{jk} = \mathbf{L}_{i,jk}$=0). As discussed, such a simplifying approximation is quite legitimate due to the suppression of higher order

angular momenta at low-energies [47]. In this case, we have

$$\Psi(\mathbf{r_1}, \mathbf{r_2}, \mathbf{r_3}) = \psi(R, \alpha_1) + \psi(R, \alpha_2) + \psi(R, \alpha_3)\,, \tag{2.83}$$

so that, for instance with particle $i = 1$ as the spectator, Eq. (2.79) becomes

$$[T_R + T_{\alpha_1} - E]\,\psi(R, \alpha_1) + V(\sqrt{2}R\sin\alpha_1)\Big(\psi(R, \alpha_1) + \psi(R, \alpha_2) + \psi(R, \alpha_3)\Big) = 0\,. \tag{2.84}$$

Similarly, the other two more equations with the particles $i = 2, 3$ as spectators can be furnished through cyclic permutations. However, these three equations can be reduced to a single equation by exploiting the fact that the averages of $\psi(R, \alpha_2)$ and $\psi(R, \alpha_3)$ over the solid angles Ω_{23} and $\Omega_{1,23}$ is given by the following integral over the component wavefunction $\psi(R, \alpha_1)$:

$$\Big\langle \psi(R, \alpha_2) \Big\rangle_{\hat{r}_{23}, \hat{r}_{1,23}} = \Big\langle \psi(R, \alpha_3) \Big\rangle_{\hat{r}_{23}, \hat{r}_{1,23}} = \frac{2}{\sqrt{3}} \int_{|\frac{\pi}{3} - \alpha_1|}^{\frac{\pi}{2} - |\frac{\pi}{6} - \alpha_1|} \mathrm{d}\eta\, \frac{\sin(2\eta)}{\sin(2\alpha_1)}\, \psi(R, \eta)\,. \tag{2.85}$$

By using the above result, the so-called *low-energy Faddeev equation*, becomes an *integro-differential equation*:

$$[T_R + T_\alpha - E]\,\psi(R, \alpha) = -V(\sqrt{2}R\sin\alpha)\left[\psi(R, \alpha) + \frac{4}{\sqrt{3}} \int_{|\frac{\pi}{3} - \alpha|}^{\frac{\pi}{2} - |\frac{\pi}{6} - \alpha|} \mathrm{d}\eta\, \frac{\sin(2\eta)}{\sin(2\alpha)}\, \psi(R, \eta)\right] \tag{2.86}$$

A possible solution $\psi(R, \alpha)$ to the Eq. (2.86) for a fixed hyper-radius R could be be obtained *via* an adiabatic expansion in terms of a complete set of hyperangular function $\phi_n(R, \alpha)$:

$$\psi(R, \alpha) = \frac{1}{R^{5/2}\sin(2\alpha)} \sum_n f_n(R)\phi_n(R, \alpha)\,. \tag{2.87}$$

Since, the pre-factor $1/\sin(2\alpha)$ diverges at the two end-points $\alpha = 0$ and $\alpha = \frac{\pi}{2}$, the boundary condition implies that the solution is regular only if $\phi_n(R, \alpha)$ vanishes at these points. Using Eq. (2.87), we obtain an integro-differential eigenvalue equation in the single variable α with the hyper-radius R as a parameter, namely,

$$\left[\frac{\partial^2}{\partial\alpha^2} + \lambda_n(R)\right]\phi_n(R, \alpha) = \frac{2mR^2}{\hbar^2} V(\sqrt{2}R\sin\alpha)\left[\phi_n(R, \alpha) + \frac{4}{\sqrt{3}} \int_{|\frac{\pi}{3} - \alpha|}^{\frac{\pi}{2} - |\frac{\pi}{6} - \alpha|} \mathrm{d}\eta\, \phi_n(R, \eta)\right] \tag{2.88}$$

The eigenvalue $\lambda_n(R)$ for the above equation defines the channel potentials in terms of the hyper-radial variable R:

$$\mathscr{V}_n(R) = \frac{\hbar^2}{2mR^2}[\lambda_n(R) - 4]\,. \tag{2.89}$$

Since, the operator on the right hand side of Eq. (2.88)) is non-hermitian, the hyperangular eigenfunctions functions $\phi_n(R, \alpha)$ in general do not constitute an orthogonal spectrum in

variable α. In fact their inner product define a matrix element $G_{nm}(R)$ dependent on hyper-radius R:

$$G_{nm}(R) = \int_0^{\pi/2} \mathrm{d}\alpha\, \phi_n^*(R,\alpha)\phi_m(R,\alpha)\,. \tag{2.90}$$

By inserting the aforementioned adiabatic expansion of $\psi(R,\alpha)$ for fixed R in the low-energy Faddeev equation, Eq. (2.86), projecting onto the n^{th} channel by convoluting with $\phi_n^*(R,\alpha)$, followed by a multiplication by the inverse $G_{nm}^{-1}(R)$, we obtain the following coupled-channel equations for the hyper-radial function $f(R)$:

$$\left[\frac{\hbar^2}{2m}\left(-\frac{\partial^2}{\partial R^2}+\frac{15}{4R^2}\right)+\mathscr{V}_n(R)\right] f_n(R) + \sum_m \left[2P_{nm}(R)\frac{\partial}{\partial R}+Q_{nm}(R)\right] f_m(R) = E f_n(R)\,, \tag{2.91}$$

where the hyper-radial coupling potentials P_{nm} and Q_{nm} are given by

$$\begin{aligned} P_{nm}(R) &= -\frac{\hbar^2}{2m}\sum_k G_{nk}^{-1}(R)\int_0^{\pi/2}\mathrm{d}\alpha\,\phi_k^*(R,\alpha)\,\frac{\partial\phi_m(R,\alpha)}{\partial R}\,, \\ Q_{nm}(R) &= -\frac{\hbar^2}{2m}\sum_k G_{nk}^{-1}(R)\int_0^{\pi/2}\mathrm{d}\alpha\,\phi_k^*(R,\alpha)\,\frac{\partial^2\phi_m(R,\alpha)}{\partial R^2}\,. \end{aligned} \tag{2.92}$$

Again invoking the adiabatic hyperspherical approximation [48], the off-diagonal (i.e., $m \neq n$) channel potentials may be neglected, thereby converting the system of coupled equations into a set of uncoupled eigenvalue equations in the hyper-radial variable R. Moreover, by choosing a region of R in which the eigenvalues $\lambda_n(R)$ are by and large insensitive to the variation in R, the diagonal terms $P_{nn}(R)$ and $Q_{nn}(R)$ can also be suppressed. Thus, by neglecting the diagonal coupling potentials the set of uncoupled eigenvalue equations reduce into standard radial Schrödinger equations with a hyper-radial potentials $\mathscr{V}_n(R)$:

$$\left[\frac{\hbar^2}{2m}\left(-\frac{\mathrm{d}^2}{\mathrm{d}R^2}+\frac{15}{4R^2}\right)+\mathscr{V}_n(R)\right] f_n(R) \approx E f_n(R)\,. \tag{2.93}$$

2.2.4 Channel Eigenvalues $\lambda_n(R)$

Let us consider the following two cases for the two-body potential $V(r)$:

Case I: First, we consider the case where the two-body potential is vanishingly small, in which case Eq. (2.88) becomes

$$\left[\frac{\partial^2}{\partial\alpha^2}+\lambda_n(R)\right]\phi_n(R,\alpha) = 0\,, \tag{2.94}$$

having the solutions of the form

$$\phi_n(R,\alpha) = C_1 \cos\sqrt{\lambda_n(R)}\alpha + C_2 \sin\sqrt{\lambda_n(R)}\alpha\,. \tag{2.95}$$

Applying the boundary conditions for the hyperangular function $\phi_n(R,\alpha)$:

- For $\alpha = 0$, $\phi_n(R,0) = 0$, implies $C_1 = 0$.
- For $\alpha = \frac{\pi}{2}$, $\phi_n\left(R,\frac{\pi}{2}\right) = 0$, implies

$$\lambda_n(R) = 4(n+1)^2\,, \quad n = 0,1,2,... \tag{2.96}$$

  noting that the lowest channel eigenvalue λ_0 must be non-trivial.

Hence, for vanishing two-body potential, the eigenfunctions of the integro-differential equation, Eq. (2.88), are given by

$$\phi_n(R,\alpha) \sim \sin\left[2(n+1)\alpha\right]\,, \tag{2.97}$$

with the corresponding hyperspherical potentials being

$$\mathscr{V}_n(R) = 4n(n+2)\frac{\hbar^2}{2mR^2}\,. \tag{2.98}$$

Case II: In the second case, we consider that the two-body potential is short-ranged. In this case, there exists the following two regions of R and α where the integro-differential eigenvalue equation, Eq. (2.88), can be analytically solved:

- In the first scenario, the term $R\sin\alpha$ is much larger than the effective-range (r_0) of interaction potential, such that the term proportional to $V(\sqrt{2}R\sin\alpha)$ in Eq. (2.88) can be neglected in comparison to $\lambda_n(R)$. Consequently, the integro-differential equation in this region reduces to the form

$$\left[\frac{\partial^2}{\partial\alpha^2} + \lambda_n(R)\right]\phi_n^{(\alpha-\text{high})}(R,\alpha) \approx 0\,. \tag{2.99}$$

  In this case only the boundary condition for the upper end-point $\alpha = \frac{\pi}{2}$ is relevant, and leads to the solution

$$\phi_n^{(\alpha-\text{high})}(R,\alpha) \approx \sin\left[\sqrt{\lambda_n(R)}\left(\frac{\pi}{2} - \alpha\right)\right]\,. \tag{2.100}$$

- The second scenario is just the opposite, namely, that $R\sin\alpha$ is small enough that the eigenvalues $\lambda_n(R)$ can be neglected in comparison to the $V(\sqrt{2}R\sin\alpha)$ term in Eq. (2.88). Here, $\alpha \ll 1$ implies the approximation $\sin\alpha \approx \alpha$, so that the boundary

condition for the lower end-point $\alpha = 0$ is the only relevant one. Consequently, in this case the Eq. (2.88) reduces to the form

$$\left[\frac{\partial^2}{\partial\alpha^2} - \frac{2mR^2}{\hbar^2}V(\sqrt{2}R\alpha)\right]\phi_n^{(\alpha-\text{low})}(R,\alpha) \approx \frac{2mR^2}{\hbar^2}V(\sqrt{2}R\alpha)\left[\frac{8\alpha}{\sqrt{3}}\phi_n^{(\alpha-\text{high})}\left(R,\frac{\pi}{3}\right)\right]. \quad (2.101)$$

A particular solution to the above inhomogeneous equation is given by

$$\phi_n^{(\alpha-\text{low})}(R,\alpha) = -\frac{8\alpha}{\sqrt{3}}\phi_n^{(\alpha-\text{high})}\left(R,\frac{\pi}{3}\right). \quad (2.102)$$

Whereas, the corresponding homogeneous equation is

$$\left[-\frac{\hbar^2}{2mR^2}\frac{\partial^2}{\partial\alpha^2} + V(\sqrt{2}R\alpha)\right]\phi_n^{(\alpha-\text{low})}(R,\alpha) \approx 0\,. \quad (2.103)$$

The above equation is identical to a radial Schrödinger equation for a two-body system with zero energy and two-body potential $V(\sqrt{2}R\alpha)$. With the zero-energy solution given by, say, $\psi_0(\sqrt{2}R\alpha)$, the general solution to the Eq. (2.101) is the sum of the particular solution and the homogeneous solution:

$$\phi_n^{(\alpha-\text{low})}(R,\alpha) \approx \mathcal{A}(R)\psi_0(\sqrt{2}R\alpha) - \frac{8\alpha}{\sqrt{3}}\phi_n^{(\alpha-\text{high})}\left(R,\frac{\pi}{3}\right), \quad (2.104)$$

where $\mathcal{A}(R)$ is an arbitrary unknown function of the hyper-radius R.

In particular, of interest to us is the existence of two-body universality (*vis-a-vis* two bound states), which evidently favors a large S-wave two-body scattering length compared to the effective-range ($|a_0| \gg r_0$). In this context, the low-α solution is more pertinent which holds for $\alpha \ll 1$ and $R\alpha \gg r_0$. Furthermore, the zero-energy solution $\psi_0(r)$ in this case is simply obtained in the $k \to 0$ limit of the asymptotic low-energy scattering solution $\psi_k(r)$:

$$\psi_0(r) = \lim_{k\to 0}\psi_k(r) = \lim_{k\to 0}\frac{1}{k}\sin\left[kr + \delta_0(k)\right] \sim r - a_0\,, \quad (2.105)$$

where we used the fact that as $k \to 0$, $\delta_0(k) \to -ka_0$. Thus, inserting the above result for $\psi_0(r)$ (with $r = \sqrt{2}R\alpha$) in Eq. (2.104) leads to the result:

$$\phi_n^{(\alpha-\text{low})}(R,\alpha) = \mathcal{A}(R)(\sqrt{2}R\alpha - a_0) - \frac{8\alpha}{\sqrt{3}}\phi_n^{(\alpha-\text{high})}\left(R,\frac{\pi}{3}\right). \quad (2.106)$$

2.2.5 Matching condition for the hyperangular wavefunction

In the results of Eq. (2.106), the term $\mathcal{A}(R)$ is an undetermined function of the hyper-radius. However, it may be determined by demanding the compatibility of the two aforementioned approximate solutions to Eq. (2.88) for the high-α and low-α regions [cf. Eqs. 2.111 and (2.106)]. The extrapolation of these solutions between the two domains is thus facilitated

via introducing a *matching condition* for the hyperangular wavefunction $\phi_n(R,\alpha)$ at $\alpha = 0$, namely,

$$\phi_n^{(\alpha-\text{high})}(R,0) = \phi^{(\alpha-\text{low})}(R,0)\,, \tag{2.107}$$

which immediately furnishes the unknown function:

$$\mathscr{A}(R) = -\frac{1}{a_0}\sin\left[\sqrt{\lambda_n(R)}\,\frac{\pi}{2}\right]. \tag{2.108}$$

Furthermore, the corresponding matching condition for the hyperangular derivatives of $\phi_n(R,\alpha)$, namely,

$$\left.\frac{\partial\phi_n^{(\alpha-\text{high})}(R,\alpha)}{\partial\alpha}\right|_{\alpha=0} = \left.\frac{\partial\phi_n^{(\alpha-\text{low})}(R,\alpha)}{\partial\alpha}\right|_{\alpha=0}, \tag{2.109}$$

yields the reputed *transcendental matching condition*, originally derived by Efimov [10]:

$$\cos\left(\sqrt{\lambda_n(R)}\,\frac{\pi}{2}\right) - \frac{8}{\sqrt{3}}\frac{1}{\sqrt{\lambda_n(R)}}\sin\left(\sqrt{\lambda_n(R)}\,\frac{\pi}{6}\right) = \frac{\sqrt{2}R}{a_0}\frac{1}{\sqrt{\lambda_n(R)}}\sin\left(\sqrt{\lambda_n(R)}\,\frac{\pi}{2}\right) \tag{2.110}$$

This equation leads to infinitely many solutions for the channel eigenvalues $\lambda_n(R)$ for fixed R.[7] It follows that the solutions to Eq. (2.88) for large a_0 are given by

$$\phi_n(R,\alpha) \sim \sin\left[\sqrt{\lambda_n(R)}\left(\frac{\pi}{2}-\alpha\right)\right]. \tag{2.111}$$

It is found that all solutions to Eq. (2.110) approach constant values independent of a_0 in the $R \to 0$ limit. In particular, for the lowest $(n = 0)$ channel, the $R \to 0$ limit yields a negative eigenvalue given by

$$\lambda_0(R) \xrightarrow{R\to 0} -s_0^2\left[1 + 1.897\frac{R}{a_0}\right], \tag{2.112}$$

where $s_0 = 1.00624$. For all other $(n \neq 0)$ channels, the eigenvalues $\lambda_n(R)$ turn out to be positive. Thus, it is interpreted for $R \ll |a_0| \to \infty$, only the lowest channel hyperspherical potential $\mathscr{V}_0(R \to 0)$ [cf. Eq. (2.89)] is attractive, while the rest of the channel potentials $\mathscr{V}_{n\neq 0}(R \to 0)$ are repulsive. On the other hand, for $R \to \infty$, all the hyperspherical potentials $\mathscr{V}_{n\neq 0}(R \to \infty)$ asymptote to the three-particle scattering threshold $E = 0$ reducing to the free-particle situation (Case I in the last subsection), with the only exception of $\mathscr{V}_0(R \to \infty)$ with $a_0 > 0$ which asymptotes to the (2+1)-dimer-particle scattering threshold $E = -B_2 =$

[7] Notably, the constant solution $\lambda_n(R) = 16$ is an unphysical one since it turns out to yield the *spurious solution* $\psi(R,\alpha) \propto \cos(2\alpha)$ to the low-energy Faddeev equation, Eq. (2.86), whereby the corresponding Schrödinger equation yields a trivial solution $\Psi = 0$ [12].

$-\hbar^2/(ma_0^2)$ (cf. Fig. 2.5):

$$\mathscr{V}_0(R) \overset{R\to\infty}{\longrightarrow} -\frac{\hbar^2}{ma_0^2}\left[1+\frac{8\sqrt{2}a_0}{\sqrt{3}R}e^{-\sqrt{2}\pi R/3a_0}+\frac{2a_0^2}{R^2}\right]. \tag{2.113}$$

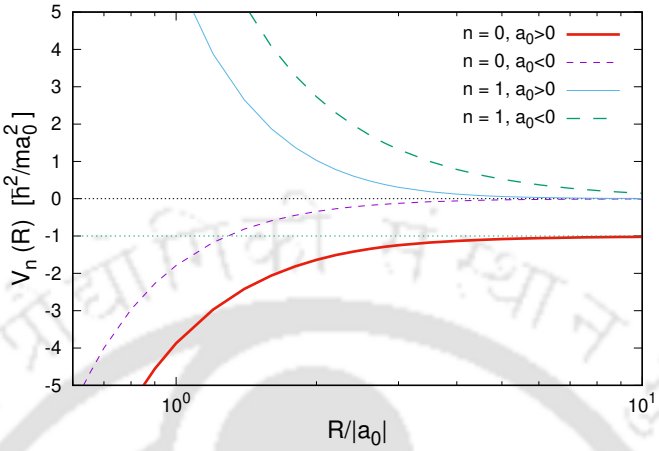

FIGURE 2.5: Variation of the first two ($n = 0, 1$) hyperspherical potentials $\mathscr{V}_n(R)$ with $R/|a_0|$, scaled in units of the dimer-particle scattering threshold energy $-E = B_2 = \hbar^2/(ma_0^2)$. The latter is depicted as the lower horizontal dotted line to which the $n = 0$ curve asymptotes as $R/|a_0| \to \infty$. The upper horizontal line depicts the three-particle scattering threshold $E = 0$. The solid curves correspond to $a_0 > 0$ and the dashed curves for $a_0 < 0$. The figure is reproduced from Ref. [12].

2.2.6 Scaling violation parameter Λ_0

In the last subsection we found that the adiabatic hyperspherical approximation for a system of identical bosons with large S-wave scattering length ($a_0 \gg r_0$) is well justified. It allows the channel coupling potentials to be $P_{nm}(R)$ and $Q_{nm}(R)$ to be neglected for both the asymptotic regions of the hyper-radius $R/|a_0| \to 0$ as well as $R/|a_0| \to \infty$. Furthermore, the channel eigenvalues $\lambda_n(R)$ in these asymptotic limits also approach constants values. In that case, Eq. (2.93) for the hyper-radial wavefunctions $f_n(R)$ reduces in the region $R \ll |a_0|$ to the standard radial Schrödinger equation for a particle of mass m in a $1/R^2$-type *singular* effective potential, with the constant $\lambda_n(0)$ determining its strength:

$$\frac{\hbar^2}{2m}\left[-\frac{\mathrm{d}^2}{\mathrm{d}R^2}+\frac{\lambda_n(0)-1/4}{R^2}\right]f_n(R) = Ef_n(R). \tag{2.114}$$

As we discussed, since only the $n = 0$ channel is attractive, while the rest are repulsive,[8] only the hyperspherical potential $\mathscr{V}_0(R)$ is likely to supports any existence of three-body bound

[8]The repulsions in the $n \neq 0$ channels may be interpreted as generalized centrifugal barriers due to the relative motion of deformation of the three-body system. Whereas, for the $n = 0$ channel the attraction is interpreted as a result of a mediated interaction between two particles by the exchange of the third particle.

states, if at all. For the region $R \ll |a_0|$, since $\lambda_0(0) = -s_0^2$, the form of $\mathcal{V}_0(R)$ is given as

$$\mathcal{V}_0(R) \xrightarrow{R\to 0} -(s_0^2+4)\frac{\hbar^2}{2mR^2}\,. \tag{2.115}$$

To capture the universal features of the system, it is necessary to determine the solution $f_0(R)$ in the asymptotically free (scale-invariant) region where the energy of the particles is purely kinetic and insensitive to the behavior of the short-distance two-body potentials $V(r_{jk})$. In other words, besides driving the system in the unitary limit ($|a_0| \to \infty$), we also consider the scaling limit of the system with vanishing two-body interaction range ($r_0 \to 0$). However, by doing so, we lose the information of the short-distance boundary condition at $R \to 0$ provided by the two-body potential $V(r_{ij})$. Nevertheless, the problem can be solved even in the scaling limit by choosing a matching point (R_0) in the scale-invariant region $r_0 \ll R_0 \ll |a_0|$ where the Eq. (2.114) is valid, and additionally demanding that the logarithmic derivative $R_0\frac{f'(R_0)}{f(R_0)}$ matches at that point.[9] Furthermore, by choosing $R_0 \ll 1/\kappa$ where $\kappa = (m|E|/\hbar^2)^{1/2}$ is the typical two-particle momentum in the asymptotically free region, the corresponding energy eigenvalue E becomes negligible compared to the channel potential $\mathcal{V}_0(R)$ and thus, be ignored. This reduces Eq. (2.114) for the $n = 0$ channel into the form

$$\frac{\hbar^2}{2m}\left[\frac{\mathrm{d}^2}{\mathrm{d}R^2} + \frac{s_0^2+1/4}{R^2}\right] f_0(R) \approx 0\,. \tag{2.116}$$

The general solution to the above equation has a power-law behavior given by

$$f_0(R) \approx C_1 R^{1/2+is_0} + C_2 R^{1/2-is_0}\,, \quad R \ll |a_0|, 1/\kappa\,. \tag{2.117}$$

where $C_{1,2}$ are constants. By demanding the absence of unphysical deeply bound dimer states, the solution for $f_0(R)$ could be transformed into the form (see Appendix A for details)

$$f_0(R) \approx A\sqrt{R}\sin\left[s_0 \ln(\kappa R) + \theta\right]\,, \tag{2.118}$$

where A is a constant and θ is a dimensionless constant (phase) that can be determined by matching the solution at long-distances $R \sim |a_0|$. This makes θ dependent on the dimensionless combination κa_0, as well as the the signs of E and a_0. The logarithmic derivative of $f_0(R)$ at matching point R_0 is given by,

$$R_0\frac{f_0'(R_0)}{f_0(R_0)} \equiv \frac{R}{f_0(R)}\frac{\mathrm{d}f_0(R)}{\mathrm{d}R}\bigg|_{R=R_0} = \frac{1}{2} + s_0\cot[s_0\ln(\kappa R_0)+\theta]\,. \tag{2.119}$$

[9] One can interpret the matching point R_0 as a short-distance cut-off below which hyperspherical configurations become immaterial for long-distance physics. Their effects are implicitly taken into account *via* boundary conditions at the matching point, such as the specification of the value of the logarithmic derivative.

Further simplification of the above equation yields

$$\Lambda_0 \equiv \kappa e^{\theta/s_0} = \frac{1}{R_0} \exp\left[\frac{1}{s_0}\cot^{-1}\left\{\frac{1}{s_0}\left(R_0\frac{f_0'(R_0)}{f_0(R_0)} - \frac{1}{2}\right)\right\}\right], \tag{2.120}$$

where the parameter Λ_0 has the dimension of wave number. As we shall see in the next subsection, such a three-body parameter leads to a logarithmic scaling violation with the emergence of a *discrete scaling-invariance* of the system signifying the occurrence of the Efimov effect in the unitary limit with $a_0 \to \pm\infty$. Low-energy observables are dependent not only on the scattering length a_0, but also on an additional three-body boundary condition, namely, the specification of the dimensionless quantity $R_0\frac{f_0'(R_0)}{f_0(R_0)}$ at the matching point R_0. In other words, the specification of the dimensionless quantity along with a short-distance scale ($R_0 \ll |a_0|$) translates into the specification of the single long-distance scale Λ_0. The emergence of a new dimensionful scale in the problem amounts to a *dimensional transmutation* due to quantum effects. Since low-energy three-body observables can be affected by the logarithmic scale violation only through their dependence on Λ_0, this parameter is often regarded as a *three-body scale-violation parameter*.

2.2.7 Efimov effect and Three-body bound states

Here we simultaneously consider the three-body system at unitarity, as well as in the scaling limit. In these limits the channel eigenvalue become independent of R, namely, $\lambda_0(0) = -s_0^2$ (where $s_0 = 1.00624$), such that the adiabatic hyperspherical approximation becomes exact. The $n = 0$ hyper-radial channel is found to be the only one with an attractive $1/R^2$ effective potential of the form:

$$V_0^{\text{eff}}(R) = -\frac{s_0^2 + 1/4}{R^2}\,. \tag{2.121}$$

The rest of the channels are repulsive and evidently do not support three-body bound states. The unexpected attraction in the $n = 0$ hyper-radial channel is the basis for the Efimov effect and is referred to as the *Efimov attraction*. The Schrödinger wavefunction, in this case, is given as

$$\Psi(\mathbf{r}_1, \mathbf{r}_2, \mathbf{r}_3) = R^{-5/2} f_0(R) \sum_{i=1}^{3} \frac{\sinh\left[s_0\left(\frac{\pi}{2} - \alpha_i\right)\right]}{\sin(2\alpha_i)}\,, \tag{2.122}$$

where the hyper-radial wavefunction $f_0(R)$ satisfies Eq. (2.93) exactly in the bound state domain with $E = -B_3 = -\hbar^2\kappa_T^2/m < 0$:

$$\left[\frac{\mathrm{d}^2}{\mathrm{d}R^2} + \frac{s_0^2 + 1/4}{R^2}\right] f_0(R) = 2\kappa_T^2 f_0(R)\,. \tag{2.123}$$

It is, however, notable that the Efimov attraction now leads to pathology that the zero-range theory for the identical three-boson system is not well-defined. Indeed, it is seen that the above equation is scale-invariant since the $1/R^2$ potential scales just like the kinetic energy operator $\mathrm{d}^2/\mathrm{d}R^2$ under a scale transformation $R \to \lambda R$, with λ as an arbitrary scaling factor. It is known that such an equation in the scaling limit can admit a solution at any value of the energy ($E \to \lambda^2 E$), and therefore its spectrum is unbounded from below. This implies that under Efimov attraction, the three-body system undergoes a collapse onto itself, a phenomenon referred to as *Thomas collapse* [16]. Of course, such a phenomenon is unphysical and can be considered as a shortcoming of the zero-range theory. This is an essential reflection of the fact that finite-range effects of interactions become important for three-boson configurations $R \lesssim r_0$ that can not be simply ignored. Either by specifying the cut-off R_0 in the scale-invariant region along with the logarithmic derivative $R_0 \frac{f_0'(R_0)}{f_0(R_0)}$, or equivalently, by introducing the intrinsic three-body parameter Λ_0, the pathology of the zero-range idealization is essentially cured. Although, all realistic interactions have non-zero range, but nevertheless they have an *universal window* of very large scattering length and very small energy where the zero-range theory is applicable and can be used to determine the three-body parameter.

Returning back to the Eq. (2.123), its solutions for the bound state hyper-radial eigenfunctions for the region $\kappa R \ll 1$ are obtained as:

$$f_0(R) \sim \sqrt{\frac{\pi R}{s_0 \sinh(\pi s_0)}} \sin\left[s_0 \ln(\kappa_T R) + \theta_0\right] ,$$

with

$$\theta_0 = -\frac{1}{2} s_0 \ln 2 - \frac{1}{2} \arg \frac{\Gamma(1 + i s_0)}{\Gamma(1 - i s_0)} . \tag{2.124}$$

The wavefunctions are seen to exhibit log-periodic oscillations in the hyper-radius with the phase of these oscillations proportional to $s_0 \ln(\kappa_T R)$. This is a typical emergent feature in the three-body system that is responsible for the logarithmic scaling violation of the wavefunction under arbitrary continuous scale transformation $R \to \lambda R$, but at the same time it is easy to check that the wavefunction is still invariant under the discrete set of scale transformations $R \to \left(e^{\pi/s_0}\right)^n R$, where $n \in \mathbb{Z}_+$. Such a feature is exactly revealed in the resulting bound energy spectrum. To see this, we now use the above solution for $f_0(R)$ in Eq. (2.120) to obtain

$$s_0 \ln(\Lambda_0 R_0) = \cot^{-1}\left[\cot[s_0 \ln(\kappa_T R_0) + \theta_0]\right] . \tag{2.125}$$

Solving for the binding wave number $\kappa = \kappa^{(n)}$, yields the discrete spectrum:

$$\begin{aligned} \kappa_T^{(n)} &= \left(e^{-\pi/s_0}\right)^{n-n_*} e^{-\theta_0/s_0} \Lambda_0 \\ &\equiv \left(e^{-\pi/s_0}\right)^{n-n_*} \kappa_* , \end{aligned} \tag{2.126}$$

where $n = n_*$ is some arbitrary integer labeling a reference level state associated with binding wave number $\kappa_T^{(n_*)} \equiv \kappa_*$.[10] The resulting spectrum for the binding energy defining the r^{th} Efimov excited trimer state with respect to the reference level (i.e., with $r = n - n_* = 1, 2, 3, ..., \infty$) is then given by [9–11]

$$B_3^{(r)} = \left(e^{-2\pi/s_0}\right)^r \frac{\hbar^2\kappa_*^2}{m}\,. \tag{2.127}$$

The Efimov effect [9–11] refers to a three-body phenomenon that describes the occurrence of infinitely many arbitrarily shallow three-body bound states with an accumulation point at the three-particle scattering threshold in the unitary limit. The energy spectrum, e.g., as displayed in Fig. 1 of Chapter 1, consists of a sequence of level states spaced geometrically with the ratios of successive binding energies approaching a universal number as the unitary limit is approached, such that

$$\lim_{a_0\to\pm\infty} \frac{B_3^{(n)}}{B_3^{(n+1)}} = e^{2\pi/s_0} = 515.03\,. \tag{2.128}$$

As earlier mentioned, the above behavior is a direct consequence of the discrete scale invariance of the system. Considering simultaneously the unitary and scaling limits of the three-boson system, the integer n_* can be taken arbitrarily large leading to the aforementioned collapse of the Efimov spectrum [16]. In reality, however, such an unphysical situation gets naturally bypassed by the finite range ($r_0 \neq 0$) of interactions that sets the energy scale of the deepest (ground state) trimer level. In that case, the reference state is identified with the ground state $n = n_* = 0$ associated with binding energy:

$$B_3^{(0)} = \frac{\hbar^2\kappa_T^{(0)\,2}}{2m} \sim \frac{\hbar^2}{mr_0^2}\,. \tag{2.129}$$

Consequently, in a realistic scenario with large but finite scattering length a_0 and a non-zero two-body interaction range r_0 (however, still $a_0 \gg r_0$), one can expect the Efimov spectrum to be bounded within the two limits:

$$-\frac{\hbar^2}{ma_0^2} \gtrsim E \gtrsim -\frac{\hbar^2}{mr_0^2}\,, \tag{2.130}$$

with the asymptotic number of such Efimov states are given by

$$N \sim \frac{s_0}{\pi} \ln \frac{|a_0|}{r_0}\,. \tag{2.131}$$

[10] Here we end up having the two *a priori* unknown quantities κ_* and Λ_0, either of which may be considered as the three-body parameter. They are, however, not independent and are related by

$$s_0 \ln(\kappa_*) = s_0 \ln(\Lambda_0) - \alpha_0\,, \quad \text{mod } \pi.$$

Specifying any one of them, either *via* phenomenological analysis or directly from experimental observation, tantamount to imposing the required three-body boundary condition for the complete specification of the three-body problem.

There will be corresponding corrections to the binding energy arising from power-law scaling violations. The leading corrections are proportional to $\kappa_T^{(n)} r_0$ which vanish as $n \to \infty$, on approaching the zero-energy threshold. Off the resonant limit, the ratio of the successive trimer level energies do not exactly scale as a universal number, whereby the expression for the Efimov level energy can be expressed as

$$B_3^{(n)} \longrightarrow \left(e^{-2\pi/s_0}\right)^n \frac{\hbar^2\kappa_*^2}{m} \quad \text{for } a_0 \to \pm\infty \text{ and } n \to \infty\,. \tag{2.132}$$

In particular in the presence of the particle-dimer scattering threshold at $E = -B_2 = -\frac{\hbar^2}{ma_0^2}$, a generic formula for the Efimov spectrum was derived in Ref. [12] which given the exact binding energy for any arbitrary Efimov bound state with binding energy $E = -B_3 < 0$ of the three-boson system:

$$B_3^{(n)} = \frac{\hbar^2}{ma_0^2} + \left[e^{-2\pi n} f(\xi)\right]^{1/s_0} \frac{\hbar^2\kappa_*^2}{m}\,, \quad \text{with} \quad \tan\xi = -\sqrt{\frac{mB_3}{\hbar^2}}a_0\,, \tag{2.133}$$

where $f(\xi)$ is an universal function of periodicity 2π. On approaching the resonant limit $f(\xi \to -\pi/2) \to 1$ (see Ref. [12] for details on this universal function). Thus, a non-trivial asymptotic discrete scaling symmetry is apparent to the three-boson system in which the three-body parameter κ_* is kept fixed while the scattering length and other kinematic variables are scaled by arbitrary positive integer powers $n \in \mathbb{Z}_+$ of the discrete scaling factor $e^{\pi/s_0} \approx 22.7$:

$$\kappa_* \to \kappa_*\,, \quad a_0 \to \left(e^{\pi/s_0}\right)^n a_0 \quad E \to \left(e^{\pi/s_0}\right)^{-2n} E\,. \tag{2.134}$$

In the next chapter of this thesis, we shall investigate the consequences of the universality of two- and three-body systems investigated in the framework of low-energy EFT. Such a methodology not only allows us to exploit the inherent universal features of few-body systems in a model-independent manner, but higher-order effects can also be systematically evaluated, including possible effects of electromagnetic and weak interactions, with a controlled estimate of the errors. This is practically unfeasible in a quantum mechanical model framework.

Chapter 3

Universality in Two- and Three-body Systems: A Low-energy EFT Perspective

3.1 Introduction

Effective Field Theory (EFT) is the most general and systematic approach to study physical systems at low-energies using available effective degrees of freedom expressed as *elementary* quantum fields. They are powerful analytical tools for model-independent quantitative study for the investigation of the universality of few-body systems. In this respect, the denomination "elementary fields" encompasses not only the standard fundamental fields in the Standard Model of particle physics but also *composite* or *clusters* fields that effectively behave as the elementary degrees of freedom relevant to the low-energy (often non-relativistic) domain of applicability of the EFT. Such fields constitute the effective degrees of freedom of the theory and appear as explicit fields in the effective Lagrangian. The validity of such a Lagrangian is defined by an appropriate *hard-scale* (M_{hi}), namely, a UV cutoff scale that sets the lowest upper bound that invalidates the effective degrees of freedom as being regarded elementary. Higher energy (or more elementary) constituents fields and their dynamics are therefore considered decoupled or "integrated out" from the picture. Of course, the information of all such UV physics is not lost, but is implicitly encoded within local couplings or contact interactions, so-called the *Low-Energy Constants* (LECs) of the EFT. Although the LECs are *a priori* undetermined in the EFT itself, they are fixed from phenomenological analysis (including Lattice QCD predictions) or from experimental observation. Thus, an EFT in essence describes a low-energy (approximate) version of a more fundamental theory in a low-energy domain having a *distinct separation of scales*. By exploiting this separation of scales low-energy observables for a given system are generally calculated. One important feature of an EFT is that it is universal, namely, once the LECs are determined from certain low-energy

processes, they could be used to make predictions for other processes at a similar range of energies. Thus, the efficacy of an EFT lies in its model-independent (universal) predictive power that surpasses potential model approaches, which are often designed to work for specific systems only, but may completely fail in their predictability in other systems.

The most general low-energy EFT Lagrangian $\mathscr{L}_{\rm EFT}$ represents an infinite string of local operators $\mathscr{O}_i\left(\{\psi\}\right)$ with increasing mass dimensions of diminishing importance, for instance, having the form:

$$\mathscr{L}_{\rm EFT}(x,\partial_x) = \sum_{n=0}^{\infty} \frac{c_n(\mu_{ren})}{M_{hi}^n} \mathscr{O}_n\left(\{\psi(x,\partial_x)\}\right) \ . \tag{3.1}$$

The local operators are constructed using all possible combinations of the fields $\{\psi\}$ (representing the degrees of freedom) evaluated at the same space-time point x but with an arbitrary number of derivatives ∂_x. The form of such operators is constrained by various low-energy global symmetries such as translational, rotational, isospin and chiral symmetry, invariance under parity, charge conjugation, time-reversal, and cluster decomposition. Especially, in the case of non-relativistic nuclear EFTs relevant to this thesis, Galilean invariance becomes more important, instead of Lorentz invariance. The c_ns denote the LECs which are defined at an arbitrary renormalization scale μ_{ren} and implicitly capture the UV physics beyond the hard scale M_{hi}. Since the EFT Lagrangian is in general constituted of operators with dimensionality $D > 4$, the theory becomes inherently non-perturbative. The infinite string of operator terms in the EFT Lagrangian at the first glance seems to question the predictability of the theory as they make the theory inherently *non-renormalizable*. However, there exists a well-defined *power-counting scheme* which re-organizes such terms by some pre-determined degree of importance, ensuring the predictability of the theory through a controlled perturbative expansion. In this way, the theory becomes effectively renormalizable in which one could simply deal with only a small number of terms relevant at the desired level of accuracy. Unlike a renormalizable QFT with a perturbative expansion in terms of a dimensionless coupling, an EFT expansion scheme organizes the Feynman scattering amplitudes (i.e., T-matrix) for a given process in a generic Taylor expansion in powers of the typical small momentum $Q \ll M_{hi}$, namely,

$$T(Q) = \sum_{\nu=0}^{\infty} T^{(\nu)}(Q) \sim \sum_{\nu=0}^{\infty} \left(\frac{Q}{M_{hi}}\right)^{\nu} F^{(\nu)}\left(c_i, Q, \mu_{ren}, M_{hi}\right) \ , \tag{3.2}$$

where $F^{(\nu)}$s denote some functions that arise from the dynamics of the fields $\{\psi\}$ which depend not only on the combination of involved particle masses and interaction couplings, but also on various dynamical scales specific of given systems. In particular, *dimensional transmutation via* quantum loop corrections can generate new short-distance scales like μ_{ren},[1]. Since renormalization amounts to a reshuffling between contributions from the LECs and the UV part

[1] In a cut-off regularization scheme the scale μ_{ren} is identified with the momentum regulator UV cut-off $\Lambda_{\rm reg}$, which must be chosen at the least larger than the hard breakdown scale.

of the loop integration, the uncertainty principle mandates such short-distance contributions to be included as an integral part of the LECs. Moreover, the perturbative expansion also helps to provide a controlled error estimate once the series expansion is truncated at a given order $\nu = \nu_{\max}$:

$$T(Q) \sim \sum_{\nu=0}^{\nu_{\max}} T^{(\nu)}(Q) = T_{\max}(Q, \mu_{ren}) + \mathcal{O}\left(\frac{Q^{\nu_{\max}+1}}{M_{hi}^{\nu_{\max}+1}}\right) . \tag{3.3}$$

Renormalization fixes the scale ($\mu_{ren} \gtrsim M_{hi}$) dependence of the LECs such that the truncated T-matrix $T_{\max}$ satisfies the renormalization group (RG) invariance:

$$\lim_{\mu_{ren}\to\infty} \frac{\mu_{ren}}{[T_{\max}(Q, \mu_{ren})]^2} \left[\frac{\mathrm{d}T_{\max}(Q, \mu_{ren})}{\mathrm{d}\mu_{ren}}\right] \approx 0 . \tag{3.4}$$

On removal of the high energy components of the order of the hard scale M_{hi} through renormalization, the dominant momentum contributions in the loop integral are of $\mathcal{O}(Q)$.

Finally, we summarize the basic utility of the low-energy EFT as follows:

- They allow a better understanding of complicated problems involving a hierarchy of different length/energy scales. When isolating the relevant degrees of freedom, new symmetries become manifest that otherwise would have remained obscured.
- They allow simple estimates using only a few relevant degrees of freedom obtainable from a perturbative power-counting, predominantly based on a *Naive Dimensional Analysis* (NDA).
- They allow computing very low-energy scattering amplitudes without having to understand the full short-distance detailed physics. Basically, the motivation behind the formulation of an EFT is based on one of two scenarios: (1) "UV completion" or the bottom-up approach, namely, that the fully known underlying high-energy dynamics is either not known or solvable at low-energies, and (2) "IR completion" or the top-down approach, namely, that even if the full underlying theory is known or solvable, it is more efficient and simpler to work with an effective low-energy theory with lesser degrees of freedom upon integrating out the heavy modes from the Lagrangian.
- They allow the extension of QCD in understanding the dynamics of nuclei which pose unexpected challenges due to the presence of shallow bound states and resonances with exotic clustering effects. Nuclear EFTs, such as Halo/Cluster EFTs [31, 32, 51],[2] are

[2]In nuclear physics, there exists a special class of exotic atomic nucleus, termed as *halo-nucleus*. They are identified by their nuclear "halo structure", *viz.* a typically tightly bound compact core consisting of a single or cluster of nuclei surrounded by a "halo" of few loosely bound *valance particles* (e.g., nucleons, mesons, and hyperons), orbiting with a radius substantially larger than that (core-halo) interaction range. Halo nuclei are formed at the extreme edges of the nuclide chart - the neutron and proton drip lines — and have short half-lives. The distinct separation of long and short-distance scales inherent to these halo-systems entails a universality description in a low-energy EFT framework. For a recent review on Halo/Cluster EFT see Ref. [32].

designed to effectively tackle such non-perturbative effects by incorporating modified power-counting schemes for addressing their multi-scale nature involving *fine-tuning* between long- and shorts-distance physics systems, where either certain *leading order* (LO) interactions are needed to be iterated to all orders, or exactly solve some dynamical equations.

- Unlike potential model approaches, the EFT framework does not suffer from ambiguities of on-shell and off-shell interactions. Equipped with a well-defined power-counting scheme, one can avoid such ambiguities through the explicit inclusion of higher-order effects from higher-dimensional operators in a controlled systematic manner.

- They allow an *a priori* estimate of the theoretical uncertainty which arises from working at a given order in the perturbative expansion (with the only exception of a near-threshold bound or resonance state where there is a significant departure from NDA).

In this chapter, we review the basic tenets of low-energy EFT needed to understand the non-perturbative dynamics of two- and three-body nuclear systems, and the role of universality in the manifestation of their bound states. We shall especially demonstrate the general working principles of EFT through the simplest setting comprising of a three-body system of interacting identical bosons in the S-wave. In particular, we consider a zero-range toy model (i.e., range of the inter-particle interaction $r_0 \to 0$) which favors a LO EFT analysis. Not to mention that by including internal degrees of freedom like spin and isospin, or by introducing different types of nuclei (termed as *heteronuclear systems*) add a certain degree of complications in the mathematical description of the EFT, they however do not grossly affect the inherent universal features, provided that the net quantum numbers and mass ratios of the particles do not change appreciably. Nevertheless, multi-component systems exhibit a richer Efimov spectrum than systems of identical particles. With additional parameters introduced in the theory for such systems, Efimov universality can get strongly restricted (cf. discussion in Chapter 1). The influence of heteronuclear components in specific S-wave three-body systems, such as in exotic mesonic nuclei (e.g., the D^0nn system) and hypernuclei (e.g., Ξ^-nn, $\Lambda\Lambda t$ and $\Lambda\Lambda h$ systems) with two identical fermions, shall be the topic of investigation in the following chapters of the thesis. Hence, in this chapter we only adhere to a simplistic toy-model EFT description, which eventually motivates the construction of a more practicable nuclear EFT, namely, the *pionless EFT* ($\not\pi$EFT) [2–7].

Pionless EFT is a standard EFT framework employed in understanding the dynamics of very low-energy nuclear systems which are insensitive to the details of mechanisms associated with the exchange of pions. This fact makes it possible to describe such systems with the explicit pion fields integrated out from the dynamics of the system. This is because the typical dynamical momentum scale Q inherent to the system is very small in comparison to the pion mass m_π, identified as the *breakdown* scale of the theory, i.e., $Q \ll M_{hi} \simeq m_\pi$. This, in essence, implies that pions other than being explicitly included in the $\not\pi$EFT Lagrangian as on-shell external degrees of freedom, off-shell generation of pions in quantum loops is potentially

excluded. Consequently, pion number remains conserved in all the interaction vertices of the theory, while the corresponding LECs parameterize the UV effects of the unresolved pion-loops. Figure 3.1 illustrates the pion being integrated out from the non-local Yukawa interaction $V_{NN\pi}$ between two nucleons mediated *via* an off-shell pion. If $\pm\mathbf{k}$ ($\pm\mathbf{k}'$) denote the incoming (outgoing) CM frame momenta of the scattered nucleons, and $\mathbf{q} = \mathbf{k} - \mathbf{k}'$ is the momentum transfer, then the corresponding *one-pion-exchange* propagator admits a generic low-energy expansion for $\mathbf{q}^2 \ll m_\pi^2$:

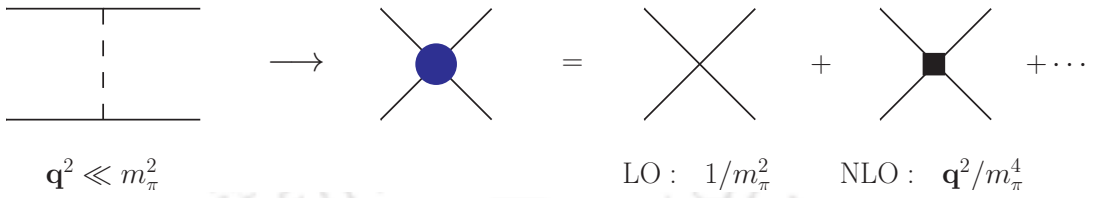

FIGURE 3.1: The Yukawa NN interaction mediated by the non-local one-pion-exchange at low-energies gets reduced to an infinite sequence of contact interactions with increasing order in effective-range expansion, whose sum is represented by the tree-order effective (local) vertex (circular blob).

$$\langle \mathbf{k}'|V_{NN\pi}|\mathbf{k}\rangle \sim \frac{1}{\mathbf{q}^2+m_\pi^2} = \frac{1}{m_\pi^2} - \frac{\mathbf{q}^2}{m_\pi^4} + \cdots = \frac{1}{m_\pi^2}\left[1 + \mathcal{O}\left(\frac{\mathbf{q}^2}{m_\pi^2}\right)\right] . \tag{3.5}$$

The resulting infinite string of (local) contact interactions terms of diminishing relevance lends credence to the construction of the $\not\pi$EFT with a power-counting that is formally equivalent to the well-known Bethe's *Effective-Range Expansion* (ERE) [42–44].[3] This is evidently seen by Fourier transforming the above series into configuration space, thereby obtaining an infinite series of delta-functions with a growing number of derivatives representing range corrections. Constructing an EFT by including only the (dominant) LO non-derivative contact interactions therefore constitutes a *zero-range approximation* with an inherent *continuous scaling symmetry*. However, the versatility of $\not\pi$EFT lies not merely in reproducing the "tree-level" predictions of *Effective-Range Theory* (ERT) [42–44] to arbitrary precision, but also in capturing important off-shell few-body effects through quantum loop corrections, often arising beyond the range of the inter-particle forces. Especially, non-perturbative effects of fine-tuned two-body threshold bound states or *dimers* are systematically incorporated by including irrelevant operators (in the RG sense) with large anomalous dimensions. Equipped with a modified power-counting for two-body contact interactions, so-called the *Q-counting scheme* [2–7], the occurrence of two-body universality mandates an expansion around a *non-trivial UV fixed point* (in contrast to ordinary perturbative NDA based counting scheme requiring an ERE around a *trivial fixed point*) [8]. In Sec. 3.2 we present the basic EFT formalism is associated with an S-wave two-body system, where in particular we obtain the LO renormalized T-matrix in the presence of a shallow dimer. The dimer pole allows tuning of the two-body contact coupling to reproduce low-energy observables to arbitrary precision thereof. However, by going to the three-body sector, we show that the EFT predictability in estimating low-energy

[3] Only for elastic scattering without relativistic corrections $\mathcal{O}(\frac{\mathbf{q}^2}{m_\pi^2})$ the ERT and pionless EFT are equivalent.

three-body observables crucially relies on fixing a dynamical three-body parameter using a single *genuine three-body datum* (besides the knowledge of the two-body scattering length). As elucidated in Sec. 3.3, S-wave universality in the three-body sector mandates the inclusion of a regulator scale ($\Lambda_{\rm reg}$) dependent LO *three-body force* (3BF) needed to renormalize non-analytic UV enhancements in the Faddeev-like integral equations, which manifest whenever the three-body system exhibits an *UV limit cycle*. In that case, the LO 3BF exhibits a characteristic *log-periodic* function of $\Lambda_{\rm reg}$ with cyclic singularities denoting successive formation of Efimov bound states. Since the introduction of a UV-finite momentum cut-off in the integral equation is in effect equivalent to a non-zero 3-body interaction range $\sim 1/\Lambda_{\rm reg}$, the continuous scaling-invariance gets manifestly broken by logarithmic scaling-violations into a residual *discrete scaling-symmetry*. Thus, in all ${}^{\not\pi}$EFT can indeed serve as a precision computational tool to investigate the qualitative effects of low-energy universality. The foundations of this EFT framework have been extensively discussed over two decades in a large repository of works in the literature (see e.g., [1–6, 8, 12, 52–57] and more references therein). For our ensuing discussion on the two- and three-body system of strongly interacting bosons, we closely follow the treatments as presented in the review works of Refs. [12, 58, 59]. The major EFT works carried out in this thesis, as presented in Chapters 4, 5, and 6, predominantly rely on the general techniques discussed in the following two sections.

3.2 Two-body Sector

At low-energies the scattering cross sections are generally dominated by S-wave scattering. For a binary system of identical bosons, the low-energy two-body dynamics stem from the most general non-relativistic effective Lagrangian constituting all possible local two-body S-wave interactions having the generic form [1–5]:

$$\mathscr{L}_2^{({}^{\not\pi}\mathrm{EFT})} = B^\dagger\left[i\partial_t + \frac{\nabla^2}{2m}\right]B - \frac{C_0}{4}\left(B^\dagger B\right)^2 - \frac{C_2}{4}\left[(BB)^\dagger\, B\left(\overleftarrow{\nabla} - \overrightarrow{\nabla}\right)^2 B + \mathrm{h.c.}\right] + \cdots . \quad (3.6)$$

Here, m is the mass of boson represented by the B-field, $C_{0,2,\cdots}$ are the two-body LECs which parametrize the short-distance physics and the ellipses denote higher-order derivative operator terms not needed for our discussion. The couplings are fixed from the empirical knowledge of the two-body parameters, such as those occurring in the ERE formula for the S-wave scattering phase-shift δ_0, namely [42–44],

$$k\cot\delta_0(k) = -\frac{1}{a_0} + \frac{r_0}{2}k^2 + \mathcal{O}\left(\frac{k^4}{M_{hi}^2}\right), \quad (3.7)$$

where $k = |\mathbf{k}| = \sqrt{m\mathscr{E}}$ is the CM momentum of the $B-B$ binary system having total CM kinetic energy $\mathscr{E}$. The parameters a_0 and r_0 are S-wave scattering length and effective range of the system, respectively, and $M_{hi} \sim m_\pi$ is the ${}^{\not\pi}$EFT hard-scale. The above expansion is

analytic in the external kinetic energy of the bosons with a radius of convergence bounded by the nearest t-channel singularity, e.g., the *pion-cut* in nucleon-nucleon (NN) scattering. For non-relativistic elastic scattering let us recall the form the S-matrix in the S-wave after dropping the overall factor of $(2\pi)^3\delta^3(\mathbf{k}-\mathbf{k}')$ for conservation of linear momentum:

$$S^{l=0}(k) = e^{i2\delta_0(k)} = 1 + \frac{4ik}{k\cot\delta_0(k) - ik} = 1 + i\frac{k\mu}{\pi}T(k;\mathscr{E})\,, \tag{3.8}$$

where $\mu = m/2$ reduced mass of the two-boson system and the corresponding on-shell T-matrix is[4]

$$T(k;\mathscr{E}) = \frac{4\pi}{\mu}\frac{1}{k\cot\delta_0(k) - ik}\,, \tag{3.9}$$

Consequently, for small momenta, the T-matrix admits a *naive* perturbative expansion in powers of k given that the S-wave two-body parameters are all of the natural size $r_0, a_0 \sim 1/m_\pi$, *viz.*

$$T(k;\mathscr{E}) = -\frac{4\pi a_0}{\mu}\left[1 - ia_0k + (a_0r_0/2 - a_0^2)k^2 + \mathcal{O}\left(\frac{k^3}{M_{hi}^3}\right)\right]\,. \tag{3.10}$$

As briefly discussed in the last section, such an NDA-based expansion is likely to fail in the vicinity of a threshold bound (real or virtual) states say, $k \sim \pm i\gamma_0$ for $\mathscr{E} < 0$ when certain two-body parameters, such as the scattering length $a_0 \sim 1/\gamma_0$, do not retain their natural size, being unconstrained by the underlying nature of the short-distance interactions. In that case, the corresponding ERE is known to get modified into the form [45]:

$$k\cot\delta_0(k) = -\gamma_0 + \frac{\rho_0}{2}(k^2+\gamma_0^2) + w(k^2+\gamma_0^2)^2 + \cdots\,, \tag{3.11}$$

where the parameters $\rho, w, \cdots$ are needed to be phenomenologically fixed to reproduce scattering/bound state data.

Hence, in order to construct the appropriate EFT, the power-counting must reflect the additional emergent scales, such as the binding momenta γ_0 of the $B-B$ bound system, and the associated *unnatural scaling* of the scattering length a_0, which typically becomes much larger than the interaction length scale r_0. To this end, we discuss two distinct scenarios: one in which the S-wave scattering length is of natural size, i.e., $|a_0| \sim 1/M_{hi}$ governed by trivial fixed-points of the two-body couplings, and the other in which a_0 scales unnaturally, i.e., $|a_0| \gg 1/M_{hi}$, governed by a non-trivial RG fixed point in the space of couplings. The latter one is the more interesting scenario having classic realistic examples in nuclear physics, such as in the NN scattering process, in which the S-wave strong interaction scattering lengths in both ${}^1S_0$ and ${}^3S_1$ channels become significantly larger than the corresponding effective-range, e.g.,

$$a_0^{(np)}({}^1S_0) = -23.714\text{ fm}\,, \qquad r_0^{(np)}({}^1S_0) = 2.73\text{ fm}\,.$$

[4]Note that for distinguishable two-particle systems, the T-matrix has a factor of 2π rather than 4π.

3.2.1 Natural scaling scenario

If $Q \sim k \ll M_{hi} \sim m_\pi$ is a generic small momentum scale, then, in this case, $|a_0| \sim r_0 \sim 1/M_{hi}$. In other words, all the underlying dynamics are based on the single momentum scale $M_{hi} \sim m_\pi$, identified as the breakdown scale of the EFT. In this case, the radius of convergence of the ERE is also at least as large as the breakdown scale dominated by the nearest t-channel singularity (pion-cut). The corresponding power-counting scheme in this case is based on the standard NDA-based perturbative momentum expansion utilizing *Dimensional Regularization*. Figure 3.2 depicts the generic Feynman amplitude for the S-wave $B-B$ scattering process to any arbitrary order ν in the CM frame. The first diagram in the figure represents the generic sum of all the Feynman vertex amplitudes truncated up to a fixed order in derivative interactions, say, $C_{2\nu_{\rm max}}\nabla^{2\nu_{\rm max}} \sim \mathcal{O}\left[(k/M_{hi})^{2\nu_{\rm max}}\right]$:

FIGURE 3.2: The bubble chain sequence of Feynman diagrams representing contributions to the S-wave $B-B$ scattering process in the CM frame of the loop diagram arising from the local operator. The solid lines denote B-field propagators and the dark blobs denote the sum of tree-order local interaction vertices to any arbitrary order.

$$iT^{(\rm tree)}_{\rm max}(k;\mathscr{E}) = -iC_0 - iC_2k^2 - \cdots - iC_{2\nu_{\rm max}}k^{2\nu_{\rm max}} = -i\sum_{\nu=0}^{\nu_{\rm max}} C_{2\nu}k^{2\nu}\,. \tag{3.12}$$

Then the truncation errors are of $\mathcal{O}\left[(k/M_{hi})^{2\nu_{\rm max}+1}\right]$. Apart from tree-level diagrams, we encounter loop diagrams, all of which have the generic form:

$$\begin{aligned}\mathcal{J}_\nu(\mathscr{E}) &= \frac{i}{2}(\mu_{ren}/2)^{4-D}\int\frac{{\rm d}^Dq}{(2\pi)^D}\frac{\mathbf{q}^{2\nu}}{\left[q_0-\frac{\mathbf{q}^2}{2m}+i\eta\right]\left[\mathscr{E}-q_0-\frac{\mathbf{q}^2}{2m}+i\eta\right]}\\ &= -\mu(2\mu\mathscr{E})^\nu(-2\mu\mathscr{E}-i\eta)^{(D-3)/2}\,\Gamma\left(\frac{3-D}{2}\right)\frac{(\mu_{ren}/2)^{4-D}}{(4\pi)^{(D-1)/2}}\\ &= (2\mu\mathscr{E})^\nu\left(\frac{\mu}{4\pi}\right)\sqrt{-2\mu\mathscr{E}-i\eta} = -i\left(\frac{\mu}{4\pi}\right)k^{2\nu+1}\,.\end{aligned} \tag{3.13}$$

Since the above loop contributions for any order ν are UV finite, the $D\to 4$ limit can be straightforwardly taken due to the absence of poles at $D=4$. Consequently, the couplings $C_{2\nu}$, in this case, are independent of the renormalization scale μ_{ren}. Nevertheless, since the scheme (in principle) amounts to subtracting the $1/(D-4)$ pole from a possible UV divergent loop before taking the $D\to 4$ limit, akin to what is done in standard QFT, the power counting is often termed as the *Minimal Subtraction* (MS) scheme. In particular, the essential feature in this scheme is that powers of loop momenta q get converted into powers of external momenta k. Moreover, the tree-level vertex amplitude $T^{(\rm tree)}_{\rm max}$ [cf. Eq. (3.10)] (truncated up to the fixed

order $2\nu_{\rm max}$ in the derivative interactions) along with the loop integral $\mathcal{I}_0$, when iterated to all orders leads to the infinite sequence bubble diagrams, Fig. 3.2, also contributing at the same order $\mathcal{O}\left[(k/M_{hi})^{2\nu_{\rm max}}\right]$:

$$T_{\rm max}(k;\mathcal{C}) = -\frac{\sum_{\nu=0}^{\nu_{\rm max}} C_{2\nu} k^{2\nu}}{1+i(\mu k/4\pi)\sum_{\nu=0}^{\nu_{\rm max}} C_{2\nu} k^{2\nu}}\,. \tag{3.14}$$

For instance, restricting only to the LO $\not\pi$EFT with the non-derivative interaction proportional to C_0, we find $T^{(0)} = -C_0$, which arises solely from the tree-order vertex graph, and $T^{(1)} = iC_0^2\mu k/(4\pi)$ which arise from the one-loop graph with two tree-order vertices. Matching to the corresponding LO ERT result obtained in Eq. (3.10), it follows that $C_0 = 4\pi a_0/\mu$. A similar expression is obtained using a momentum cut-off regularization [59]. In essence, such perturbative power-counting leads to universal results up to arbitrary sub-leading orders, irrespective of the regularization scheme used. To this end, we summarize the general MS power-counting scheme applicable up to arbitrary sub-leading orders, provided $k|a_0| \ll 1$ is satisfied:

- Each non-relativistic boson propagator, namely,

$$iS_B(k) = \frac{i}{k_0 - \frac{\mathbf{k}^2}{2m} + i\eta}\,, \tag{3.15}$$

  scales as $\sim m/Q^2 \sim \mathcal{O}(Q^{-2})$;

- Each loop integral measure scales as $\sim \mathcal{O}(Q^5)$;[5]

- Each interaction vertex of order ν scales as $C_{2\nu}\nabla^{2\nu} \sim \mathcal{O}(Q^{2\nu})$, since the general scaling of the two-body LECs $C_{2\nu}$ can be shown to be of $\mathcal{O}(1)$ [2–6]:

$$C_{2\nu} \sim \frac{4\pi}{\mu M_{hi}^{2\nu+1}} \sim \mathcal{O}(Q^0) \quad \forall\ \nu \in \mathbb{Z}_+\,, \tag{3.16}$$

  with $\mu = m/2$ being the reduced mass of the two-boson $(B-B)$ system.

- Each two-body Feynman graph contributing at the fixed order $\mathcal{O}(Q^\nu)$, with $L \leq \nu$ loops and $\mathcal{V}_{2r}$ interaction vertices with $2r$ derivatives, scale as [59]

$$T^{(\nu)} \sim \mathcal{O}(Q^\nu)\,; \quad \nu = 3L + 2 + \sum_{r=0}(2r-2)\mathcal{V}_{2r} \geq 0\,. \tag{3.17}$$

[5] This is easily seen as follows:

$$\int \mathrm{d}^4 q \sim \int \mathrm{d}q_0 \int d^3\mathbf{q} \sim \frac{Q^2}{2\mu}\cdot Q^3 = \frac{Q^5}{2\mu}\,,$$

3.2.2 Unnatural scaling scenario: Fine-tuning

Again, if $Q \sim k \ll M_{hi} \sim m_\pi$ is a generic small momentum scale, in the current scaling scenario the scattering length becomes unnaturally large compared to its effective-range $|a_0| \gg r_0 \sim 1/M_{hi}$, which supports shallow bound (real or virtual) states with binding energy $\mathscr{E} = -B_2 < 0$ and momenta $\gamma_0 = \sqrt{2\mu B_2} \sim 1/|a_0|$. Such an EFT scenario in which the existence of emergent dynamical scales vitiate the natural perturbative scaling in terms of the inverse powers of the hard scale is termed *fine-tuning*. Fine-tuned two-body systems are ubiquitous in nuclear physics, say, for an S-wave binary system of neutrons with large scattering length, $a_{nn} = -18.63$ fm $\gg r_{nn} \sim 1/m_\pi \sim 0.5$ fm, which yields the virtual bound *di-neutron* system. Here, the T-matrix expansion, Eq. 3.10, has little practical use since it rapidly breaks down in the vicinity of the bound state poles in the complex Riemann sheet $k \to i\gamma_0 \sim i/|a_0|$, far below $|k| \to M_{hi}$. The breakdown of the expansion parameter is an unpleasant situation for the EFT potentially precluding a proper estimation of the theoretical error. This inherent problem is attributed due to the *anomalous* enhancement of the coupling $C_{2\nu} \sim 4\pi a_0^{\nu+1}/(\mu M_{hi}^\nu)$ in the current scenario, in comparison to the MS scaling, Eq. (3.16).

To effectively tackle this conundrum a new power counting is introduced that incorporates a perturbative expansion of the T-matrix up to a fixed order in $k/M_{hi} \ll 1$, along with non-perturbative resummation of $a_0 k \gtrsim 1$ up to all orders (to contrast the perturbative expansion carried out in Eq. (3.10) for $|a_0|k \ll 1$). In this way one obtains the on-shell T-matrix as

$$T(k;\mathscr{E}) = -\frac{4\pi}{\mu}\frac{1}{(1/a_0 + ik)}\left[1 + \frac{r_0/2}{(1/a_0+ik)}k^2 + \frac{(r_0/2)^2}{(1/a_0+ik)^2}k^4 + \cdots\right]. \tag{3.18}$$

Evidently, the T-matrix now scales as $T^{(\nu)} \sim \mathcal{O}(Q^\nu)$, where unlike the previous scenario the perturbative momentum expansion begins at $\nu = -1$ instead of $\nu = 0$. The first two terms of amplitude expansion become[6]

$$T^{(-1)}(k;\mathscr{E}) = -\frac{4\pi}{\mu}\frac{1}{(1/a_0+ik)} \qquad \text{and} \qquad T^{(0)}(k;\mathscr{E}) = -\frac{4\pi}{\mu}\frac{r_0 k^2/2}{(1/a_0+ik)^2}\,. \tag{3.19}$$

Since any single Feynman graph in a valid EFT should scale as a positive power of the small momentum Q, the fact that $T^{(-1)} \sim \mathcal{O}(Q^{-1})$ suggests that $T^{(-1)}$ could only arise out of resumming an infinite number of graphs. Moreover, the presence of shallow bound state poles limits the range of the perturbative description, thereby demanding a non-perturbative scheme to generate poles in the T-matrix. In this context, Weinberg [60] had pointed out that using the MS scheme one can reproduce $T^{(-1)}$ *via* "bubble resumming" the LO contact interaction C_0 to all orders [cf. Fig. 3.2)], namely,

$$T^{(-1)}(k;\mathscr{E}) = C_0 + C_0\mathcal{I}_0(\mathscr{E})C_0 + C_0\mathcal{I}_0(\mathscr{E})C_0\mathcal{I}_0(\mathscr{E})C_0 + \cdots = \frac{-C_0}{1 + \left(\frac{C_0\mu}{4\pi}\right)ik}\,. \tag{3.20}$$

[6]It must be noted that for distinguishable particles the expressions for the T-matrix should have a factor of 2π instead of 4π.

where $\mathcal{J}_0(\mathscr{E})$ is the two-body bubble integral given by Eq. (3.13) for $\nu = 0$. Now, comparing Eqs. (3.19) and (3.20), we obtain $C_0 = 4\pi a_0/\mu$. The scaling of $T_2^{(-1)} \sim \mathcal{O}(Q^{-1})$ suggests that the individual graphs in the bubble sum must also scale as $\mathcal{O}(Q^{-1})$. Then, the resulting power-counting implies that the tree-level LO vertex graph must count as $C_0 \sim \mathcal{O}(Q^{-1})$, while each additional loop $\mathcal{J}_0$ with a C_0 vertex counts as $C_0\mathcal{J}_0 \sim \mathcal{O}(1)$. This is all quite transparent justifying the bubble resummation. Nonetheless, according to the naive MS scaling of the individual graphs, namely, $C_0[C_0\mu Q]^L \sim (4\pi a_0/\mu)(a_0 Q)^L$, with L being the number of loops, each term in bubble sum is bigger than the preceding one for $|a_0 Q| \gtrsim 1$. This leads to the conclusion that the sequence of graphs is manifestly divergent, in spite of knowing the fact that they sum up to something small.

One way of resolving this apparent dichotomy is to employ dimensional regularization equipped with a novel subtraction scheme, termed as *Power Divergence Subtraction* (PDS) [1–5]. Here, not only does one subtract the $1/(D-4)$ pole corresponding to the logarithmic divergence, but also the $1/(D-3)$ pole corresponding to a power-law sub-divergence at $D = 4$. Since $\mathcal{J}_\nu$ in Eq. (3.13) has a pole at $D = 3$, it may be removed by adding the following counterterm:

$$\delta\mathcal{J}_\nu(\mathscr{E};\mu_{ren}) = -(2\mu\mathscr{E})^\nu \frac{\mu}{4\pi}\frac{\mu_{ren}}{(D-3)}\,. \tag{3.21}$$

Thus, the PDS scheme modified loop integral in $D = 4$ becomes

$$\mathcal{J}_\nu^{PDS}(\mathscr{E};\mu_{ren}) = \mathcal{J}_\nu(\mathscr{E}) + \delta\mathcal{J}_\nu(\mathscr{E};\mu_{ren}) = -(2\mu\mathscr{E})^\nu \frac{\mu}{4\pi}(\mu_{ren} + ik)\,, \tag{3.22}$$

leading to the fixed order ($\nu_{\max}$) result for the renormalized T-matrix:

$$T_{\max}(k;\mathscr{E}) = -\frac{4\pi}{\mu}\left[\frac{4\pi}{\mu\sum_{\nu=0}^{\nu_{\max}} C_{2\nu}k^{2\nu}} + \mu_{ren} + ik\right]^{-1}. \tag{3.23}$$

In particular, restricting to a LO $\not\pi$EFT analysis where C_0 is the only relevant LEC, the bubble sum in the PDS scheme is given by

$$T^{(-1)}(k;\mathscr{E}) = -\frac{4\pi}{\mu}\frac{1}{\left[\frac{4\pi}{\mu C_0} + \mu_{ren} + ik\right]}\,. \tag{3.24}$$

Matching to the corresponding LO ERT result obtained in Eq. (3.19), and also using the fact that at LO we can write $k\cot\delta_0 = -1/a_0 = -\gamma_0 + \mathcal{O}\left(k^2/M_{hi}^2\right)$, we obtain[7]

$$\frac{4\pi}{\mu C_0} = \gamma_0 - \mu_{ren} \qquad \Longrightarrow \qquad C_0(\mu_{ren}) = \frac{4\pi}{\mu}\left[\frac{1}{1/a_0 - \mu_{ren}}\right]. \tag{3.27}$$

[7]Similar results are obtained in a cut-off regularization scheme by introducing a sharp momentum cut-off $\Lambda_{\rm reg}$ in the UV limit of the loop integrals. The corresponding expression for the LO T-matrix is obtained with the essential replacement $\mu_{ren} \mapsto 2\Lambda_{\rm reg}/\pi$ [59]:

$$T^{(\rm LO)}(k;\mathscr{E}) = -C_0\left[1 + \frac{\mu C_0}{2\pi^2}\left(\Lambda_{\rm reg} - \frac{\pi}{2}\sqrt{-2\mu\mathscr{E} - i\eta}\right)\right]^{-1}. \tag{3.25}$$

This contrasts the previous MS counting scheme where C_0 is independent of the subtraction scale μ_{ren}. The explicit incorporation of the subtraction scale in the T-matrix sets the scale of C_0, instead of having its scale set by $\gamma_0 \sim 1/|a_0|$, provides immediate benefits. By either choosing $\mu_{ren} = 0$ or $\mu_{ren} \sim M_{hi} \gg \gamma_0$ we can essentially recover the MS scaling $C_0 \sim 4\pi/\mu M_{hi}$. However, a more useful regulator-independent power-counting scheme, so-called the Q-counting scheme [2–6], emerges for the choice of the subtraction scale taken to be the same order as the external low-momentum scale, viz. $\mu_{ren} \sim |k| \sim \gamma_0 \sim 1/|a_0| \sim Q \ll M_{hi} \sim 1/r_0$. This is distinguished from the natural scenario where either the hard scale or the interaction range $r_0 \sim 1/m_\pi$ solely accounts for all relevant dynamics, such that $k \sim Q \sim 1/|a_0| \sim M_{hi} \sim 1/r_0$. The new scheme now explicitly keeps track of the linear divergences and allows fine-tuning between the LEC C_0 and the UV contributions from the loops to produce shallow dimers.

In general for $\mu_{ren} \sim \gamma_0 \sim |k| \sim Q$ and $a_0|k| \gg 1$, by Taylor expanding the above T-matrix, Eq. (3.24), and comparing with the ERE result, Eq. (3.18), one can derive the scaling of all the higher dimensional couplings C_{2n} [2–6]:

$$C_{2\nu}(\mu_{ren}) \sim \frac{4\pi}{\mu M_{hi}^{\nu}\,(\mu_{ren})^{\nu+1}} \sim \mathcal{O}(1/Q^{\nu+1}) \quad \forall\ \nu \in \mathbb{Z}_+\,, \tag{3.28}$$

with $\mu = m/2$ being the reduced mass of the binary system. We can now enumerate the general Q-counting rules applicable for the fine-tuned system with a large scattering length:

- Each non-relativistic boson propagator scales as $\mathcal{O}(Q^{-2})$;
- Each loop integral measure scales as $\sim \mathcal{O}(Q^5)$;
- Each interaction vertex of order ν scales as $C_{2\nu}\nabla^{2\nu} \sim \mathcal{O}(Q^{\nu-1})$;
- Each two-body Feynman graph contributing at the fixed order $\mathcal{O}(Q^\nu)$, with L loops and $\mathcal{V}_{2r}$ interaction vertices with $2r$ derivatives, scales as [59]

$$T^{(\nu)} \sim \mathcal{O}(Q^\nu)\ ; \quad \nu = 3L + 2 + \sum_{r=0}(r-3)\mathcal{V}_{2r} \geq -1\,. \tag{3.29}$$

Thus, for example at low-energies in proximity to the S-wave dimer $-\mathscr{E} = B_2 \sim 1/(2\mu a_0^2)$, restricting to the LO analysis in Q-counting (i.e., for $\nu = -1$), an infinite number of loops with only C_0 interactions are needed to be (non-perturbatively) resummed. Such an infinite sequence of bubble diagrams, all contributing at the same order in the Q-counting (cf.

The renormalization of $T^{(\mathrm{LO})}$ can be implemented by matching to the two-body S-wave scattering length using the relation leading to the regulator-dependent result for the LO coupling C_0, namely,

$$C_0(\Lambda_{\mathrm{reg}}) = \frac{4\pi a_0}{\mu}\left(1 - \frac{2a_0\Lambda_{\mathrm{reg}}}{\pi}\right)^{-1}. \tag{3.26}$$

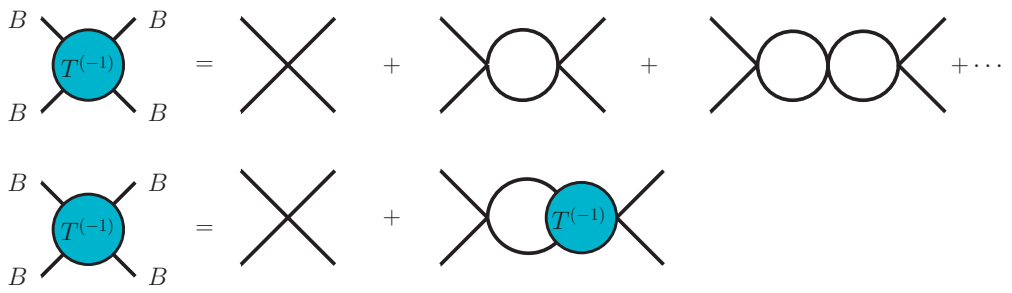

FIGURE 3.3: The leading order (LO) two-body S-wave T-matrix $\hat{T}^{(-1)}$, obtained by resumming the bubble graphs containing only the C_0 contact interaction. It is compactly represented as a Lippmann-Schwinger integral equation, $\hat{T}^{(-1)} = \hat{V} + \hat{V}\hat{G}_0\hat{T}^{(-1)}$, where $\hat{V}$ denotes two-body contact interaction operator associated with the coupling C_0, and $\hat{G}_0$ is the two-particle free Green's function.

Fig. 3.3), yields a shallow dimer. However, at the next-to-leading-order (NLO) in the power counting (i.e., for $\nu = 0$) the C_2 interactions vertices contribute to the dynamics. Being $1/M_{hi}$ suppressed compared to the leading C_0 interactions, the C_2 constitutes a perturbative correction. Such a bubble resummation with only the C_0 interaction leads to a *Lippmann-Schwinger series* for the on-shell two-body S-wave scattering amplitude $T^{(-1)}$ expressed explicitly as the integral equation:

$$T^{(-1)}(k;\mathscr{E}) = -C_0 - \frac{1}{2}C_0^2 \int \frac{\mathrm{d}^4 q}{(2\pi)^4 i} \frac{i}{q_0 - \mathbf{q}^2/2m + i\eta} \frac{i}{\mathscr{E} - q_0 - \mathbf{q}^2/2m + i\eta} T^{(-1)}(k;\mathscr{E}), \quad (3.30)$$

where q_0, $\mathbf{q}$ are temporal and spatial parts of loop four-momentum q. After renormalization, it yields the LO physical scattering amplitude, say, for the bound state domain with CM energy $\mathscr{E} < 0$ and momentum $k = i\sqrt{-2\mu\mathscr{E} - i\eta}$:

$$T^{(-1)}(k;\mathscr{E}) = \frac{4\pi}{\mu} \frac{1}{-1/a_0 + \sqrt{-2\mu\mathscr{E} - i\eta}}\,. \quad (3.31)$$

where the physical S-wave $B - B$ scattering length is given at the on-shell point:

$$a_0 = -\frac{\mu}{4\pi} \lim_{k\to 0} T^{(-1)}(\mathscr{E} = k^2/2\mu)\,, \quad (3.32)$$

where we again note the factor of 4π in the above definition relevant to the system of indistinguishable particles, instead of the standard factor of 2π for distinguishable particles.

3.2.3 RG analysis of two-body couplings

The β-functions for the two-body LEC C_{2n} are easily determined by demanding the renormalization scale ($\mu_{ren} \equiv \lambda$) independence of the on-shell T-matrix, namely,

$$\lambda \frac{\mathrm{d}}{\mathrm{d}\lambda}\left[\frac{1}{T(k;\mathscr{E})}\right] = 0\,, \quad \text{where} \quad T(k;\mathscr{E}) = -\frac{\sum C_{2\nu}(\lambda)\, k^{2\nu}}{1 + i(\mu k/4\pi)\sum C_{2\nu}(\lambda)\, k^{2\nu}}\,, \quad (3.33)$$

which for $\nu \geqslant 0$ the above relations yield the β-functions [4]:

$$\beta_{2\nu} \equiv \lambda \left[\frac{\mathrm{d}C_{2\nu}(\lambda)}{\mathrm{d}\lambda}\right] = \frac{\mu}{4\pi}\lambda \sum_{\alpha=0}^{\nu} C_{2\alpha}(\lambda)\, C_{2(\nu-\alpha)}(\lambda)\,, \tag{3.34}$$

where $\mu = m/2$ being the reduced mass of the $B-B$ system. In particular, the LO one-loop diagram (cf. Fig. 3.3) yields the β-function for the coupling C_0:

$$\beta_0 = \frac{\mu}{4\pi}\lambda C_0^2\,, \tag{3.35}$$

which leads to the RG flow equation

$$\frac{\mathrm{d}}{\mathrm{d}\lambda}C_0(\lambda) = \frac{\mu}{4\pi}C_0^2(\lambda)\,. \tag{3.36}$$

By integrating the above equation between two different renormalization scales λ and λ_0, we obtain the equation for evolution of the coupling $C_0(\lambda)$, namely,

$$C_0(\lambda) = \frac{C_0(\lambda_0)}{1 + C_0(\lambda_0)\mu(\lambda_0 - \lambda)/4\pi}\,. \tag{3.37}$$

By utilizing the boundary condition at $\lambda = 0$ provided by comparing Eqs. (3.19) and (3.20), namely, $C_0(0) = 4\pi a_0/\mu$, we once again arrive at the same universal result, Eq. (3.27), as in the last subsection,[8]

$$C_0(\lambda) = \frac{4\pi}{\mu}\left[\frac{1}{1/a_0 - \lambda}\right].$$

It is interesting to consider the so-called *unitary* or *resonant limit* of the $B-B$ system where the S-wave two-body scattering length diverges ($a_0 \to \pm\infty$) and the corresponding partial cross-section saturates the unitary bound $\sigma^{l=0} \leq 8\pi/k^2$. In such a limit there is a dimer state formed exactly at the threshold with zero binding energy, i.e., $B_2 \sim 1/(2\mu a_0^2) \to 0$. Then, it is clear that in this limit

$$\lambda\frac{\mathrm{d}}{\mathrm{d}\lambda}\left[\lambda C_0(\lambda)\right] = 0 \tag{3.39}$$

Thus, for the LO contact interactions in the $B-B$ system to generate a threshold bound state, $C_0(\lambda)$ must be located in the vicinity of a non-trivial UV fixed point in the RG space of all two-body couplings. Notably, the existence of such a non-trivial fixed point is independent of the regularization scheme, and can be realized as follows: Since C_0 is a dimensionful coupling with mass dimension -2, one must first define a dimensionless counterpart of C_0, namely,

$$g_2(\lambda) = \frac{\mu}{4\pi}\lambda C_0(\lambda) = \frac{\lambda a_0}{1 - \lambda a_0}\,, \tag{3.40}$$

[8] In fact, the general solution to the coupled RG equation, Eq. (3.34) can be obtained as [4]:

$$C_{2\nu}(\mu_{ren}) = \frac{4\pi}{\mu(-\mu_{ren} + 1/a_0)}\left(\frac{r_0/2}{-\mu_{ren} + 1/a_0}\right)^{\nu} + \mathcal{O}\left(\frac{1}{(\mu_{ren})^n}\right). \tag{3.38}$$

As the momentum scale, λ is varied with various positive and negative fixed values of a_0, the above equation maps out RG trajectories illustrated in Fig. 3.4. For every given trajectory there exists two fixed points $g_2 = 0$ and $g_2 = -1$, which correspond to the zeros of the β-function

$$\beta_2 = \lambda \left[\frac{\mathrm{d}}{\mathrm{d}\lambda} g_2(\lambda) \right] = g_2(\lambda) \left[1 + g_2(\lambda) \right] . \tag{3.41}$$

At the fixed points the $B-B$ system exhibits *conformal invariance*. A trivial fixed point that

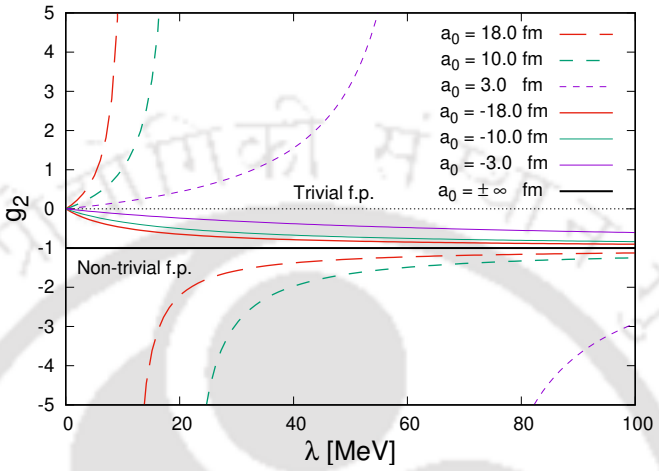

FIGURE 3.4: Renormalization group trajectory for the dimensionless coupling g_2 as a function of the momentum scale λ for several fixed positive and negative values of the S-wave $B-B$ scattering length a_0. Evidently, RG flow indicates the existence of two fixed points (f.p.): first, a trivial infrared fixed point $g_2 = 0$ as $\lambda \to 0$ (dotted horizontal line), and second, a non-trivial ultraviolet fixed point $g_2 = -1$ as $\lambda \to \infty$ (solid horizontal line). Since the latter fixed point corresponds to $a_0 \to \pm\infty$ it represents the unitary limit of two-body interactions. For $a_0 > 0$ the poles in the RG trajectory correspond to the formation of two-body bound states.

is obtained at $g_2 = 0$ in the infrared limit $\lambda \to 0$, is not particularly interesting since the system becomes non-dynamical (free system) with vanishing two-body interactions. However, the non-trivial fixed point that is obtained at $g_2 = -1$ in the ultraviolet limit $\lambda \to \infty$ is generally of interest being identified as the unitary limit of two-body interactions as $a_0 \to \pm\infty$. In particular, for $a_0 > 0$ we find that the RG trajectories develop poles at $\lambda_0 = \gamma_0 \sim 1/a_0$, corresponding to the formation of (real bound) $B-B$ dimer states. The deeply-bound poles progressively turn into shallow-bound poles with increasing scattering length a_0 ultimately leading to a threshold bound state with binding momenta $\gamma_0 \to 0$ for $a_0 \to \infty$. Whereas for $a_0 < 0$ no such poles manifest with smooth RG trajectories extending between the two-fixed points.

3.2.4 Auxiliary field formalism

In the context of studying three-body dynamics with two-body (real or virtual) bound subsystems having large scattering lengths, it is convenient to introduce auxiliary *dimer* fields or

dimerons (d) representing "bosonized" dimers. Ideally, the bare auxiliary fields do not propagate and even have a "wrong sign" in the kinetic terms (see following two-body Lagrangian). Hence, the content of the original theory remains unchanged by the addition of such *ghost* fields "by hand". For the case of a spinless bosonic system an equivalent two-body Lagrangian [alternative to Eq. 3.6] in terms of the dimeron fields has been constructed [52–54]:

$$\mathscr{L}_2^{(\mathrm{BHvK})} = B^\dagger\left[i\partial_t + \frac{\nabla^2}{2m}\right]B - d^\dagger\left[i\partial_t + \frac{\nabla^2}{4m} - \Delta_d\right]d - y_0\left(d^\dagger B^2 + B^{\dagger 2}d\right) + \cdots . \quad (3.42)$$

The dimeron fields are essentially employed to cancel the quadratic terms such as $(B^\dagger B)^2$ in Eq. (3.6), so that all interactions between the B-fields are now mediated *via* the dimer exchange process, with y_0 as the dBB interaction coupling. The quantity Δ_d is a free parameter related to the binding energy of the dimeron such that the bare or tree-level dimeron propagator is the simple non-dynamical term i/Δ_d. Quantum loop corrections, however, allow the dimerons to propagate. It turn out that, by virtue of *reparametrization invariance* of the theory, the above Lagrangian is equivalent to the original two-body Lagrangian presented in Eq. (3.6). One can easily demonstrate this equivalence (up to terms suppressed by inverse powers of the heavy boson mass m) that using a Hubbard-Stratonovich transformation, leading to the connection between the LO two-body couplings of the respective Lagrangians: $C_0 \mapsto 4y_0^2/\Delta_d$.

In the context of Halo/Cluster EFT, where the dimeron formalism has been extensively used, the earlier discussed scaling under the non-perturbative Q-counting scheme has been modified as [31, 32, 51]:

$$y_0^2 \sim \frac{C_0^2}{2\mu C_2} \sim \frac{2\pi M_{hi}}{\mu^2} \sim \mathcal{O}(1) \qquad \text{and} \qquad \Delta_d \sim \frac{C_0}{2\mu C_2} \sim \frac{M_{hi}\,\mu_{ren}}{2\mu} \sim \mathcal{O}(Q)\,, \quad (3.43)$$

where $\mu = m/2$ is the reduced mass of the $B-B$ system and $\mu_{ren} \sim \gamma_0 \sim \mathcal{O}(Q)$ is the generic dynamical low-momentum scale of the order of the binding momenta γ_0 of the dimeron. Consequently, using field re-definitions in trading away the time derivatives in favor of space derivatives, the kinetic term of the d-field becomes sub-leading compared to the term proportional to Δ_d. In that case, the Q-counting leads to an infinite sequence of Feynman graphs, as illustrated in Fig. 3.5, each contributing at the same order as the static dimeron propagator $i\Delta_d^{-1} \sim \mathcal{O}(Q^{-1})$. Consequently, they must all be resummed to the leading order to yield the dynamical "dressed" unrenormalized dimeron propagator: [9]

$$i\Delta^{(0)}(q_0,\mathbf{q}) = \frac{i\pi}{y_0^2\mu}\left[\frac{\pi\Delta_d}{y_0^2\mu} + \mu_{ren} - \sqrt{-2\mu q_0 + \mathbf{q}^2/4 - i\eta}\right]^{-1} . \quad (3.45)$$

[9] The corresponding bare propagator in the sharp momentum cut-off regularization scheme is given by [59]

$$i\Delta^{(0)}(q_0,\mathbf{q}) = \frac{i\pi}{y_0^2\mu}\left[\frac{\pi\Delta_d}{y_0^2\mu} + \frac{2}{\pi}\Lambda_{\mathrm{reg}} - \sqrt{-2\mu q_0 + \mathbf{q}^2/4 - i\eta}\right]^{-1} . \quad (3.44)$$

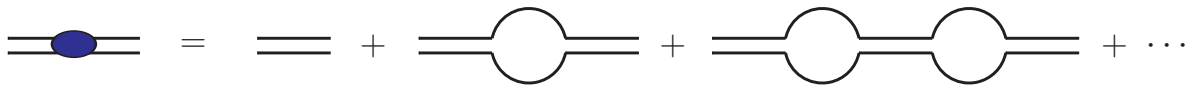

FIGURE 3.5: The renormalized dressed d-field propagator in which the solid lines denote the B-fields.

We note its similarity to the resummed two-body T-matrix at LO $T^{(-1)}$, Eq. (3.24), with the center-of-mass kinetic energy $\mathscr{E} \to q_0 - \mathbf{q}^2/(4m)$, where $q_0(\mathbf{q})$ is kinetic energy (momentum) of the dimeron . Upon renormalization using Eq. (3.27) and the leading order relation among the two-body parameters, namely, $C_0 \mapsto 4y_0^2/\Delta_d$, the renormalized dressed dimeron propagator becomes

$$i\Delta(q_0, \mathbf{q}) = \frac{i\pi}{y_0^2 \mu} \left[\frac{1}{a_0} - \sqrt{-2\mu q_0 + \mathbf{q}^2/4 - i\eta} \right]^{-1} . \tag{3.46}$$

If the scattering length $a_0 > 0$, then the renormalized propagator has a pole at $q_0 = -1/(2\mu a_0^2) + \mathbf{q}^2/(4m)$, corresponding to the existence of a real-bound state dimer with the binding energy $B_2 = 1/(2\mu a_0^2)$ and an overall kinetic energy $\mathbf{q}^2/(4m)$ of its CM. In the low-energy threshold limit, i.e., with $\mathbf{p} \to 0$, the renormalized dimeron propagator has a residue (wave function renormalization constant) given by

$$\mathcal{Z}_d = \left[\frac{\mathrm{d}\Delta^{-1}(q_0, \mathbf{0})}{\mathrm{d}q_0} \right]^{-1}_{q_0 = -B_2} = \frac{\pi}{y_0^2 \mu^2 a_0} , \tag{3.47}$$

such that at close proximity to the pole position, the dimeron propagator has the dominant behavior given by

$$\Delta(q_0, \mathbf{q}) \approx \frac{\mathcal{Z}_d}{q_0 + 1/(2\mu a_0^2) - \mathbf{q}^2/4 + i\eta} . \tag{3.48}$$

3.3 Three-body Sector

We now describe the low-energy dynamics of S-wave scattering associated with an interacting system of three indistinguishable bosons ($B - B - B$). Figure. 3.6 is a diagrammatic illustration of the various re-scattering among the two-body subsystems. Excluding the *genuine* 3BF diagrams shown in the second row, the scattering diagrams in the first row constitute only the two-body interaction y_0, and thus described by same leading order EFT Lagrangian, Eq. (3.42). According to the Q-counting scheme, a simple investigation shows that these diagrams contribute at the same order. For example, the tree-level diagram in the first row can be considered as a one-boson (B) exchange process between the incoming and outgoing dimerons (d). Since the tree diagram contains two dBB vertices ($y_0^2 \sim M_{hi}/\mu^2$) and one B propagator ($iS_B \sim \mu/Q^2$), this amounts to a net contribution of order $\sim M_{hi}/(\mu Q^2)$. The adjacent one-loop re-scattering diagram contains two additional dBB vertices, two additional B propagators, a dimeron propagator ($i\Delta \sim \mu/M_{hi}Q$) and a loop integral ($\sim Q^5/\mu$), thereby

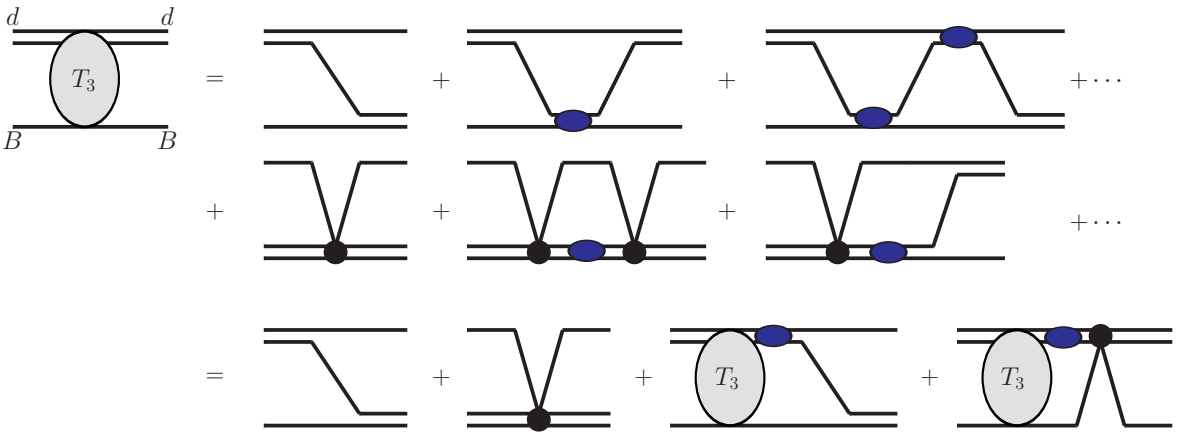

FIGURE 3.6: Three-body integral equation for the spinless three-boson S-wave scattering amplitude T_3. In the Q-counting scheme, all graphs in the first line contribute as $\sim M_{hi}/(\mu Q^2)$, while those in the second line with three-body contact interactions contribute as $\sim 1/(\mu Q^4)$. The single line denotes a (boson) B-field propagator, the double line denotes a static (dimeron) d-field propagator, and the double line with an oval blob represents a fully dressed (dynamical) renormalized dimeron propagator. The dark-filled circle denotes the insertion of a leading-order three-body force or contact interaction.

indicating that the one-loop diagram also scales as $\sim M_{hi}/(\mu Q^2)$, like the tree-graph. In essence, inspection shows that every re-scattering graph in the first row precisely contributes at the same leading order, necessitating a resummation of all such graphs. Besides, one also requires the infinite sequence of 3BF diagrams (second row) which may be shown to contribute at the leading order, and hence needed to be resummed as well. The power-counting for such three-body graphs is described later in this section. However, unlike the resummation in the two-body sector [cf. Eq. (3.30)] which entails a simple summation of a geometric series, the same is impracticable in the three-body sector. As contradistinction, here we must incorporate a non-perturbative resummation of all three-body graphs in the form of a "one-loop" *Fredholm* integral equation (third row of Fig. 3.6) which is solved self-consistently for the T-matrix T_3 using numerical methods. As was noted in Chapter 2, the *Faddeev equations* in the standard sense, comprise a set of coupled *integro-differential* quantum mechanical equations determining the wavefunction of a three-body system in the coordinate-space representation. They are numerically solved using finite range model potential with well-defined kernels (belonging to the *Hilbert-Schmidt class* of operators with finite *Schmidt-norm*). In contrast, our zero-range toy-model of the interacting three-boson system involves integral equations in momentum-space having ill-defined kernels, originating from the non-self-adjoint character of the underlying three-body Hamiltonian [61, 62]. Such a zero-range "Faddeev-like" integral equations in the momentum representation is termed as an *Skornyakov-Ter-Martirosyan* (STM) equations [13, 14]. Despite ambiguities in their solutions, the STM equations have the primary advantage of fitting naturally into an EFT framework based on a diagrammatic (perturbative) or Lagrangian-based approach. This contrasts with the inherently non-perturbative Hamiltonian-based potential-model approach for solving three-body Faddeev equations.

The biggest advantage, however, lies in the manner of introducing 3BF operator terms. This

is achieved quite naturally *via* the STM framework, without the requirement of introducing *ad hoc* three-body potentials which often leads to very cumbersome treatments (e.g., see Ref. [35] for an effective quantum mechanical approach that also includes a genuine three-body wavefunction). The ambiguity due to the non-self-adjointness of the Hamiltonian is solved by cutting off the effective interactions at short distances. This is accomplished in the EFT by introducing, e.g., a sharp momentum UV cutoff $\Lambda_{\rm reg}$ in the integral equations which becomes a free parameter of the theory. This kind of regularization method implicitly necessitates the introduction of cutoff-dependent three-body couplings needed to renormalize the artificial cutoff dependence of the STM equations. To this end, we introduce additional non-derivatively coupled three-body interactions in the effective Lagrangian, for instance,

$$\mathscr{L}_3^{(\not\pi{\rm EFT})} = \frac{D_0(\Lambda_{\rm reg})}{36}(B^\dagger B)^3 + \cdots, \qquad \text{(standard form)}$$

and

$$\mathscr{L}_3^{(\rm BHvK)} = -d_0(\Lambda_{\rm reg})\left(d^\dagger d\right)\left(B^\dagger B\right) + \cdots, \quad \text{(dimerized form)} \tag{3.49}$$

for the respective standard and dimerized forms, with the contact interaction couplings scaling unnaturally at the leading order, namely, $D_0 \sim d_0 \sim 1/(\mu Q^4)$. In this case, the $B-B-B$ system exhibits three-body (Efimov) universality.[10] The values of the 3BF couplings can be fixed using an additional three-body datum (e.g., three-body binding energy) in realistic situations. The ellipses denote derivative 3BF terms which are naturally sub-leading. Figure 3.6 (second row) displays all re-scattering diagrams with insertions of leading-order three-body contact interactions. These graphs are similarly resummed into an integral equation that yields contributions of order $\sim 1/(\mu Q^4)$, and hence, equally important as the set of graphs in the first row with two-body interactions only. Together they constitute all possible non-perturbative contributions to the scattering amplitude at leading order.

3.3.1 Amplitude and integral Equation

Assuming the manifestation of Efimov universality, the natural choice of the reference frame is the boson-dimeron ($B-d$) CM frame, with the relative external momenta being $-\mathbf{k}, \mathbf{k}$ ($-\mathbf{p}, \mathbf{p}$) for the incoming (outgoing) boson and dimeron respectively. With the total three-body CM kinetic energy as E, their energies are taken as E_B, $E-E_B$ (E'_B, $E-E'_B$) for the incoming (outgoing) particles. Using standard Feynman rules which follow from the EFT Lagrangians, Eqs. (3.42) and (3.49), we easily obtain the following Faddeev-like STM integral equation for the unrenormalized scattering amplitude T_3 corresponding to the second line of

[10] For *natural* systems without three-body universality, the scaling of the 3BF couplings are instead governed by NDA scaling, $D_0 \sim d_0 \sim 1/(2\mu M_{hi}^4)$. Thus, the corresponding 3BF terms are considered sub-leading in the EFT Lagrangian.

Fig. 3.6, namely,

$$T_3\left(\mathbf{p},\mathbf{k};E\right) = -\left[\frac{4y_0^2}{E-E_B'-E_B-(\mathbf{p}+\mathbf{k})^2/2m+i\eta}+d_0(\Lambda_{\rm reg})\right] + \frac{i\pi}{\mu y_0^2}\int^{\Lambda_{\rm reg}}\frac{\mathrm{d}^4q}{(2\pi)^4}\left[\frac{4y_0^2}{E-E_B'-q_0-(\mathbf{p}+\mathbf{q})^2/2m+i\eta}+d_0(\Lambda_{\rm reg})\right] \times\frac{1}{q_0-\mathbf{q}^2/2m+i\eta}\,\frac{T_3\left(\mathbf{q},\mathbf{k};E\right)}{1/a_0-\sqrt{-2\mu(E-q_0)+\mathbf{q}^2/4-i\eta}} \tag{3.50}$$

where $q_0(\mathbf{q})$ is the temporal (spatial) part of loop momentum with the three-momentum integral cut-off in the UV region at $|\mathbf{q}|=\Lambda_{\rm reg}$. Using Cauchy's residue theorem, the integral over q_0 can be evaluated by choosing the pole, $q_0=\mathbf{q}^2/2m$, making one of the boson propagators inside the loop integration on-shell. Further simplifications is achieved by choosing either one or both the initial and final states on-shell. For instance, with the full on-shell choice $E_B=\mathbf{k}^2/2m$ and $E_B'=\mathbf{p}^2/2m$, we obtain

$$T_3\left(\mathbf{p},\mathbf{k};E\right) = -4my_0^2\left[\frac{1}{mE-(\mathbf{p}^2+\mathbf{p}\cdot\mathbf{k}+\mathbf{k}^2)+i\eta}+\frac{d_0(\Lambda_{\rm reg})}{4my_0^2}\right] - 8\pi\int^{\Lambda_{\rm reg}}\frac{\mathrm{d}^3\mathbf{q}}{(2\pi)^3}\left[\frac{1}{mE-(\mathbf{p}^2+\mathbf{p}\cdot\mathbf{q}+\mathbf{q}^2)+i\eta}+\frac{d_0(\Lambda_{\rm reg})}{4my_0^2}\right] \times\frac{T_3\left(\mathbf{q},\mathbf{k};E\right)}{-1/a_0+\sqrt{-2\mu E+3\mathbf{q}^2/4-i\eta}}\,. \tag{3.51}$$

Especially in the context of S-wave scattering process, we consider the projection of the unrenormalized amplitude onto the $l=0$ partial wave renormalized amplitude given by

$$T_3\left(p,k;E\right)\equiv\frac{\mathcal{I}_d}{2}\int_{-1}^{1}\mathrm{d}\left(\cos\theta_{\hat{\mathbf{p}}\cdot\hat{\mathbf{q}}}\right)\;T_3\left(\mathbf{p},\mathbf{k};E\right)\,, \tag{3.52}$$

such that boson-dimeron *elastic* scattering amplitude is obtained by evaluating the renormalized scattering amplitude at the on-shell point, $p=|\mathbf{p}|=k=|\mathbf{k}|$ and $E=-B_2+3k^2/(4m)$, with dimer binding energy $B_2=1/(2\mu a_0^2)$. Furthermore, in the threshold limit, one obtains the three-body scattering length as

$$a_3^{(Bd)}=-\frac{m}{3\pi}\lim_{k\to0}\;T_3\left(k,k;\frac{3k^2}{4m}-B_2\right). \tag{3.53}$$

It is conventional to re-define the dimension-full three-body coupling $d_0(\Lambda_{\rm reg})$ in terms of a dimensionless coupling $g_3(\Lambda_{\rm reg})$ such that $T_3(p,k;E)$ has a well-defined asymptotic behavior as $\Lambda_{\rm reg}\to\infty$, namely,

$$d_0(\Lambda_{\rm reg})=-\frac{4my_0^2}{\Lambda_{\rm reg}^2}g_3(\Lambda_{\rm reg})\,. \tag{3.54}$$

This leads to the 3BF renormalized STM integral equation for the three-boson system, originally derived in Ref. [54]:

$$T_3(p,k;E) = \frac{8\pi}{\mu a_0}\left[\frac{1}{2pk}\ln\left(\frac{p^2+k^2+pk-mE-i\eta}{p^2+k^2-pk-mE-i\eta}\right)+\frac{g_3(\Lambda_{\rm reg})}{\Lambda^2}\right] + \frac{4}{\pi}\int_0^{\Lambda_{\rm reg}} dq\; q^2\left[\frac{1}{2pq}\ln\left(\frac{p^2+q^2+pq-mE-i\eta}{p^2+q^2-pq-mE-i\eta}\right)+\frac{g_3(\Lambda_{\rm reg})}{\Lambda^2}\right] \times \frac{T_3(q,k;E)}{-1/a_0+\sqrt{3q^2/4-\mu E-i\eta}}. \tag{3.55}$$

The above equation must be numerically solved to obtain the three-body eigenenergies and scattering lengths in the respective kinematical domains.[11] In this case, the STM equation is one-dimensional in the sense that $B-d$ scattering involves a single-channel elastic process $B+d \to B+d$. In realistic situations with non-zero spin-isospin degrees of freedom, the processes involve coupled elastic and inelastic channels, thereby requiring multi-dimensional representations. For instance, the iso-doublet ($I=1/2$, $J^P=1/2^+$) system ($^{\;\;5}_{\Lambda\Lambda}$H , $^{\;\;5}_{\Lambda\Lambda}$He) and the $\Xi^- nn$ ($I=3/2$, $J^P=1/2^+$) systems dealt in this thesis, will involve three and two coupled-channel scattering processes, respectively, along with additional re-coupling coefficients necessary for projecting the individual diagrams onto the appropriate spin-isospin channels. The details of such analysis are presented in the following two chapters (also see Refs. [63, 64]).

3.3.2 RG analysis of three-body coupling

The RG behavior of the three-body system is deduced quite naturally in EFT framework by studying the cut-off regulator ($\Lambda_{\rm reg}$) dependence of the 3BF *via* the STM integral equation, Eq. (3.55). The introduction of UV regulator $\Lambda_{\rm reg}$ repairs the non-self-adjoint pathology associated with the STM equation making the scattering amplitude T_3 well-behaved asymptotically. But this comes at a cost: the continuous scaling-symmetry gets partially broken in to a residual discrete scaling-symmetry that manifests as a sequence of singularity with quasi-logarithmic periodicity in the running of the 3BF coupling, $g_3 = g_3(\Lambda_{\rm reg})$. Figure. 3.7 clearly demonstrates the occurrence of such cyclic singularities, attributing to the successive formation of Efimov-bound states and thereby suggesting the onset of an emergent RG limit cycle. This feature can be checked analytically by investigating the asymptotic nature of the integral equation in the unitary and scaling limits. In other words, with p taken as the off-shell (outgoing) momentum having the same order of magnitude as the loop momenta q, we examine the integral equations in the limit $E, 1/|a_0|, k \ll p \sim q \sim \Lambda_{\rm reg} \lesssim \infty$, whereby the 3BF terms $\propto g_3(\Lambda_{\rm reg})/\Lambda^2_{\rm reg} \approx 0$ may be dropped, and the integral equations can be well

[11] It must be understood that the three-body bound states are obtained in the negative energy kinematical region, $E < \mathscr{E}_d$, namely below the boson-dimeron breakup threshold $\mathscr{E}_d \sim -B_2$. While the $B-d$ scattering solutions correspond to energies, $\mathscr{E}_d \leq E < 0$, namely the kinematical region in between the boson-dimeron and three-boson breakup thresholds.

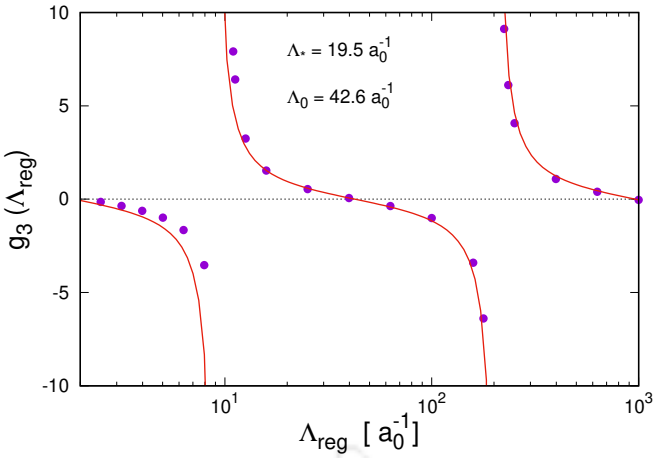

FIGURE 3.7: Demonstration of RG limit cycle.The regulator scale ($\Lambda_{\rm reg}$) dependence of the three-body coupling $g_3 = g_3(\Lambda_{\rm reg})$ for the $B-B-B$ system. The input three-body datum is the S-wave boson-dimeron ($B-d$) scattering length $a_3^{(Bd)} = 1.56a_0$. The parameters, Λ_* and $\Lambda_{\rm reg}^{(0)}$, are obtained by fitting the approximate analytical formula for the running of g_3, Eq. (3.60) (solid curve), to the data points obtained by numerically solving the STM equation (3.55), thereby reproducing the result of Ref. [54]. The singularities correspond to the ground and first excited Efimov states, cf. Fig. (1.1) of Chapter 1.

approximated by considering just the homogeneous parts (i.e., excluding all tree-level contributions). Thus, with no other relevant scales in the theory, the STM equations become *dilation invariant* and an additional *inversion symmetry* under the transformation $q \to 1/q$. To this effect, the asymptotic solution for T_3 scales as a pure power-law with an undetermined exponent, $T_3(p) \sim p^{s-1}$. Thus, the resulting STM equation (3.55) becomes

$$p^{s-1} = \frac{4}{\sqrt{3}\pi p}\int_0^\infty {\rm d}q\; q^{s-1}\ln\left[\frac{p^2+pq+q^2}{p^2-pq+q^2}\right], \tag{3.56}$$

which after a change of variable, $q = xp$, becomes

$$1 = \frac{4}{\sqrt{3}\pi}\int_0^\infty dx\; x^{s-1}\ln\left[\frac{1+x+x^2}{1-x+x^2}\right]. \tag{3.57}$$

A *Mellin transformation* finally reduces the STM equation to the very same transcendental relation, obtained in the previous chapter (cf. Eq. (2.110) of Chapter 2) by solving the low-energy Faddeev equation in the limit of the hyperradial coordinate $R \to 0$, namely,

$$1 - \frac{8}{\sqrt{3}s}\frac{\sin\left(\frac{\pi s}{6}\right)}{\cos\left(\frac{\pi s}{2}\right)} = 0\,. \tag{3.58}$$

Solving the above equation yields a set of complex solutions for the exponent, namely, $s = \pm i s_0$, where $s_0 = 1.00624\cdots$ is obtained in the present case. As discussed at length in Chapter 2, the asymptotic value s_0 parametrizes the exact discrete scaling behavior of the system in the unitary limit with the $B-B$ scattering length $a_0 \to \pm\infty$. This formally indicates the manifestation of Efimov effect [9–11] in the $B-B-B$ system, namely, the emergence of a geometric sequence of arbitrary shallow three-particle level state accumulation to zero-energy

$(E = 0)$ threshold. However, with the $B - B$ subsystems having finite scattering length and non-zero interaction range, i.e., $a_0 \ll r_0$ (i.e., tuned away from the unitary as well as scaling limits), the binding energies $B_3^{(n)}$ $(n \in \mathbb{Z}_+)$ are expected to lie geometrically between the two bounds [9–11]:

$$\frac{1}{ma_0^2} \gtrsim B_3^{(n)} \gtrsim \frac{1}{mr_0^2}\,, \quad \text{with} \quad B_3^{(n)} \overset{n\to\infty}{\longrightarrow} \frac{\kappa_*^2}{m}\left(e^{-2\pi/s_0}\right)^n . \tag{3.59}$$

where the multiplicative factor $\lambda_0 = e^{-\pi/s_0}$ characterizes the inherent discrete scaling behavior of the Efimov spectrum (cf. Fig. (1.1) in Chapter 1). Such a parameter (λ_0) is universal because it only depends on the gross features of the three-body system, such as the mass ratios of the bound particles and the overall quantum statistics of the system, irrespective of the fine details such as the nature of the individual bound particles and the short-distance interaction potentials. In this context, Bedaque *et al.* [54] deduced an approximate analytical expression for the typical log-periodic running of the dimensionless three-body coupling $g_3 = g_3(\Lambda_{\rm reg})$, given by

$$g_3(\Lambda_{\rm reg}) \sim -\aleph\, \frac{\sin\left[s_0 \ln(\Lambda_{\rm reg}/\Lambda_*) - \arctan(1/s_0)\right]}{\sin\left[s_0 \ln(\Lambda_{\rm reg}/\Lambda_*) + \arctan(1/s_0)\right]}\,. \tag{3.60}$$

with $\aleph = 0.879$ being a numerical coefficient introduced to improve the overall fit to the corresponding non-asymptotic result. Such an RG orbit for the coupling g_3 with a periodic dependence on the cut-off parameter when the latter increases to infinity is termed as a limit cycle. The underlying principle ensures that the family of effective theories with finite cut-offs yields predictions that are guaranteed to remain independent of the respective cut-offs. In the above expression, the parameter Λ_* [12] denotes an emergent three-body dynamical parameter that results from the logarithmic scaling-violation $\sim \ln(\Lambda_*|a_0|)$. This parameter is likewise fixed using a three-body datum, such as the trimer binding energy B_3 or the $B - d$ scattering length $a_3^{(Bd)}$. Alternatively, the scale dependence of $g_3(\Lambda_{\rm reg})$ may be determined by numerically solving the STM equation (3.55) at non-asymptotic scales for a given two-body input a_0 and three-body datum (e.g., B_3, $a_3^{(Bd)}$, etc.). In Fig. 3.7, we reproduce the result of Ref. [54], displaying the approximate RG limit cycle with quasi-periodic singularities associated with the successive formation of new Efimov states as $\Lambda_{\rm reg} \to \infty$. The data points correspond to our numerical evaluations, while the solid curve is the fit to these data using the analytical formula of Bedaque *et al.*, Eq. (3.60). To this end one may extract the three-body parameters, such as Λ_* and s_0, using the momentum scaling relations,

$$\Lambda_{\rm reg}^{(n)} = \left(e^{\pi/s_0}\right)^n \Lambda_{\rm reg}^{(0)} \quad \text{as } n \to \infty\,,$$

and

$$\Lambda_{\rm reg}^{(0)} = \exp\left[\frac{\arctan(1/s_0)}{s_0}\right]\Lambda_*\,, \tag{3.61}$$

[12] In Chapter 2, the analogous three-body parameter κ_* was identified as the binding momentum/wave number of the Efimov ground state in the unitary limit, see Eq. (2.126).

where $\Lambda_{\rm reg} = \Lambda_{\rm reg}^{(n)}$ represents the $n^{\rm th}$ zero of the three-body coupling $g_3 = g_3(\Lambda_{\rm reg}^{(n)})$. The typical non-asymptotic values $\tilde{s}_0$ expected in this case depend on $\Lambda_{\rm reg}^{(n)}$, and hence, differ from the cutoff independent asymptotic value, $\tilde{s_0}(\Lambda_{\rm reg}^{(n)}) \to 1.00624\cdots$, which restores the exact scaling-symmetry of the STM equation as $\Lambda_{\rm reg}^{(n)} \to \infty$. For a discussion on the asymptotic convergence of the residual scale dependence on $\tilde{s}_0$, we refer to the discussion in Chapter 5 in the context of the analysis of the $\Xi^- nn$ ($I = 3/2$, $J^P = 1/2^+$) systems (also see Refs. [64]).

Chapter 4

${}^{5}_{\Lambda\Lambda}$H and ${}^{5}_{\Lambda\Lambda}$He hypernuclei examined in halo/cluster EFT

4.1 Introduction

In this chapter, we use low energy pionless halo/cluster EFT to examine the doubly strange ($S = -2$) ${}^{5}_{\Lambda\Lambda}$H and ${}^{5}_{\Lambda\Lambda}$He hypernuclei. This work has been recently published in Physical Review C [64]. The various experimental [65–77] and theoretical [78–90] investigations over several decades on the doubly strange ($S = -2$) s-shell light double-Λ-hypernucler systems, such as, ${}^{3}_{\Lambda\Lambda}$n, ${}^{4}_{\Lambda\Lambda}$n, ${}^{4}_{\Lambda\Lambda}$H, ${}^{4}_{\Lambda\Lambda}$He, ${}^{5}_{\Lambda\Lambda}$H, ${}^{5}_{\Lambda\Lambda}$He and ${}^{6}_{\Lambda\Lambda}$He, have elicited keen interest in the study of exotic hypernuclei in the strangeness nuclear physics community. Such multistrange systems can provide stringent tests for probing the microscopic mechanisms for the flavor SU(3) baryon-baryon interaction in the strangeness $S = -2$ channel. In particular, essential information about the Λ-Λ interaction is expected to be obtained from these studies, which may hold definitive clues to the longstanding quest for the controversial *H-dibaryon*, an exotic six-quark ($J = 0$, $I = 0$) deeply bound state, originally predicted by Jaffe in 1977 using the *bag-model* [78]. Different perspectives regarding the existence of the H particle have been obtained in *ab initio* calculations over the years. For example, the *dispersion relations* based analysis [91] on the ${}^{12}\mathrm{C}(K^-, K^+\Lambda\Lambda X)$ reaction data from the KEK-PS Collaboration [68], yielded an estimate of the ${}^1\mathrm{S}_0$ double-Λ scattering length, namely, $a_{\Lambda\Lambda} = -1.2 \pm 0.6$ fm, that was well at odds with a possible $\Lambda\Lambda$ bound state. While lattice QCD simulations [92–96] with significantly larger pion masses yielded extrapolated results suggesting positive indications of a $\Lambda\Lambda$ bound state, albeit a shallow one in the flavor SU(3) limit. However, apparently by going to the physical point, it tends to get pushed to the double-Λ threshold, eventually dissolving into the continuum once SU(3) breaking effects are considered [97, 98]. In fact, of late the HAL QCD $(2+1)$-flavor coupled-channel lattice simulation [99] closer to the physical point ($m_\pi^{\mathrm{Lat}} \simeq 146$ MeV, $m_K^{\mathrm{Lat}} \simeq 525$ MeV) has yielded a rather small magnitude of the ${}^1\mathrm{S}_0$ double-Λ scattering length, $a_{\Lambda\Lambda} = -0.81 \pm 0.23$ fm, casting a significant doubt on the

very existence of the H-particle. This is consistent with the current theoretically accepted (albeit broad) range, namely, -1.92 fm $\lesssim a_{\Lambda\Lambda} \lesssim -0.5$ fm, set by the fairly recent *thermal correlation model* based investigations [100–102] on *Au + Au Relativistic Heavy-Ion Collisions* (RHIC) data from STAR Collaboration [71], which is unlikely to support any $\Lambda\Lambda$ bound state. It is interesting in this regard that the same RHIC data previously analyzed by the STAR Collaboration themselves [71] estimated a positive scattering length, $a_{\Lambda\Lambda} = 1.10 \pm 0.37$ fm. Nevertheless, the rather recent Λ-Λ femtoscopic analysis of p-p and p-Pb collision data from the ALICE Collaboration [76, 77] yielded a $\Lambda\Lambda$ virtual bound state of energy ≈ 3.2 MeV, thereby favoring a scattering length consistent with the above range. In short, although these analyses are clearly equivocal in their resolution of the H particle conjecture, they evidently concur on a weakly attractive Λ-Λ interaction with no deeply bound state.

With the discovery of ${}^{\;\;6}_{\Lambda\Lambda}$He in the hybrid-emulsion experiment KEK-E373 [65], so-called the "NAGARA" event, along with indications of the conjectured ${}^{\;\;4}_{\Lambda\Lambda}$H bound state in the BNL-AGS E906 production experiment [66], arguments on the existence of double-Λ-hypernuclei have gained a firm foothold fostering a prolific area of modern research. A whole gamut of theoretical investigations on the double-Λ-hypernuclei followed since then. As for the $J = 1/2$ iso-doublet mirror partners, namely, ${}^{\;\;5}_{\Lambda\Lambda}$H and ${}^{\;\;5}_{\Lambda\Lambda}$He, until rather recently most of these investigations have been focusing on establishing phenomenological potential models. In particular, there exists both *ab initio* and *cluster* model approaches involving three- and four-body Faddeev-Yakubovsky calculations and variational methods [80–87]. In some of these model analyses, the binding energy difference between the two isospin partners has been studied using dynamical effects of mixing between different channels, such as ΣN, $\Sigma\Sigma$, and ΞN. Of these, it is believed that the dominant contribution arises from the $\Lambda\Lambda$ - ΞN mixing channel. Because of this channel coupling the value of the hypernuclear binding energy (otherwise, commonly referred to in the literature as the *double-Λ-separation energy*) $B_{\Lambda\Lambda}$ of ${}^{\;\;5}_{\Lambda\Lambda}$He significantly exceeds that of ${}^{\;\;5}_{\Lambda\Lambda}$H. However, such model approaches are often nonsystematic with conflicting conclusions based on *ad hoc* assumptions, whereby little perception can be gained regarding the underlying binding mechanisms inherent to these systems. It is, thus, timely to supplement the multitude of the existing model results with a general model-independent prediction based on universal arguments in few-body systems.

In a recent pioneering effort, the first microscopic *pionless effective field theory* ($\not\pi$EFT) based many-body analysis using *Stochastic Variational Method* (SVM) has been reported on some of the lightest double-Λ-hypernuclei for $A \leq 6$ [90]. This kind of *ab initio* Hamiltonian constructed $\not\pi$EFT technique utilizing only elementary baryonic (NN, $N\Lambda$, $\Lambda\Lambda$ two-body and NNN, $N\Lambda N$, $\Lambda N\Lambda$ three-body) interactions were first applied to calculations of few-nucleon systems for lattice-nuclei [103–105] and later extended to the analysis of s-shell Λ-hypernuclei [106]. Through a *leading order* (LO) assessment of the onset of double-Λ-hypernuclei binding, the work of Ref. [90] quantitatively demonstrates the robust possibility of the iso-doublet partners (${}^{\;\;5}_{\Lambda\Lambda}$H , ${}^{\;\;5}_{\Lambda\Lambda}$He), as the lightest particle stable double-Λ-hypernuclei,

thereby discounting ${}^{3}_{\Lambda\Lambda}\mathrm{n}$, ${}^{4}_{\Lambda\Lambda}\mathrm{n}$ and ${}^{4}_{\Lambda\Lambda}\mathrm{H}$ as possible bound states. Interestingly, as a parallel qualitative assessment to supplement the aforementioned rigorous numerical analysis, we re-examine the $({}^{5}_{\Lambda\Lambda}\mathrm{H}\,,\,{}^{5}_{\Lambda\Lambda}\mathrm{He})$ iso-doublet pair in view of a plausible cluster or *halo* nuclear nature using universal arguments in physics. Particularly, in the context of standard $\not\pi$EFT framework we investigate the correlations between their bound state characteristics and the S-wave $({}^{4}_{\Lambda}\mathrm{H}\text{-}\Lambda\,,\,{}^{4}_{\Lambda}\mathrm{He}\text{-}\Lambda)$ scattering processes, respectively, in the kinematical region below the $({}^{3}\mathrm{H}\,,\,{}^{3}\mathrm{He})+\Lambda+\Lambda$ breakup thresholds. In this way, through a prototypical model-independent study we assess the role of low-energy Λ-Λ interactions in giving rise to universal correlations between three-body observables of such s-shell double-Λ-hypernuclei and their possible formations thereof.

A low-energy EFT constitutes a systematic model-independent approach with low-energy observables expanded in a perturbative expansion in terms of a small parameter, namely, $\epsilon \sim Q/\Lambda_H \ll 1$, where Q is a generic small momentum and Λ_H is the ultraviolet (UV) cutoff scale which limits the applicability of the perturbative scheme. The effective degrees of freedom consistent with the low-energy symmetries of the system are then identified in terms of which the Lagrangian of the system is constructed and expanded in increasing order of derivative interaction. The corresponding coefficients (low-energy constants) are fixed from phenomenological data. The heavy degrees of freedom above the hard scale Λ_H are integrated out and their effects are implicitly encoded in these couplings. In the so-called *halo/cluster* EFT formalism, the ${}^{5}_{\Lambda\Lambda}\mathrm{H}$ and ${}^{5}_{\Lambda\Lambda}\mathrm{He}$ systems can be regarded as the double-Λ *halo*-nuclear states, namely, $\Lambda\Lambda t$ ($t \equiv {}^{3}\mathrm{H}$, i.e., the *triton*) and $\Lambda\Lambda h$ ($h \equiv {}^{3}\mathrm{He}$, i.e., the *helion*), respectively, with $T \equiv t, h$ being the compact core that can be considered elementary at scales chosen well below the breakup of ${}^{4}_{\Lambda}\mathrm{H}$ and ${}^{4}_{\Lambda}\mathrm{He}$.

The erstwhile emulsion works [67, 70, 107] have indicated evidences of particle stable states of ${}^{4}_{\Lambda}\mathrm{H}$ and ${}^{4}_{\Lambda}\mathrm{He}$ Λ-hypernuclei. The existence of these states was recently reconfirmed by high-resolution decay π^- and γ-ray spectroscopic measurements carried out by the A1 Collaboration at MAMI [73, 74] and the E13 Collaboration at J-PARC [72, 75], respectively. The extracted $J^p = 0^+$ ground state Λ-*separation energies* ($\mathscr{B}_\Lambda[0^+]$) of ${}^{4}_{\Lambda}\mathrm{H}$ and ${}^{4}_{\Lambda}\mathrm{He}$ are 2.157 ± 0.077 MeV and 2.39 ± 0.05 MeV, respectively, whereas those corresponding to the $J^p = 1^+$ first excited state ($\mathscr{B}_\Lambda[1^+]$) are 1.067 ± 0.08 MeV and 0.984 ± 0.05 MeV, respectively (cf. level scheme depicted in Fig. 4.1). Thus, the typical momentum scale Q associated with these single Λ-hypernuclei can be naively identified with mean binding momentum of the ground and first excited states, namely, $\bar{Q} \sim \sqrt{\mu_{\Lambda T}\,(\mathscr{B}_\Lambda[0^+] + \mathscr{B}_\Lambda[1^+])} \approx 50$ MeV, with $\mu_{\Lambda T} = M_\Lambda M_T/(M_\Lambda + M_T)$ being the reduced mass of these ΛT subsystems. On the other hand, the experimental binding energies ($\mathscr{B}_T$) of the triton and helion cores being 8.48 MeV and 7.72 MeV, respectively, the *breakdown* scale of our EFT framework may be associated with the corresponding binding momentum scale $\Lambda_H \sim \sqrt{2\mu_{dN}\mathscr{B}_T} \sim m_\pi$ of the cores, with μ_{dN} being the reduced mass of the deuteron (d) and nucleon (N) system, and m_π is the pion mass. Consequently, the expansion parameter is conservatively estimated to be at the most

$\epsilon \sim \bar{Q}/m_\pi \lesssim \sqrt{2\mu_{\Lambda T}\mathscr{B}_\Lambda[0^+]}/m_\pi \approx 0.4$, a value reasonably small to support a valid EFT framework.

A practical computational framework for investigating three-body dynamics is thus provided by the $\not\pi$EFT without explicit inclusion of pion. This has become a popular tool for investigating shallow bound state systems of nucleons and other hadrons (for reviews and relatively recent works, e.g., see Refs. [3, 4, 6, 12, 52–54, 79, 88, 89, 108, 109] and other references therein). Such a framework provides the most general approach to handling the dynamics of finely tuned systems with large scattering lengths and cross-sections, nearly saturating the unitary bound. This happens presumably in the vicinity of nontrivial RG fixed points of the two-body contact couplings. Recently, a large number of works on $\not\pi$EFT have appeared dealing with low-energy universal physics of three-body systems. A typical signature of the onset of such universality is the appearance of a RG limit cycle resulting from the breakdown of an exact to a discrete scaling symmetry, accompanied by the emergence of a geometric tower of arbitrary shallow three-body Efimov bound states [9, 12]. In the context of hypernuclear physics, the Efimov effect and its universal role in the prediction of three-body exotic bound states have been discussed in a number of theoretical works [79, 88, 89, 108, 110] based on $\not\pi$EFT at LO. In the ensuing analysis, we use a similar set-up to investigate whether any remnant universal feature inherent to the $\Lambda\Lambda T$ system indicates Efimov-like bound state character. However, the current paucity of phenomenological information to constrain the various low-energy parameters of the theory is a major hurdle in our approach which precludes a robust prediction of the existence of Efimov-like bound states in the ${}^{\;\;5}_{\Lambda\Lambda}$H and ${}^{\;\;5}_{\Lambda\Lambda}$He systems. As demonstrated in our analysis, a crucial piece of information required as input to the EFT analysis is a three-body datum, namely, the three-body binding or double-Λ-separation energy $B_{\Lambda\Lambda}$ of a given mirror partner, for which there are currently no available experimental estimates. For this purpose, we rely on suitable predictions based on existing potential models, e.g., the *ab initio* SVM analysis of Nemura *et al.* [86]. Moreover, the predictability of our halo/cluster EFT framework depends on fixing several two-body parameters from the following phenomenological information:

- the measured ground and first-excited state Λ-separation energies $\mathscr{B}_\Lambda[J^P = 0^+, 1^+]$ of the mirror Λ-hypernuclei (${}^{\;\;4}_{\Lambda}$H , ${}^{\;\;4}_{\Lambda}$He), which we take from Refs. [67, 72–75] (cf. Fig. 4.1); and
- second, the value of the S-wave double-Λ scattering length $a_{\Lambda\Lambda}$, for which we consider an acceptable range of values from various phenomenological analyses [90, 91, 99–102, 111–113], constrained by the recent RHIC data [71].

Based on these inputs, the three-body integral equations completely determine the $B_{\Lambda\Lambda}$ - $a_{\Lambda\Lambda}$ correlations for the $\Lambda\Lambda T$ systems, using which preliminary estimates of the corresponding S-wave three-body scattering lengths $a_{\Lambda\Lambda T}$ are predicted. Such EFT-predicted scattering

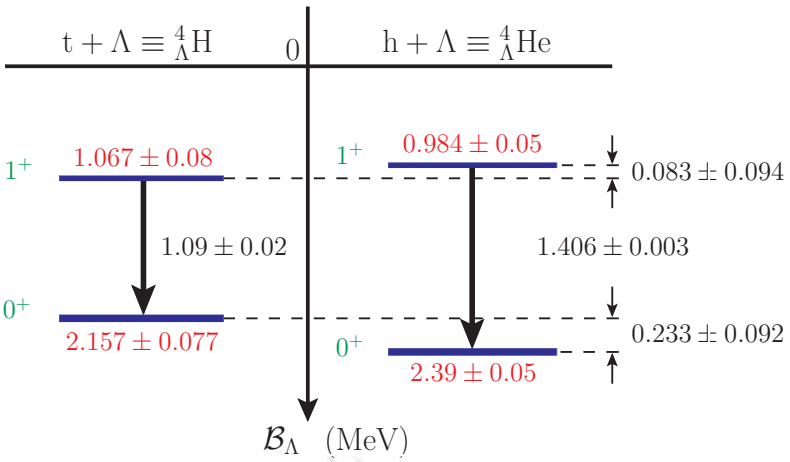

FIGURE 4.1: Level energy ($\mathcal{B}_\Lambda$) scheme with the ground ($J^P = 0^+$) state of ${}^4_\Lambda$H and the first-excited ($J^P = 1^+$) states of the mirror partners (${}^4_\Lambda$H, ${}^4_\Lambda$He) taken from the recent high-resolution spectroscopic measurements at MAMI [73, 74] and J-PARC [72, 75], respectively. The ground state energy of ${}^4_\Lambda$He on the other hand is taken from the erstwhile emulsion work of Ref. [67]. The figure is adapted from Refs. [74, 114].

lengths induce universal correlations between three-body observables, as elucidated by the so-called *Phillips-lines* [115] (cf. Fig. 4.11). Furthermore, for the recently suggested benchmark value, $a_{\Lambda\Lambda} = -0.80$ fm, in Ref. [90], the Λ-separation energies, $\mathcal{B}_\Lambda({}^5_{\Lambda\Lambda}\text{H}) = 2.295$ MeV and $\mathcal{B}_\Lambda({}^5_{\Lambda\Lambda}\text{He}) = 2.212$ MeV, are deduced.

This chapter is organized as follows. In Sec. 4.2 we present the basic set-up of the ${}^{\not\pi}$EFT formalism necessary for $\Lambda\Lambda T$ system. There we display the most general LO effective Lagrangian and the coupled system of integral equations for the $\Lambda\Lambda T$ system, with appropriate scale-dependent three-body contact interactions that describe RG limit cycle behavior. Section 4.3 contains our numerical results of solving the integral equations in both bound and scattering domains. In particular, through our study of the $B_{\Lambda\Lambda}$ - $a_{\Lambda\Lambda}$ correlations, we present preliminary estimates of the $\Lambda\Lambda T$ scattering lengths and the corresponding Λ-separation energies. Finally, in Sec. 4.4 we present our summary with concluding remarks. A brief discussion on the one- and two-body non-relativistic propagators in ${}^{\not\pi}$EFT is relegated to Appendix B.

4.2 Theoretical Framework For $\Lambda\Lambda T$ System

4.2.1 Effective Lagrangian

We use the theoretical framework of pionless effective field theory to investigate the bound states of the double-Λ-hypernuclear mirror systems (${}^5_{\Lambda\Lambda}$H , ${}^5_{\Lambda\Lambda}$He). In this approach, the effective Lagrangian is constructed manifestly nonrelativistic on the basis of available symmetries of the relevant low-energy degrees of freedom. In our case, the explicit elementary degrees of freedom involves two Λ-hyperon *halo* fields and the generic *core* field, $T \equiv t, h$, representing one of the two mirrors (isospin) partners, namely, the triton (t) or the helion (h). In addition,

it is convenient to introduce auxiliary dimer fields to unitarize and renormalize the two-body sectors [12, 54, 116–118]. Our formalism includes three such dimer fields, namely, the spin-singlet (^{1}S$_0$) field $u_0 \equiv (\Lambda T)_s$, the spin-triplet (^{3}S$_1$) field $u_1 \equiv (\Lambda T)_t$, and the spin-singlet $\Lambda\Lambda$-dibaryon field $u_s \equiv (\Lambda\Lambda)_s$.[1] Notably, these u_0 and u_1 dimer states correspond to the experimentally observed spin-singlet (0^+) ground state and spin-triplet (1^+) excited state of the mirror hypernuclei ($^4_\Lambda$H , $^4_\Lambda$He) [67, 70, 72–75, 107].

The full nonrelativistic LO $\not\pi$EFT Lagrangian can be expressed as the following string of terms:

$$\mathscr{L} = \mathscr{L}_\Lambda + \mathscr{L}_T + \mathscr{L}_{u_0} + \mathscr{L}_{u_1} + \mathscr{L}_{u_s} + \mathscr{L}_{3-body} \,. \tag{4.1}$$

The one-body Lagrangian contains the contributions of the elementary fields, namely, the Λ-hyperon and the spin-1/2 core T, and is given as

$$\mathscr{L}_\Lambda = \Lambda^\dagger \left[i\partial_t + \frac{\nabla^2}{2M_\Lambda} + \cdots \right] \Lambda \,, \tag{4.2}$$

$$\mathscr{L}_T = T^\dagger \left[i\partial_t + \frac{\nabla^2}{2M_T} + \cdots \right] T \,, \tag{4.3}$$

where M_Λ and M_T are the respective masses of the elementary fields. Next, we display the two-body parts of the Lagrangian, namely,

$$\mathscr{L}_{u_0} = -u_0^\dagger \left[i\partial_t + \frac{\nabla^2}{2(M_\Lambda + M_T)} + \cdots \right] u_0 - y_0 \left[u_0^\dagger \left(T^{\rm T} \hat{\mathbb{P}}^{(^1{\rm S}_0)}_{(\Lambda T)} \Lambda \right) + {\rm h.c.} \right] + \cdots \,, \tag{4.4}$$

$$\mathscr{L}_{u_1} = -(u_1)^\dagger_j \left[i\partial_t + \frac{\nabla^2}{2(M_\Lambda + M_T)} + \cdots \right] (u_1)_j - y_1 \left[(u_1)^\dagger_j \left(T^{\rm T} \hat{\mathbb{P}}^{(^3{\rm S}_1)}_{(\Lambda T)\, j} \Lambda \right) + {\rm h.c.} \right] + \cdots \,, \tag{4.5}$$

$$\mathscr{L}_{u_s} = -u_s^\dagger \left[i\partial_t + \frac{\nabla^2}{4M_\Lambda} + \cdots \right] u_s - y_s \left[u_s^\dagger \left(\Lambda^{\rm T} \hat{\mathbb{P}}^{(^1{\rm S}_0)}_{(\Lambda\Lambda)} \Lambda \right) + {\rm h.c.} \right] + \cdots \,, \tag{4.6}$$

where the spin-singlet and spin-triplet projection operators are given as

$$\hat{\mathbb{P}}^{(^1{\rm S}_0)}_{(\Lambda\Lambda)} = -\frac{i}{2}\sigma_2 \,, \quad \hat{\mathbb{P}}^{(^1{\rm S}_0)}_{(\Lambda T)} = -\frac{i}{\sqrt{2}}\sigma_2 \,, \quad \hat{\mathbb{P}}^{(^3{\rm S}_1)}_{(\Lambda T)\, j} = -\frac{i}{\sqrt{2}}\sigma_2\sigma_j \,, \tag{4.7}$$

with σ_j ($j = 1, 2, 3$) being the Pauli spin matrices. In the above equations the couplings y_0, y_1, and y_s are two-body contact interactions between the respective dimer and their constituent elementary fields. Adopting the power-counting scheme for the contact interactions apposite to finely tuned systems [3, 4, 6], these LO couplings are easily fixed as [119–121]

$$y_0 = y_1 = \sqrt{\frac{2\pi}{\mu_{\Lambda T}}} \,, \quad \text{and} \quad y_s = \sqrt{\frac{4\pi}{M_\Lambda}} \,. \tag{4.8}$$

[1] Notably, in the investigation of the low-energy S-wave $\Lambda\Lambda T$ dynamics, the triplet state $u_t \equiv (\Lambda\Lambda)_t$ does not contribute, being Pauli-blocked.

The ellipses in all the above Lagrangians denote subleading order terms containing four or higher derivative operators that do not contribute to our LO analysis. For pedagogical reasons a brief description of the one- and two-body nonrelativistic propagators used in the construction of the Faddeev-type coupled integral equations is presented in Appendix B.

Finally, as demonstrated later in this section, since the $\Lambda\Lambda T$ three-body systems are found to exhibit RG limit cycle behavior, the set of integral equations [cf. Eqs. (4.11) and (4.12)] becomes ill-defined in the asymptotic UV limit, and a regulator, say, in the form of a sharp momentum cutoff $\Lambda_{\rm reg}$ must be introduced to obtain regularized finite results. In that case, the basic tenet of the EFT [54] demands the introduction of non-derivatively coupled LO counterterms to renormalize the *artificial* regulator ($\Lambda_{\rm reg}$) dependence of the integral equations. For the $\Lambda\Lambda T$ ($J=1/2, I=1/2$) mirror systems, there exists two equivalent choices for the subsystem spin rearrangements that determine the elastic channels, namely, $u_0\Lambda \to u_0\Lambda$ (denoted "type-A"), and $u_1\Lambda \to u_1\Lambda$ (denoted "type-B"). With the type-A, and -B choices of the elastic channels, the three-body counterterm Lagrangians are[2]

$$\mathscr{L}^{(A)}_{\text{3-body}} = -\frac{g_3^{(A)}(\Lambda_{\rm reg})}{\Lambda_{\rm reg}^2}\Bigg[-\frac{M_T y_0^2}{2}(u_0\Lambda)^\dagger(u_0\Lambda)+\frac{M_T y_0 y_1}{2}(u_0\Lambda)^\dagger\left(\mathbf{u}_1\cdot\boldsymbol{\sigma}\Lambda\right) - \frac{M_\Lambda y_s y_0}{\sqrt{2}}(u_0\Lambda)^\dagger(u_s T)+\text{h.c.}\Bigg], \tag{4.9}$$

$$\mathscr{L}^{(B)}_{\text{3-body}} = -\frac{g_3^{(B)}(\Lambda_{\rm reg})}{\Lambda_{\rm reg}^2}\Bigg[\frac{M_T y_1^2}{6}\left(\mathbf{u}_1\cdot\boldsymbol{\sigma}\Lambda\right)^\dagger\left(\mathbf{u}_1\cdot\boldsymbol{\sigma}\Lambda\right)+\frac{M_T y_0 y_1}{2}\left(\mathbf{u}_1\cdot\boldsymbol{\sigma}\Lambda\right)^\dagger(u_0\Lambda) - \frac{M_\Lambda y_s y_1}{\sqrt{2}}\left(\mathbf{u}_1\cdot\boldsymbol{\sigma}\Lambda\right)^\dagger(u_s T)+\text{h.c.}\Bigg]. \tag{4.10}$$

The regulator-dependent three-body running couplings $g_3^{(A)}(\Lambda_{\rm reg})$ and $g_3^{(B)}(\Lambda_{\rm reg})$ which are used to absorb the scale dependence of the integral equations are *a priori* undetermined in the EFT. Hence they must be phenomenologically fixed from essential three-body data. A typical signature that Efimov physics [9, 12] is manifest in the three-body system is that the RG behavior of the three-body couplings $g_3^{(A)}$ and $g_3^{(B)}$ displays a characteristic quasi-log cyclic periodicity as a function of the regulator scale $\Lambda_{\rm reg} \ll \infty$. As originally suggested by Wilson [122], this unambiguously implies the onset of an RG limit cycle. Here we note that exact universality demands both three-body couplings to be identical which in principle should not depend on the details of the two-body subsystems. However, in practice, certain nominal qualitative differences do appear in the estimation of these scale-dependent couplings, as seen in our results presented in the next section. This is primarily due to the specific choice of the renormalization schemes we have adopted in the treatments of the type-A and type-B

[2] In this work, we have excluded a third possible choice "type-C" of the elastic scattering channel, namely, $u_s T \to u_s T$, which can not be physically associated with any realizable scattering of particle-stable two-body asymptotic states, given that $u_s \equiv (\Lambda\Lambda)_s$ is unbound. Furthermore, we have chosen a renormalization scheme where we only included the three-body force in the respective elastic channels [cf. discussion below Eq. (4.15)]. Consequently, a three-body force in the channel $u_s T \to u_s T$ is missing in our analysis.

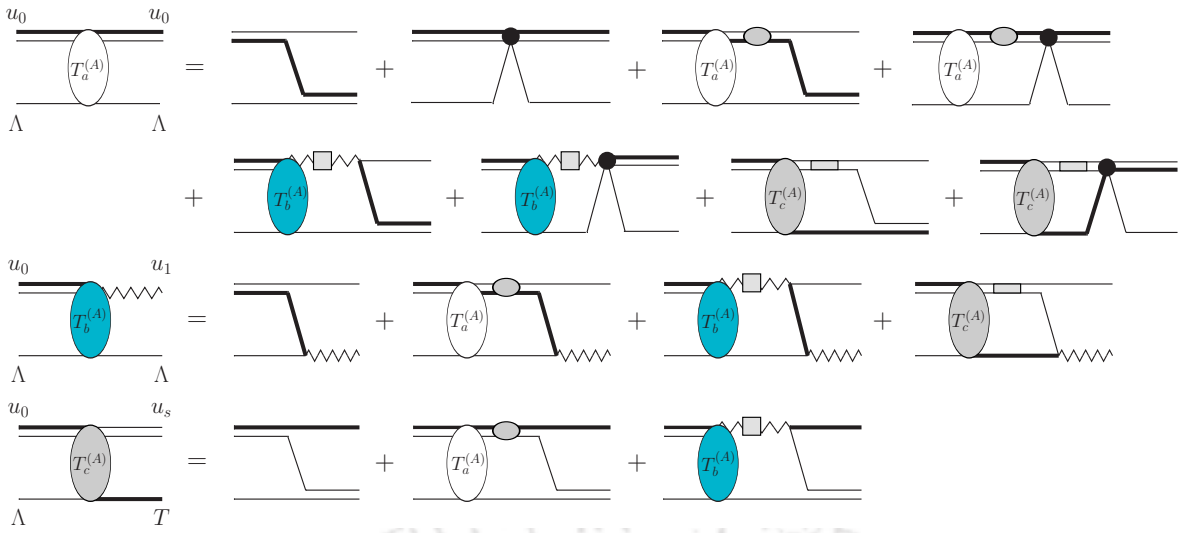

FIGURE 4.2: Feynman diagrams for the coupled-channel integral equations, with $u_0\Lambda \to u_0\Lambda$ (type-A) choice as the elastic channel. The thin (thick) lines denote the Λ-hyperon (core $T \equiv t, h$) field propagators. The double lines denote the renormalized propagators for the spin-singlet dimer fields u_0 and u_s, and the zigzag lines denote the renormalized propagators for the spin-triplet dimer field u_1. The dark-filled circles denote the leading-order three-body contact interactions, while the square, oval, and rectangular gray blobs represent dressings of the dimer propagators with resummed loops.

integral equations [cf. discussion below Eq. (4.15)]. However, such differences do not have any significant influence on the qualitative nature of the results of this work.

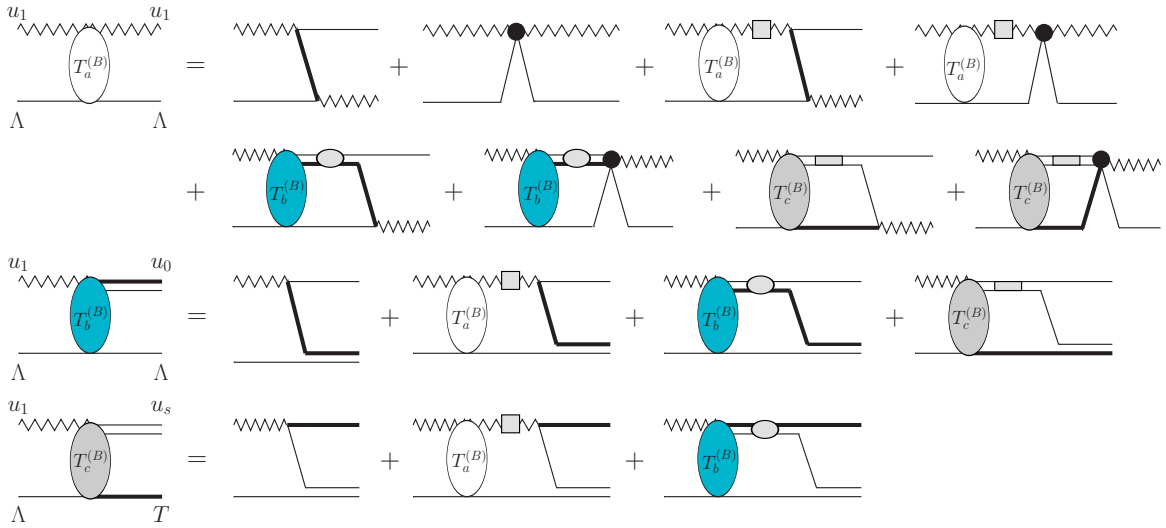

FIGURE 4.3: Feynman diagrams for the coupled-channel integral equations, with $u_1\Lambda \to u_1\Lambda$ (type-B) choice for the elastic channel. The thin (thick) lines denote the Λ-hyperon (core $T \equiv t, h$) field propagators. The double lines denote the renormalized propagators for the spin-singlet dimer fields u_0 and u_s, and the zigzag lines denote the renormalized propagators for the spin-triplet dimer field u_1. The dark-filled circles denote the leading-order three-body contact interactions, while the square, oval, and rectangular gray blobs represent dressings of the dimer propagators with resummed loops.

4.2.2 Integral equations

In Figs. 4.2 and 4.3, we display the Feynman diagrams contributing to the S-wave elastic processes, namely, $u_0\Lambda \to u_0\Lambda$ (type-A) and $u_1\Lambda \to u_1\Lambda$ (type-B), in terms of the *half-off-shell* S-wave projected amplitudes, $T_a^{(A,B)}(p,k;E)$, $T_b^{(A,B)}(p,k;E)$ and $T_c^{(A,B)}(p,k;E)$. While $T_a^{(A,B)}(p,k;E)$ denotes the elastic amplitudes, $T_b^{(A,B)}(p,k;E)$ and $T_c^{(A,B)}(p,k;E)$ are the amplitudes for the inelastic processes, $u_{0,1}\Lambda \to u_{1,0}\Lambda$ and $u_{0,1}\Lambda \to u_s T$, respectively. Here k (p) is the relative on-shell (off-shell) three-body center-of-mass momentum for the $u_{0,1}$ - Λ scattering processes in the initial (final) states, and $E = \mathscr{E}_{2(s,t)}^{thr} + k^2/(2\mu_{\Lambda(\Lambda T)})$ is the total center-of-mass kinetic energy measured with respect to the *three-particle breakup* threshold ($E = 0$). In other words, for each $\Lambda\Lambda T$ three-body system, there exist two *particle-dimer breakup* thresholds, viz. the deeper $\Lambda + u_0$ breakup threshold, $\mathscr{E}_{2(s)}^{thr} = -\gamma_0^2/(2\mu_{\Lambda T})$, and the shallower $\Lambda + u_1$ breakup threshold, $\mathscr{E}_{2(t)}^{thr} = -\gamma_1^2/(2\mu_{\Lambda T})$ (cf. discussions in Sec. 4.3). Here γ_0 and γ_1 are the respective binding momenta of the singlet $u_0 \equiv (\Lambda T)_s$ and triplet $u_1 \equiv (\Lambda T)_t$ two-body subsystems, and $\mu_{\Lambda(\Lambda T)} = M_\Lambda(M_\Lambda + M_T)/(2M_\Lambda + M_T)$ is the reduced masses of the Λ - $(\Lambda T)_{s,t}$ three-body system. Using standard Feynman rules, the S-wave projected amplitudes for the different elastic and inelastic channels can be easily worked out. With the type-A and type-B choices of the elastic channels, the two sets of coupled integral equations for the $\Lambda\Lambda T$ mirror partners are given as [13, 14, 123, 124]

$$
\begin{aligned}
T_a^{(A)}(p,k;E) = &-\frac{1}{2}(y_0^2 M_T)\,\mathscr{K}_{(a)}^{A}(p,k;E) \\
&+\frac{M_T}{\mu_{\Lambda T}}\int_0^{\Lambda_{\rm reg}}\frac{\mathrm{d}q\,q^2}{2\pi}\,\mathscr{K}_{(a)}^{A}(p,q,\Lambda_{\rm reg};E)\,\mathscr{D}_0(q,E)\,T_a^{(A)}(q,k;E) \\
&-\frac{y_0}{y_1}\frac{\sqrt{3}M_T}{\mu_{\Lambda T}}\int_0^{\Lambda_{\rm reg}}\frac{\mathrm{d}q\,q^2}{2\pi}\,\mathscr{K}_{(a)}^{A}(E;p,q)\,\mathscr{D}_1(q,E)\,T_b^{(A)}(q,k;E) \\
&+\frac{y_0}{y_s}\sqrt{8}\int_0^{\Lambda_{\rm reg}}\frac{\mathrm{d}q\,q^2}{2\pi}\,\mathscr{K}_{(b2)}^{A}(p,q;E)\,\mathscr{D}_s(q,E)\,T_c^{(A)}(q,k;E)\,, \\
T_b^{(A)}(p,k;E) = &\frac{\sqrt{3}}{2}(y_0 y_1 M_T)K_{(a)}(p,k;E) \\
&-\frac{y_1}{y_0}\frac{\sqrt{3}M_T}{\mu_{\Lambda T}}\int_0^{\Lambda_{\rm reg}}\frac{\mathrm{d}q\,q^2}{2\pi}\,K_{(a)}(p,q;E)\,\mathscr{D}_0(q,E)\,T_a^{(A)}(q,k;E) \\
&-\frac{M_T}{\mu_{\Lambda T}}\int_0^{\Lambda_{\rm reg}}\frac{\mathrm{d}q\,q^2}{2\pi}\,K_{(a)}(p,q;E)\,\mathscr{D}_1(q,E)\,T_b^{(A)}(q,k;E) \\
&+\frac{y_1}{y_s}\sqrt{24}\int_0^{\Lambda_{\rm reg}}\frac{\mathrm{d}q\,q^2}{2\pi}\,K_{(b2)}(p,q;E)\,\mathscr{D}_s(q,E)\,T_c^{(A)}(q,k;E)\,, \\
T_c^{(A)}(p,k;E) = &-\frac{1}{\sqrt{2}}(y_0 y_s M_\Lambda)\,K_{(b1)}(p,k;E) \\
&+\frac{y_s}{y_0}\frac{\sqrt{2}M_\Lambda}{\mu_{\Lambda T}}\int_0^{\Lambda_{\rm reg}}\frac{\mathrm{d}q\,q^2}{2\pi}\,K_{(b1)}(p,q;E)\,\mathscr{D}_0(q,E)\,T_a^{(A)}(q,k;E) \\
&+\frac{y_s}{y_1}\frac{\sqrt{6}M_\Lambda}{\mu_{\Lambda T}}\int_0^{\Lambda_{\rm reg}}\frac{\mathrm{d}q\,q^2}{2\pi}\,K_{(b1)}(p,q;E)\,\mathscr{D}_1(q,E)\,T_b^{(A)}(q,k;E)\,, \qquad (4.11)
\end{aligned}
$$

and,

$$
\begin{aligned}
T_a^{(B)}(p,k;E) &= \frac{1}{2}(y_1^2 M_T)\mathscr{K}^B_{(a)}(p,k;E) \\
&\quad - \frac{M_T}{\mu_{\Lambda T}}\int_0^{\Lambda_{\rm reg}} \frac{{\rm d}q\, q^2}{2\pi}\, \mathscr{K}^B_{(a)}(p,q,\Lambda_{\rm reg};E)\, \mathscr{D}_1(q,E)\, T_a^{(B)}(q,k;E) \\
&\quad - \frac{y_1}{y_0}\frac{\sqrt{3}M_T}{\mu_{\Lambda T}}\int_0^{\Lambda_{\rm reg}} \frac{{\rm d}q\, q^2}{2\pi}\, \mathscr{K}^B_{(a)}(p,q;E)\, \mathscr{D}_0(q,E)\, T_b^{(B)}(q,k;E) \\
&\quad + \frac{y_1}{y_s}\sqrt{24}\int_0^{\Lambda_{\rm reg}} \frac{{\rm d}q\, q^2}{2\pi}\, \mathscr{K}^B_{(b2)}(p,q;E)\, \mathscr{D}_s(q,E)\, T_c^{(B)}(q,k;E)\ , \\
T_b^{(B)}(p,k;E) &= \frac{\sqrt{3}}{2}(y_1 y_0 M_T)K_{(a)}(p,k;E) \\
&\quad - \frac{y_0}{y_1}\frac{\sqrt{3}M_T}{\mu_{\Lambda T}}\int_0^{\Lambda_{\rm reg}} \frac{{\rm d}q\, q^2}{2\pi}\, K_{(a)}(p,q;E)\, \mathscr{D}_1(q,E)\, T_a^{(B)}(q,k;E) \\
&\quad + \frac{M_T}{\mu_{\Lambda T}}\int_0^{\Lambda_{\rm reg}} \frac{{\rm d}q\, q^2}{2\pi}\, K_{(a)}(p,q;E)\, \mathscr{D}_0(q,E)\, T_b^{(B)}(q,k;E) \\
&\quad + \frac{y_0}{y_s}\sqrt{8}\int_0^{\Lambda_{\rm reg}} \frac{{\rm d}q\, q^2}{2\pi}\, K_{(b2)}(p,q;E)\, \mathscr{D}_s(q,E)\, T_c^{(B)}(q,k;E)\ , \\
T_c^{(B)}(p,k;E) &= -\sqrt{\frac{3}{2}}(y_1 y_s M_\Lambda)K_{(b1)}(p,k;E) \\
&\quad + \frac{y_s}{y_1}\frac{\sqrt{6}M_\Lambda}{\mu_{\Lambda T}}\int_0^{\Lambda_{\rm reg}} \frac{{\rm d}q\, q^2}{2\pi}\, K_{(b1)}(p,q;E)\, \mathscr{D}_1(q,E)\, T_a^{(B)}(q,k;E) \\
&\quad + \frac{y_s}{y_0}\frac{\sqrt{2}M_\Lambda}{\mu_{\Lambda T}}\int_0^{\Lambda_{\rm reg}} \frac{{\rm d}q\, q^2}{2\pi}\, K_{(b1)}(p,q;E)\, \mathscr{D}_0(q,E)\, T_b^{(B)}(q,k;E)\,, \qquad (4.12)
\end{aligned}
$$

respectively, where in the above equations the two-body couplings y_0, y_1, and y_s are determined by using Eq. (4.8). The S-wave projected two-point Green's functions [cf. Eq. (B.3) in Appendix B], namely,

$$
\begin{aligned}
\mathscr{D}_0(q,E) &= \frac{1}{\gamma_0 - \sqrt{q^2\frac{\mu_{\Lambda T}}{\mu_{\Lambda(\Lambda T)}} - 2\mu_{\Lambda T}E - i\eta} - i\eta}\,, \\
\mathscr{D}_1(q,E) &= \frac{1}{\gamma_1 - \sqrt{q^2\frac{\mu_{\Lambda T}}{\mu_{\Lambda(\Lambda T)}} - 2\mu_{\Lambda T}E - i\eta} - i\eta}\,, \\
\mathscr{D}_s(q,E) &= \frac{1}{\frac{1}{a_{\Lambda\Lambda}} - \sqrt{q^2\frac{M_\Lambda}{2\mu_{T(\Lambda\Lambda)}} - M_\Lambda E - i\eta} - i\eta}, \qquad (4.13)
\end{aligned}
$$

contain the contributions of the u_0, u_1, and u_s intermediate dimer states, with $\mu_{T(\Lambda\Lambda)} = (2M_\Lambda M_T)/(2M_\Lambda + M_T)$, which is the reduced mass of the T-$(\Lambda\Lambda)_s$ three-body system. The T-exchange interaction kernel $K_{(a)}$, and the two possible Λ-exchange interaction kernels, $K_{(b1)}$ and $K_{(b2)}$, can be expressed as

$$
K_{(a)}(p,\kappa;E) = \frac{1}{2p\kappa}\ln\left[\frac{p^2+\kappa^2+\frac{2\mu_{\Lambda T}}{M_T}p\kappa - 2\mu_{\Lambda T}E}{p^2+\kappa^2-\frac{2\mu_{\Lambda T}}{M_T}p\kappa - 2\mu_{\Lambda T}E}\right],
$$

and

$$K_{(b1)}(p,\kappa;E) = \frac{1}{2p\kappa}\ln\left[\frac{\frac{M_\Lambda}{2\mu_{\Lambda T}}p^2+\kappa^2+p\kappa-M_\Lambda E}{\frac{M_\Lambda}{2\mu_{\Lambda T}}p^2+\kappa^2-p\kappa-M_\Lambda E}\right],$$
$$K_{(b2)}(p,\kappa;E) = \frac{1}{2p\kappa}\ln\left[\frac{p^2+\frac{M_\Lambda}{2\mu_{\Lambda T}}\kappa^2+p\kappa-M_\Lambda E}{p^2+\frac{M_\Lambda}{2\mu_{\Lambda T}}\kappa^2-p\kappa-M_\Lambda E}\right], \tag{4.14}$$

respectively, where the generic momentum $\kappa \equiv k\,(q)$ denotes the on-shell (loop) momenta. The inclusion of the regulator ($\Lambda_{\rm reg}$) dependent three-body contact interaction couplings $g_3^{(A,B)} = g_3^{(A,B)}(\Lambda_{\rm reg})$ modifies the one-particle exchange interaction kernels, $K_{(a)}$ and $K_{(b2)}$, in the respective elastic channels as:[3]

$$\mathscr{K}^{A,B}_{(a)}(p,\kappa,\Lambda_{\rm reg};E) = \left[K_{(a)}(p,\kappa;E) - \frac{g_3^{(A,B)}(\Lambda_{\rm reg})}{\Lambda^2_{\rm reg}}\right],$$
$$\mathscr{K}^{A,B}_{(b2)}(p,\kappa,\Lambda_{\rm reg};E) = \left[K_{(b2)}(p,\kappa;E) - \frac{g_3^{(A,B)}(\Lambda_{\rm reg})}{\Lambda^2_{\rm reg}}\right]. \tag{4.15}$$

Here we point out that in this work we used a minimal prescription of introducing the scale-dependent three-body couplings only in the elastic channels. In general, the most systematic method of renormalization is to include them in all the inelastic channels as well, e.g., as done in Refs. [79, 110]. In the present case, we find that the latter method leads to certain uncontrollable numerical instabilities in determining the limit cycle behaviors of $g_3^{(A,B)}(\Lambda_{\rm reg})$. This is perhaps due to the simultaneous admixture of the negative $(\Lambda\Lambda)_s$ and positive $(\Lambda T)_{s,t}$ two-body scattering lengths associated with the virtual and real bound state dimers, respectively. Hence, we took recourse to the former simplistic prescription. Either way, since these unknown scale-dependent three-body couplings are needed to be fixed phenomenologically during evaluations of the integral equations, they are expected to get accordingly renormalized in the different coupled channels. Thereby, the essential qualitative features of our investigations of the three-body bound states (e.g., the quasiperiodicity of the RG limit cycle) are by and large expected to remain unaffected. This issue is elucidated later in our results presented in the forthcoming section.

4.2.3 Three-body scattering lengths

The coupled integral equations displayed in the previous subsection must be renormalized and then solved numerically to yield predictions for the $\Lambda\Lambda T$ three-body scattering amplitudes. For a given on-shell relative momentum $k = |\mathbf{k}|$ and three-body center-of-mass kinetic energy E, the kinematical scattering domain lies between the particle-dimer breakup thresholds

[3] Note that the sign convention for the dimensionless three-body couplings $g_3^{(A,B)}$ are taken opposite to the corresponding coupling g_3 for the three-boson system, as followed in Chapter 3 [cf. Eq. (3.55)], accounting for the negative sign in front of $g_3^{(A,B)}$ in the above expressions for $\mathscr{K}^{A,B}_{(a)}$ and $\mathscr{K}^{A,B}_{(b2)}$.

$\mathscr{E}^{thr}_{2(s,t)}$ and the three-particle breakup threshold, i.e., $\mathscr{E}^{thr}_{2(s,t)} < E < 0$. In contrast with the kinematical domain of three-body bound states ($E < \mathscr{E}^{thr}_{2(s,t)}$ with imaginary k) free of singularities, the integral equations in the scattering domain develop singularities associated with poles of the $(\Lambda T)_{s,t}$-dimer propagators $\mathscr{D}_{0,1}(q,E)$ for certain values of the loop momenta q. For the type-A integral equations, the only poles are those that arise from the $\mathscr{D}_0(q,E)$ propagator insertions at $q=k$. While for the type-B integral equations poles arise due to the insertions of both $(\Lambda T)_{s,t}$-dimer propagators, namely, $\mathscr{D}_1(q,E)$ has a pole at $q=k$ and $\mathscr{D}_0(q,E)$ has a pole at $q=\sqrt{k^2+(\gamma_0^2-\gamma_1^2)(\mu_{\Lambda(\Lambda T)}/\mu_{\Lambda T})}$. To avoid these poles, a *principal value* prescription must be applied in the appropriate loop integrals to extract the three-body scattering amplitudes. Furthermore, it is numerically advantageous to express the otherwise complex-valued integral equations below the three-particle breakup threshold in terms of the real-valued renormalized K-matrix elements $\mathbb{K}^{(A,B)}_{a,b,c}(p,k;E)$ for the respective choice of the elastic processes, viz. $u_{(0,1)}\Lambda \to u_{(0,1)}\Lambda$. To this end we display the principal value prescription modified renormalized K-matrix integral equations:

$$
\begin{aligned}
\mathbb{K}^{(A)}_{a}(p,k;E) = &-\frac{M_T}{4\mu_{\Lambda T}}\mathscr{M}^{A(0)}_{(a)}(p,k;E)\\
&-\frac{M_T}{2\pi\mu_{\Lambda T}}\mathscr{P}\int_0^{\Lambda_{\rm reg}}\mathrm{d}q\,q^2\,\frac{\mathscr{M}^{A(0)}_{(a)}(p,q,\Lambda_{\rm reg};E)\,\mathbb{K}^{(A)}_{a}(q,k;E)}{q^2-k^2}\\
&+\frac{\sqrt{3}M_T}{2\pi\mu_{\Lambda T}}\frac{y_0}{y_1}\int_0^{\Lambda_{\rm reg}}\mathrm{d}q\,q^2\,\frac{\mathscr{M}^{A(0)}_{(a)}(p,q,\Lambda_{\rm reg};E)\,\mathbb{K}^{(A)}_{b}(q,k;E)}{q^2-k^2+\frac{\mu_{\Lambda(\Lambda T)}}{\mu_{\Lambda T}}(\gamma_0^2-\gamma_1^2)}\\
&-\frac{\sqrt{2}}{\pi}\frac{y_0}{y_s}\mathscr{P}\int_0^{\Lambda_{\rm reg}}\mathrm{d}q\,q^2\,\frac{\mathscr{M}^{A(0)}_{(b2)}(p,q,\Lambda_{\rm reg};E)\,\mathbb{K}^{(A)}_{c}(q,k;E)}{q^2-k^2}\,,\\
\mathbb{K}^{(A)}_{b}(p,k;E) = &\frac{\sqrt{3}M_T}{4\mu_{\Lambda T}}\frac{y_1}{y_0}\,M^{(1)}_{(a)}(p,k;E)\\
&+\frac{\sqrt{3}M_T}{2\pi\mu_{\Lambda T}}\frac{y_1}{y_0}\mathscr{P}\int_0^{\Lambda_{\rm reg}}\mathrm{d}q\,q^2\,\frac{M^{(1)}_{(a)}(p,q;E)\,\mathbb{K}^{(A)}_{a}(q,k;E)}{q^2-k^2}\\
&+\frac{M_T}{2\pi\mu_{\Lambda T}}\int_0^{\Lambda_{\rm reg}}\mathrm{d}q\,q^2\,\frac{M^{(1)}_{(a)}(p,q;E)\,\mathbb{K}^{(A)}_{b}(q,k;E)}{q^2-k^2+\frac{\mu_{\Lambda(\Lambda T)}}{\mu_{\Lambda T}}(\gamma_0^2-\gamma_1^2)}\\
&-\frac{\sqrt{6}}{\pi}\frac{y_1}{y_s}\mathscr{P}\int_0^{\Lambda_{\rm reg}}\mathrm{d}q\,q^2\,\frac{M^{(1)}_{(b2)}(p,q;E)\,\mathbb{K}^{(A)}_{c}(q,k;E)}{q^2-k^2}\,,\\
\mathbb{K}^{(A)}_{c}(p,k;E) = &\frac{M_\Lambda}{2\sqrt{2}\mu_{\Lambda T}}\frac{y_s}{y_0}\,M_{(b1)}(p,k;E)\\
&+\frac{M_\Lambda}{\sqrt{2}\pi\mu_{\Lambda T}}\frac{y_s}{y_0}\mathscr{P}\int_0^{\Lambda_{\rm reg}}\mathrm{d}q\,q^2\,\frac{M_{(b1)}(p,q;E)\,\mathbb{K}^{(A)}_{a}(q,k;E)}{q^2-k^2}\\
&+\sqrt{\frac{3}{2}}\frac{M_\Lambda}{\pi\mu_{\Lambda T}}\frac{y_s}{y_1}\int_0^{\Lambda_{\rm reg}}\mathrm{d}q\,q^2\,\frac{M_{(b1)}(p,q;E)\,\mathbb{K}^{(A)}_{b}(q,k;E)}{q^2-k^2+\frac{\mu_{\Lambda(\Lambda T)}}{\mu_{\Lambda T}}(\gamma_0^2-\gamma_1^2)}\,,
\end{aligned}
\tag{4.16}
$$

for the type-A elastic channel with $E \equiv E_A = \mathscr{E}^{thr}_{2(s)} + k^2/(2\mu_{\Lambda(\Lambda T)})$, and

$$\begin{aligned}
\mathbb{K}^{(B)}_a(p,k;E) &= \frac{M_T}{4\mu_{\Lambda T}}\mathscr{M}^{B(1)}_{(a)}(p,k;E) \\
&\quad + \frac{M_T}{2\pi\mu_{\Lambda T}}\,\mathscr{P}\!\int_0^{\Lambda_{\rm reg}} \mathrm{d}q\, q^2\, \frac{\mathscr{M}^{B(1)}_{(a)}(p,q,\Lambda_{\rm reg};E)\,\mathbb{K}^{(B)}_a(q,k;E)}{q^2-k^2} \\
&\quad + \frac{\sqrt{3}M_T}{2\pi\mu_{\Lambda T}}\frac{y_1}{y_0}\,\mathscr{P}\!\int_0^{\Lambda_{\rm reg}} \mathrm{d}q\, q^2\, \frac{\mathscr{M}^{B(1)}_{(a)}(p,q,\Lambda_{\rm reg};E)\,\mathbb{K}^{(B)}_b(q,k;E)}{q^2-k^2-\frac{\mu_{\Lambda(\Lambda T)}}{\mu_{\Lambda T}}(\gamma_0^2-\gamma_1^2)} \\
&\quad - \frac{\sqrt{6}}{\pi}\frac{y_1}{y_s}\,\mathscr{P}\!\int_0^{\Lambda_{\rm reg}} \mathrm{d}q\, q^2\, \frac{\mathscr{M}^{B(1)}_{(b2)}(p,q,\Lambda_{\rm reg};E)\,\mathbb{K}^{(B)}_c(q,k;E)}{q^2-k^2}\,, \\
\mathbb{K}^{(B)}_b(p,k;E) &= \frac{\sqrt{3}M_T}{4\mu_{\Lambda T}}\frac{y_0}{y_1}\,M^{(0)}_{(a)}(p,k;E) \\
&\quad + \frac{\sqrt{3}M_T}{2\pi\mu_{\Lambda T}}\frac{y_0}{y_1}\,\mathscr{P}\!\int_0^{\Lambda_{\rm reg}} \mathrm{d}q\, q^2\, \frac{M^{(0)}_{(a)}(p,q;E)\,\mathbb{K}^{(B)}_a(q,k;E)}{q^2-k^2} \\
&\quad - \frac{M_T}{2\pi\mu_{\Lambda T}}\,\mathscr{P}\!\int_0^{\Lambda_{\rm reg}} \mathrm{d}q\, q^2\, \frac{M^{(0)}_{(a)}(p,q;E)\,\mathbb{K}^{(B)}_b(q,k;E)}{q^2-k^2-\frac{\mu_{\Lambda(\Lambda T)}}{\mu_{\Lambda T}}(\gamma_0^2-\gamma_1^2)} \\
&\quad - \frac{\sqrt{2}}{\pi}\frac{y_0}{y_s}\,\mathscr{P}\!\int_0^{\Lambda_{\rm reg}} \mathrm{d}q\, q^2\, \frac{M^{(0)}_{(b2)}(p,q;E)\,\mathbb{K}^{(B)}_c(q,k;E)}{q^2-k^2}\,, \\
\mathbb{K}^{(B)}_c(p,k;E) &= \frac{\sqrt{3}M_\Lambda}{2\sqrt{2}\mu_{\Lambda T}}\frac{y_s}{y_1}\,M_{(b1)}(p,k;E) \\
&\quad + \sqrt{\frac{3}{2}}\,\frac{M_\Lambda}{\pi\mu_{\Lambda T}}\frac{y_s}{y_1}\,\mathscr{P}\!\int_0^{\Lambda_{\rm reg}} \mathrm{d}q\, q^2\, \frac{M_{(b1)}(p,q;E)\,\mathbb{K}^{(B)}_a(q,k;E)}{q^2-k^2} \\
&\quad + \frac{M_\Lambda}{\sqrt{2}\pi\mu_{\Lambda T}}\frac{y_s}{y_0}\,\mathscr{P}\!\int_0^{\Lambda_{\rm reg}} \mathrm{d}q\, q^2\, \frac{M_{(b1)}(p,q;E)\,\mathbb{K}^{(B)}_b(q,k;E)}{q^2-k^2-\frac{\mu_{\Lambda(\Lambda T)}}{\mu_{\Lambda T}}(\gamma_0^2-\gamma_1^2)}\,,
\end{aligned} \tag{4.17}$$

for the type-B elastic channel with $E \equiv E_B = \mathscr{E}^{thr}_{2(t)} + k^2/(2\mu_{\Lambda(\Lambda T)})$. The symbol "$\mathscr{P}$" stands for a principal value integral which involves rewriting the complex-valued dimer propagators with $i\eta$ prescription in terms of real-valued propagators, namely,

$$\frac{1}{q^2-k^2-i\eta} = \mathscr{P}\frac{1}{q^2-k^2} + i\pi\delta(q^2-k^2)\,, \tag{4.18}$$

and

$$\begin{aligned}
\frac{1}{q^2-k^2-\frac{\mu_{\Lambda(\Lambda T)}}{\mu_{\Lambda T}}(\gamma_0^2-\gamma_1^2)-i\eta} &= \mathscr{P}\frac{1}{q^2-k^2-\frac{\mu_{\Lambda(\Lambda T)}}{\mu_{\Lambda T}}(\gamma_0^2-\gamma_1^2)} \\
&\quad + i\pi\delta\left(q^2-k^2-\frac{\mu_{\Lambda(\Lambda T)}}{\mu_{\Lambda T}}(\gamma_0^2-\gamma_1^2)\right).
\end{aligned} \tag{4.19}$$

The S-wave projected Λ and T-exchange interactions kernels, in this case, are rewritten as:

$$
\begin{aligned}
M_{(a)}^{(0,1)}(p,\kappa;E) &= \left(\frac{\mu_{\Lambda(\Lambda T)}}{\mu_{\Lambda T}}\right) K_{(a)}(p,\kappa;E)\left(\gamma_{0,1}+\sqrt{p^2\frac{\mu_{\Lambda T}}{\mu_{\Lambda(\Lambda T)}}-2\mu_{\Lambda T}E}\right), \\
M_{(b1)}(p,\kappa;E) &= K_{(b1)}(p,\kappa;E)\left(\frac{p^2-k^2}{\frac{1}{a_{\Lambda\Lambda}}-\sqrt{p^2\frac{M_\Lambda}{2\mu_{T(\Lambda\Lambda)}}-M_\Lambda E}}\right), \\
M_{(b2)}^{(0,1)}(p,\kappa;E) &= \left(\frac{\mu_{\Lambda(\Lambda T)}}{\mu_{\Lambda T}}\right) K_{(b2)}(p,\kappa;E)\left(\gamma_{0,1}+\sqrt{p^2\frac{\mu_{\Lambda T}}{\mu_{\Lambda(\Lambda T)}}-2\mu_{\Lambda T}E}\right),
\end{aligned}
\tag{4.20}
$$

and the corresponding three-body force modified $\Lambda_{\rm reg}$ dependent kernels needed are:

$$
\begin{aligned}
\mathscr{M}_{(a)}^{A,B(0,1)}(p,\kappa,\Lambda_{\rm reg};E) &= \left(\frac{\mu_{\Lambda(\Lambda T)}}{\mu_{\Lambda T}}\right) \mathscr{K}_{(a)}^{A,B}(p,\kappa,\Lambda_{\rm reg};E)\left(\gamma_{0,1}+\sqrt{p^2\frac{\mu_{\Lambda T}}{\mu_{\Lambda(\Lambda T)}}-2\mu_{\Lambda T}E}\right), \\
\mathscr{M}_{(b2)}^{A,B(0,1)}(p,\kappa,\Lambda_{\rm reg};E) &= \left(\frac{\mu_{\Lambda(\Lambda T)}}{\mu_{\Lambda T}}\right) \mathscr{K}_{(b2)}^{A,B}(p,\kappa,\Lambda_{\rm reg};E)\left(\gamma_{0,1}+\sqrt{p^2\frac{\mu_{\Lambda T}}{\mu_{\Lambda(\Lambda T)}}-2\mu_{\Lambda T}E}\right)
\end{aligned}
\tag{4.21}
$$

where $\kappa = k\,(q)$ is the on-shell (loop) momentum. In the above integral equations, the unrenormalized complex-valued amplitudes $T_a^{(A,B)}(p,k;E)$ are related to the renormalized real-valued K-matrix elements $\mathbb{K}_{a,b,c}^{(A,B)}(p,k;E)$ by the following relations:

$$
\begin{aligned}
\frac{\mathbb{K}_a^{(A)}(p,k;E)}{k^2-p^2} &= \left(\frac{\mu_{\Lambda T}}{4\pi\gamma_0}\right)\frac{\sqrt{Z_0}\,T_a^{(A)}(p,k;E)\sqrt{Z_0}}{\gamma_0-\sqrt{q^2\frac{\mu_{\Lambda T}}{\mu_{\Lambda(\Lambda T)}}-2\mu_{\Lambda T}E}}, \\
\frac{\mathbb{K}_b^{(A)}(p,k;E)}{k^2-p^2-\frac{\mu_{\Lambda(\Lambda T)}}{\mu_{\Lambda T}}(\gamma_0^2-\gamma_1^2)} &= \left(\frac{\mu_{\Lambda T}}{4\pi\gamma_0}\right)\frac{\sqrt{Z_0}\,T_b^{(A)}(p,k;E)\sqrt{Z_0}}{\gamma_1-\sqrt{q^2\frac{\mu_{\Lambda T}}{\mu_{\Lambda(\Lambda T)}}-2\mu_{\Lambda T}E}}, \\
\frac{\mathbb{K}_c^{(A)}(p,k;E)}{k^2-p^2} &= \left(\frac{\mu_{\Lambda T}}{4\pi\gamma_0}\right)\frac{\sqrt{Z_0}\,T_c^{(A)}(p,k;E)\sqrt{Z_0}}{\frac{1}{a_{\Lambda\Lambda}}-\sqrt{q^2\frac{M_\Lambda}{2\mu_{T(\Lambda\Lambda)}}-M_\Lambda E}},
\end{aligned}
\tag{4.22}
$$

for the type-A amplitudes, and

$$
\begin{aligned}
\frac{\mathbb{K}_a^{(B)}(p,k;E)}{k^2-p^2} &= \left(\frac{\mu_{\Lambda T}}{4\pi\gamma_1}\right)\frac{\sqrt{Z_1}\,T_a^{(B)}(p,k;E)\sqrt{Z_1}}{\gamma_1-\sqrt{q^2\frac{\mu_{\Lambda T}}{\mu_{\Lambda(\Lambda T)}}-2\mu_{\Lambda T}E}}, \\
\frac{\mathbb{K}_b^{(B)}(p,k;E)}{k^2-p^2+\frac{\mu_{\Lambda(\Lambda T)}}{\mu_{\Lambda T}}(\gamma_0^2-\gamma_1^2)} &= \left(\frac{\mu_{\Lambda T}}{4\pi\gamma_1}\right)\frac{\sqrt{Z_1}\,T_b^{(B)}(p,k;E)\sqrt{Z_1}}{\gamma_0-\sqrt{q^2\frac{\mu_{\Lambda T}}{\mu_{\Lambda(\Lambda T)}}-2\mu_{\Lambda T}E}}, \\
\frac{\mathbb{K}_c^{(B)}(p,k;E)}{k^2-p^2} &= \left(\frac{\mu_{\Lambda T}}{4\pi\gamma_1}\right)\frac{\sqrt{Z_1}\,T_c^{(B)}(p,k;E)\sqrt{Z_1}}{\frac{1}{a_{\Lambda\Lambda}}-\sqrt{q^2\frac{M_\Lambda}{2\mu_{T(\Lambda\Lambda)}}-M_\Lambda E}},
\end{aligned}
\tag{4.23}
$$

for the type-B amplitudes, where $Z_{0,1}$ are the $u_{0,1}$-dimer field wave function renormalization constants, defined as the residues of the renormalized dressed dimer propagators $\Delta_{0,1}(k_0,\mathbf{k})$

[cf. Eq. (B.3) in Appendix B]:

$$\begin{aligned} Z_0^{-1} &= \left.\frac{d[\Delta_0^{-1}(k_0,\mathbf{0})]}{dk_0}\right|_{k_0=-\mathscr{B}_\Lambda[0^+]} = \frac{\mu_{\Lambda T}^2 y_0^2}{2\pi\gamma_0}\,, \\ Z_1^{-1} &= \left.\frac{d[\Delta_1^{-1}(k_0,\mathbf{0})]}{dk_0}\right|_{k_0=-\mathscr{B}_\Lambda[1^+]} = \frac{\mu_{\Lambda T}^2 y_1^2}{2\pi\gamma_1}\,. \end{aligned} \tag{4.24}$$

Finally, the $J = 1/2$ S-wave $\Lambda\Lambda T$ scattering lengths corresponding to the constituent spin-singlet and spin-triplet ΛT subsystems are obtained by numerically solving the above K-matrix equations for the renormalized on-shell elastic-scattering amplitudes $\mathbb{K}_a^{(A,B)}(k,k)$, and then taking the threshold limit according to the definition

$$a_{3(s,t)} = -\lim_{k\to 0}\mathbb{K}_a^{(A,B)}(k,k)\,. \tag{4.25}$$

It is notable that neither of the two three-body scattering lengths $a_{3(s,t)}$ can be considered as physical observables. On the other hand, albeit practical difficulties, it may not be entirely impossible to extract the effective three-body scattering length $a_{\Lambda\Lambda T}$ at low-energies from the $(2J+1)$-*spin averaged* S-wave elastic cross-section $\sigma_{\Lambda\Lambda T}^{el}$ by using the relation

$$a_{\Lambda\Lambda T} = \sqrt{\frac{1}{4}a_{3(s)}^2 + \frac{3}{4}a_{3(t)}^2}\,, \tag{4.26}$$

vis-a-vis, the prescription:

$$\begin{aligned} \sigma_{\Lambda\Lambda T}^{el} &= \frac{1}{4}\sigma_{3(s)}(\text{type-A}) + \frac{3}{4}\sigma_{3(t)}(\text{type-B})\,; \\ a_{3(s,t)} &= \lim_{k\to 0}\sqrt{\frac{1}{4\pi}\sigma_{3(s,t)}(\text{type-A,B})}\,, \\ a_{\Lambda\Lambda T} &= \lim_{k\to 0}\sqrt{\frac{1}{4\pi}\sigma_{\Lambda\Lambda T}^{el}}\,. \end{aligned} \tag{4.27}$$

Thus, our EFT framework provides a viable prescription to determine the three-body scattering lengths via numerical solutions to the renormalized K-matrix integral equations. Having said that it must be borne in mind that as yet there exists no experimental facility capable of extracting these scattering lengths by measuring the above elastic cross sections. The unstable nature of the Λ-hyperon poses immense technical challenges to be used either as targets or projectiles in scattering experiments. Nevertheless, the purpose of the present exercise is to demonstrate the kind of prototypical analysis that may be necessary whenever such information becomes available from future experimental investigations.

4.2.4 Asymptotic bound state analysis

In the investigation of three-body bound state characteristics in the $\Lambda\Lambda T$ cluster systems, the emergence of RG limit-cycle behavior could be easily checked by studying the UV limit of

the coupled integral equations where the off-shell or loop momenta is asymptotically large, i.e., $q, p \sim \Lambda_{\rm reg} \to \infty$, while the on-shell energy and relative momenta is small, i.e., $E, k \sim \gamma_{0,1} \sim 1/a_{\Lambda\Lambda} \ll p, q$. In this limit the inhomogeneous parts as well as the $\Lambda_{\rm reg}^{-2}$ suppressed three-body contributions to the integral equations drop out. After suitable redefinitions of the half-off-shell amplitudes, they may be shown to scale for generic off-shell asymptotic momenta κ as $T^{(A,B)}_{a,b,c}(\kappa \to \infty) \sim \kappa^{s-1}$. Finally through a sequence of *Mellin transformations*, both sets of integral equations reduce to same transcendental form:

$$1 = \left(\frac{M_T}{2\pi\mu_{\Lambda T}C_1}\right)\left[\frac{2\pi}{s}\frac{\sin\left[s\sin^{-1}(a/2)\right]}{\cos[\pi s/2]}\right] + \left(\frac{M_\Lambda}{\pi^2\mu_{\Lambda T}C_1C_2}\right)\left[\frac{2\pi}{s}\frac{\sin\left[s\cot^{-1}\sqrt{4b-1}\,\right]}{\cos[\pi s/2]}\right]^2, \quad (4.28)$$

where

$$a = \frac{2\mu_{\Lambda T}}{M_T} \quad , \quad b = \frac{M_\Lambda}{2\mu_{\Lambda T}}\,,$$
$$C_1 = \sqrt{\frac{\mu_{\Lambda T}}{\mu_{\Lambda(\Lambda T)}}} \quad , \quad C_2 = \sqrt{\frac{M_\Lambda}{2\mu_{T(\Lambda\Lambda)}}}\,. \quad (4.29)$$

Solving for the exponent s in the above equation yields the following imaginary values:

$$s = \pm i s_0^\infty \begin{cases} s_0^\infty = 1.03517... & \text{for } {}^{5}_{\Lambda\Lambda}\mathrm{H} \\ s_0^\infty = 1.03516... & \text{for } {}^{5}_{\Lambda\Lambda}\mathrm{He}\,. \end{cases} \quad (4.30)$$

The small numerical difference between the values of the asymptotic limit cycle parameter s_0^∞ reflects their universal character with reasonably good isospin symmetry in the three-body sector. The imaginary solutions can be formally attributed to the existence of Efimov states in the *unitary limit* of the two $\Lambda\Lambda T$ mirror clusters, and parametrize the onset of discrete scaling invariance. A detailed exposition of this kind of asymptotic analysis leading to the Efimov effect is found in Ref. [12]. In the next section, we present a qualitative assay of our numerical results for the non-asymptotic solutions to the integral equations and their possible implications in the low-energy domain.

4.3 Results and Discussion

For our numerical evaluations, we use the masses of the particles as displayed in Table. 4.1. As a comparison with our already obtained asymptotic limit cycle parameter s_0^∞ for each mirror hypernuclei, the analogous non-asymptotic parameter s_0 may be obtained by studying the RG behavior of the three-body couplings $g_3^{(A,B)}(\Lambda_{\rm reg})$ for non-asymptotic kinematics. The s_0 parameter is, however, nonuniversal in character and sensitive to the cutoff variations. Nevertheless, it may be shown that as $\Lambda_{\rm reg} \to \infty$, $s_0 \to s_0^\infty$ [109]. We note that currently there is no empirical three-body information available to constraint $g_3^{(A,B)}$. Thus, we adopt a strategy similar to the earlier pursued works [88, 89, 109]. We assume that ${}^{5}_{\Lambda\Lambda}\mathrm{H}$ and ${}^{5}_{\Lambda\Lambda}\mathrm{He}$

Particle	Symbol	Mass (MeV)	Binding energy (MeV)
Λ-hyperon	Λ	1115.683	-
Triton ^{3}H	t	2808.921	8.48
Helion ^{3}He	h	2808.391	7.72

TABLE 4.1: Particle data used in our calculations [125].

already form Efimov-like bound cluster states and thereby investigate the RG of $g_3^{(A,B)}$ by choosing two sets of values of the three-body binding or double-Λ-separation energies[4] ($B_{\Lambda\Lambda}$) for the mirror partners, predicted by the *ab initio* coupled channel potential model of Nemura *et al.* [86] using SVM analysis (cf. Table. 4.2). These predictions correspond to the two representative S-wave double-Λ scattering lengths, namely, $a_{\Lambda\Lambda} = -0.91$ and -1.37 fm, taken from the old Nijmegen hard-core potential models, mND$_S$ and ND$_S$, respectively, of Ref. [111], but consistent with the constraints based on recent theoretical analyses [100–102] based on RHIC data [71].

In Fig. 4.4 we demonstrate the cutoff regulator dependence of the three-body coupling $g_3^{(A,B)} = g_3^{(A,B)}(\Lambda_{\rm reg})$ for the $\Lambda\Lambda t$ system. The characteristic quasiperiodic cyclic singularities reminiscent of the asymptotic limit cycle associated with the successive formation of three-body bound states are clearly evident in the non-asymptotic domain. Our finding in the three-body sector reveals good isospin symmetry between the two double-Λ-hypernuclear mirror partners with very little discernible difference in the RG behavior of each partner. Consequently, for brevity, we do not display the result for the $\Lambda\Lambda h$ system. As already pointed out, ideally the scale dependence of the type-A and type-B three-body couplings should be identical. However, owing to the small qualitative differences in rearrangements between the two types of elastic reaction channels where we only choose to introduce the counterterms (cf. Figs. 4.2 and 4.3), the type-B limit cycle plots are nominally shifted leftwards and downwards with respect to the type-A limit cycle plots. In particular, due to considerable sensitivity to the small cutoff region, $\Lambda_{\rm reg} \lesssim 200$ MeV, the $N = 0$ branch which is altogether washed out in the type-B plot, is still manifest in the type-A plot (top left corner). However, this branch

[4]The double-Λ-separation energy $B_{\Lambda\Lambda}$, as commonly referred to in the context of potential model analyses, is interpreted in our EFT framework as the three-body eigenenergy, $-E = B_{\Lambda\Lambda}$, obtained as the likely ground-state solution to the homogeneous part of the integral equations. Additionally, in the cluster model framework, it is conventional to define an *incremental binding energy* $\Delta B_{\Lambda\Lambda}$ which is related to $B_{\Lambda\Lambda}$ (measured with respect to the $\Lambda\Lambda T$ three-particle breakup threshold) as [80]

$$\Delta B_{\Lambda\Lambda} = B_{\Lambda\Lambda} - 2\mathcal{B}_\Lambda^{avg}\,, \tag{4.31}$$

where,

$$\mathcal{B}_\Lambda^{avg} = \frac{1}{4}\mathcal{B}_\Lambda[0^+] + \frac{3}{4}\mathcal{B}_\Lambda[1^+]\,, \tag{4.32}$$

is the $(2J+1)$ *spin averaged* Λ-separation energy of the singlet and triplet two-body subsystems (interpreted in the EFT as the $(\Lambda T)_{s,t}$ subsystem averaged binding energy). Thus, the predicted values of $B_{\Lambda\Lambda}$ from past *ab initio* potential model analysis, such as in Ref. [86], may be used to supplant the old results of $\Delta B_{\Lambda\Lambda}$ by reevaluating them using the recent experimental inputs for the Λ-separation energies of the ground (singlet) and first (triplet) excited states of the ($^4_\Lambda$H , $^4_\Lambda$He) mirrors [72–75].

ΛΛ-Hypernuclear mirror (a , b) Sets	S-wave ΛΛ Scattering length $a_{\Lambda\Lambda}$ (fm)	ΛΛ-Separation energy $B_{\Lambda\Lambda}$ (MeV) [86]	Incremental binding energy $\Delta B_{\Lambda\Lambda}$ (MeV) reevaluated (this work)	Critical cutoff $\Lambda_{\rm crit}^{(n=0)}$ (MeV) (with $g_3^{(A,B)}=0$)	cutoff $\Lambda_{\rm pot}^{(n=0)}$ (MeV) (with $g_3^{(A,B)}=0$)
Ia ($^{5}_{\Lambda\Lambda}$H)	**-0.91** (mND$_S$) [111]	**3.750**	1.071	235.028	437.654
Ib ($^{5}_{\Lambda\Lambda}$He)	**-0.91** (mND$_S$) [111]	**3.660**	0.989	269.621	429.833
IIa ($^{5}_{\Lambda\Lambda}$H)	-1.37 (ND$_S$) [111]	4.050	1.381	205.448	403.285
IIb ($^{5}_{\Lambda\Lambda}$He)	-1.37 (ND$_S$) [111]	3.960	1.289	234.522	396.332

TABLE 4.2: Two sets of predictions for the three-body binding or double-Λ-separation energy $B_{\Lambda\Lambda}$ for the ($^{5}_{\Lambda\Lambda}$H , $^{5}_{\Lambda\Lambda}$He) mirrors using the coupled-channel potential model SVM analysis of Nemura *et al.* [86]. The corresponding double-Λ scattering lengths used are two representative values based on the old Nijmegen hard-core potential models [111] (names in parentheses) consistent with the currently accepted range, -1.92 fm $\lesssim a_{\Lambda\Lambda} \lesssim -0.5$ fm [100–102], as constrained by the recent RHIC data [71]. The values of the incremental binding energies $\Delta B_{\Lambda\Lambda}$ are obtained utilizing the recent experimental input for the Λ-separation energies of the ground (singlet) and first (triplet) excited states of the ($^{4}_{\Lambda}$H , $^{4}_{\Lambda}$He) mirrors [72–75]. Furthermore, with the three-body contact interactions excluded from our integral equations, the critical cutoffs, $\Lambda_{\rm reg}=\Lambda_{\rm crit}^{(n=0)}$ (see text), associated with the ground ($n=0$) state Efimov-like trimers for each mirror double-Λ-hypernuclei, are also displayed. The rightmost column shows our adjusted cutoff values, $\Lambda_{\rm reg}=\Lambda_{\rm pot}^{(n=0)}$, which reproduce the above values of $B_{\Lambda\Lambda}$ as ground state eigenenergies. The paired ($B_{\Lambda\Lambda}$, $a_{\Lambda\Lambda}$) data points for cases Ia and Ib (shown in bold) are used to normalize our solutions.

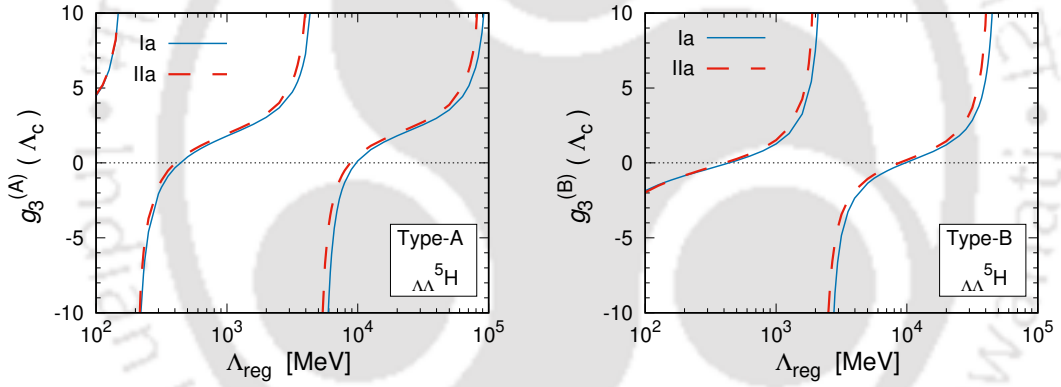

FIGURE 4.4: The non-asymptotic RG limit cycle behaviors of the three-body couplings $g_3^{(A,B)}=g_3^{(A,B)}(\Lambda_{\rm reg})$ for the $\Lambda\Lambda t$ system. Two representative choices for the S-wave double-Λ scattering lengths are considered, namely, $a_{\Lambda\Lambda}=-0.91$ fm (Ia) and -1.37 fm (IIa), based on the Nijmegen hard-core potential models, mND$_S$ and ND$_S$, respectively [111], and compatible with the range of values constrained by the recent phenomenological analyses [100–102] of RHIC data [71]. The corresponding three-body binding or double-Λ-separation energies $B_{\Lambda\Lambda}$ (cf. Table 4.2) used as input to our integral equations, are the predictions of the *ab initio* potential model analysis of Ref. [86]. The corresponding results for the $\Lambda\Lambda h$ system being almost identical are not displayed for brevity.

is not associated with the formation of an Efimov state. The ground ($n=N-1=0$) state on the other hand is associated with the $N=1$ branch. Nevertheless, the regulator values, $\Lambda_{\rm reg}=(\Lambda_{\rm reg})_N$, at which these couplings successively vanish remain unaltered in the two types of limit cycle plots. In each case the non-asymptotic RG limit cycle parameter s_0 can

be calculated via the relation

$$s_0 = \frac{\pi}{\ln\left[\frac{(\Lambda_{\rm reg})_{N+1}}{(\Lambda_{\rm reg})_N}\right]}; \quad N = 1, 2, \cdots \tag{4.33}$$

where $(\Lambda_{\rm reg})_N$ is the momentum cutoff corresponding to the Nth zero of $g_3^{(A,B)}$. Using, say, the $N = 1, 2$ values of $\Lambda_{\rm reg}$ we obtain $s_0 = \pi/\ln[(\Lambda_{\rm reg})_2/(\Lambda_{\rm reg})_1] \approx 1.03$, which is nearly the same as the asymptotic values of s_0^∞ given in Eq. (4.30), irrespective of the chosen type of elastic channel. It is also notable that our s_0 or s_0^∞ values agree well with typical values anticipated from the universal calibration curve for a mass imbalanced three-body system [12], namely, the plot of $\exp(\pi/s_0)$ versus the mass ratio m_1/m_3, with $m_1 = m_2 \equiv M_\Lambda$ and $m_3 \equiv M_T \neq m_{1,2}$.

Next, we report on our regulator ($\Lambda_{\rm reg}$) dependence of $B_{\Lambda\Lambda}$ (cf. Fig. 4.5) obtained by numerically solving the homogeneous parts of the two sets of integral equations [cf. Eqs. (4.11) and (4.12)], excluding the three-body contact interaction, i.e., $g_3^{(A,B)} = 0$. Here we again consider the two representative S-wave double-Λ scattering lengths, namely, $a_{\Lambda\Lambda} = -0.91$ fm and -1.37 fm [111–113], compatible with the range, -1.92 fm $\lesssim a_{\Lambda\Lambda} \lesssim -0.5$ fm [100–102], constrained by RHIC data [71]. It may be noted that both choices (type-A and type-B) for the elastic channels yield identical cutoff dependence. Furthermore, both the double-Λ-hypernuclear mirror partners yield nearly identical results, apart from the expected "mismatch" in threshold region (see inset plot of Fig. 4.5). Thus, it is interesting that despite the significant spin-dependent *charge symmetry breaking* reflected in the two-body binding energies, e.g., $\delta\mathscr{B}_\Lambda[0^+] \gtrsim 200$ keV, the corresponding difference of the spin-averaged binding energies, $\delta\mathscr{B}_\Lambda^{avg} \sim 5$ keV, is surprisingly small. This is easily seen using Eq. (4.32) with $\mathscr{B}_\Lambda^{avg}[{}^4_\Lambda\mathrm{H}] = 1.3395$ MeV and $\mathscr{B}_\Lambda^{avg}[{}^4_\Lambda\mathrm{He}] = 1.3355$ MeV, based on the recent spectroscopic measurements [72–75] [cf. Table. 4.3 and also Fig. 4.1]. Such a "spin averaging" effect apparently gets implicitly reflected in the unrenormalized (regulator dependent) eigenenergies, $E(\Lambda_{\rm reg}) \equiv -B_{\Lambda\Lambda}$, obtained via our integral equations with $g_3^{(A,B)}(\Lambda_{\rm reg}) = 0$. The resulting difference of the double-Λ-separation energy ($B_{\Lambda\Lambda}$) between the $({}^5_{\Lambda\Lambda}\mathrm{H}\,,\ {}^5_{\Lambda\Lambda}\mathrm{He})$ mirror partners is evidently large, $\delta B_{\Lambda\Lambda}(\Lambda_{\rm crit}^{(n=0)}) \gtrsim 200$ keV, around the particle-dimer thresholds, $\Lambda_{\rm reg} = \Lambda_{\rm crit}^{(n=0)}$ (i.e., the ground ($n = 0$) state *critical cutoff* scales for the mirror partners[5]). However, this difference rapidly vanishes asymptotically ($\Lambda_{\rm reg} \to \infty$), ultimately leading to good charge and isospin symmetry. This feature will also be apparent in our $B_{\Lambda\Lambda}$ - $a_{\Lambda\Lambda}$ correlation results presented later in Table. 4.4. Notably, due to the absence of the three-body contact interactions to renormalize the integral equations, $B_{\Lambda\Lambda}$ is quite sensitive to the cutoff variations, which increase with increasing cutoff above the respective $\Lambda + u_0$ breakup thresholds. Moreover, it is apparent that the eigenenergies are also sensitive to the input double-Λ scattering lengths, with $B_{\Lambda\Lambda}$ increasing with increasing $|a_{\Lambda\Lambda}|$.

[5]In our case in general, $\Lambda_{\rm reg} = \Lambda_{\rm crit}^{(n)}$, denotes the nth critical cutoff, defined as the cutoff scale at which the nth Efimov bound state emerges just above the *deeper* particle-dimer ($\Lambda + u_0$) breakup threshold $E = \mathscr{E}_{2(s)}^{thr}$.

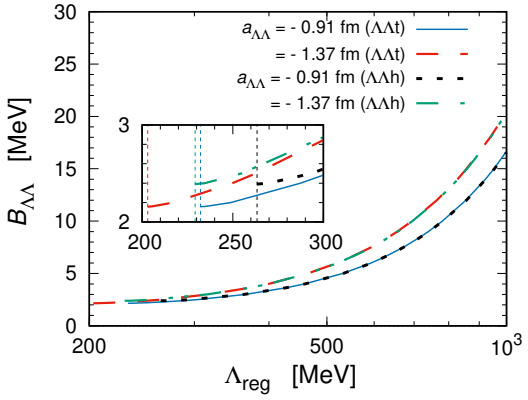

FIGURE 4.5: The cutoff regulator ($\Lambda_{\rm reg}$) dependence of the three-body binding or the double-Λ-separation energy $B_{\Lambda\Lambda}$ (with respect to the three-particle threshold) of $\Lambda\Lambda T$ mirror systems with the three-body couplings $g_3^{(A,B)}$ excluded. The plots correspond to the results for both choices of the elastic channels. Two representative choices for the double-Λ scattering lengths are considered, namely, $a_{\Lambda\Lambda} = -0.91$ fm and -1.37 fm, based on the old Nijmegen hard-core potential models, mND$_S$ and ND$_S$, respectively [111], and consistent with the recent theoretical constraints [100–102] based on RHIC data [71]. The vertical lines in the inset plot denote the critical cutoffs, $\Lambda_{\rm reg} = \Lambda_{\rm crit}^{(n=0)}$, defined with respect to the deeper particle-dimer thresholds, namely, the $\Lambda + u_0$ thresholds. Apart from the threshold regions, the results of both mirror partners are almost identical.

Λ-Hypernuclear mirror states	$\mathscr{B}_\Lambda[J^P]$ (MeV)	$\gamma_{\Lambda T} \overset{!}{\rightsquigarrow} (2\mu_{\Lambda T}\mathscr{B}_\Lambda[J^P])^{1/2}$ (MeV)
${}^4_\Lambda$H $[0^+]$	2.157 [73, 74]	$\gamma_0 \overset{!}{\rightsquigarrow}$ 58.692
${}^4_\Lambda$H (1^+)	1.067 [72, 75]	$\gamma_1 \overset{!}{\rightsquigarrow}$ 41.280
${}^4_\Lambda$He $[0^+]$	2.39 [67]	$\gamma_0 \overset{!}{\rightsquigarrow}$ 61.779
${}^4_\Lambda$He (1^+)	0.984 [72, 75]	$\gamma_1 \overset{!}{\rightsquigarrow}$ 39.641

TABLE 4.3: Λ-separation energies $\mathscr{B}_\Lambda[J^P = 0^+, 1^+]$ of the mirror states of $({}^4_\Lambda\text{H}, {}^4_\Lambda\text{He})$ corresponding to the central values of the experimental results of Refs. [67, 72–75] and summarized in Fig. 4.1. In our EFT they are to be identified ("$\overset{!}{\rightsquigarrow}$" denotes correspondence) with the particle-dimer breakup thresholds $-\mathscr{E}^{thr}_{2(s,t)}$ for the $\Lambda\Lambda T$ systems or equivalently, the $u_{0,1} \equiv (\Lambda T)_{s,t}$ dimer binding energies. The corresponding binding momenta $\gamma_{\Lambda T} \equiv \gamma_{0,1}$ are inputs to our integral equations.

We emphasize that, although in our EFT framework the $u_{0,1} \equiv (\Lambda T)_{s,t}$ two-body subsystems introduce two relevant energy scales $\mathscr{E}^{thr}_{2(s,t)}$, it is the larger of the two particle-dimer thresholds, namely, the $\Lambda + u_0$ (singlet-dimer) threshold that is effectively associated with the formation of Efimov states. In fact, irrespective of the chosen (type-A,B) elastic channels, our numerical evaluations of the integral equation only yield trimer states which are deeper than the $\Lambda + u_0$ thresholds, viz. $B_{\Lambda\Lambda} > \mathscr{B}_\Lambda[0^+]$ provided $\Lambda_{\rm reg} > \Lambda_{\rm crit}^{(n=0)}$. No numerically stable eigensolutions are obtained in the energy domain, $\mathscr{E}^{thr}_{2(s)} < E < \mathscr{E}^{thr}_{2(t)}$, lying in between the two thresholds. Thus, we should re-emphasize the correspondence of the $\Lambda\Lambda T \to \Lambda + u_0$ breakup threshold energies $\mathscr{E}^{thr}_{2(s)}$ of the respective double-Λ-hypernuclear mirror partners to the $(\Lambda T)_s$ subsystem binding energies, vis-a-vis the Λ-separation energies $\mathscr{B}_\Lambda[0^+]$ of the ground ($J^P = 0^+$) state of

the $({}^{4}_{\Lambda}\mathrm{H}\,,{}^{4}_{\Lambda}\mathrm{He})$ mirror partners, namely,

$$B_{\Lambda\Lambda}(\Lambda^{(n=0)}_{\rm crit}) \equiv -\mathscr{E}^{thr}_{2(s)} = \frac{\gamma_0^2}{2\mu_{\Lambda T}} \overset{!}{\rightsquigarrow} \mathscr{B}_{\Lambda}[0^+] \tag{4.34}$$
$$= \begin{cases} 2.157 \text{ MeV } [72\text{–}74] & \text{for } {}^{4}_{\Lambda}\mathrm{H}[0^+]\,, \\ 2.39 \text{ MeV } [67] & \text{for } {}^{4}_{\Lambda}\mathrm{He}[0^+]\,. \end{cases}$$

Here, the currently accepted central values of experimentally determined Λ-separation energies [67, 72–75] [cf. Table. 4.3 and also Fig. 4.1] is used to fix the two-body input parameters of the $(\Lambda T)_{s,t}$ systems, namely, the binding momenta, defined by the correspondence, $\gamma_{0,1} \overset{!}{\rightsquigarrow} \sqrt{2\mu_{\Lambda T}\mathscr{B}_{\Lambda}[J^P=0^+,1^+]}$, which reflect the information regarding the two breakup thresholds in our integrals equations. These critical cutoffs for the ground $(n=0)$ states were tabulated earlier in Table. 4.2. The rightmost column in the same table also displays our cutoff values, $\Lambda_{\rm reg} = \Lambda^{(n=0)}_{\rm pot}$ that reproduce the double-Λ-separation energies $B_{\Lambda\Lambda}$ of Ref. [86], begin interpreted as the plausible Efimov ground $(n=0)$ state eigenenergies. Although the $\Lambda^{(n=0)}_{\rm pot}$ values are significantly larger than the canonical hard scale of a $\not\pi$EFT, namely, $\Lambda_H \sim m_\pi$, they are nevertheless within a reasonable ballpark in context of hypernuclear systems where one-pion exchanges are forbidden by virtue of isospin invariance. A more reasonable choice of our EFT hard scale consistent with the low-energy symmetries, in this case, could be $\Lambda_H \gtrsim 2m_\pi$, with the Λ-Λ interactions known to be dominated by $\pi\pi$ or the *σ-meson* exchange mechanism. It is, however, not inconceivable that a momentum scale of this magnitude is inconsistent with the $\Lambda\Lambda T$ bound cluster *ansatz*, whereby the very existence of the core fields, $T \equiv t, h$ becomes questionable.

In Figs. 4.6 and 4.7, for each choice (type-A, -B) of the elastic channel, we plot our predictions for the $B_{\Lambda\Lambda}$ - $a_{\Lambda\Lambda}$ correlation using different values of the three-body couplings $g_3^{(A,B)}$ at appropriate cutoff scales. Solutions to each set of integral equations [i.e., Eqs. (4.11) and (4.12)] are normalized to a single (paired) data point which is conveniently taken from the *ab initio* potential model analysis of Ref. [86], each for ${}^{5}_{\Lambda\Lambda}\mathrm{H}$ and ${}^{5}_{\Lambda\Lambda}\mathrm{He}$, namely, the data points "Ia" ($B_{\Lambda\Lambda} = 3.750$ MeV, $a_{\Lambda\Lambda} = -0.91$ fm) and "Ib" ($B_{\Lambda\Lambda} = 3.660$ MeV, $a_{\Lambda\Lambda} = -0.91$ fm), respectively (cf. Table. 4.2). In particular, our EFT results for the choice of the regulator, $\Lambda_{\rm reg} = 200$ MeV, corresponding to the three-body couplings, $g_3^{(A)} = -28.461$ and $g_3^{(B)} = -0.8606$ for ${}^{5}_{\Lambda\Lambda}\mathrm{H}$, and $g_3^{(A)} = -25.252$ and $g_3^{(B)} = -0.8362$ for ${}^{5}_{\Lambda\Lambda}\mathrm{He}$, agrees reasonably well with the existing regulator-independent potential model results [80, 81, 83, 84, 86] (provided of course that the original model predictions of $B_{\Lambda\Lambda}$ or $\Delta B_{\Lambda\Lambda}$, based on the superannuated $\mathscr{B}_{\Lambda}[0^+,1^+]$ experimental data [67, 107] are reevaluated using the current data [72–75]).[6]

[6]The past potential model analyses used different three-body techniques to determine either $B_{\Lambda\Lambda}$ or $\Delta B_{\Lambda\Lambda}$ in one of two ways: (i) *ab initio* determination, using elementary two- and three-body baryonic interactions, and (ii) cluster model determination, relying on the elementary four-body inputs (or equivalently, the two-body inputs in our particle-dimer cluster scenario), namely, the Λ-separation energies $\mathscr{B}_{\Lambda}[0^+,1^+]$ of $({}^{4}_{\Lambda}\mathrm{H}\,,{}^{4}_{\Lambda}\mathrm{He})$ from old emulsion studies [67, 107]. With the advent of the recent high-precision data on $\mathscr{B}_{\Lambda}[0^+,1^+]$ from MAMI and J-PARC [72–75], the old emulsion works have now been superseded. Consequently, all model data points displayed in Figs. 4.6 and 4.7 correspond to our reevaluated $B_{\Lambda\Lambda}$ values from the old $\Delta B_{\Lambda\Lambda}$ model results using the current data *via* Eq. (4.31). There is, however, a caveat to these figures: in the absence of

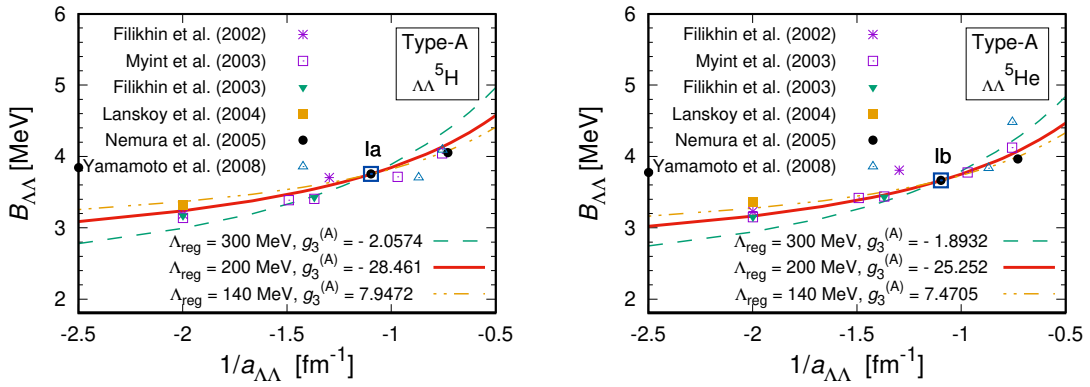

FIGURE 4.6: The double-Λ-separation energies $B_{\Lambda\Lambda}$ of ${}^{5}_{\Lambda\Lambda}$H (left panel) and ${}^{5}_{\Lambda\Lambda}$He (right panel) as a function of the inverse of the S-wave double-Λ scattering length $a^{-1}_{\Lambda\Lambda}$ using different values of the three-body coupling $g_3^{(A)}$ at appropriate cutoff scales $\Lambda_{\rm reg}$. These results correspond to the type-A choice of the elastic channel obtained using integral equations (4.11). The displayed data points correspond to our reevaluations [via Eq. (4.31)] of the past potential model-based predictions of Refs. [80, 81, 83, 84, 86] using the current experimental input for the Λ-separation energies $\mathcal{B}_\Lambda[0^+, 1^+]$ of $({}^{4}_{\Lambda}\mathrm{H}, {}^{4}_{\Lambda}\mathrm{He})$ [72–75]. In particular, the two data points, namely, "Ia": ($B_{\Lambda\Lambda} = 3.750$ MeV, $a_{\Lambda\Lambda} = -0.91$ fm) for ${}^{5}_{\Lambda\Lambda}$H and "Ib": ($B_{\Lambda\Lambda} = 3.660$ MeV, $a_{\Lambda\Lambda} = -0.91$ fm) for ${}^{5}_{\Lambda\Lambda}$He (large open squares), taken from Ref. [86] best serve to normalize our solutions to the integral equations.

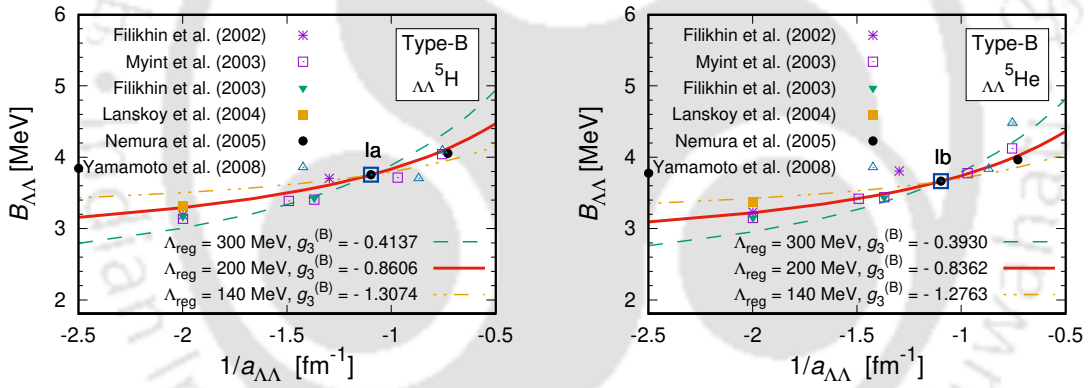

FIGURE 4.7: The double-Λ-separation energies $B_{\Lambda\Lambda}$ of ${}^{5}_{\Lambda\Lambda}$H (left panel) and ${}^{5}_{\Lambda\Lambda}$He (right panel) as a function of the inverse of the S-wave double-Λ scattering length $a^{-1}_{\Lambda\Lambda}$ using different values of the three-body coupling $g_3^{(B)}$ at appropriate cutoff scales $\Lambda_{\rm reg}$. These results correspond to the type-B choice of the elastic channel obtained using integral equations (4.12). The displayed data points correspond to our reevaluations [via Eq. (4.31)] of the past potential model-based predictions of Refs. [80, 81, 83, 84, 86] using the current experimental input for the Λ-separation energies $\mathcal{B}_\Lambda[0^+, 1^+]$ of $({}^{4}_{\Lambda}\mathrm{H}, {}^{4}_{\Lambda}\mathrm{He})$ [72–75]. In particular, the two data points, namely, "Ia": ($B_{\Lambda\Lambda} = 3.750$ MeV, $a_{\Lambda\Lambda} = -0.91$ fm) for ${}^{5}_{\Lambda\Lambda}$H and "Ib": ($B_{\Lambda\Lambda} = 3.660$ MeV, $a_{\Lambda\Lambda} = -0.91$ fm) for ${}^{5}_{\Lambda\Lambda}$He (large open squares), taken from Ref. [86] best serve to normalize our solutions to the integral equations.

To this end, each solid red curve in the figures represents our EFT generated *calibration curve* reflecting the inherent nature of the $B_{\Lambda\Lambda}$ - $a_{\Lambda\Lambda}$ correlations of the $\Lambda\Lambda T$ mirror systems. Thus, in the remaining part of our analysis, we use the correlation plots corresponding to

updated results of the old cluster model analyses [80, 81, 83, 84], it is likely that some of the our reevaluated $B_{\Lambda\Lambda}$ "model data points" may be nominally faulty in using the old model $\Delta B_{\Lambda\Lambda}$ inputs, owing to a certain degree of residual dependence on the superannuated $\mathcal{B}_\Lambda[0^+, 1^+]$ data.

$\Lambda_{\rm reg} = 200$ MeV to predict $B_{\Lambda\Lambda}$ for arbitrary values of $a_{\Lambda\Lambda}$. Our preferred choice of the normalization point Ia and Ib deserves some comments. First of all, it is notable that the value of $a_{\Lambda\Lambda} = -0.91$ fm of the Ref. [111] agrees closely with the most recent (2+1)-flavor coupled-channel lattice QCD simulation value of $a_{\Lambda\Lambda} = -0.81$ fm, as obtained by the HAL QCD Collaboration [99]. This is the primary reason for the above preference of two normalization points. Nevertheless, the choice, "IIa" ($a_{\Lambda\Lambda} = -1.37$ fm, $B_{\Lambda\Lambda} = 4.05$ MeV) and "IIb" ($a_{\Lambda\Lambda} = -1.37$ fm, $B_{\Lambda\Lambda} = 3.96$ MeV), as normalization data points from the phenomenological model analysis (ND_S) of the same Ref. [86], that correspond to the scattering length $a_{\Lambda\Lambda} = -1.37$ fm [111], yields almost identical looking EFT calibration curves as in Figs. 4.6, and 4.7. Hence, for brevity, we do not display the calibration plots corresponding to the "IIa" and "IIb" normalization points. Both the type "I" and type "II" calibration curves yield equally good fits to the rest of the other model data points. In contrast, choosing the rest of the model data points for the purpose of normalization yield calibration curves with substantially poorer fits. Consequently, either of the two choices I and II of the normalization data points could, in principle, be used to obtain our results. Therefore, the agreement with the lattice value of $a_{\Lambda\Lambda}$ is the only rationale behind our preferred normalization points.

The final part of our EFT analysis is concerned with the preliminary estimation of the S-wave three-body scattering lengths $a_{\Lambda\Lambda T}$, namely, the ${}^{4}_{\Lambda}\mathrm{H}$ - Λ and ${}^{4}_{\Lambda}\mathrm{He}$ - Λ scattering lengths. For this purpose, we numerically solve the two sets of coupled integral equations for the renormalized on-shell elastic K-matrix elements $\mathbb{K}_a^{A,B}(k,k)$ in each case [cf. Eqs. (4.16) and (4.17)], which yield the scattering lengths in the threshold limit ($k \to 0$). Care must be taken to bypass the poles of the dimer propagators originating in the kinematical scattering domain close to the respective particle-dimer thresholds. In this regard, we have implemented a numerical methodology of solving a multidimensional generalization of principal value prescription modified integral equations, originally developed by Kowalski and Noyes [126, 127] (see also Ref. [50, 59]) for the one-dimensional case.

Figures 4.8 and 4.9 display the cutoff scale dependence of the Λ - $(\Lambda t)_{s,t}$ scattering lengths for the ${}^{4}_{\Lambda}\mathrm{H}[0^+, 1^+]$ - Λ scattering processes for the two input double-Λ scattering lengths, namely, $a_{\Lambda\Lambda} = -0.91$ fm and -1.37 fm [111]. In this case, the results for the $\Lambda\Lambda T$ mirror partners are imperceptibly close to each other, so that we graphically display the results for only one of them, say, the $\Lambda\Lambda t$ system, although a consolidated summary of our numerical predictions for both mirror partners is tabulated in Table. 4.4. It is, however, worth mentioning that in contrast with our universal LO EFT prediction with very little observable difference between the $\Lambda\Lambda T$ mirrors, somewhat large isospin-breaking corrections have been reported for these systems in the context of existing potential-model analyses. This leads to significant differences in the model predictions of the two- and three-body binding energies [84, 128]. Such precision effects are not captured without a subleading-order EFT calculation, which is beyond the present scope.

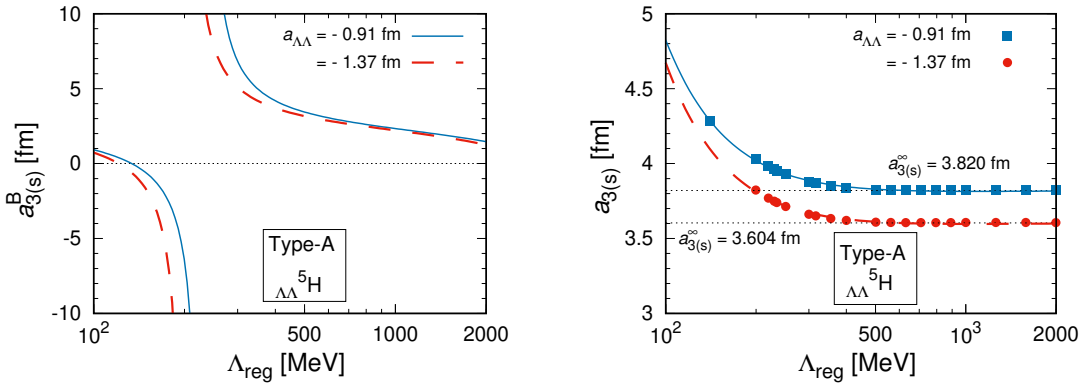

FIGURE 4.8: The EFT predicted regulator ($\Lambda_{\rm reg}$) dependence of the $J = 1/2$ S-wave Λ - $(\Lambda t)_s$ scattering length $a_{3(s)}$ for the ${}^{4}_{\Lambda}$H$[0^+]$ - Λ scattering without (left panel) and with (right panel) the three-body coupling $g_3^{(A)}$. Two representative values of the Nijmegen hard-core potential model extracted double-Λ scattering lengths are used, namely, $a_{\Lambda\Lambda} = -0.91$, -1.37 fm [111], which are consistent with recent RHIC data analyses [100–102]. The input double-Λ-separation energies $B_{\Lambda\Lambda}$ needed to fix $g_3^{(A)}(\Lambda_{\rm reg})$ for renormalization are obtained by using our EFT calibration curves (solid red line in Fig. 4.6; see also Table. 4.4). The unrenormalized (bare) scattering length is denoted $a^{B}_{3(s)}$. The smooth curves in the right panel represent fits to the data points based on the power series ansatz, Eq. (4.35). The corresponding results for $\Lambda\Lambda h$ or ${}^{4}_{\Lambda}$He$[0^+]$ - Λ scattering being similar, are not displayed.

In contrast with little or no quantitative difference in results corresponding to each choice (type-A, -B) of the bound-state solutions, significant qualitative differences arise in the respective scattering domains. In the left panel plots of Figs. 4.8 and 4.9, which exclude the three-body contact interactions, the unregulated (bare) scattering amplitudes $a^{\rm B}_{3(s,t)}$ depend sensitively on the cutoff scale and diverge for specific values of $\Lambda_{\rm reg}$ associated with the successive emergence of three-body bound states. Moreover for $\Lambda_{\rm reg} \lesssim 200$ MeV, the very first pole-like feature seen in the unrenormalized type-A amplitude in Fig. 4.8, is missing from the unrenormalized type-B amplitude displayed in Fig. 4.9. This feature is concomitant with the associated limit cycle behavior of the three-body systems (cf. Fig.4.4) where the $N = 0$ branch is found to be altogether missing in the type-B plots. Nevertheless, such unphysical singularities in the scattering amplitude are renormalized by the introduction of the scale-dependent couplings $g_3^{(A,B)}(\Lambda_{\rm reg})$, as revealed in the right panel plots which are free of singularities. We find that the renormalized scattering lengths $a_{3(s,t)}$ smoothly decreases with increasing $\Lambda_{\rm reg}$ converging asymptotically for $\Lambda_{\rm reg} \gtrsim 500$ MeV. These asymptotic values $a_{3(s,t)}(\Lambda_{\rm reg} \to \infty)$ precisely yield our EFT predictions of the three-body scattering lengths corresponding to type-A,B choices of the elastic channels. To obtain the asymptotic values $a^{\infty}_{3(s,t)}$, we use the power series fitting ansatz for small $\bar{Q}/\Lambda_{\rm reg}$, namely,

$$a_{3(s,t)}(\Lambda_{\rm reg}) = a^{\infty}_{3(s,t)}\left[1+\alpha_{s,t}\left(\frac{\bar{Q}}{\Lambda_{\rm reg}}\right)+\beta_{s,t}\left(\frac{\bar{Q}}{\Lambda_{\rm reg}}\right)^2+\cdots\right], \tag{4.35}$$

applied to our generated data points, as shown in the figures, obtained as solutions to the renormalized K-matrix equations (4.16) and (4.17). As estimated earlier, $\bar{Q} \sim 50$ MeV can be

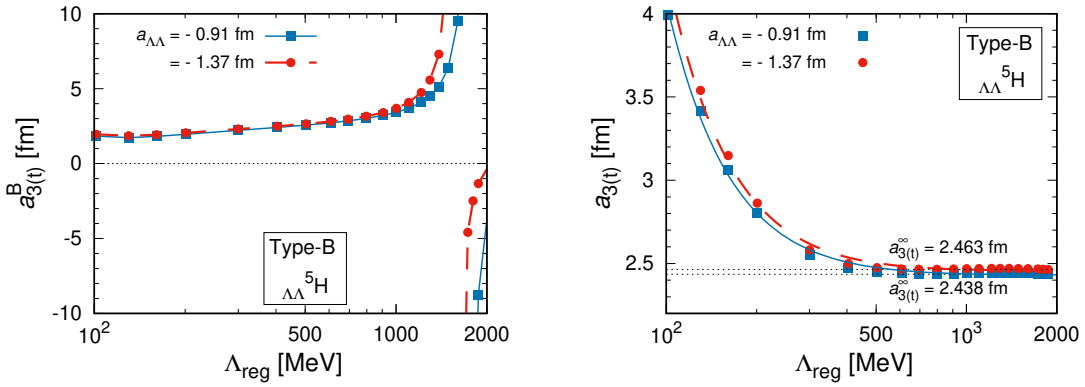

FIGURE 4.9: The EFT predicted regulator ($\Lambda_{\rm reg}$) dependence of the $J = 1/2$ S-wave Λ - $(\Lambda t)_t$ scattering length $a_{3(t)}$ for the ${}^{4}_{\Lambda}$H$[1^+]$ - Λ scattering without (left panel) and with (right panel) the three-body coupling $g_3^{(B)}$. Two representative values of the Nijmegen hard-core potential model extracted double-Λ scattering lengths are used, namely, $a_{\Lambda\Lambda} = -0.91, -1.37$ fm [111], which are consistent with recent RHIC data analyses [100–102]. The input double-Λ-separation energies $B_{\Lambda\Lambda}$ needed to fix $g_3^{(B)}(\Lambda_{\rm reg})$ for renormalization are obtained by using our EFT calibration curves (solid red line in Fig. 4.7; see also Table. 4.4). The unrenormalized (bare) scattering length is denoted $a^{B}_{3(t)}$. The smooth curves in the right panel represent fits to the data points based on the power series ansatz, Eq. (4.35). The corresponding results for $\Lambda\Lambda h$ or ${}^{4}_{\Lambda}$He$[1^+]$ - Λ scattering being similar, are not displayed.

conveniently taken as the generic momentum scale of the underlying dynamics, with $\alpha_{s,t}$, $\beta_{s,t}$ and $a^{\infty}_{3(s,t)}$ being the fitting parameters. Thus, the corresponding fitting curves, as displayed Figs. 4.8 and 4.9 (right panel plots), yield the respective three-body scattering lengths by extrapolating to $\Lambda_{\rm reg} \to \infty$. We note that a similar *ansatz* was recently used in the SVM ${}^{\not\pi}$EFT calculation of Ref. [90] to estimate the Λ-separation energies $\mathscr{B}_\Lambda$ of the $({}^{5}_{\Lambda\Lambda}$H, ${}^{5}_{\Lambda\Lambda}$He) mirror partners.

Table. 4.4 summarizes our numerical estimates of the S-wave renormalized type-A, -B three-body scattering lengths $a_{3(s,t)} \equiv a_{3(s,t)}(\Lambda_{\rm reg} \to \infty)$, as well as the *spin-averaged* values $a_{\Lambda\Lambda T}$ for different $a_{\Lambda\Lambda}$ inputs within the current theoretically feasible range, -1.92 fm $\lesssim a_{\Lambda\Lambda} \lesssim -0.5$ fm, based on RHIC data analyses [100–102].[7] The chosen $a_{\Lambda\Lambda}$ values range from those extracted from the old Nijmegen potential models (e.g., NHC-F, NSC97e, ND, ND$_S$, mND$_S$) [111–113], including more recent ones based on dispersion techniques [91] and RHIC thermal correlation model analysis [100–102], and up to the most recent ones based on lattice simulations by the HAL QCD Collaboration [99]. In particular, a representative value of $a_{\Lambda\Lambda} = -0.8$ fm was suggested in the recent SVM ${}^{\not\pi}$EFT calculation [90], using which $\mathscr{B}_\Lambda$ of ${}^{5}_{\Lambda\Lambda}$H was predicted to be about 1.14 MeV. This value can be compared with our estimation displayed in Table. 4.5, which in our $\Lambda\Lambda t$ cluster scenario may be naively obtained as

$$\begin{aligned} \mathscr{B}_\Lambda\left({}^{5}_{\Lambda\Lambda}\mathrm{H}\right) &= \Delta B_{\Lambda\Lambda}\left({}^{5}_{\Lambda\Lambda}\mathrm{H}\right) + \mathscr{B}^{avg}_{\Lambda}\left({}^{4}_{\Lambda}\mathrm{H}\right) \\ &= B_{\Lambda\Lambda}(\mathrm{Avg}) - \mathscr{B}^{avg}_{\Lambda}({}^{4}_{\Lambda}\mathrm{H})\,, \end{aligned} \tag{4.36}$$

[7] In contrast, the same RHIC data previously analyzed by the STAR Collaboration [71] suggested a positive value of the scattering length. It is notable, however, that our analysis in this work is *only* justified on the basis of a virtual bound $\Lambda\Lambda$ state. Hence, we restrict our analysis to negative $a_{\Lambda\Lambda}$ values only.

Hypernucleus ($J=\frac{1}{2}$)	Scattering length $a_{\Lambda\Lambda}$ (fm) from potential models	Type-A $B_{\Lambda\Lambda}$ (MeV) from calibration curve	Type-A $a_{3(s)}(\Lambda_{\rm reg}\to\infty)$ (fm)	Type-B $B_{\Lambda\Lambda}$ (MeV) from calibration curve	Type-B $a_{3(t)}(\Lambda_{\rm reg}\to\infty)$ (fm)	$(2J+1)$ averaged $a_{\Lambda\Lambda T}$ (fm)
${}^{\ 5}_{\Lambda\Lambda}$H	-0.50 (NSC97e) [112, 113]	3.236	4.258	3.292	2.388	2.968
	-0.60 (DR) [91]	3.377	4.109	3.418	2.404	2.925
	-0.73 (NHC-F) [111]	3.544	3.964	3.567	2.420	2.885
	-0.77 (ND) [112, 113]	3.592	3.927	3.610	2.425	2.875
	-0.80 (SVM) [90]	3.627	3.902	3.641	2.428	2.868
	-0.81 (HAL QCD) [99]	3.639	3.894	3.651	2.429	2.866
	-0.91 (mND$_S$) [111]	**3.750** [86]	3.821	**3.750** [86]	2.438	2.847
	-1.20 (DR) [91]	4.030	3.668	3.997	2.456	2.809
	-1.25 (RHIC) [100–102]	4.073	3.648	4.034	2.459	2.804
	-1.32 (NHC-F) [111]	4.131	3.622	4.085	2.462	2.797
	-1.37 (ND$_S$) [111]	4.170	3.605	4.119	2.463	2.793
	-1.80 (DR) [91]	4.461	3.493	4.374	2.473	2.764
	-1.92 (RHIC) [100–102]	4.530	3.470	4.434	2.474	2.757
${}^{\ 5}_{\Lambda\Lambda}$He	-0.50 (NSC97e) [112, 113]	3.163	4.714	3.221	1.831	2.841
	-0.60 (DR) [91]	3.298	4.461	3.341	1.837	2.740
	-0.73 (NHC-F) [111]	3.460	4.229	3.484	1.843	2.649
	-0.77 (ND) [112, 113]	3.506	4.173	3.525	1.845	2.628
	-0.80 (SVM) [90]	3.541	4.134	3.555	1.846	2.613
	-0.81 (HAL QCD) [99]	3.552	4.121	3.565	1.846	2.608
	-0.91 (mND$_S$) [111]	**3.660** [86]	4.012	**3.660** [86]	1.849	2.567
	-1.20 (DR) [91]	3.934	3.793	3.899	1.853	2.485
	-1.25 (RHIC) [100–102]	3.976	3.766	3.935	1.854	2.474
	-1.32(NHC-F) [111]	4.032	3.730	3.984	1.854	2.461
	-1.37(ND$_S$) [111]	4.071	3.707	4.018	1.854	2.452
	-1.80 (DR) [91]	4.357	3.558	4.266	1.853	2.396
	-1.92 (RHIC) [100–102]	4.425	3.528	4.324	1.852	2.384

TABLE 4.4: The EFT predicted $J = 1/2$ S-wave $\Lambda\Lambda T$ scattering lengths $a_{\Lambda\Lambda T}$ [cf. Eq. (4.26)] of the double-Λ-hypernuclear mirror partners (${}^{\ 5}_{\Lambda\Lambda}$H, ${}^{\ 5}_{\Lambda\Lambda}$He), obtained for the central values of the S-wave scattering length $a_{\Lambda\Lambda}$ based on various phenomenological analyses, e.g., old Nijmegen potential models (e.g., NHC-F, NSC97e, ND, ND$_S$, mND$_S$) [111–113], dispersion relations (DR) [91], thermal correlation model of relativistic heavy-ion collisions (RHIC) [100–102], *ab initio* $\not\pi$EFT (SVM) [90], and lattice QCD (HAL QCD) [99], consistent with the currently accepted range, -1.92 fm $\lesssim a_{\Lambda\Lambda} \lesssim -0.5$ fm [100–102]. All the displayed double-Λ-separation energies $B_{\Lambda\Lambda}$, excepting the two normalization values taken from the potential model *ab initio* SVM analysis of Ref. [86] (shown in bold), are obtained using our calibration curves for the choice of the cutoff scale, $\Lambda_{\rm reg} = 200$ MeV.

where

$$B_{\Lambda\Lambda}(\text{Avg}) = \frac{1}{2}\Big[B_{\Lambda\Lambda}(\text{type-A}) + B_{\Lambda\Lambda}(\text{type-B})\Big] \tag{4.37}$$

is the ordinary mean of the type-A and type-B double-Λ-separation energies of ${}^{\ 5}_{\Lambda\Lambda}$H obtained from Table. 4.4. Likewise, we also obtain the estimate for $\mathcal{B}_\Lambda$ (${}^{\ 5}_{\Lambda\Lambda}$He), as displayed in Table. 4.5. Consequently, the difference between the two Λ-separation energies, namely, $\mathcal{B}_\Lambda({}^{\ 5}_{\Lambda\Lambda}\text{He}) - \mathcal{B}_\Lambda({}^{\ 5}_{\Lambda\Lambda}\text{H}) = 9$ keV, yields a naive estimate of the charge-symmetry-breaking effects inherent to these double-Λ-hypernuclei. This is indeed small in comparison with that in the two-body sector where $\delta\mathcal{B}_\Lambda[0^+] \sim 200$ MeV and $\delta\mathcal{B}_\Lambda[1^+] \sim 100$ MeV. However, the charge asymmetry noted here does not directly reflect anything regarding the underlying low-energy EFT dynamics with no isospin-breaking terms included in the effective Lagrangian at LO, but rather a consequence of using physical masses and phenomenologically fixed inputs. Nevertheless, given the broad range of acceptable input values of the S-wave double-Λ scattering lengths, namely, with $\delta a_{\Lambda\Lambda} \approx 1.42$ fm, the corresponding variations in the spin-averaged three-body scattering lengths turn out to be quite nominal, i.e., $\delta a_{\Lambda\Lambda T} \lesssim 0.4$ fm. But, it may

Hypernucleus ($J=\frac{1}{2}$, $I=\frac{1}{2}$)	This work, Eq. (4.36) $\mathcal{B}_\Lambda$ (MeV)	Ref. [90] $\mathcal{B}_\Lambda$ (MeV)
${}^{5}_{\Lambda\Lambda}$H	2.295	$1.14\pm0.01^{+0.44}_{-0.26}$
${}^{5}_{\Lambda\Lambda}$He	2.212	-

TABLE 4.5: The Λ-separation energies, namely, $\mathcal{B}_\Lambda({}^{5}_{\Lambda\Lambda}\mathrm{H})$ and $\mathcal{B}_\Lambda({}^{5}_{\Lambda\Lambda}\mathrm{He})$, corresponding the representative value, $a_{\Lambda\Lambda} = -0.80$ fm. The result for ${}^{5}_{\Lambda\Lambda}$H of Ref. [90] is displayed for comparison.

be noticed that in contrast particularly the type-A scattering lengths $a_{3(s)}$ exhibit significant variations depending on the ($a_{\Lambda\Lambda}$, $B_{\Lambda\Lambda}$) inputs. In fact, the behavior, of $a_{3(s)}$ and $a_{3(t)}$ turn out to be quite the opposite, with the former increasing and the latter decreasing with both $|a_{\Lambda\Lambda}|$ and $B_{\Lambda\Lambda}$ decreasing.

Furthermore, in order to demonstrate the sensitivity of the three-body scattering length (a_3) to the preferred choice of the normalization data points, we can instead choose the IIa and IIb calibration plots (not explicitly displayed in this chapter) to measure the variation of the spin-averaged three-body scattering length $a_{\Lambda\Lambda T}$ with respect to the respective central values, from those obtained with the normalization points, Ia and Ib, for both the iso-doublet mirrors. As evident from Fig. 4.10, we find a maximum deviation of the spin-averaged three-body scattering length of $\Delta a_{\Lambda\Lambda T} \sim \pm 3\%(\pm 1\%)$ for the ${}^{5}_{\Lambda\Lambda}$He (${}^{5}_{\Lambda\Lambda}$H) systems.

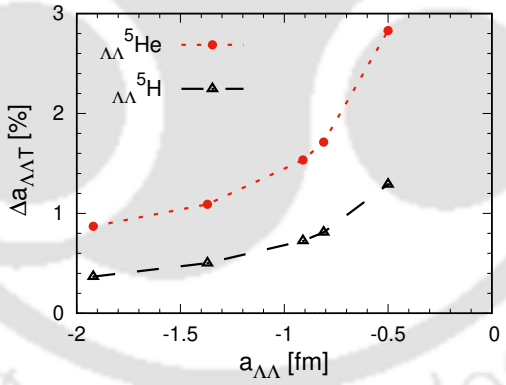

FIGURE 4.10: Percentage variation $\Delta a_{\Lambda\Lambda T}$ of spin-averaged three-body scattering length with respect to the respective central values, obtained with the two different normalization points, Ia and IIa, for the ${}^{5}_{\Lambda\Lambda}$H system, and, Ib and IIb, for the ${}^{5}_{\Lambda\Lambda}$He system.

The above-discussed features are depicted clearly in the Phillips-line plots [115] shown in upper the panels of Fig. 4.11, for each choice (type-A, -B) of the elastic channel. Interestingly, the variation of the spin-averaged scattering length $a_{\Lambda\Lambda T}$, in what may be termed as the "physical" Phillips plot (lower panel) turns out to be significantly moderate. Evidently, the type-A Phillips plots are in accordance with the expected behavior of the three-body binding energies varying inversely as the three-body scattering lengths, accounting for their characteristic negative slopes. In contrast, the observed positive slope of the type-B Phillips

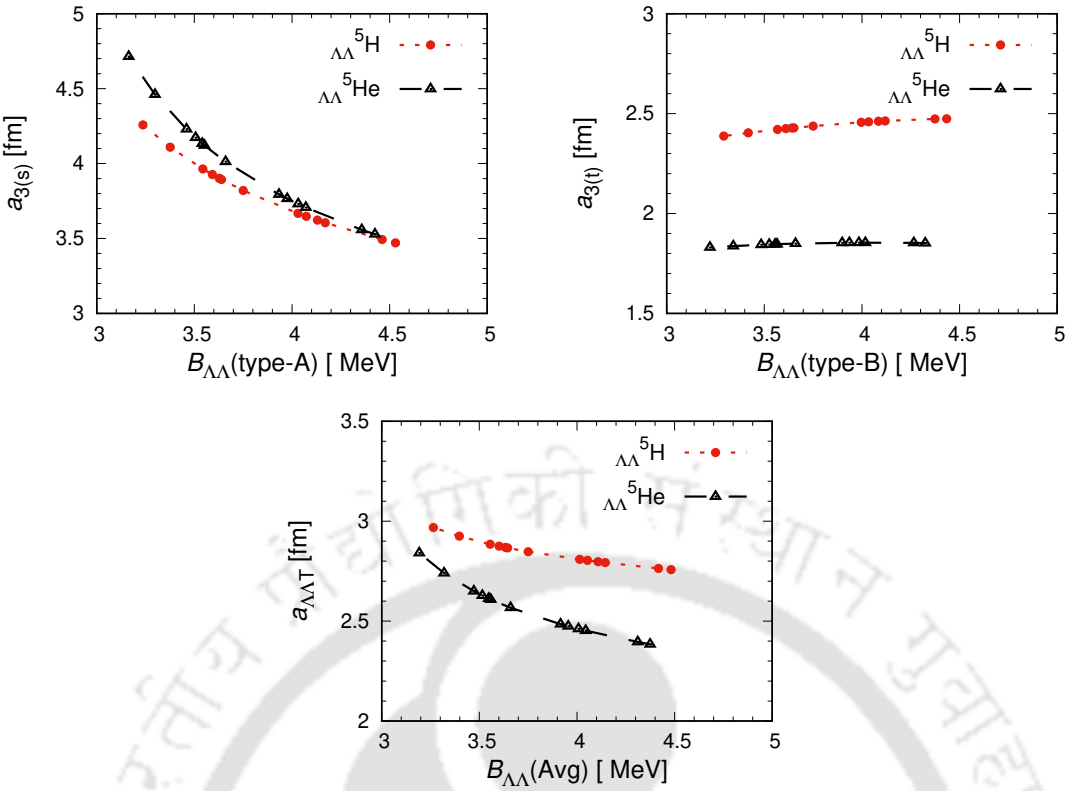

FIGURE 4.11: Phillips-lines for the type-A elastic channel, i.e., ${}^{4}_{\Lambda}$H$[0^+]$ - Λ and ${}^{4}_{\Lambda}$He$[0^+]$ - Λ scatterings (upper left panel) and the type-B elastic channel, i.e., ${}^{4}_{\Lambda}$H$[1^+]$ - Λ and ${}^{4}_{\Lambda}$He$[1^+]$ - Λ scatterings (upper right panel) are displayed. The lower panel displays the "physical" Phillips-lines corresponding to the spin-averaged scattering lengths $a_{\Lambda\Lambda T}$ plotted as a function the mean values of the three-body binding energy, namely, $B_{\Lambda\Lambda}(\text{Avg}) = \frac{1}{2}\left[B_{\Lambda\Lambda}(\text{type-A}) + B_{\Lambda\Lambda}(\text{type-B})\right]$, obtained from Table. 4.4.

plot may seem rather counter-intuitive. It is noteworthy that these contrasting type-A, -B results, are neither dependent on the nature of the three-body contact interactions used nor any artifact of the renormalization methods adopted in each case [cf. discussion below Eq. (4.15)]. This is easily understood by comparing the plots for the unrenormalized type-A, -B scattering lengths, which exhibit the same contrasting features. In this context, we also note that in determining $a_{3(s)}$, only the dynamics near the deeper threshold, namely, the particle-dimer $\Lambda + u_0$ threshold, are relevant, whereas the dynamics of both thresholds $(\Lambda + u_{0,1})$ contribute in the determination of $a_{3(t)}$. Although an unambiguous physical reasoning behind this contrasting behavior could not be ascertained, a plausible explanation may be attributed to the underlying nature of the off-shell dynamics arising due to the complex interplay between the two thresholds.

To test this hypothesis we took the strategy of considering a hypothetical (unphysical) scenario in which the triplet and singlet ΛT subsystems are completely decoupled from each other to avoid the simultaneous contribution of both the particle-dimer thresholds for each $\Lambda\Lambda T$ systems. In other words, this is essentially tantamount to the removal of the triplet-dimer field u_1 contributions in the type-A integral equations (4.11), and the singlet-dimer field u_0 contributions in the type-B integral equations (4.12). The resulting $\Lambda\Lambda T$ dynamics become

considerably simpler reducing into a system of two coupled-channel integral equations in each case. It is found that, in these reduced systems, the type-A elastic channel does not exhibit a limit cycle behavior any longer, while the type-B elastic channels continue to exhibit limit cycles but instead follow a very different value of the asymptotic parameter, namely, $s_0'^{\infty} \approx 0.84$, for each mirror system. Subsequently, it may indeed be checked that the estimation of the scattering lengths $a_{3(s,t)}$ leads to the expected natures of the Phillips-lines with negative slopes. This ostensibly indicates the plausible role of the simultaneous particle-dimer thresholds resulting in the atypical nature of the type-B Phillips-lines. However, a more satisfactory explanation of this feature demands a thorough understanding of the off-shell dynamics, perhaps hinting at the need for a more fundamental (microscopic) four- or five-body calculation, including the triton/helion two- or three-body break-up channels. However, this is beyond the present scope of the work. Finally, the fact that our results converge asymptotically for momentum scales significantly larger than m_π, the canonical hard scale of $\not\pi$EFT, there is an indication of the apparent insensitivity of the three-body dynamics to the Λ-Λ (two-body) correlations. In this regard, our findings corroborate the two previous $\not\pi$EFT analyses [88, 89] based on similar three-body calculations of ${}^{4}_{\Lambda\Lambda}$H and ${}^{6}_{\Lambda\Lambda}$He double-Λ-hypernuclei.

4.4 Summary and Conclusions

In summary, this work presents an assay of the putative doubly strange ($S = -2$) mirror double-Λ-hypernuclei (${}^{5}_{\Lambda\Lambda}$H , ${}^{5}_{\Lambda\Lambda}$He) in the context of a LO pionless EFT. In this framework, the systems are conjectured as shallow three-particle halo-bound clusters, viz. the iso-doublet pair ($\Lambda\Lambda t$, $\Lambda\Lambda h$) in the $J = 1/2$ channel. The numerical methodology presented here closely resembles the approaches of Refs. [88, 89, 108, 109]. By solving the Faddeev-like coupled integral equations [13, 14, 123, 124] for each choice (type-A, -B) of the constituent $(\Lambda T)_{s,t}$ subsystem spin introduced in the elastic channel, we presented a qualitative RG based study of the cutoff dependence of the three-body contact interactions. In particular, we investigated the dynamical interplay between the different constituent two-body subsystems, namely, the virtual bound ${}^1\mathrm{S}_0$ $\Lambda\Lambda$ cluster (with $a_{\Lambda\Lambda} < 0$), and the $(\Lambda T)_{s,t}$ bound clusters (equivalently, the two-body spin-singlet and spin-triplet bound states, i.e., ${}^{4}_{\Lambda}$H$[J = 0^+, 1^+]$ and ${}^{4}_{\Lambda}$He$[J = 0^+, 1^+]$), whose interplay could plausibly lead to the emergence of three-body shallow bound states. This is formally suggested by the appearance of RG limit cycles in the running of the three-body couplings $g_3^{(A,B)}(\Lambda_{\mathrm{reg}})$. In the unitary limit, this also implies that a discrete sequence of Efimov states emerges from the three-particle threshold [9], and simultaneously with our LO theory in the *scaling limit*, the ground-state energy collapses to negative infinity (Thomas effect [16]). Of course, such universal phenomena are *de facto* unrealistic and disappear for interactions with nonvanishing range (finite momentum cutoff) and finite scattering lengths. Nevertheless, for energies in proximity to the particle-dimer thresholds (sufficiently far from

open channels involving transmutations into particles like $\Sigma, \Xi, \cdots$) with reasonably fine-tuned Λ-T and Λ-Λ correlation strengths, it can not be precluded that any remnant universal feature leads to the formation of Efimov-like trimers.

For our numerical analysis, we considered different choices of the input double-Λ scattering lengths within the currently acceptable range, -1.92 fm $\lesssim a_{\Lambda\Lambda} \lesssim -0.5$ fm [100–102], along with the inputs for the $\Lambda + u_{0,1}$ particle-dimer thresholds provided by the up-to-date experimental information on the Λ-separation energies of the $({}^{4}_{\Lambda}\mathrm{H}\,, {}^{4}_{\Lambda}\mathrm{He})$ mirror hypernuclei [67, 72–75]. By appropriate fixing of the three-body contact interactions using the RG limit cycles at the typical cutoff scale, $\Lambda_{\rm reg} \sim 200$ MeV, a fairly good agreement of our EFT predicted $B_{\Lambda\Lambda}$ - $a_{\Lambda\Lambda}$ correlations was obtained with existing potential models [80, 81, 83, 84, 86] (provided that the $B_{\Lambda\Lambda}$ are reevaluated from their old model prediction of $B_{\Lambda\Lambda}$ using updated experimental inputs). This agreement, of course, relied on the efficacy in choosing our normalization points, taken from the *ab initio* potential model analysis of Nemura *et al.* [86]. In this case the double-Λ-separation energy $B_{\Lambda\Lambda}$ could be identified with the eigenenergy of the ground ($n = 0$) state Efimov-like trimer, with the provision that our halo/cluster $\not\pi$EFT analysis could be extended to include $\pi\pi$ or σ-meson exchange interactions with an adjusted breakdown scale, $\Lambda_H \gtrsim 2m_\pi$. But whether such physically realizable bound states can be *de facto* supported in our EFT framework remains contentious, depending crucially on support from experimental or lattice QCD data which are currently altogether missing. Future feasibility studies from the much-awaited production experiments, like PANDA and CBM at FAIR [129–131], and JPARC-P75 [132], are likely to explicate more on the inherent character of these hypernuclei. Besides, predictions based on LO EFT analyses are by and large qualitative in nature and must be supplemented by subleading order precision analyses for robust assessments. This should naturally address issues such as the compatibility with the low-energy cluster picture at momentum scales, $Q \gtrsim \Lambda_H$, potentially probing the short-distance degrees of freedom beyond the breakup scales of the triton and helion cores.

Finally, to demonstrate the predictive power of our EFT analysis, we presented preliminary estimates of the Λ-separation energies $\mathscr{B}_\Lambda$ of the two double-Λ-hypernuclear mirrors of interest and the previously undetermined S-wave three-body scattering lengths for the ${}^{4}_{\Lambda}\mathrm{H}$ - Λ and ${}^{4}_{\Lambda}\mathrm{He}$ - Λ scattering processes. Needless to say, with the scarcity of pertinent empirical inputs, a theoretical error analysis based on such empirical estimates serves little purpose and, hence, was not attempted in this work. Nevertheless, the accuracy of our results evidently relies on the precise nature of the $B_{\Lambda\Lambda}$ - $a_{\Lambda\Lambda}$ correlations, with the latter being still poorly constrained currently. Subject to the inherent limitation pertaining to the ambiguity in the normalization of the solutions to the integrals equations, our EFT methodology demands a three-body empirical input which is provided by the $B_{\Lambda\Lambda}$ model predictions of Nemura *et al.* Subsequently, the correlation plots with both types of normalization points I and II self-consistently determine the three-body scattering lengths $a_{\Lambda\Lambda T}$. In particular, the scale variation of the renormalized scattering lengths was found to asymptotically converge

for $\Lambda_{\rm reg} \gtrsim 500$ MeV which is well beyond the hard scale of standard $\not\pi$EFT. Thus, the three-body dynamics are most likely insensitive to the low-energy Λ-Λ two-body interactions, unless the hard-scale Λ_H of the effective theory could be augmented sufficiently beyond without potentially invalidating the basic halo/cluster *ansatz*. This supports the earlier claim made in Refs. [88, 89] based on similar investigations of the other double-Λ-hypernuclear cluster systems, such as ${}^{\;\;4}_{\Lambda\Lambda}$H and ${}^{\;\;6}_{\Lambda\Lambda}$He. Although short-distance mechanisms beyond the realm of our EFT can certainly influence the formation of such exotic-bound hypernuclear clusters, this does not preclude the possible role of low-energy off-shell effects that may not be accessible in a three-body halo/cluster EFT framework without involving microscopic four- or five-body calculations. Such an endeavor, however, goes beyond the scope of the simple qualitative nature of this work. To this end, we reiterate once more that our estimates of the scattering lengths $a_{\Lambda\Lambda T}$ should serve for demonstrative purposes only, given the current limitations of performing $\Lambda\Lambda T$ scattering experiments in testing their validity thereof.

Chapter 5

Investigation of $\Xi^- nn$ $(S = -2)$ Hypernucleus in Low-energy halo EFT

5.1 Introduction

In this chapter, we will discuss the light Ξ-hypernucleus $\Xi^- nn$ system in low-energy pionless halo effective field theory. The work of this chapter is published in the EPJST journal [63]. The physics of hypernuclei has gained considerable attention in the strangeness nuclear physics community through numerous studies of exotic hypernuclei (for recent reviews, see e.g., Refs. [33, 57, 133–136]). Such studies have also proven to have important consequences in the astrophysics of neutron stars where strange matter is expected to appear at their cores (e.g., see Refs. [137–139]). Especially, the strangeness $S = -2$ sector has engendered for a long time a great deal of activity behind ideas, such as the existence of the putative *H-dibaryon* and other light Ξ-*hypernuclei* or to seek a resolution to the well-known *hyperon (Y) puzzle* [140, 141]. For instance, with regard to the feasibility of the H-particle, as conjectured by Jaffe more than 40 years ago [78], no definite conclusion has been reached till date, despite the extensive theoretical [92, 94, 95, 97, 98, 142–150] and experimental investigations [151, 152]. It has been recognized that a thorough understanding of the role and character of the underlying YNN and YYN three-body forces (3BFs) is vital to resolving some of these contentious issues.[1] Especially, to stabilize neutron stars with masses larger than twice the solar mass $(2M_\odot)$ against gravitational collapse, the sole inclusion of NN, YN, and YY two-body interactions becomes questionable, as they lead to considerable *softening* of the *equation-of-state* (EoS) [153] of the dense baryonic matter. The answer probably lies in the inclusion of an admixture of NNN, ΛNN, $\Lambda\Lambda N$ and ΞNN 3BFs that may be the key in estimating the correct stiffness of the EoS governing the stability of the cores. Notably, the *Quantum Monte Carlo* simulations by Lonardini *et al.* [154, 155] have already shown encouraging indication that the inclusion of ΛNN 3BF compensates the excessive overbinding

[1] Here, the symbol N represents a nucleon, and Y represents a hyperon.

due to the ΛN interactions, ostensibly resolving the "B_Λ-overbinding" problem. Further work in this direction is necessary for a comprehensive understanding of the 2017 observation of gravitational waves from two-neutron star mergers by the LIGO Scientific Collaboration [156].

In 2001, the NAGARA event [65] from the KEK E373 emulsion experiment undoubtedly provided the first evidence of the light double-Λ hypernuclei ${}^{6}_{\Lambda\Lambda}$He, demonstrating that the $S = -2$ $\Lambda\Lambda$ interactions are less attractive than the $S = -1$ ΛN counterparts. On the other hand, the feasibility of a light Ξ-hypernuclei based on the state-of-the-art experimental [157–159] and theoretical [160–168] studies remain largely equivocal since they were first claimed in 1959 in the experimental work of Wilkinson *et al.* [169]. This is primarily due to the acute scarcity of $S = -2$ empirical information[2] needed to determine the underlying character of the hypernuclear interactions. All that one finds in the literature are a few scattered upper bounds for $\Xi^- p \to \Xi^- p$ (elastic) and $\Xi^- p \to \Lambda\Lambda$ (inelastic) cross sections from emulsion experiments [172–174] for laboratory frame momenta in the range $500 - 600$ MeV. Thus, it is no surprise that different existing model analyses lead to substantially contrasting views regarding the nature of the ΞN potentials, ranging from moderately or weakly attractive [157, 167, 172–180], even vanishing [181], to weakly repulsive [182]. In fact, the KISO event [159] from the KEK E373 experiment in 2015, which undeniably confirmed the particle-stable Ξ-hypernucleus ${}^{15}_{\Xi}$C (interpreted as the ground state of a deeply bound Ξ^-–^{14}N cluster system with binding energy 4.38 ± 0.25 MeV), at the least corroborated that the constituent ΞN channels are attractive. Specifically, the updated (*Extended-soft-core* ESC08c) Nijmegen model *G-matrix* analyses [183, 184] have predicted that the ΞN two-body system in the maximal spin-isospin ($i = 1, j^p = 1^+$) channel is strongly attractive and forms a near-threshold bound state with large positive ${}^3S_1$ scattering length, namely, $a_{\Xi n}^{(j=1)} = 4.911$ fm. On the contrary, the ($i = 1, j^p = 0^+$) channel was predicted to be predominantly repulsive with small ${}^1S_0$ scattering length, namely, $a_{\Xi n}^{(j=0)} = 0.579$ fm. Using a potential model involving *Faddeev equations*, the putative two-body bound state in the former attractive ΞN channel, so-called the *deuteron** (D^*), was estimated to have a binding energy of 1.56 MeV (1.67 MeV) with (without) taking into consideration the latter repulsive ΞN channel [165, 166]. However, the very recent updated *Extended-soft-core* ESC16 potential model [185] has denied any possibility of deuteron-like D^* in the ($i = 1, j^p = 0^+$) channel, and the corresponding two-body scattering length they found to be $a_{\Xi n}^{(j=1)} = 0.144$ fm. In a contrasting scenario compared to ESC08c potential model, the recent SU(3) chiral effective field theory (EFT) predictions from the relativistic leading order (LO) analysis of Ref. [179], as well as the non-relativistic *next-to-leading order* (NLO) *in-medium* G-matrix analysis of Ref. [180], have practically ruled out the possibility of a particle-stable ΞN bound state in the (1,1) channel. It is noteworthy that both EFT analyses were constrained by the recent HAL QCD lattice results [99] and the

[2]Due to the current impracticability of Ξ-hyperon scattering experiments, accurate data is difficult to procure. However, study of pertinent correlations in heavy-ion collisions or highly energetic proton-proton scattering in future facilities like ALICE and PANDA could certainly improve the present scenario [170, 171].

aforementioned empirical upper bounds from $\Xi^- p$ cross-sections data [172–174, 178]. Interestingly, the recent Faddeev calculations [136, 150, 162, 164–166] relying either on the updated ΞN Nijmegen ESC08c potential model [183, 184] as input for the $I = 3/2$, $J^P = 1/2^+$ channel, or on the recent HAL QCD based $\Lambda\Lambda - \Xi N$ separable interaction potential [99] as input for the $I = 1/2$, $J^P = 1/2^+$ channel, have hinted at the feasibility of a deeply bound ΞNN state in the former channel and a three-body $\Xi NN - \Lambda\Lambda N$ resonance state (i.e., either as a $\Lambda\Lambda N$ resonance state or a ΞNN quasi-bound state) in the latter.[3] These facts ostensibly imply that the ΞN interactions are predominantly attractive in nature.

5.2 Halo $\not{\pi}$EFT of $\Xi^- nn$

Prompted by this unresolved scenario, we present in this work an alternative qualitative assessment regarding the viability of a putative $\Xi^- nn$ two-neutron *halo-bound* state in the $I = 3/2$, $J^P = 1/2^+$ channel. In particular, the reasons motivating our study of the ΞNN system in this maximal spin-isospin channel are as follows:

- First, the decoupling of this channel from the strong decay into the $\Lambda\Lambda N$ channel is forbidden by isospin conservation.[4]

- Second, the Pauli principle works favorably in supporting stable ΞNN bound states.

- Third, the absence of Coulomb effects to a great extent simplifies the EFT construction of the coupled integral equations in the momentum-space [12], the so-called STM or *Skornyakov-Ter-Martirosyan* equations [13, 14] (cf. section 3.3.1).

[3] Even a contrasting viewpoint is obtained in the ΞNN system in the light of the more recent variational calculation using *Gaussian expansion* method [167] with Nijmegen ΞN potential [183, 184]. Oddly enough, their findings indicate a rather strongly attractive $I = 1/2$, $J^P = 1/2^+$ channel with a three-body bound state with binding energy 7.20 MeV, while the $I = 3/2$, $J^P = 1/2^+$ channel is less attractive without a bound state.

[4] The ΞNN system in the $I = 1/2$, $J^P = 1/2^+$ channel, on the other hand, has profound astrophysical importance in the context of EoS of neutron star matter. It has been recognized that $\Xi NN \to \Lambda\Lambda N$ transmutations could contribute to an intricate balance between the ordinary nucleonic and hyperonic matter accumulating at the stellar cores, inducing a natural "pressure control" mechanism for the build-up of neutron and lepton Pauli pressures in the high-density matter. Moreover, the ΛNN and $\Lambda\Lambda N$ three-body observables can additionally serve to fine-tune the stiffness of the EoS in a controlled way. In this regard, a series of chiral constituent quark model analyses by Garcilazo *el al.* [186–188] using Faddeev equations suggested the importance of $\Xi NN - \Lambda\Lambda N$ couplings in obtaining a three-body bound state, so-called the $S = -2$ *hypertriton* (with binding energy ~ 0.5 MeV), given that the $\Lambda\Lambda N$ system is by and large unbound. However, such a bound state mechanism seems fundamentally at odds with Efimov universality, since the feasibility of Efimov states gets substantially weakened or disappears in proximity to open decay or reaction channels [109, 189]. Thus, it seems rather unlikely that the above-reported bound state is manifestly Efimov-like in character. This calls for a rigorous model-independent assessment which is beyond the scope of a simplistic qualitative treatment as pursued in this work.

In this work, we use halo $\not\pi$EFT at LO to assess the feasibility of a $\Xi^- nn$ bound state in the $I = 3/2$, $J = 1/2$ channel primarily based on Efimov universality. This may be reflected through a study of the EFT regulator scale dependence of the RG limit cycle exhibited by the three-body contact interaction coupling (see Chapter 3 for basic details regarding few-body universality, RG limit cycle and Efimov effect in the context of EFT analysis). Despite existing uncertainties regarding the exact nature of ΞN interactions, we adopt a certain scenario motivated by the results from a series of recent *constituent quark cluster* potential model (CQCM) analyses [162, 164–166] based on Faddeev calculations. These analyses rely on the fact that the ${}^3S_1$ $\Xi^- n$ sub-system is dominantly attractive and bound with large *positive* S-wave scattering length, namely, $a_{\Xi n}^{(j=1)} = 4.911$ fm, taken from the Nijmegen ESC08c model [183, 184]. It is especially noted in some of these model studies that if one included the real bound ${}^3S_1$ channel as the only $\Xi^- n$ sub-system channel, the $\Xi^- nn$ system exhibited a three-body deeply bound state. On the other hand, no bound state is obtained with only the ${}^1S_0$ $\Xi^- n$ sub-system channel included with the Nijmegen model predicted small S-wave scattering length, namely, $a_{\Xi n}^{(j=0)} = 0.579$ fm [183, 184].[5] Here we report analogous qualitative features arising in the context of our EFT framework as well. This probably hints at the consistency of our halo EFT results with those reported earlier in the above-mentioned model analyses. In particular, the Faddeev-type coupled integral equations in the momentum space are found not to exhibit an RG limit cycle with only the repulsive ${}^1S_0$ $\Xi^- n$ sub-system channel included implying an unbound $\Xi^- nn$ system. On the other hand, we find that an *asymptotic* RG limit cycle (cf. section 3.3.2) is always manifest in the presence of the $\Xi^- n$ triplet channel, irrespective of the inclusion of the $\Xi^- n$ singlet channel. However, a full-fledged numerical evaluation of the integral equations using conventional auxiliary fields, or the so-called *dibaryon* formalism [8, 52, 53] (cf. section 3.2.4 for details), becomes a challenging task, especially when dealing with the repulsive $\Xi^- n$ sub-system with a small positive scattering length. The problem is attributed to the presence of an unphysically deep pole in the ${}^1S_0$ $\Xi^- n$ dibaryon propagator [cf. Eq. (5.8)] corresponding to an unnaturally large binding momentum, $\gamma_{\Xi n}^{(0)} \approx 1/a_{\Xi n}^{(0)} \approx 340$ MeV (estimated using the the Nijmegen ESC08c model [183, 184]). Since there is no straightforward way of "renormalizing" the effect of such a deep two-body pole, the EFT evidently breaks down. Thus, in this work we take recourse to a simplistic study of the $\Xi^- nn$ system to look for the possible emergence of physically realizable Efimov-like trimers by completely excluding the repulsive ${}^1S_0$ $\Xi^- n$ channel (as done in e.g., Ref. [162]). Notably, in our halo EFT formalism the triplet dibaryon pole position defines the $n + (\Xi^- n)_t$ particle-triplet-dimer break-up threshold, beyond which the $\Xi^- nn$ trimer levels are expected to emerge. The trimer binding energies correspond to the eigensolutions to the coupled integral equations for a given finite value of a UV sharp momentum cut-off regulator [12] (cf. section 3.3.1).

[5] It is notable that the ${}^1S_0$ nn sub-system channel is *virtual* bound with large *negative* S-wave scattering length, namely, $a_{nn} = -18.63$ fm [30].

In the ensuing EFT analysis, we present a qualitative investigation of the regulator scale dependence of an *a priori* undetermined three-body contact interaction coupling introduced for the purpose of renormalization. Through this study we hope to establish a correspondence between our EFT results with those obtained in the potential model analyses by Garcilazo *et al.* [162, 164–166]. Our analysis serves as a consistency check between both types of approaches. In particular, based on existing model estimates for the three-body binding energy, we give a *naive* window of possible estimates of the S-wave three-body scattering length associated with the elastic $n-(\Xi^- n)_t$ scattering process. These predictions in turn induce a striking feature of three-body universality, the so-called *Phillips line* [115], namely, the fact that different model potentials tuned to the same input two-body scattering data (i.e., $a_{\Xi n}^{(j=1)}$ and a_{nn}) yield a highly correlation result for the $\Xi^- nn$ binding energy and the corresponding three-body scattering length. Albeit approximations considered in our simplistic model independent treatment, such universal correlations are expected to reflect robust features of the thee-body system.

5.2.1 Effective Lagrangian and Formalism

In a simplified picture, the $\Xi^- nn$ system may be visualized as a two-neutron halo with the two loosely bound neutrons orbiting about the Ξ^--hyperon "elementary" core, forming a shallow bound state with a diffuse structure. Such universal class of systems exploits the distinct separation of scale between the typical dynamical scale, $Q \sim \gamma_{\Xi n}^{(1)} \approx 1/a_{\Xi n}^{(1)} \sim 40$ MeV, associated with the "attractive pole" momentum of the ${}^3S_1$ $\Xi^- n$ dibaryon propagator (ignoring possible artifact due to the deep pole at $\gamma_{\Xi n}^{(0)} \approx 1/a_{\Xi n}^{(0)} \sim 340$ MeV associated with the repulsive ${}^1S_0$ $\Xi^- n$ sub-system), and the breakdown scale $\Lambda_H \sim m_\pi$ of standard $\not\pi$EFT [1–6, 8, 12, 52–56]. This implies that $\epsilon \sim Q/m_\pi \sim 1/3$ defines a reasonable expansion parameter that is amenable to a EFT treatment. A concise description on the general principles and methodology of $\not\pi$EFT framework used in the analyses of two- and three-body universality is provided in chapter-3. The effective Lagrangian is constructed on the basis of all possible available low-energy symmetries ($\mathscr{P}$, $\mathscr{C}$, $\mathscr{T}$ and Galilean invariance) and degrees of freedom. The interaction vertices are represented by local contact interactions and the Lagrangian is expressed in a derivative expansion of the fundamental fields. For our system, the fundamental degrees of freedom consist of the Ξ^--hyperon and neutron (n) fields. The LO non-relativistic Lagrangian is free from derivative terms and expressed as a sum of one-, two- and three-body parts, namely,

$$\mathscr{L}_{\not\pi\text{EFT}} = \mathscr{L}_{1-\text{body}} + \mathscr{L}_{2-\text{body}} + \mathscr{L}_{3-\text{body}} \ . \tag{5.1}$$

Below we consider each of the components of the effective Lagrangian separately.

One-body part. The terms $\mathscr{L}_\Xi$ and $\mathscr{L}_n$ constitute the one-body Lagrangian $\mathscr{L}_{1-\text{body}}$ corresponding to the kinetic part of the Ξ^--hyperon and neutron fields respectively, and are

Particle	Mass Symbol	Numerical Value (MeV)
Ξ-Hyperon	M_Ξ	1321.710
Neutron (n)	M_n	939.565

TABLE 5.1: PDG [191] values of particle masses considered in the analysis.

expressed in the physical basis as

$$\mathscr{L}_{1-\text{body}} = \mathscr{L}_\Xi + \mathscr{L}_n \ , \tag{5.2}$$

where

$$\begin{aligned} \mathscr{L}_\Xi &= \Xi^\dagger \left[i\partial_t + \frac{\nabla^2}{2M_\Xi} \right] \Xi \ , \\ \mathscr{L}_n &= n^\dagger \left[i\partial_t + \frac{\nabla^2}{2M_n} \right] n \ , \end{aligned} \tag{5.3}$$

where M_Ξ, and M_n are the physical masses of the Ξ^--hyperon and neutron fields respectively, as given in Table 5.1. It follows that the non-relativistic propagators associated with these fundamental fields are given by

$$\begin{aligned} iS_\Xi(p_0, \mathbf{p}) &= \frac{i}{p_0 - \frac{\mathbf{p^2}}{2M_\Xi} + i\eta} \ , \\ iS_n(p_0, \mathbf{p}) &= \frac{i}{p_0 - \frac{\mathbf{p^2}}{2M_n} + i\eta} ; \quad \eta \to 0 \ , \end{aligned} \tag{5.4}$$

where p_0 and $\mathbf{p}$ are temporal and spatial parts of the generic four-momentum p^μ.

Two-body part. In $\not\pi$EFT, as we discussed in Chapter 3, to deal with the formation of shallow S-wave bound states one needs to *unitarize* the two-body sector by employing the Q-counting rule [2–7]. To efficiently capture such two-body physics in the vicinity of a *non-trivial fixed-point* described by the RG of the two-body contact interactions, it was suggested to introduce auxiliary *dimer* fields in the effective Lagrangian [8, 12, 52, 53, 55] (also, see section 3.2.4). Thus, for the heteronuclear $\Xi^- nn$ system we need to introduce two types of dimer fields, namely, the isospin-spin triplet $(i = 1, j = 1)$ $\Xi^- n$ dibaryon field u_1 and the isospin-triplet spin-singlet $(i = 1, j = 0)$ nn dibaryon field u_0. Here we re-emphasize that the iso-triplet spin-singlet $(i = 1, j = 0)$ $\Xi^- n$ sub-system channel is considered decoupled from the picture as its physics lies beyond the realm of our halo EFT formalism. The corresponding two-body LO Lagrangian (written in the physical basis) in terms of the dibaryon fields is expressed as

$$\mathscr{L}_{2-\text{body}} = \mathscr{L}_{u_0} + \mathscr{L}_{u_1} \ , \tag{5.5}$$

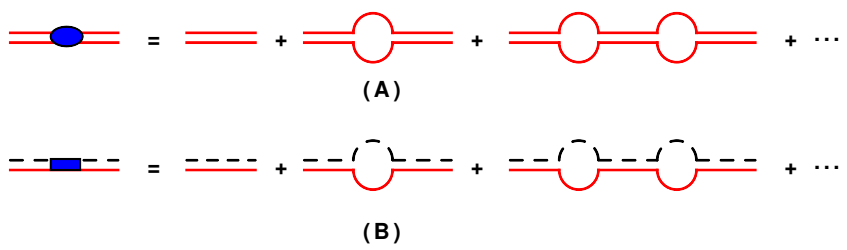

FIGURE 5.1: The renormalized dressed propagators for (upper pannel) ${}^1S_0$ nn, and (lower pannel) ${}^3S_1$ $\Xi^- n$ dibaryon fields. The dashed lines represent the Ξ^--hyperon field propagator and the solid lines represent the neutron field propagator.

where

$$\begin{aligned}
\mathscr{L}_{u_0} &= -(u_0)^{a\dagger}\left[i\partial_t + \frac{\nabla^2}{4M_n}\right](u_0)^a - y_0\left[(u_0)^{a\dagger}\left(n^T \hat{\mathscr{P}}^{(1,0)\,a}_{(nn)}\, n\right) + \text{h.c.}\right] , \\
\mathscr{L}_{u_1} &= -(\mathbf{u}_1)^{a\dagger}_k\left[i\partial_t + \frac{\nabla^2}{2(M_\Xi + M_n)}\right](\mathbf{u}_1)^a_k - y_1\left[(\mathbf{u}_1)^{a\dagger}_k\left(n^T \hat{\mathscr{P}}^{(1,1)\,a}_{(\Xi n)\,k}\,\Xi\right) + \text{h.c.}\right] ,
\end{aligned} \tag{5.6}$$

noting that the "wrong signs" in front of the respective kinetic terms suggest the non-dynamical or quasi-particle nature of the dibaryon fields. Here, $\hat{\mathscr{P}}^{(1,1)\,a}_{(\Xi n)\,k} = \frac{1}{2}\tau^2\tau^a\sigma_2\sigma_k$, and $\hat{\mathscr{P}}^{(1,0)\,a}_{(nn)} = \frac{1}{\sqrt{8}}\tau^2\tau^a\sigma_2$ are the spin-isospin projection operators, with σ_k and τ^a $(k, a = 1, 2, 3)$ being the Pauli matrices in the spin and isospin spaces respectively. The two-body non-derivatively coupled LO contact interactions or LECs $y_{0,1}$ between the respective dibaryons and their constituent elementary fields encode all UV physics that remain unresolved in the EFT. These couplings are easily fixed by the prescription given in Ref. [120]:

$$y_1 = \sqrt{\frac{2\pi}{\mu}}\,, \quad \text{and} \quad y_0 = \sqrt{\frac{4\pi}{M_n}}\,, \tag{5.7}$$

where $\mu = M_n M_\Xi/(M_n + M_\Xi) = 549.174$ MeV is the reduced mass of $\Xi^- n$ two-body subsystem. Next, we spell out the renormalized "dressed" (unitarized) propagators for the nn and $\Xi^- n$ dibaryon fields (cf. Fig. 5.1) consistent with the Q-counting scheme [2–7]:

$$\begin{aligned}
i\mathscr{D}_0(p_0, \mathbf{p}) &= \frac{4\pi}{y_0^2 M_n}\frac{i}{\gamma^{(0)}_{nn} - \sqrt{-M_n(p_0 - \frac{\mathbf{p}^2}{4M_n}) - i\eta} - i\eta} , \\
i\mathscr{D}_1(p_0, \mathbf{p}) &= \frac{2\pi}{y_1^2 \mu}\frac{i}{\gamma^{(1)}_{\Xi n} - \sqrt{-2\mu(p_0 - \frac{\mathbf{p}^2}{2(M_n+M_\Xi)}) - i\eta} - i\eta} ; \quad \eta \to 0 ,
\end{aligned} \tag{5.8}$$

where at the LO in $\not\pi$EFT, we have $\gamma^{(0)}_{nn} \to 1/a_{nn}$ and $\gamma^{(1)}_{\Xi n} \to 1/a^{(1)}_{\Xi n}$, as the (1,0) nn and (1,1) $\Xi^- n$ dibaryon (virtual or real bound) binding momenta respectively. It may be noted that the two scattering lengths are the only two-body input parameters in our LO EFT. Other parameters, such as S-wave effective range r_{nn} and $r_{\Xi n}$ formally contribute at NLO in the Q-counting scheme, which is beyond the scope of this work.

Three-body part. Formally the $\Xi^- nn$ three-body system with a possible fine-tuned two-body sector exhibits the well-known Efimov effect close to the unitary or resonant limit of the two-body interactions. This is reflected by the fact that the integral equations for the system with only two-body contact interactions become ill-defined in the asymptotic UV limit. The inherent reason for this anomalous UV behavior is the partial breakdown of the expected *fixed-point scaling* invariance of the system in the vicinity of bound states into the onset of a *discrete scaling* symmetry. A possible remedy to this problem, for instance, may be obtained by including a sharp momentum UV cut-off regulator $\Lambda_{\rm reg}$ in the integral equations, thereby, formally introducing another free parameter in the LO EFT (in addition to the two S-wave scattering lengths in the two-body sector). This simultaneously necessitates the introduction of LO three-body contact interactions (3BFs) as counterterms with scale dependent couplings, such as $g_3 = g_3(\Lambda_{\rm reg})$, to renormalize the artificial cut-off dependence. The resulting atypical scaling behavior gets reflected through the emergence of an RG limit cycle behavior in the 3BF couplings (for a pedagogical review on this topic, see Ref. [12]; also see section 3.3.2). Here we present a certain choice of the LO three-body Lagrangian consistent with the reparametrization symmetries of the coupled system of integral equation, and given by

$$\begin{aligned}\mathscr{L}_{3-\rm body} \;=\; -\frac{g_3(\Lambda_{\rm reg})}{\Lambda_{\rm reg}^2}\Bigg[&\frac{M_\Xi y_1^2}{2}\Big\{(\mathbf{u}_1)_l^a\;\hat{\mathscr{P}}_l^{ab}\;n\Big\}^\dagger\Big\{(\mathbf{u}_1)_k^c\;\hat{\mathscr{P}}_k^{cb}\;n\Big\}\\ &-\frac{\sqrt{3}M_n y_0 y_1}{\sqrt{2}}\Big\{(\mathbf{u}_1)_l^a\;\hat{\mathscr{P}}_l^{ab}\;n\Big\}^\dagger\Big\{u_0^c\;\hat{\mathscr{P}}^{cb}\;\Xi\Big\}+\text{h.c.}\Bigg],\end{aligned} \tag{5.9}$$

where the spin-isospin projection operators have the following forms:

$$\begin{aligned}\Big[\hat{\mathscr{P}}_k^{cb}\Big]_{\alpha\beta} &= \frac{1}{3\sqrt{3}}\Big[(\tau^c\tau^b)_{\alpha\beta}+\delta_{cb}\delta_{\alpha\beta}\Big]\sigma_k\;,\\ \Big[\hat{\mathscr{P}}^{cb}\Big]_{\alpha\beta} &= \frac{1}{3}\Big[(\tau^c\tau^b)_{\alpha\beta}+\delta_{cb}\delta_{\alpha\beta}\Big]\;,\end{aligned} \tag{5.10}$$

with $\alpha,\beta=1,2$ being the isospin-1/2 SU(2) indices [192]. The cut-off dependence of g_3 is *a priori* undetermined in the EFT and can be fixed only using a three-body datum, e.g., the three-body binding energy B_3 or the corresponding scattering length a_3.[6] However, none of this empirical information is available currently, either from experimental data or from *ab initio* lattice QCD simulations. Due to such an acute paucity of data, it becomes imperative to rely on some of the erstwhile phenomenological models, before our LO EFT analysis, can be made viable to yield some qualitative insight. Thus, for example, here we rely on the $\Xi^- nn$ binding energy estimates from the Faddeev calculations provided by the potential model analyses of Refs. [161, 162, 164–166].

[6]The three-body datum in this case is analogous to the information on parameters, such as Λ_* or κ_*, in addition to the two-body scattering length a_0, necessary for the description of the Efimov spectrum, as detailed in Appendix C for a three-boson system.

5.2.2 Coupled STM Integral Equations

For the sake of theoretical analysis, we study the $\Xi^- nn$ system in both the kinematical three-body bound and scattering domains. For this purpose, we choose a representative elastic reaction channel corresponding to the low-energy $1 + 2 \to 1 + 2$ scattering process with dominant S-wave contribution, namely,

$$n + (\Xi^- n)_t \longrightarrow n + (\Xi^- n)_t \ . \tag{5.11}$$

Here we must emphasize that this "reference" scattering process is chosen solely for demonstrating our theoretical methodology, irrespective of the infeasibility of performing such experiments at current facilities. The chosen reaction channel yields a set of two coupled *Fredholm-type* integral equations in the momentum space. While their eigenvalues yield all possible allowed trimer binding energies (B_3), the eigenvectors yield the scattering amplitudes of the coupled elastic and inelastic channels. In Fig. 5.2, we display the relevant Feynman diagrams for the above-mentioned scattering process expressed in term of the two *half-off-shell* S-wave projected scattering amplitudes, namely, $t_A(k, p; E)$ representing the elastic process $n + u_1 \to n + u_1$, and $t_B(k, p)$ representing the inelastic process $n + u_1 \to \Xi^- + u_0$. Here $k = |\mathbf{k}|$ ($p = |\mathbf{p}|$) denotes the on-shell (off-shell) incoming (outgoing) relative three-momentum in the center-of-mass (CM) system, and E is the total CM kinetic energy of the three-body system, given by

$$E = \pm \frac{k^2}{2\mu_{n(n\Xi)}} - B_2 \quad ; \quad B_2 = \frac{\left(\gamma^{(1)}_{\Xi n}\right)^2}{2\mu} = 1.47 \text{ MeV} \, , \tag{5.12}$$

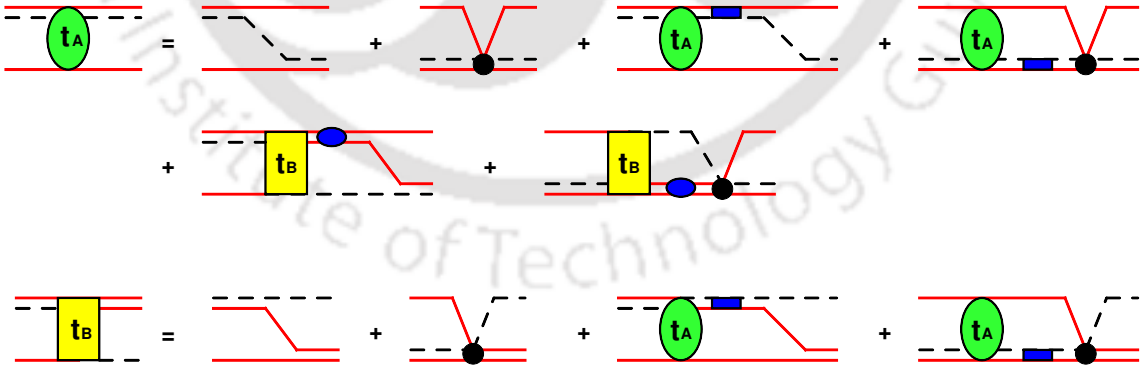

FIGURE 5.2: Feynman diagrams for the representative coupled channel elastic scattering process, $n + (\Xi^- n)_t \to n + (\Xi^- n)_t$, where "$t$" is used to denotes the ${}^3S_1$ $\Xi^- n$ sub-system. The solid (dash) line represents the neutron (Ξ^--hyperon) propagator. The off-shell double lines with insertions of the small empty oval (square) blobs represent the renormalized dressed ${}^1S_0$ nn (u_0) and ${}^3S_1$ $\Xi^- n$ (u_1) dibaryon field propagators. The large blob t_A (t_B) denotes the elastic (inelastic) half-off-shell scattering amplitude for the $n + u_1 \to n + u_1$ ($n + u_1 \to \Xi^- + u_0$) scattering processes. The dark blobs represent the insertions of leading order three-body contact interactions.

where the "−" sign is applicable for the kinematical three-body bound state domain and the "+" sign for the scattering domain. B_2 is the CM binding energy of a possible shallow-bound $(\Xi^- n)_t$ sub-system which also sets the scale for the particle-triplet-dimer $(n + u_1)$ break-up threshold energy,[7] and $\mu_{n(n\Xi)} = M_n(M_\Xi + M_n)/(2M_n + M_\Xi) = 663.768$ MeV is the corresponding reduced mass of three-body (particle-dimer) system. The construction methodology of the integral equations is similar to those employed in several earlier $\not\pi$EFT works [64, 88, 89, 108, 109] (also see section 3.3.1). The renormalized S-wave projected coupled (elastic and inelastic channels) STM integral equations (a detailed calculation is presented in Appendix C) with the introduced cut-off regulator $\Lambda_{\rm reg}$ are given as[8]

$$\begin{aligned} t_A^{(R)}(p,k;E) &= Z_{\Xi n}\frac{(y_1^2 M_\Xi)}{2}\left[K_{(a)}(p,k;E) - \frac{g_3(\Lambda_{\rm reg})}{\Lambda_{\rm reg}^2}\right] \\ &\quad - \frac{M_\Xi}{2\pi\mu}\int_0^{\Lambda_{\rm reg}} dq\, q^2 \left[K_{(a)}(p,q;E) - \frac{g_3(\Lambda_{\rm reg})}{\Lambda_{\rm reg}^2}\right] \\ &\qquad \times \mathscr{D}_1\left(E - \frac{q^2}{2M_n}, \mathbf{q}\right) t_A^{(R)}(q,k;E) \\ &\quad + \frac{\sqrt{6}y_1}{\pi y_0}\int_0^{\Lambda_{\rm reg}} dq\, q^2 \left[K_{(b2)}(p,q;E) - \frac{g_3(\Lambda_{\rm reg})}{\Lambda_{\rm reg}^2}\right] \\ &\qquad \times \mathscr{D}_0\left(E - \frac{q^2}{2M_\Xi}, \mathbf{q}\right) t_B^{(R)}(q,k;E)\ , \end{aligned} \tag{5.13}$$

and

$$\begin{aligned} t_B^{(R)}(p,k;E) &= -Z_{\Xi n}\sqrt{\frac{3}{2}}\,(y_1 y_0 M_n)\left[K_{(b1)}(p,k;E) - \frac{g_3(\Lambda_{\rm reg})}{\Lambda_{\rm reg}^2}\right] \\ &\quad + \sqrt{\frac{3}{2}}\frac{M_n y_0}{\mu\pi y_1}\int_0^{\Lambda_{\rm reg}} dq\, q^2 \left[K_{(b1)}(p,q;E) - \frac{g_3(\Lambda_{\rm reg})}{\Lambda_{\rm reg}^2}\right] \\ &\qquad \times \mathscr{D}_1\left(E - \frac{q^2}{2M_n}, \mathbf{q}\right) t_A^{(R)}(q,k;E)\ , \end{aligned} \tag{5.14}$$

where the term $K_{(a)}$ denotes the S-wave projected Ξ-exchange interaction kernel, while $K_{(b_1,b_2)}$ are two different variants of the n-exchange interaction kernel, namely,

$$K_{(a)}(p,\kappa;E) = \frac{1}{2p\kappa}\ln\left(\frac{p^2+\kappa^2+ap\kappa-2\mu E}{p^2+\kappa^2-ap\kappa-2\mu E}\right)\ , \tag{5.15}$$

[7] In our halo EFT formalism B_2 corresponds to the pole position of the u_1 dibaryon propagator. Its value may be compared with the binding energy of the putative D^* state in the (1,1) ΞN channel, as predicted by the potential model analyses of Refs. [165, 166, 183, 184].

[8] Note that the sign convention for the dimensionless three-body couplings g_3 are taken opposite to the corresponding coupling g_3 for the three-boson system, as followed in Chapter 3 [cf. Eq. (3.55)], accounting for the negative sign in front of g_3 in the above expressions for $t_{A,B}^{(R)}$.

$$K_{(b_1)}(p,\kappa;E) = \frac{1}{2p\kappa}\ln\left(\frac{bp^2+\kappa^2+p\kappa-M_nE}{bp^2+\kappa^2-p\kappa-M_nE}\right),$$
$$K_{(b_2)}(p,\kappa;E) = \frac{1}{2p\kappa}\ln\left(\frac{p^2+b\kappa^2+p\kappa-M_nE}{p^2+b\kappa^2-p\kappa-M_nE}\right). \quad (5.16)$$

The generic momentum κ denotes either the incoming on-shell relative momentum (k) or the loop momentum (q). Also, $a = 2\mu/M_\Xi$ and $b = M_n/(2\mu)$ are two mass-dependent parameters. The above half-off-shell renormalized amplitudes are related to the corresponding unrenormalized amplitudes $t_{A,B}(p,k;E)$ by

$$t^{(R)}_{A,B}(p,k;E) = \sqrt{Z_{\Xi n}}\, t_{A,B}(p,k;E)\, \sqrt{Z_{\Xi n}}\,, \quad (5.17)$$

where

$$Z^{-1}_{\Xi n} = \frac{y_1^2\mu^2}{2\pi\gamma^{(1)}_{\Xi n}}, \quad (5.18)$$

is the wavefunction renormalization associated with the possible bound $(\Xi^- n)_t$ sub-system. Finally, the renormalized elastic amplitude is used to obtain the S-wave $n-(\Xi^- n)_t$ three-body scattering length by considering the threshold limit of the on-shell momentum $k \to 0$, namely,

$$a_3 = -\lim_{k\to 0}\frac{\mu_{n(n\Xi)}}{2\pi}\, t^{(R)}_A(k,k)\,. \quad (5.19)$$

5.2.3 Asymptotic Analysis

In order to assess that the coupled STM integral equations indeed have the potentiality to yield three-body bound state solutions, one needs to check for the possible manifestation of the Efimov effect at the asymptotic UV limit as $\Lambda_{\rm reg} \to \infty$ [12] (cf. section 3.3.2). In this case, all other low-energy/momentum scales in the problem, e.g., $E, \gamma^{(1)}_{\Xi n}, \gamma^{(0)}_{nn}, k \ll p, q \sim \Lambda_{\rm reg} \lesssim \infty$, become irrelevant, and the integral equations can be well approximated by considering only the homogeneous parts (i.e., excluding the tree diagram contributions in Fig. 5.2) and dropping all the k dependence and three-body interactions (g_3) terms. Thus, with no other relevant scales in the theory, the STM equations become *dilation* invariant and symmetric under the inversion transformation $q \to 1/q$. Consequently, the half-off-shell channel amplitudes exhibit a power-law scaling, namely, $t_{A,B}(\kappa) \sim \kappa^{s-1}$, with $\kappa \sim \Lambda_{\rm reg}$ and a complex-valued exponent s, an undetermined three-body parameter. By performing a sequence of *Mellin* transformations the integral equations can be converted into a single transcendental equation that solves for the exponent s, namely,

$$1 = \frac{M_\Xi}{2\mu C_1}\left[\frac{\sin[s\sin^{-1}(a/2)]}{s\cos(\pi s/2)}\right] + \frac{3M_n}{\mu C_1 C_2}\left[\frac{\sin[s\cot^{-1}\sqrt{4b-1}]}{s\cos(\pi s/2)}\right]^2, \quad (5.20)$$

where

$$C_1 = \sqrt{\frac{\mu}{\mu_{n(n\Xi)}}}, \quad \text{and} \quad C_2 = \sqrt{\frac{M_n}{2\mu_{\Xi(nn)}}}\,, \tag{5.21}$$

and $\mu_{\Xi(nn)} = 2M_nM_\Xi/(2M_n + M_\Xi) = 775.942$ MeV is the reduced mass of the $\Xi^- + u_0$ particle-dimer system. Solving Eq. (5.20) yields an imaginary solution, i.e., $s = \pm is_0^\infty = \pm i0.803391\cdots$. The solution immediately suggests the existence of an asymptotic UV RG limit cycle with a discrete scaling symmetry associated with the scale factor, $\lambda_\infty = e^{\pi/s_0^\infty} = 49.919712\cdots$. This formally implies that our LO EFT manifests Efimov effect in the unitary limit of the Ξ^-nn system. Consequently, it becomes imperative to include scale-dependent 3BF as counterterms in the effective Lagrangian to renormalize the ill-defined asymptotic limit of the STM equations with two-body interaction. As elucidated by power counting arguments in the section 3.3, such non-derivative 3BF terms are naturally enhanced to get promoted to LO for consistency of the renormalization scheme [52, 53]. Here we must, however, mention that the asymptotic scaling exponent $s_0^\infty = 0.803391\cdots$ considerably differs from the expected value, $(s_0^\infty)_{\text{expect}} \sim 1.01$, based on the universal RG limit cycle scaling depending on the relative three-particle mass ratios [12]. This difference is attributed to the effect of excluding the isospin-triplet spin-singlet (1,0) Ξ^-n sub-system channel from the STM equations whose dynamics are not directly amenable to our low-energy EFT description.

5.3 Results and Discussion

In this section, we present the results of our preliminary investigation of the sharp cut-off regulator (Λ_{reg}) dependence of the Faddeev-type STM integral equations (5.13) and (5.14), at non-asymptotic low-energy scales. For the sake of numerical evaluations, we use the particle masses as presented in Table 5.1, while the S-wave scattering lengths $a_{nn} = -18.63$ fm [30] and $a_{\Xi n}^{(j=1)} = 4.911$ fm [183, 184][9] constitute the principal input two-body parameters in our LO EFT framework. In the last section, our asymptotic analysis demonstrated the evidence of Efimov effect at the unitary limit of the Ξ^-nn system with an RG limit cycle discrete scaling symmetry determined by the multiplicative factor $\lambda_\infty = e^{\pi/s_0^\infty} \sim 50$. With $\kappa^{(1)} \equiv \gamma_{\Xi n}^{(1)} \sim 40$ MeV as the typical momentum scale of the problem, it is natural to expect that the next higher momentum scale appears at $\kappa^{(2)} \equiv \lambda_\infty\gamma_{\Xi n}^{(1)} \sim 2$ GeV $\gg \Lambda_H \sim m_\pi$, which is well beyond the accessibility of our low-energy EFT description. Hence, it is likely that at the most one Efimov-like state emerges as a plausible bound Ξ^-nn hypernucleus, if at all. Figure 5.3 shows the cut-off dependence of the three-body contact interaction coupling $g_3(\Lambda_{\text{reg}})$. In the absence of datum to constrain the unknown coupling g_3, our *strategy* is to

[9]For our calculation we have taken $a_{\Xi n}^{(j=1)} = 4.911$ fm rather than $a_{\Xi n}^{(j=1)} = 0.144$ fm from Ref.[185]. However, considering the very small value of $a_{\Xi n}^{(j=1)} = 0.144$ fm the three-body Ξ^-nn bound state is not possible within the acceptable range of cut-off scale Λ_{reg}.

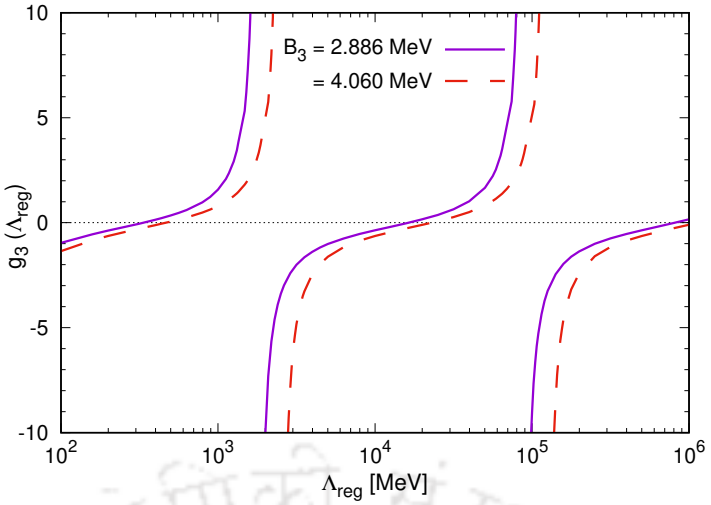

FIGURE 5.3: The approximate RG limit cycle behavior of the three-body coupling g_3 for the $\Xi^- nn$ ($I = 3/2$, $J = 1/2$) system as a function of the cut-off scale $\Lambda_{\rm reg}$. The results are obtained by numerically solving the STM integral equations (5.13) and (5.14). The input three-body binding energies $B_3 = 2.886$, 4.06 MeV, are predictions from the Faddeev calculation based potential models [162, 166]. The input S-wave spin-isospin triplet $\Xi^- n$ scattering length $a_{\Xi n}^{(j=1)} = 4.911$ fm is provided by the recent ESC08c Nijmegen potential model analyses [183, 184].

hypothetically assume at the very outset that the $\Xi^- nn$ system is bound, with ground state eigenenergy ($E = -B_3$) coinciding with the existing (Faddeev calculations) model predictions of Refs. [162, 164–166]. We thereby fix our benchmark range of input values of the $\Xi^- nn$ binding energy, namely, between $B_3 = 2.886$ MeV taken from Ref. [166], and $B_3 = 4.06$ MeV taken from Ref. [162]. Notably, both predictions rely on the same two-body input parameters (e.g., $a_{\Xi n}^{(1)} = 4.911$ fm) provided by the recent ESC08c Nijmegen model analyses [183, 184].[10] The figure displays the typical quasi-periodic log-singularities of *approximate* RG limit cycles for the two aforementioned limiting B_3 inputs. The corresponding non-asymptotic scale factor, $\lambda_n \lesssim \lambda_\infty$, may be obtained by considering the ratio of two successive cut-offs where the three-body coupling vanishes, i.e., if $g_3\left(\Lambda_{\rm reg}^{(n)}\right) = g_3\left(\Lambda_{\rm reg}^{(n+1)}\right) = 0$, then

$$\lambda_n = \frac{\Lambda_{\rm reg}^{(n+1)}}{\Lambda_{\rm reg}^{(n)}} \; ; \quad n = 1, 2, .., \infty \; , \tag{5.22}$$

where $\Lambda_{\rm reg}^{(n)}$ is the cut-off corresponding to $n^{\rm th}$ zero of g_3. Table 5.2 displays some of the estimated non-asymptotic scale factors λ_n corresponding to successive pairs of zeros of each RG limit cycle obtained for the two limiting input B_3 values. In each case, the scale factor λ_n is obtained close to yet less than the asymptotic value λ_∞. By progressively choosing larger pairs of the successive zeros of g_3, i.e., with $n \to \infty$, λ_n is found to converge rapidly to λ_∞.

[10] The predicted value $B_3 = 2.886$ MeV obtained in Faddeev calculation analysis of Ref. [166] resulted from considering both the repulsive (1,0) and attractive (1,1) ΞN channels. Whereas, the value $B_3 = 4.06$ MeV obtained in the Faddeev analysis of Ref. [162] resulted from considering only the latter attractive channel. Nevertheless, irrespective of these details, we consider these predicted values as given three-body inputs to our EFT analysis.

Binding Energy B_3 (MeV)	$n \in \mathbb{Z}_+$	n^{th} zero of g_3 $\Lambda_{\text{reg}}^{(n)}$ (MeV)	$(n+1)^{\text{th}}$ zero of g_3 $\Lambda_{\text{reg}}^{(n+1)}$ (MeV)	Scale factor $\lambda_n = \Lambda^{(n+1)}/\Lambda^{(n)}$
2.886 [166]	1	334.283	16344.134	$48.893105\cdots$
	2	16344.134	815412.631	$49.890232\cdots$
	3	815412.631	40704680.527	$49.919119\cdots$
	4	40704680.527	2031965537.021	$49.919702\cdots$
4.06 [162]	1	465.937	22919.007	$49.189069\cdots$
	2	22919.007	1143628.429	$49.898690\cdots$
	3	1143628.429	57089119.370	$49.919290\cdots$
	4	57089119.370	2849872042.899	$49.919706\cdots$

TABLE 5.2: The approximate RG limit cycle behavior with the discrete scaling symmetry factor $\lambda_n \to \lambda_\infty$, obtained by solving the integral equations (5.13) and (5.14) for the $\Xi^- nn$ ($I = 3/2$, $J = 1/2$) system. Here, results for $n \leq 4$ display a rapid convergence of the scale parameter toward the asymptotic limit, $\lambda_\infty = 49.919712\cdots$. The input three-body binding energies $B_3 = 2.886$, 4.06 MeV are predictions from the Faddeev calculation based on potential models [162, 166] with input S-wave $\Xi^- n$ $^3S_1$ scattering length $a_{\Xi n}^{(1)} = 4.911$ fm, provided by the ESC08c Nijmegen potential model analyses [183, 184].

Next, in Fig. 5.4 we display the cut-off variation of the binding energy B_3 excluding the 3BF terms, i.e., with $g_3 = 0$ in the STM equations. In particular, due to the ambiguities concerning the precise nature of the (1,1) ΞN sub-system interactions between different existing phenomenological analyses [157, 167, 172–184], we consider here two representative scenarios with contrasting perspectives as elucidated below (both cases can formally lead to the emergence of Efimov-like states):

- First, the scenario with the input positive $(\Xi^- n)_t$ scattering length, e.g., $a_{\Xi n}^{(j=1)} = 4.911$ fm, as predicted by the updated ESC08c Nijmegen potential model analyses of Refs. [183, 184], suggests a strongly attractive $^3S_1$ $\Xi^- n$ sub-system commensurate with the likely existence of a threshold bound state (D^*) [165, 166]. Consequently, in the three-body sector with a pair of likely bound $(\Xi^- n)_t$ sub-systems and a virtual bound nn sub-system, the $\Xi^- nn$ system assumes a halo-bound *samba-configuration* [24] structure emerging from the particle-triplet-dimer $(n + (\Xi^- n)_t)$ break-up threshold at the CM energy $E = -B_2$. This corresponds to the solid (red) line curve in the left panel of Fig. 5.4, representing the regulator dependence of the *relative* binding energy $B_d = B_3 - B_2$, for the ground ($n = 0$) Efimov-like state which appears at the *critical cut-off* scale $\Lambda_{\text{crit}}^{(0)} \approx 80$ MeV.

- Second, the scenario with the input negative $(\Xi^- n)_t$ scattering length, e.g., as predicted by the two recent SU(3) chiral EFT analyses, namely, $a_{\Xi n}^{(j=1)} = -0.09$ fm [179] and -1.17 fm [180], suggests a weakly attractive $^3S_1$ $\Xi^- n$ sub-system that is unlikely to exhibit any two-body bound state. Consequently, in the three-body sector with no bound two-body sub-systems, the $\Xi^- nn$ system assumes a bound *borromean-configuration* [24]

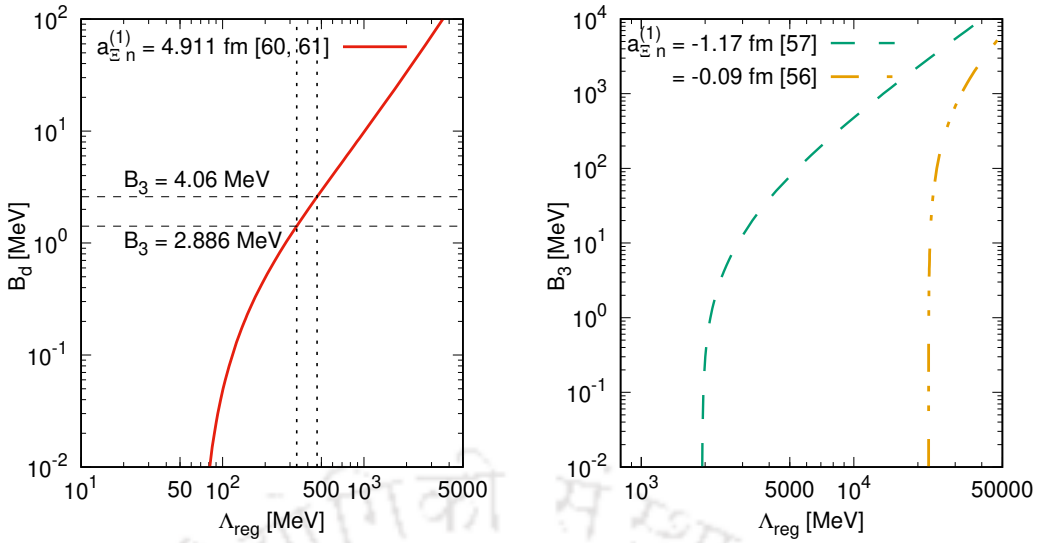

FIGURE 5.4: Cut-off regulator ($\Lambda_{\rm reg}$) dependence of the three-body binding energy of the $\Xi^- nn$ ($I = 3/2$, $J = 1/2$) system, obtained by solving the coupled integral equations (5.13) and (5.14), excluding the three-body contact interactions [i.e. $g_3(\Lambda_{reg}) = 0$]. **Left panel:** Three-body binding energy $B_d = B_3 - B_2$, relative to the $n+(\Xi^- n)_t$ particle-dimer threshold $-E = B_2 = 1.47$ MeV, with the input S-wave ${}^3S_1$ $\Xi^- n$ scattering length $a^{(1)}_{\Xi n} = 4.911$ fm, as predicted by the recently updated ESC08c Nijmegen potential model analyses [183, 184]. The regulator-independent predictions, namely, $B_3 = 2.886$ MeV and 4.06 MeV, from the Faddeev calculation-based potential model analyses [162, 166] for the same $a^{(j=1)}_{\Xi n}$ input are displayed for comparison. **Right panel:** Three-body binding energy B_3 relative to the three-particle threshold with input $a^{(j=1)}_{\Xi n} = -0.09\,, -1.17$ fm, as predicted by the two recent SU(3) chiral EFT analyses [179, 180].

structure emerging from the three-particle break-up threshold $E = 0$. This corresponds to the two broken line curves in the right panel of Fig. 5.4, representing the regulator dependence of B_3 for the respective ground Efimov-like states which appear above the threshold at the critical values, $\Lambda^{(0)}_{\rm crit} \approx 1940$ MeV for Ref. [180] and 22470 MeV for Ref. [179].

Evidently, with such large critical cut-offs, the latter scenario most likely not be supported in our low-energy EFT framework, *vis-a-vis*, the Efimov-like ground state does not physically manifest as a bound Ξ-hypernucleus. In contrast, the small critical cut-off in the former scenario lies well within the EFT validity domain, indicating an encouraging prospect for a potentially feasible $\Xi^- nn$ Efimov state. In what follows, we shall only discuss our results pertaining to the former choice of the $\Xi^- nn$ scenario.

In the absence of the three-body contact interactions for renormalization our results for the three-body binding energy exhibit considerable sensitivity to the cut-off variations. Figure 5.4 also compares our results with the regulator-independent predictions for the $\Xi^- nn$ binding energy from the potential models [162, 166] which also rely on the two-body inputs from the Nijmegen ESC08c model analyses [183, 184]. We find that our scale-dependent eigenenergies from the STM equations reproduce the model predictions, namely, $B_3 = 2.886$ MeV

of Ref. [166] and $B_3 = 4.06$ MeV of Ref. [162] at the cut-off scales $\Lambda_{\rm reg} \approx 334$ MeV and $\Lambda_{\rm reg} \approx 465$ MeV respectively. The same result is demonstrated more conspicuously in Fig. 5.5 where we plot the variation of the eigenenergy B_3 by (hypothetically) varying the scattering length $a^{(1)}_{\Xi n} > 0$ for several fixed cut-offs $\Lambda_{\rm reg}$ excluding 3BF terms. The chosen potential model predicted range, 2.886 MeV $\lesssim B_3 \lesssim$ 4.06 MeV, as demarcated by the horizontal band in the figure, is well constrained within our regulator range, 334 MeV $\lesssim \Lambda_{\rm reg} \lesssim$ 465 MeV.[11] In particular, our summary Table 5.3 displays the $\Lambda_{\rm reg}$ values at which our EFT solutions reproduce several more of the existing Faddeev calculation-based model predictions for the $\Xi^- nn$ binding energy [162, 164–166]. Although the above regulator range apparently seems well beyond the expected $\not\pi$EFT hard scale $\Lambda_H \sim m_\pi$, the model results may still be accommodated within the framework of a modified EFT having an extended domain of validity. Consequently, such a modified halo $\not\pi$EFT should have a larger breakdown scale, say, $\widetilde{\Lambda}_H \lesssim 500$ MeV, where interactions between the Ξ-hyperon and neutron are possibly dominated by two-pion ($\pi\pi$) or σ-meson exchange mechanisms. We note that one-pion exchanges are typically ruled out by isospin invariance in strong processes.

Finally, we give a simple demonstration of the predictability of our EFT framework. To this end, we attempt a *naive* estimation of the $\Xi^- nn$ ($I = 3/2$, $J = 1/2$) three-body scattering length, or more precisely the $n - (\Xi^- n)_t$ elastic S-wave scattering length a_3, by utilizing

[11] Note that such an unrenormalized result by excluding the three-body force g_3 is otherwise physically ill-defined. However, given that currently there exists no three-body datum (e.g., three-body scattering length a_3) necessary to fix this regulator dependence of g_3, only a crude estimate of the EFT regulator range consistent with our benchmark range of B_3 values is implied here.

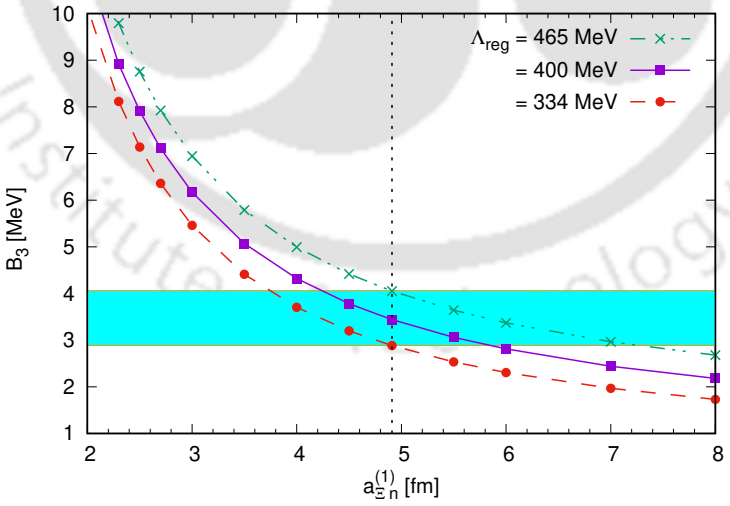

FIGURE 5.5: Variation of the three-body binding energy B_3 of the $\Xi^- nn$ ($I = 3/2$, $J = 1/2$) system as a function of input positive values of the S-wave $^3S_1$ $\Xi^- n$ scattering length $a^{(1)}_{\Xi n}$ for fixed cut-offs $\Lambda_{\rm reg}$ excluding three-body interactions. The horizontal shaded band represents our benchmark range of values of B_3 considered between the limits, $B_3 = 2.886$ MeV and 4.06 MeV, predicted by the Faddeev calculation based potential model analyses [162, 166]. The vertical dotted line represents our choice of the input scattering length $a^{(1)}_{\Xi n} = 4.911$ fm, as predicted by the recently updated ESC08c Nijmegen potential model analyses [183, 184].

the potential model predicted three-body binding energy information from Refs. [162, 164–166]. Here we need to solve our coupled STM integral equations (5.13) and (5.14) in the kinematical scattering domain. Subsequently, the three-body scattering length is obtained by considering the on-shell threshold limit of the renormalized elastic scattering amplitude $t_A^{(R)}$ [cf. Eq. (5.19)]. Solving the STM equations with the 3BF terms excluded (i.e., with $g_3 = 0$) leads to strong regulator dependence with the resulting amplitude displaying quasi-periodic singularities akin to the limit cycle behavior (cf. left panel of Fig. 5.6). Such divergences are renormalized by introducing the 3BF counterterms with the running coupling $g_3(\Lambda_{\rm reg})$ already fixed using the RG limit cycles corresponding to model predicted B_3 inputs (cf. Fig. 5.3).

Figure 5.6 (right panel) depicts the regulator dependence of the three-body scattering length $a_3(\Lambda_{\rm reg})$ renormalized by the 3BF terms. As mentioned, the scale dependence of the 3BF coupling $g_3(\Lambda_{\rm reg})$ is fixed using the RG limit cycles corresponding to the potential model inputs for B_3 [162, 166]. The renormalized plots still exhibit a residual regulator dependence stemming from the low cut-off scale sensitivity of the counterterms owing to the decoupling of most underlying physics. However, for sufficiently large cut-off, say $\Lambda_{\rm reg} \gtrsim 400$ MeV, most of the underlying low-energy three-body dynamics are well captured in our solutions to the integral equations. Consequently, renormalizing a_3 using the counterterms becomes more

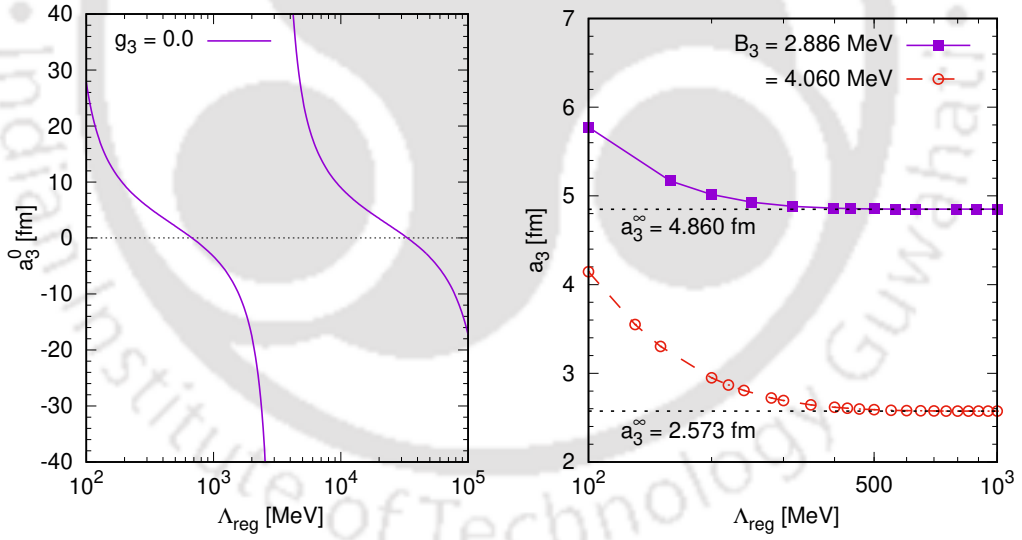

FIGURE 5.6: Regulator ($\Lambda_{\rm reg}$) dependence of the $n - (\Xi^- n)_t$ elastic S-wave three-body scattering length a_3, obtained by solving the coupled integral equations (5.13) and (5.14) with input S-wave scattering length $a_{\Xi n} = 4.911$ fm, taken from the updated Nijmegen model analyses [183, 184]. **Left panel:** The unrenormalized scattering length $a_3 \to a_3^0$ excluding the three-body coupling, i.e., $g_3 = 0$. **Right panel:** The renormalized scattering length including the three-body coupling $g_3 \neq 0$. The scale dependence of $g_3(\Lambda_{\rm reg})$ is determined using the respective RG limit cycles (cf. Fig. 5.3) corresponding to the two three-body inputs, $B_3 = 2.886$ MeV and 4.06 MeV, taken from the Faddeev calculation model analyses [162, 166]. Our predictions, namely, $a_3^\infty = 4.860$ fm and 2.573 fm, correspond to the respective asymptotic limits.

effective at large $\Lambda_{\rm reg}$ leading to a well-defined asymptotic limit:

$$a_3^{\infty} = \lim_{\Lambda_{\rm reg}\to\infty} a_3(\Lambda_{\rm reg})\,. \tag{5.23}$$

Hence, for each B_3 input a constant value a_3^{∞} is obtained, as demanded by renormalization invariance, representing our predicted three-body scattering length. In particular, our limiting benchmark inputs, $B_3 = 2.886$ MeV and 4.06 MeV, lead to $a_3^{\infty} = 4.860$ fm and 2.573 fm respectively. In addition, our summary Table 5.3 displays some intermediate results corresponding to two other existing model predictions, namely, $B_3 = 3.89$ MeV and 3.00 MeV, from the Faddeev calculations analyses of Refs. [164, 165]. Here we point out that for possible negative choice of the ${}^3S_1$ $\Xi^- n$ scattering length, such as the two recent SU(3) chiral EFT predictions, namely, $a_{\Xi n}^{(1)} = -0.09$, -1.17 fm [179, 180], the $(\Xi^- n)_t$ sub-system is unbound with no kinematical particle-dimer scattering domain below the three-particle break-up threshold, i.e., $E < 0$.

Our predicted range of three-body scattering lengths represents a *naive* ballpark estimate based on the induced universal correlations which are expected to manifest in a halo-bound

Scattering length $a_{\Xi n}^{(1)}$(fm)	Binding energy B_3 (MeV)	Cut-off $\Lambda_{\rm reg}^{(g_3=0)}$ (MeV)	Scattering length a_3^{∞} (fm)
4.911 (Nijmegen model) [183, 184]	2.886 [166]	334	4.860
	2.89 [164]	335	4.849
	3.00 [165]	348	4.562
	4.06 [162]	465	2.573
-0.09 (Relativistic Chiral EFT) [179]	2.886 [166]	22590	-
	2.89 [164]	22591	-
	3.00 [165]	22595	-
	4.06 [162]	22633	-
-1.17 (G-matrix Chiral EFT) [180]	2.886 [166]	2333	-
	2.89 [164]	2334	-
	3.00 [165]	2345	-
	4.06 [162]	2440	-

TABLE 5.3: Summary of our EFT results with three different input S-wave ${}^3S_1$ $\Xi^- n$ scattering lengths, namely, $a_{\Xi n}^{(1)} = 4.911$ fm, taken from the updated ESC08c Nijmegen model analyses [183, 184], $a_{\Xi n}^{(1)} = -0.09$ fm, taken from the relativistic LO chiral EFT analysis [179], and $a_{\Xi n}^{(1)} = -1.17$ fm, taken from the NLO chiral EFT-based non-relativistic G-matrix analysis [180]. Displayed are the regulator scales $\Lambda_{\rm reg}^{(g_3=0)}$ at which the Efimov ground state eigenenergy (by excluding g_3) reproduces each of several existing potential model predictions on the three-body binding energies B_3 of the $\Xi^- nn$ system [162, 164–166]. Also summarized are our predicted three-body scattering length (a_3^{∞}) corresponding to each model input for B_3, with the three-body coupling $g_3(\Lambda_{\rm reg})$ determined by the respective RG limit cycles. The results corresponding to the $a_{\Xi n}^{(1)} < 0$ scenario have no kinematical particle-dimer scattering domain for $E < 0$ and the three-body system is likely to remain unbound. In contrast, the $a_{\Xi n}^{(1)} > 0$ scenario shows encouraging prospect for a physically realizable $\Xi^- nn$ Efimov state.

$\Xi^- nn$ system, albeit approximations considered in the analysis. To elucidate one of the inherent universal features, it is worth demonstrating the B_3 versus a_3^∞ correlations corresponding to our preferred choice of the input $\Xi^- n$ scattering length, namely, $a_{\Xi n}^{(1)} = 4.911$ fm [183, 184]. This yields the well-known Phillips line correlation plot for the $\Xi^- nn$ system, as depicted in Fig. 5.7. The curve diverges as $B_3 \to B_2 = 1.47$ MeV, the $n + (\Xi^- n)_t$ particle-triplet-dimer threshold, whenever an Efimov-like bound state emerges at zero-energy threshold (i.e., with $B_d = B_3 - B_2 = 0$). A second virtual bound three-body state with a large negative value of a_3^∞ is expected to emerge around $B_3^{(\text{virt})} = e^{\pi/s_0} B_2 \approx 70$ MeV, where the Phillips line diverges again. However, the latter state lies outside the domain of validity of standard $\not\pi$EFT with an estimated breakdown energy scale $-E_{\text{break}} \sim 14$ MeV, as determined by the three-body binding momentum of the order of the pion mass, i.e., $\gamma_3 = \sqrt{-2\mu_{n(n\Xi)} E_{\text{break}}} \sim m_\pi$. The four data points displayed in the figure correspond to the B_3 predictions from the potential model analyses [162, 164–166], all of which rely on the same two-body input from the Nijmegen model analyses, namely, $a_{\Xi n}^{(1)} = 4.911$ fm [183, 184] (cf. Table 5.3). The fact that the Phillips plot evidently reflects a certain degree of compatibility of the potential model inputs with our EFT description is an important qualitative finding of this work. In the event of possible future availability of phenomenological three-body data, a more rigorous NLO EFT analysis (explicitly including effective range terms) may be helpful to substantiate such connections on a better footing.

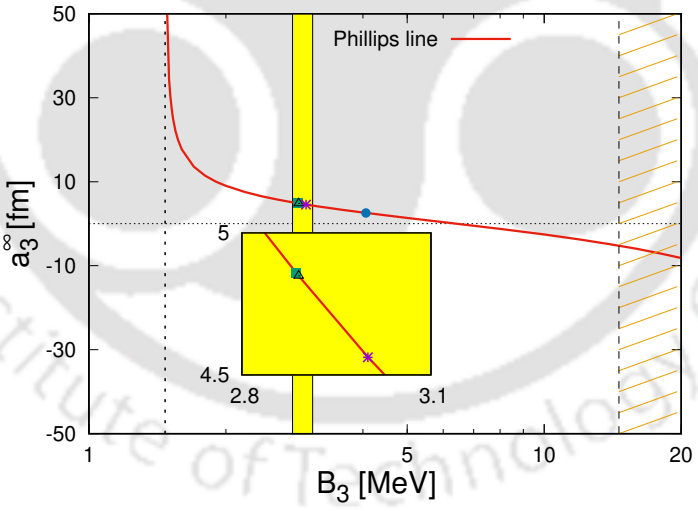

FIGURE 5.7: Phillips line correlation for the $(I = 3/2,\ J = 1/2)$ $\Xi^- nn$ system corresponding to the input ${}^3S_1$ $\Xi^- n$ scattering length $a_{\Xi n}^{(1)} = 4.911$ fm, as predicted by the updated ESC08c Nijmegen model analyses [183, 184]. The data points correspond to the input values of the three-body binding energy $B_3 = 2.886$, 2.89, 3.00 and 4.06 MeV, predicted by the potential model analyses [162, 164–166]. The vertical dotted line on the left represents the $n + (\Xi^- n)_t$ particle-dimer threshold at $B_3 = B_2 = 1.47$ MeV, while the hashed region, $B_3 \gtrsim 14$ MeV, represents the expected breakdown region of our halo EFT description.

5.4 Summary and Conclusions

A knowledge of few-body dynamics in light ($S = -2$) Ξ-hypernuclei can serve as an essential input to the neutron star EoS for a possible explanation of their stabilities with masses $\gtrsim 2M_\odot$. In this regard, the $\Xi^- nn$ ($I = 3/2$, $J^P = 1/2^+$) three-body system is one of the simplest systems to investigate the nature of the underlying 3BF. The reason is the stability of this channel against strong decays and the absence of Coulomb interactions. However, the impracticability of performing Ξ-hyperon scattering experiments and the lack of empirical data thereof have so far eluded rigorous determination of essential few-body observables. Thus, a general qualitative insight relying solely on low-energy universality is needed to illuminate specific characteristics of the underlying interactions that may reflect the emergence of exotic halo-bound states.

Here we used the framework of leading order halo EFT in a speculative study to explore the feasibility that the $\Xi^- nn$ system is Efimov-bound. Notably, the presence of the predominantly repulsive ${}^1S_0$ $\Xi^- n$ sub-system channel potentially leads to the generation of anomalously deep two- and three-body unphysical bound states beyond the breakdown scale of the theory. In our current simplistic approach, as a first approximation, such unphysical contributions are avoided on an *ad hoc* basis by explicitly decoupling this channel in the construction of our integral equations. Our asymptotic analysis of the $\Xi^- nn$ integral equations revealed the formal appearance of Efimov states in the unitary limit associated with an RG limit cycle with a discrete scaling factor, $s_0^\infty = 0.803391\cdots$. The factor, however, differs from the expected value $(s_0^\infty)_{\text{expect}} \approx 1.01$, as governed by the universality of three-particle mass ratios [12], owing to the decoupling of the ${}^1S_0$ $\Xi^- n$ channel. Such scaling differences can certainly influence various numerical estimates in the low-energy non-asymptotic domain, but the general qualitative features are likely to remain unchanged with the inclusion of both spin channels.[12]

Evidently, the unavailability of empirical three-body datum to fix the scale dependence of the three-body coupling $g_3(\Lambda_{\text{reg}})$ is a major drawback of our approach which prevents robust predictions. Thus, we relied on several existing Faddeev calculation-based potential model analyses [162, 164–166] for the input three-body binding energy B_3 in the reasonable benchmark range, $2.886 - 4.06$ MeV. Moreover, the ${}^{\not\pi}$EFT formalism requires the two-body inputs, namely, the ${}^1S_0$ nn scattering length $a_{nn} = -18.63$ [191], and the ${}^3S_1$ $\Xi^- n$ scattering length $a_{\Xi n}^{(1)}$. For the choice of the latter, we considered two contrasting scenarios, given the current ambiguities in regard to the underlying nature of the interactions in the spin-isospin triplet (1,1) $\Xi^- n$ channel. In the first scenario, we considered the prediction, $a_{\Xi n}^{(1)} = 4.911$ fm, from the recently updated Nijmegen model analyses [183, 184], which is based on the notion of a strongly attractive likely bound $(\Xi^- n)_t$ sub-system. In the second scenario, we considered the predictions of two contemporary SU(3) chiral EFT analyses, namely, $a_{\Xi n}^{(1)} = -0.09$ fm [179],

[12] In either case we expect to find robust three-body universal features, such as the quasi-periodic RG limit cycle behavior of the three-body coupling and the induced Phillips line correlations.

based on a relativistic calculation, and $a^{(1)}_{\Xi n} = -1.17$ fm [180], based on a non-relativistic in-medium G-matrix calculation, both concurring on a moderately attractive nature of the $(\Xi^- n)_t$ sub-system channel. With both the chiral EFT inputs, our investigations hinted at a predominantly unbound $\Xi^- nn$ system. In contrast with the input, $a^{(1)}_{\Xi n} = 4.911$ fm, the first scenario indicated favourable prospects for a physically realizable $\Xi^- nn$ Efimov-like ground, with the proviso that our $\not\pi$EFT formalism could be extended (with $\widetilde{\Lambda}_H \gtrsim 500$ MeV) to accommodate interactions mediated by $\pi\pi$ or σ-meson exchanges. Specifically, our eigensolutions (B_3) to the integral equations (excluding the 3BF terms) could reproduce the benchmark range of model inputs for the cut-off regulator values in the range $\Lambda_{\rm reg} \approx 335 - 464$ MeV.

Finally, as a simple demonstration of the predictive power of our EFT formalism, we evaluated the three-body S-wave $n - (\Xi^- n)_t$ scattering length to lie in the range, $a_3^\infty \approx 2.6 - 4.9$ fm, corresponding to the same aforementioned benchmark range of model inputs for B_3. Given the very speculatory nature of the present study and the indeterminable three-body scattering length from present-day experiments, the numerical figures for a_3^∞ are by all means *naive* ballpark estimates. Nevertheless, they are indicative of the emergent universal features of a prospective Efimov-bound $\Xi^- nn$ system which induces three-body correlations like the Phillips line. Such universal three-body features are robust against ambiguities in the two-body description given that the three-body datum is reliable. Consequently, our obtained results reasonably guesstimate similar qualitative results expected from more rigorous $\not\pi$EFT-based future investigations with systematic inclusion of both $\Xi^- n$ sub-system spin channels. Needless to emphasize that our conclusions tacitly relied on the presumed halo-bound structure of the $\Xi^- nn$ system, *viz.* a strongly attractive and bound ${}^3S_1$ $\Xi^- n$ sub-system and a predominantly weak (attractive or repulsive) ${}^1S_0$ $\Xi^- n$ sub-system with small scattering length.

A more systematic (realistic) approach requires a modification of the dibaryon formalism of the $\not\pi$EFT power counting, as well as including subleading order range effects. However, such a modified EFT analysis is beyond the scope of the present work and must be certainly explored as a possible future endeavor when more data will become available from upcoming experiments, such as ALICE [170] and FAIR [171]. Moreover, a next-to-leading order analysis would involve additional unknown three-body parameters in the theory thereby requiring more empirical inputs which are currently non-procurable.

Chapter 6

Universal Characteristics of Efimovian D^0nn System *via* Faddeev Techniques

6.1 Introduction

Few-body universality refers to the general long-distance/low-energy characteristics of few-body systems that is insensitive to short-distance/high-energy details of interactions. They can manifest themselves in sharply contrasting manners. A common example of universality is what is manifested in the two-body sector accompanied by the occurrence of shallow two-body *dimers* whenever the S-wave two-body scattering length a_0 becomes positive and in fact much larger than the corresponding interaction range r_0. A renormalization group (RG) analysis of the two-body contact interactions reveals the proximity of a *non-trivial infrared fixed-point* that concurs with the *unitary limit* of the two-body interactions. However, in the pioneering works of Efimov and Danilov [9–11, 61], a rather peculiar universal behavior was demonstrated in a three-boson system interacting *via* a short-distant two-body $\sim 1/r^2$ singular potential, with the scattering lengths *fine-tuned* to the unitary limit. Solving the Faddeev equations [34] in the *hyperspherical* co-ordinate representation led to the emergence of a sequence of geometrically spaced arbitrarily shallow S-wave *trimers* accumulating to zero energy threshold as $|a_0| \to \infty$. Such an emergent so-called *Efimov effect* [9–12, 15, 61] heralds the partial breakdown of exact scale invariance of the system into a *discrete scaling* behavior. A study of the scale dependence of the three-body contact interactions shows the onset of a renormalization group (RG) *limit cycle* [12].

Over the past two decades, Efimov universality has been extensively investigated in the $\not\pi$EFT [2–6, 12] using the momentum-space version of Faddeev scattering equations, so-called the STM equations [13, 14], in a wide variety of three-body nuclear systems. These include ordinary shallow-bound nuclei (e.g., ^{3}H, ^{3}He, ^{5}He, ^{6}He, ^{11}Li, ^{12}Be, ^{14}Be, ^{18}C, ^{20}C, etc.) [7, 31, 38, 46, 52, 53, 55], exotic nuclear clusters such as hypernuclei (e.g., ${}^{3}_{\Lambda}$H, $nn\Lambda$, ${}^{4}_{\Lambda\Lambda}$He, ${}^{5}_{\Lambda\Lambda}$H, ${}^{5}_{\Lambda\Lambda}$He, ${}^{6}_{\Lambda\Lambda}$He, $\Xi^- nn$, etc.) [63, 64, 79, 88, 108, 110, 193], as well as pure mesonic

clusters including heavy charm and bottom mesons [109, 194, 195] (also see Chapters 4 and 5 of this thesis). In addition, we refer the reader to Ref. [57] for a recent exhaustive review of applications of $\not\pi$EFT in the search and analyses of exotic Efimov bound states. In particular, some of these putative bound states constitute a special universal class of exotic nuclear systems termed as *halo nuclei*. Their quantum descriptions are defined in terms of few physical scales independent of range and other details of short-distance pairwise interactions. Such systems have been extensively exploited to explore three-body universality [25–29]. Often the *neutron rich* three-body hadronic clusters are identified as good halo-bound candidates owing to their typical diffuse structure with large radii and a few loosely held "valence" neutrons orbiting about their compact cores. The core itself may either consist of a single structureless particle (as in our case), or a hadronic cluster with excitation energies much larger than the halo-neutron separation energies. This characteristic scale separation makes them amenable to a low-energy EFT description. Especially, to tackle the multi-scale S-wave threshold dynamics of halo nuclei at scales typically lower than in standard $\not\pi$EFT, an important variant, so-called the *halo EFT* [7, 31], is needed to be employed (for a recent review see Ref. [32]). Such a framework provides a starting point in exploring the possible existence and low-energy characteristics of a putative $2n$ halo-bound D^0nn ($J = 0, T = 3/2$) system, as previously initiated in Refs. [109, 195].

Concurrently, meson-nucleon interactions have garnered a lot of interest in view of their role in strangeness physics in explaining hadronic *clustering* phenomena. This led to the identification of a large number of exotic bound systems of mesons, nucleons, and hyperons. Especially, the interaction of (anti-) kaons with nucleons or nuclei gained considerable impetus since the seminal works of Dalitz [196–200], leading to the discovery of the well-known resonance state $\Lambda(1405)$ right below the $\bar{K}N$ threshold, thereby establishing a strongly attractive nature of $\bar{K}N$ interaction in $T = 0$ isospin channel. This subsequently prompted a flurry of theoretical investigations on possible formation of exotic kaonic nuclei using various potential model analyses [201–214] (also see Ref. [33] for a recent review). However, it is well-known that dynamics of decay into other coupled open-channels tend to "wash out" various emergent features of three-body universality diminishing the likelihood of formation of Efimov states [109, 189, 194, 195]. Thus, given that the $\Lambda(1405)$ has a large decay width $\Gamma \sim 40 - 70$ MeV, in comparison to its binding energy ~ 20 MeV, it is expected that an Efimov-like $\bar{K}NN$ ($J = 0, T = 1/2$) bound state is practically unfeasible. Furthermore, the $\not\pi$EFT work of Ref. [109] employing a sharp momentum cut-off regulator ($\Lambda_{\rm reg}$) in the Faddeev integral equations demonstrated that the particle-stable $\bar{K}NN(J = 0, T = 3/2)$ system remains largely unbound *via* Efimov attraction, with a critical cut-off $\gtrsim 2$ GeV $\gg m_\pi$ (where m_π is the pion mass), that is too large to fit into a low-energy EFT description.

An analogous situation arises in the charm sector with a predominantly attractive DN ($T = 0$) channel leading the resonance state $\Lambda_c^+(2595)$ just below the DN threshold [215, 216] having an identical quantum number as $\Lambda(1405)$. However, unlike $\Lambda(1405)$, $\Lambda_c^+(2595)$ has a narrow width $\Gamma \sim 2.6$ MeV, making it more stable. Furthermore, the potential model analysis of

Ref. [217] posits that the $DNN\,(J=0,T=1/2)$ system is likely to form a deeply-bound trimer with binding energy $\sim$ 250 MeV. However, assessing its Efimov signature has been difficult, complicated by the presence of resonance and Coulomb effects. In contrast, the somewhat less attractive *quasi-bound* DN $(T=1)$ channel being manifestly free of resonance and Coulomb effects, may prove to be more favorable in exhibiting three-body universal signatures in the $DNN\,(J=0,T=3/2)$ channel, as hinted in Ref. [218]. Indeed in Ref. [109] it was demonstrated that the DN $(T=1)$ channel manifests two-body universality upon invoking a *zero-coupling limit* (ZCL) model idealization that excluded coupled-channel effects. Furthermore, invoking the ZCL ansatz in the three-body sector, the neutron separation energy arguably becomes much smaller compared to the excitation energy of D^0-meson to the $D^{*0}(2007)$ resonance state. The distinct separation of scales thereby allowed an halo-EFT [32] description of the S-wave $D^0nn\,(J=0,T=3/2)$ system. By solving the Faddeev-like integral equations for the three-body scattering amplitudes, the analysis in Ref. [109] demonstrated that an Efimov-like D^0nn threshold ground state becomes feasible at a sufficiently small critical cut-off $\sim$ 40 MeV, relative to the EFT hard scale $\sim m_\pi$. This indicated encouraging prospects for the S-wave D^0nn system as a feasible Efimovian candidate.

The work in this chapter aims to employ the Faddeev techniques developed in Refs. [24, 35–38, 46] to formulate an effective non-relativistic quantum mechanical method to assess the geometrical structure of the plausible S-wave D^0nn bound system. Such an EFT-inspired description provides a viable means to correlate in a model-independent way the low-energy structure with the expected qualitative features of such a universal halo-bound Efimov state. Such structural predictions could not only shed light on the inherent character of the hadronic clustering mechanisms but also provide valuable inputs for other *ab initio* calculations including lattice QCD simulations. The contents of this chapter is organized in the following way: In Sec. 6.2, we begin by presenting a brief outline of the general operator formalism of deriving the notable Faddeev equations [34, 50] for an arbitrary three-body system. We then extend the formalism to describe a $2n$ halo-bound D^0nn system. In Sec. 6.3, we employ a Jacobi momentum representation to build a complete set of basis states using partial wave decomposition needed to describe the component wavefunctions, representing all possible re-arrangements of the binary (two-body) subsystems. By projecting the operator form of the Faddeev equations onto the chosen basis, we derive in Sec. 6.4 a set of coupled integral equations describing the dynamics of the coupled spin and isospin channels for the D^0nn system. We subsequently establish a one-to-one correspondence with the analogous STM integral equations derived in Ref. [109] in the context of $\not\pi$EFT [1] whose solutions determine the low-energy D^0nn observables. In Sec. 6.5, we demonstrate the reconstruction of the full three-body D^0nn wavefunction in terms of different re-arrangements channels (cf. Fig. 6.3). We then show how the solution to component wavefunctions can be used to extract various structural features of a plausible Efimov-bound D^0nn system, namely, the one- and two-body

[1] In our case of the D^0nn system, with the D^0-meson identified as the structureless core, the halo-EFT becomes equivalent to $\not\pi$EFT.

matter density form factors, their corresponding mean square radii, and the $n - D^0 - n$ opening angle. In Sec. 6.6 we report the results of our numerical evaluations in the context of ZCL model idealization and discuss the universal physics implications. We finally conclude this chapter in Sec. 6.7 by presenting a brief summary of this work with some concluding remarks and outlook.

6.2 Faddeev Equations in Quantum Mechanics

At non-relativistic energies, the quantum mechanics of determining the dynamics of scattering of three interacting particles is obtained *uniquely* by numerically solving a set of three linear integral equations called the Faddeev equations. In contrast to two-body dynamics determined solely in terms of single particle motions, the three-body problem is complicated by the presence of two relative motions which are not mutually independent. This leads to the occurrence of three two-body fragmentation or *rearrangement* channels ($\alpha = 1, 2, 3$) and one *break-up* channel ($\alpha = 0$), thereby requiring additional boundary conditions than one would expect in solving the standard three-body Schrödinger equation, or equivalently, a single *Lippmann-Schwinger* (LS) equation, such as[2]

$$|\Psi_\alpha^{(+)}\rangle = |\phi_\alpha\rangle + \lim_{\varepsilon\to 0} \frac{1}{E_\alpha + i\varepsilon - H_\alpha}(V - V_\alpha)|\Psi_\alpha^{(+)}\rangle\,, \quad \alpha = 0, 1, 2, 3\,. \tag{6.1}$$

Here the three-particle scattering state $|\Psi_\alpha^{(+)}\rangle$ in the channel α is related to the corresponding asymptotic state $|\phi_\alpha\rangle$ with bound particles $\beta \neq \alpha$ and $\gamma \neq \alpha$ *via* the *Möller* scattering relation [219]:

$$|\Psi_\alpha^{(+)}\rangle = \lim_{\varepsilon\to 0} \frac{i\varepsilon}{E_\alpha + i\varepsilon - H}|\phi_\alpha\rangle\,, \quad \alpha = 0, 1, 2, 3\,, \tag{6.2}$$

where $H_\alpha = H_0 + V_\alpha$ is the channel Hamiltonian which is the sum of the free Hamiltonian (kinetic energy of the three-body system) H_0 and the channel potential V_α, and $H = H_0 + V$ is the full three-body Hamiltonian. The essential problem in dealing with such an LS equation is that it does not define the solution $|\Psi_\alpha^{(+)}\rangle$ uniquely, since the scattering state $|\Psi_\beta^{(+)}\rangle$, $\beta \neq \alpha$, also satisfies the corresponding homogeneous equation:

$$|\Psi_\beta^{(+)}\rangle = \lim_{\varepsilon\to 0} \frac{1}{E_\beta + i\varepsilon - H_\alpha}(V - V_\alpha)|\Psi_\beta^{(+)}\rangle\,. \tag{6.3}$$

This criterion of non-uniqueness is the main reason for disregarding LS equations in multi-particle scattering ($n > 2$). It is therefore imperative to consider an augmented version of the LS equations in a three-body problem satisfying extra boundary conditions, leading us to the Faddeev equations [34]. Moreover, Faddeev's ingenious idea of decomposing the full three-body wavefunction into *partitions* carefully avoids the issue of disconnected contributions

[2]Here we shall use spectator notation throughout, with the subscript index denoting the spectator particle.

to the three-body scattering kernel. This becomes advantageous from the point of view of numerical evaluations. In the following subsection, we provide only a basic schematic for deriving the coupled set of integral equations in operator formalism for an arbitrary three-body system beginning from the three-body Schrödinger equation. In the subsection following that we determine the specific operator form of the Faddeev equation for the D^0nn system, exploiting the symmetries of an S-wave $2n$ halo-bound system.

6.2.1 Operator formalism

The Faddeev equation exploits the simplicity of break-up of the three-body system into a (2+1)-body system, namely, a binary subsystem interacting with a third spectator particle. The essential idea to introduce the idea of partitioning the effective three-body interaction potential into a sum of three pair-wise interaction potentials corresponding to all possible (2+1)-body re-arrangements, namely,

$$V(\mathbf{r_1}, \mathbf{r_2}, \mathbf{r_3}) = V_1(r_{23}) + V_2(r_{31}) + V_3(r_{12})\,, \tag{6.4}$$

where $V_k(r_{ij})$ is the interaction potential between the particles i and j, with k being the spectator particle. Simultaneously, one decomposes the full three-body wavefunction $|\Psi_\alpha\rangle$, for a given channel $\alpha = 0, 1, 2, 3$, into three component *Faddeev partition* wavefunctions $|\psi_{\alpha,i}\rangle$ (i being the spectator particle index), given by

$$|\Psi_\alpha^{(+)}\rangle = \sum_{i=1}^{3} |\psi_{\alpha,i}\rangle\,, \tag{6.5}$$

Suppressing the "(+)" symbol in the superscript, as well as the channel index α, we begin by first writing the three-body Schrödinger equation for the channel in the following operator notation

$$|\Psi\rangle = G_0(z) \sum_i V_i |\Psi\rangle\,, \tag{6.6}$$

where the free Green's function or resolvent operator (representing the three-body propagator) is given by

$$G_0(z) \equiv (z - H_0)^{-1}\,. \tag{6.7}$$

where $z = E + i0$ is the total three-body energy. Next, using Eq. (6.5) we express a single component wavefunction as

$$|\psi_i\rangle = G_0(z)V_i|\Psi\rangle = G_0(z)V_i|\psi_i\rangle + G_0(z)V_i \sum_{j\neq i} |\psi_j\rangle\,. \tag{6.8}$$

Further simplification of the above equation may be achieved by solving for the $|\psi_i\rangle$ component, namely,

$$|\psi_i\rangle = (1 - G_0(z)V_i)^{-1} G_0(z)V_i \sum_{i\neq j} |\psi_j\rangle \,. \tag{6.9}$$

The operator in front of the summation can be iterated to all orders which eventually yields the two-body T-matrix, represented by the familiar LS equation for that channel:

$$\begin{aligned} t_i(z) = V_i \,(1 - G_0(z)V_i)^{-1} &= V_i + V_i G_0(z) V_i + V_i G_0(z) V_i G_0(z) V_i + \cdots \,, \\ &= V_i + V_i G_0(z) \,[V_i + V_i G_0(z) V_i + \cdots] \\ &= V_i + V_i G_0(z) t_i(z) \end{aligned} \tag{6.10}$$

Thus, we obtain the familiar form *homogeneous* Faddeev equations,

$$|\psi_i\rangle = G_0(z) t_i(z) \sum_{i\neq j} |\psi_j\rangle \,. \tag{6.11}$$

Consequently, to satisfy the correct boundary conditions for a given initial channel $\alpha = \alpha_0$, $|\psi_{\alpha,i}\rangle$ must obey the *inhomogeneous* Faddeev equations expressed in the compact form:

$$|\psi_{\alpha_0,i}\rangle = |\phi_{\alpha_0}\rangle \delta_{i,\alpha_0} + G_0(z) t_i(z) \sum_{j\neq i} |\psi_{\alpha_0,j}\rangle \,. \tag{6.12}$$

As for example, if the initial channel is specified as $\alpha_0 = 1$, then we express the Faddeev equations in the standard matrix form:

$$\begin{bmatrix} |\psi_1\rangle \\ |\psi_2\rangle \\ |\psi_3\rangle \end{bmatrix} = \begin{bmatrix} |\phi_1\rangle \\ 0 \\ 0 \end{bmatrix} + G_0(z) \begin{bmatrix} 0 & t_1(z) & t_1(z) \\ t_2(z) & 0 & t_2(z) \\ t_3(z) & t_3(z) & 0 \end{bmatrix} \begin{bmatrix} |\psi_1\rangle \\ |\psi_2\rangle \\ |\psi_3\rangle \end{bmatrix} . \tag{6.13}$$

In the following subsection, we specialize to the D^0nn system and derive the corresponding operator form of the Faddeev equation.

6.2.2 Faddeev Equation For D^0nn system

The EFT analysis presented in Refs. [109, 195] demonstrated that the S-wave $D^0nn\,(J = 0, T = 3/2)$ system is likely to manifest Efimov states with the DN $(T = 1)$ interactions tuned in close proximity to the unitary limit with the couplings to sub-threshold decay channels eliminated. With such a ZCL idealization, the otherwise quasi-bound DN state with small complex D^0n S-wave scattering length turned into a real-bound state with real-valued scattering length that was found to become quite large (see Ref. [109] for details of extraction of the scattering lengths in the framework of a dynamical coupled-channel model). Invoking such a ZCL scenario, the D^0nn system could be pictured as a $2n$-halo nuclei with three two-body fragmentation channels: two $n + (D^0n)$ channels, each representing a bound D^0n

subsystem with a spectator neutron, and a $D^0 + (nn)$ channel, representing a *virtual* bound nn subsystem with a spectator D^0-meson. Consequently, the D^0nn system can be described using the three Faddeev components: $|\psi_{n_1}\rangle$ and $|\psi_{n_2}\rangle$ when one of the halo-neutrons is the spectator and the core D^0-meson with the other neutron representing the binary subsystem, and $|\psi_D\rangle$ when the core D^0-meson is the spectator and the $2n$-halo-neutrons representing the binary subsystem. However, by virtue of fermionic symmetry between identical configurations $|\psi_{n_1}\rangle$ and $|\psi_{n_2}\rangle$ upon transposition of the two neutrons, the number of independent components is reduced to two. If $\mathscr{P}$ is the permutation operator swapping the two neutrons, then we demand the anti-symmetry of the full three-body wavefunction as well as its components, namely,

$$\begin{aligned}\mathscr{P}|\Psi\rangle &= \mathscr{P}\left(|\psi_{n_1}\rangle + |\psi_{n_2}\rangle + |\psi_D\rangle\right) \\ &= -|\psi_{n_2}\rangle - |\psi_{n_1}\rangle - |\psi_D\rangle = -|\Psi\rangle\,. \end{aligned} \tag{6.14}$$

Thus, with $|\psi_{n_2}\rangle$ component expressed in terms of $|\psi_{n_1}\rangle$, we effectively need two Faddeev partitions, namely, $|\psi_n\rangle$ and $|\psi_D\rangle$, describing all possible three-body re-arrangements, as depicted in Fig. 6.1. The full three-body wavefunction is then expressed as

$$|\Psi\rangle = (1 - \mathscr{P})|\psi_n\rangle + |\psi_D\rangle\,. \tag{6.15}$$

Assuming that the n-D^0 and n-n subsystems to interact *via* the *effective potentials* V_n and V_D, respectively, the two-body T-matrices t_n and t_D are obtained using the standard LS equations

$$\begin{aligned} t_n(z) &= V_n + G_0(z)V_n t_n(z)\,, \quad \text{and} \\ t_D(z) &= V_D + G_0(z)V_D t_D(z)\,. \end{aligned} \tag{6.16}$$

Finally, noting that the permutation operator $\mathscr{P}$ leaves the T-matrices t_i and potential V_i invariant, the coupled two-component homogeneous Faddeev equations for the D^0nn system are given as

$$|\psi_n\rangle = -G_0(z)t_n(z)\mathscr{P}|\psi_n\rangle + G_0 t_n(z)|\psi_D\rangle \quad \text{and} \tag{6.17}$$

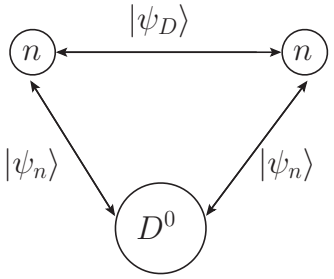

FIGURE 6.1: The Faddeev components for the D^0nn system corresponding to all possible three-particle re-arrangements.

$$
\begin{aligned}
|\psi_D\rangle &= G_0(z)t_D(z)|\psi_n\rangle - G_0 t_D(z)\mathscr{P}|\psi_n\rangle \\
&= 2G_0(z)t_D(z)|\psi_n\rangle\,,
\end{aligned}
\tag{6.18}
$$

or equivalently, expressed in the matrix form:

$$
\begin{bmatrix} |\,\psi_n\rangle \\ |\psi_D\rangle \end{bmatrix} = G_0 \begin{bmatrix} -t_n(z)\mathscr{P} & t_n(z) \\ 2t_D(z) & 0 \end{bmatrix} \begin{bmatrix} |\psi_n\rangle \\ |\psi_D\rangle \end{bmatrix}. \tag{6.19}
$$

For the total three-body energy $z = E < 0$, the above matrix equation has a nontrivial solution when the eigenvalue of the kernel matrix is unity. However, before we can attempt to solve the above equations to obtain the three-body observables of the system, the equations must be projected onto an appropriate complete basis. This takes us to the next section on constructing a set of basis states using Jacobi momentum representation.

6.3 Basis States in Jacobi Momentum Representation

The Jacobi momenta provide a convenient representation to describe the non-relativistic dynamics of the three-body system. By completely eliminating the motion of the center-of-mass of the three-body system, it expresses all the dynamics in terms of the binary subsystem's relative motion, as well as the motion of the binary subsystem relative to the spectator particle. Thus, the momentum state of an arbitrary three-body system is defined in terms of a pair of relative three-momenta: one being the relative three-momentum $\mathbf{p}$ between two particles in a chosen two-body subsystem, and the other being the three-momentum $\mathbf{q}$ of the third spectator particle relative to the center-of-mass of the chosen binary subsystem.

For concreteness, as depicted in Fig. 6.2 let us consider an arbitrary system of three *distinguishable* particles (i, j and k) with masses (m_i, m_j and m_k), and individual (laboratory/inertial frame) momentum ($\mathbf{k}_i$, $\mathbf{k}_j$ and $\mathbf{k}_k$), respectively. Then, the Jacobi momenta of the system with particle i as the spectator are defined as[3]

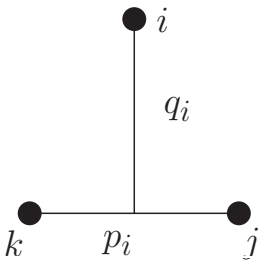

FIGURE 6.2: The Jacobi momenta ($p_i = |\mathbf{p}_i|, q_i = |\mathbf{q}_i|$) of an arbitrary three-body system.

[3]The spectator notation is used throughout the chapter. However, it must be noted that this notation is not applicable while defining the individual particle masses (m_i) and laboratory/inertial frame momenta ($\mathbf{k}_i$). Also, note that the choice of the Jacobi momenta is not unique. In fact, there are three equivalent choices for describing the same three-body system depending on which particle is chosen as the spectator. The other equivalent Jacobi momenta could be easily obtained through cyclic permutations of the indices (ijk).

$$\mathbf{p}_i = \mu_{jk}\left(\frac{\mathbf{k}_j}{m_j} - \frac{\mathbf{k}_k}{m_k}\right); \qquad \mu_{jk} = \frac{m_j m_k}{m_j + m_k}, \tag{6.20}$$

$$\mathbf{q}_i = \mu_{i(jk)}\left(\frac{\mathbf{k}_i}{m_i} - \frac{\mathbf{k}_j + \mathbf{k}_k}{m_j + m_k}\right); \qquad \mu_{i(jk)} = \frac{m_i(m_j + m_k)}{M}. \tag{6.21}$$

Here, $\mathbf{p}_i$ is the relative momentum between the particles j and k in the center-of-mass frame of the two-body subsystem, $\mathbf{q}_i$ is the relative momentum of the spectator particle i with respect to the center-of-mass of the same binary subsystem, $M = m_i + m_j + m_k$ is the total mass of the three-body system, and the $\mathbf{K} = \mathbf{k}_i + \mathbf{k}_j + \mathbf{k}_k$ is total three-body momentum.[4] Using the above choice of the Jacobi momenta, the total kinetic energy or free Hamiltonian of the three-body system is given as

$$H_0 = \frac{\mathbf{K}^2}{2M} + \frac{\mathbf{p}_i^2}{2\mu_{jk}} + \frac{\mathbf{q}_i^2}{2\mu_{i(jk)}}. \tag{6.22}$$

6.3.1 Jacobi Momentum Basis States in Quantum Mechanics

We now briefly discuss the construction of a complete set of basis states for a momentum-space quantum mechanical description of an arbitrary three-body system. For a detailed exposition, we refer the reader to the treatment in the book by W. Glöckle [50]. The basic objects are the Jacobi plane wave state vectors denoted as

$$|\mathbf{pq}\rangle_i \equiv |\mathbf{p}_i\mathbf{q}_i\rangle, \tag{6.23}$$

which satisfy the *orthonormality* relation:

$${}_i\langle\mathbf{pq}|\mathbf{p'q'}\rangle_i \equiv \langle\mathbf{p}_i\mathbf{q}_i|\mathbf{p}'_i\mathbf{q}'_i\rangle = \delta^3(\mathbf{p}_i - \mathbf{p}'_i)\,\delta^3(\mathbf{q}_i - \mathbf{q}'_i) \equiv \delta^3(\mathbf{p} - \mathbf{p}')\,\delta^3(\mathbf{q} - \mathbf{q}'), \tag{6.24}$$

as well as the *completeness* relation:

$$\int \mathrm{d}^3\mathbf{p} \int \mathrm{d}^3\mathbf{q}\, |\mathbf{pq}\rangle_i\, {}_i\langle\mathbf{pq}| \equiv \int \mathrm{d}^3\mathbf{p}_i \int \mathrm{d}^3\mathbf{q}_i\, |\mathbf{p}_i\mathbf{q}_i\rangle\langle\mathbf{p}_i\mathbf{q}_i| = 1. \tag{6.25}$$

Since these momentum states denote free-particle motions, they are eigenstates of the free Hamiltonian H_0:

$$H_0|\mathbf{p}_i\mathbf{q}_i\rangle = \left(\frac{\mathbf{p}_i^2}{2\mu_{jk}} + \frac{\mathbf{q}_i^2}{2\mu_{i(jk)}}\right)|\mathbf{p}_i\mathbf{q}_i\rangle \tag{6.26}$$

A generic partial wave projected basis can now be constructed from these plane wave states [50]:

$$\begin{aligned} |pq\,\mathbb{Q}\rangle_i &\equiv |p_i q_i\,\mathbb{Q}_i\rangle \\ &\equiv \Big|pq\{(ls)\mathfrak{j}(\lambda\sigma)\mathfrak{J}\}JM_J(t\tau)TM_T\Big\rangle_i, \end{aligned} \tag{6.27}$$

[4] $\mathbf{K} = \mathbf{0}$ in the three-body center-of-mass frame.

where $\mathbb{Q}_i$ represents the set of all the *discrete* quantum numbers of a given quantum state, defined with respect to the particle i as the spectator. For the above basis representation $\mathbb{Q}_i$ collectively denotes the following quantum numbers:[5]

- $l \implies$ quantum number for the relative orbital angular momentum of particles in binary subsystem j-k,
- $s \implies$ intrinsic spin quantum number of binary subsystem j-k,
- $\boldsymbol{\jmath} \implies$ coupling of l and s, or total spin quantum number of binary subsystem j-k,
- $t \implies$ isospin quantum number of binary subsystem j-k,
- $\lambda \equiv l_i \implies$ orbital angular momentum quantum number of spectator i relative to binary subsystem j-k,
- $\sigma \equiv s_i \implies$ intrinsic spin quantum number of spectator i,
- $\boldsymbol{\mathcal{J}} \implies$ coupling of λ and σ, or total spin quantum number of spectator i,
- $\tau \equiv t_i \implies$ isospin quantum numbers of spectator i,
- $J \implies$ coupling of $\boldsymbol{\jmath}$ and $\boldsymbol{\mathcal{J}}$, or total spin quantum number of three-body system,
- $M_J \implies$ quantum number for the z-component of total spin of three-body system,
- $T \implies$ coupling of t and τ, or total isospin quantum number of three-body system,
- $M_T \implies$ quantum number for the z-component of total isospin of three-body system.

However, it is sometimes useful to decouple the orbital angular momentum, intrinsic spin, and isospin quantum numbers of the full three-body system, rather than using the above representation in terms of the (2+1)-subsystem quantum numbers. This amounts to an unitary transformation of the $|pq\,\mathbb{Q}\rangle_i$ basis which is easily achieved *via* the well-known *Wigner's 9-j* symbol:

$$|pq\,\mathbb{Q}\rangle_i = \sum_{LS} \sqrt{\hat{\boldsymbol{\jmath}}\,\hat{\boldsymbol{\mathcal{J}}}\,\hat{L}\,\hat{S}} \begin{Bmatrix} l & s & \boldsymbol{\jmath} \\ \lambda & \sigma & \boldsymbol{\mathcal{J}} \\ L & S & J \end{Bmatrix} \Big| pq\{(l\lambda)L(s\sigma)S\}JM_J(t\tau)TM_T \Big\rangle_i , \tag{6.28}$$

where it is customary to denote the hatted quantum numbers, e.g., $\hat{\boldsymbol{\jmath}} \equiv 2\boldsymbol{\jmath} + 1$, etc. Also,

- $L \implies$ coupling of l and λ, or total orbital quantum number of three-body system,
- $S \implies$ coupling of s and σ, or total intrinsic quantum number of three-body system.

[5] Spectator notation is not applicable to individual particle quantum numbers such as l_i, s_i, t_i, etc.

These partial-wave-projected basis state vectors likewise satisfy the *orthonormality* relation:

$$ {}_i\langle pq\,\mathbb{Q}|p'q'\,\mathbb{Q}'\rangle_i = \frac{\delta(p-p')}{pp'}\frac{\delta(q-q')}{qq'}\;\delta_{\mathbb{Q}\mathbb{Q}'}\,, \tag{6.29} $$

as well as the *completeness* relation:

$$ \sum_{\mathbb{Q}}\int_0^\infty \mathrm{d}p\; p^2 \int_0^\infty \mathrm{d}q\; q^2\;|pq\,\mathbb{Q}\rangle_i\;{}_i\langle pq\,\mathbb{Q}| = 1\,, \tag{6.30} $$

such that a Faddeev component $|\psi_i\rangle$ may be expanded in the basis as follows:

$$ |\psi_i\rangle = \sum_{\mathbb{Q}}\int_0^\infty \mathrm{d}p\; p^2 \int_0^\infty \mathrm{d}q\; q^2\;{}_i\langle pq\,\mathbb{Q}|\psi_i\rangle\;|pq\,\mathbb{Q}\rangle_i\,. \tag{6.31} $$

Here we also display how we express the overlap of a plane wave vector state onto a partial wave projected state employing *spherical* and *hyperspherical harmonics*, namely,

$$ {}_i\langle \mathbf{p}'|plm_l\rangle_i = \frac{\delta(p-p')}{pp'}Y_l^{m_l}(\hat{\mathbf{p}}')\,, \tag{6.32} $$

$$ {}_i\langle \mathbf{p}'\mathbf{q}'|pq(l\lambda)LM_L\rangle_i = \frac{\delta(p-p')}{pp'}\frac{\delta(q-q')}{qq'}\mathcal{Y}_{l\lambda}^{LM_L}(\hat{\mathbf{p}}\hat{\mathbf{q}})\,. \tag{6.33} $$

The solutions to the Faddeev equations will also require us to recouple two Jacobi basis states corresponding to two different spectator representations. This corresponds to the overlap-matrix element of the form:

$$ \begin{aligned} {}_i\langle pq\,\mathbb{Q}|p'q'\,\mathbb{Q}'\rangle_j = \sum_{LS}\sum_{L'S'}\sqrt{\hat{\jmath}\hat{\mathcal{J}}\hat{L}\hat{S}}\sqrt{\hat{\jmath}'\hat{\mathcal{J}}'\hat{L}'\hat{S}'}\begin{Bmatrix} l & s & \jmath \\ \lambda & \sigma & \mathcal{J} \\ L & S & J \end{Bmatrix}\begin{Bmatrix} l' & s' & \jmath' \\ \lambda' & \sigma' & \mathcal{J}' \\ L' & S' & J' \end{Bmatrix} \\ \times {}_i\langle pq(l\lambda)L|p'q'(l'\lambda')L'\rangle_j\;\;{}_i\langle(s\sigma)S|(s'\sigma')S'\rangle_j\;\;{}_i\langle(t\tau)T|(t'\tau')T'\rangle_j\,, \end{aligned} \tag{6.34} $$

where the re-coupling matrix elements for the spins and isospins are calculated using the well-known *Wigner's 6-j* symbol:

$$ {}_i\langle(s\sigma)S|(s'\sigma')S'\rangle_j = \delta_{SS'}\sqrt{\hat{s}\hat{s}'}(-1)^{s_i+2s_j+s_k+s'}\begin{Bmatrix} s_j & s_k & s \\ s_i & S & s' \end{Bmatrix}\,, \tag{6.35} $$

and

$$ {}_i\langle(t\tau)T|(t'\tau')T'\rangle_j = \delta_{TT'}\sqrt{\hat{t}\hat{t}'}(-1)^{t_i+2t_j+t_k+t'}\begin{Bmatrix} t_j & t_k & t \\ t_i & T & t' \end{Bmatrix}\,. \tag{6.36} $$

The real work is to calculate the overlap matrix element ${}_i\langle pq(l\lambda)L|p'q'(l'\lambda')L'\rangle_j$ involving re-couplings of momenta and orbital angular momenta belonging to two different spectator representations of the Jacobi basis. The general procedure for a three-nucleon system has been pedagogically worked out in Ref. [50]. For our case of the $2n$-halo D^0nn system, the approach closely resembles the general treatment of $2n$-halo nuclei presented in Refs. [35–38, 46]. The

details of the methodology are worked out in Sec. 6.4.1.

6.3.2 Jacobi Momentum States for a $2n$-halo D^0nn System

The three different re-arrangement channels for a $2n$-halo D^0nn system is displayed in Fig.6.3. For simplicity of the analytical derivations, we find it convenient to express the mass M_D of the D^0-meson in terms of the nucleon (neutron) mass, namely $M_D = yM_n$. Depending upon the choice of the spectator, the following *equivalent* kinematical description of the D^0nn system can be given:

- **Channel-1:** D^0-meson is the spectator, and the two neutrons form the binary subsystem. In this case, the choice of the Jacobi momenta are

$$\mathbf{p}_D = \frac{1}{2}(\mathbf{k}_{n_1} - \mathbf{k}_{n_2})\,, \qquad \text{and} \tag{6.37}$$

$$\mathbf{q}_D = \frac{2\mathbf{k}_D - y(\mathbf{k}_{n_1} + \mathbf{k}_{n_2})}{y+2}\,, \tag{6.38}$$

where $\mathbf{k}_{n_1}$, $\mathbf{k}_{n_2}$, and $\mathbf{k}_D$ are individual momenta of n_1-neutron, n_2-neutron and the D^0-meson, respectively. The corresponding free Hamiltonian of the system in this representation is given by

$$H_0^{(D)} = \frac{\mathbf{p}_D^2}{2\mu_{nn}} + \frac{\mathbf{q}_D^2}{2\mu_{D(nn)}} = \frac{1}{M_n}p_D^2 + \left(\frac{y+2}{4yM_n}\right)q_D^2\,, \tag{6.39}$$

where the reduced masses are

$$\mu_{nn} = \frac{M_n}{2} \quad \text{and} \quad \mu_{D(nn)} = \frac{2M_nM_D}{M_D+M_n} = \frac{2y}{y+2}M_n\,. \tag{6.40}$$

- **Channels-2, -3:** Either n_1-neutron or n_2-neutron is the spectator, and the non-spectator neutron with the D^0-meson forms the binary subsystem. These re-arrangement channels yield identical configurations since the two neutrons are identical particles. As

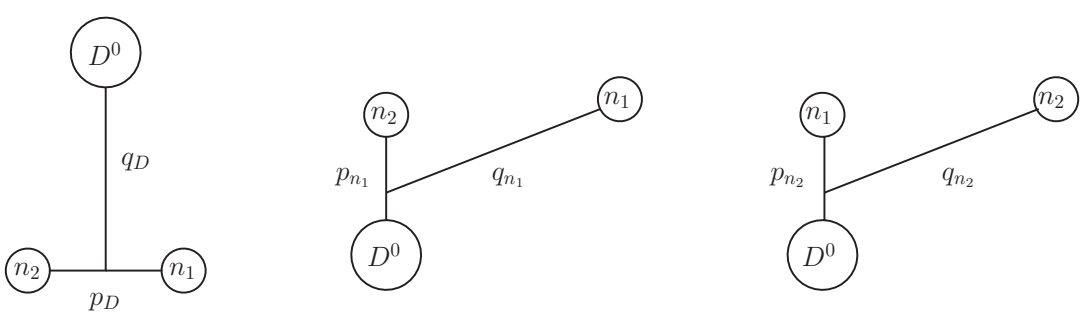

FIGURE 6.3: The re-arrangement channels and Jacobi momenta for a $2n$-halo D^0nn system.

we have noted earlier, using the permutation operator $\mathcal{P}$ the $|\psi_{n2}\rangle$ component wave-function is expressible in term of the $|\psi_{n1}\rangle$ Faddeev component. In this case, the choice of the Jacobi momenta are

$$\mathbf{p}_{n_1} = \frac{1}{y+1}\left(y\mathbf{k}_{n_2} - \mathbf{k}_D\right) , \quad \mathbf{p}_{n_2} = \frac{1}{y+1}\left(\mathbf{k}_D - y\mathbf{k}_{n_1}\right) , \tag{6.41}$$

and

$$\mathbf{q}_{n_1} = \frac{(y+1)\mathbf{k}_{n_1} - (\mathbf{k}_{n_2} + \mathbf{k}_D)}{y+2} , \quad \mathbf{q}_{n_2} = \frac{(y+1)\mathbf{k}_{n_2} - (\mathbf{k}_{n_1} + \mathbf{k}_D)}{y+2} . \tag{6.42}$$

The corresponding free Hamiltonian is

$$H_0^{(n)} = \frac{\mathbf{p}_n^2}{2\mu_{nD}} + \frac{\mathbf{q}_n^2}{2\mu_{n(nD)}} = \frac{y+1}{2yM_n}p_n^2 + \left(\frac{y+2}{2M_n(y+1)}\right)q_n^2 , \tag{6.43}$$

where the reduced masses are

$$\mu_{nD} = \frac{M_n M_D}{M_D + M_n} = \frac{y}{y+1}M_n, \quad \text{and} \quad \mu_{n(nD)} = \frac{M_n(M_D + M_n)}{M_D + 2M_n} = \frac{y+1}{y+2}M_n . \tag{6.44}$$

The partial wave projected Jacobi momentum basis states for the D^0nn system are donated as:

- $|pq\,\mathbb{Q}\rangle_D$: D^0-meson is the spectator particle,
- $|pq\,\mathbb{Q}\rangle_{n_1}$: n_1-neutron is the spectator particle,
- $|pq\,\mathbb{Q}\rangle_{n_2}$: n_2-neutron is the spectator particle.

Since the two identical neutrons have opposite spins in the binary subsystem, the $|pq\,\mathbb{Q}\rangle_D$ basis state is anti-symmetric with respect to the two neutrons. Thus, the permutation operator $\mathcal{P}$ yields eigenvalue of -1 when operated on $|pq\,\mathbb{Q}\rangle_D$:

$$\mathcal{P}|pq\,\mathbb{Q}\rangle_D = -|pq\,\mathbb{Q}\rangle_D . \tag{6.45}$$

As for the basis states $|pq\,\mathbb{Q}\rangle_{n_1}$ and $|pq\,\mathbb{Q}\rangle_{n_2}$, the binary subsystems are symmetric with respect to the non-identical particles. The action of $\mathcal{P}$ on these states simply interchanges the position of both neutrons. The parity of $\mathcal{P}$, in this case, is thus given by $(-1)^L$. Consequently, for an S-wave D^0nn system we must have

$$\mathcal{P}|pq\,\mathbb{Q}\rangle_{n_1/n_2} = |pq\,\mathbb{Q}\rangle_{n_2/n_1} . \tag{6.46}$$

6.4 Faddeev Equations in Jacobi Momentum Basis

The complete set of Jacobi momentum basis states obtained in the last section can now be used to define the Faddeev equations for the $2n$-halo D^0nn system. We now project the operator Eqs. (6.17) and (6.18) onto the partial wave basis using the completeness relation Eq. (6.30). Notably, here we can drop the summation over the set of discrete quantum numbers $\mathbb{Q}$ since we are eventually going to consider a specific set of such quantum numbers to describe the D^0nn ($J = 0$, $T = 3/2$) system. Thus, we have

$$\begin{aligned}
{}_n\langle pq\,\mathbb{Q}|\psi_n\rangle &= {}_n\langle pq\,\mathbb{Q}| - G_0(z)\,t_n(z)\,\mathcal{P}|\psi_n\rangle + {}_n\langle pq\,\mathbb{Q}|\,G_0(z)\,t_n(z)\,|\psi_D\rangle \\
&= \int_0^\infty \mathrm{d}p'\,p'^2\;\mathrm{d}q'\,q'^2 \int_0^\infty \mathrm{d}p''\,p''^2\;\mathrm{d}q''\,q''^2\;{}_n\langle pq\,\mathbb{Q}|\,G_0(z)\,t_n(z)\,|p'q'\,\mathbb{Q}'\rangle_n \\
&\quad\times\Big({}_n\langle p'q'\,\mathbb{Q}'| - \mathcal{P}|p''q''\,\mathbb{Q}''\rangle_n\;{}_n\langle p''q''\,\mathbb{Q}''|\psi_n\rangle + {}_n\langle p'q'\,\mathbb{Q}'|p''q''\,\mathbb{Q}''\rangle_D\;{}_D\langle p''q''\,\mathbb{Q}''|\psi_D\rangle\Big)\,,
\end{aligned} \tag{6.47}$$

and

$$\begin{aligned}
{}_D\langle pq\,\mathbb{Q}|\psi_D\rangle &= {}_D\langle pq\,\mathbb{Q}|\,2G_0(z)\,t_D(z)\,|\psi_n\rangle \\
&= 2\int_0^\infty \mathrm{d}p'\,p'^2\;\mathrm{d}q'\,q'^2 \int_0^\infty dp''\,p''^2\;dq''\,q''^2\;{}_D\langle pq\,\mathbb{Q}|\,G_0(z)\,t_D(z)\,|p'q'\mathbb{Q}'\rangle_D \\
&\quad\times {}_D\langle p'q'\,\mathbb{Q}'|p''q''\,\mathbb{Q}''\rangle_n\;{}_n\langle p''q''\,\mathbb{Q}''|\psi_n\rangle\,,
\end{aligned} \tag{6.48}$$

where it is understood that the integration variables are all expressed in terms of a specific choice of the spectator representation. Here, in particular, we have chosen to express the intermediate states in terms of the Jacobi momenta where a neutron is the spectator, i.e., $p' \equiv p'_n$, $p'' \equiv p''_n$, $q' \equiv q'_n$, $q'' \equiv q''_n$. Thus,

$${}_n\langle p'q'\,\mathbb{Q}'|p''q''\,\mathbb{Q}''\rangle_D \equiv {}_n\langle p'_nq'_n\,\mathbb{Q}'|p''_nq''_n\,\mathbb{Q}''\rangle_D \quad \text{and}$$

$${}_D\langle p'q'\,\mathbb{Q}'|p''q''\,\mathbb{Q}''\rangle_n \equiv {}_D\langle p'_nq'_n\,\mathbb{Q}'|p''_nq''_n\,\mathbb{Q}''\rangle_n$$

We further notice that the coupled integral equations comprise several two-body LS kernel-matrix elements of the form ${}_i\langle pq\,\mathbb{Q}|\,G_0(z)t_i(z)\,|p'q'\,\mathbb{Q}'\rangle_i$ and overlap-matrix elements of the form ${}_i\langle p'q'\,\mathbb{Q}'|p''q''\,\mathbb{Q}''\rangle_j$. Their expressions are analytically derived in the following subsections in the context of an effective quantum mechanical framework where only LO effective *separable* potentials are used for calculations. Our methodology is an essential adoption from the universality-based effective potential techniques developed in Refs. [35–37] for a resonant system of three and four bosons, which was later extended in the study of $2n$-halo nuclei such as ^{20}C in Refs [38, 46].[6]

[6]The $2n$-halo nuclei ^{20}C is ostensibly identified as an exited $n - {}^{18}\mathrm{C} - n$ Efimov cluster state [38, 46, 220–222].

6.4.1 Two-body LS kernel matrix elements: ${}_i\langle pq\,\mathbb{Q}|G_0 t_i|p'q'\,\mathbb{Q}'\rangle_i$

In Chapter 2, we presented a derivation of the general form of the two-body T-matrix[7] [cf. Eq. (2.52)] starting from an S-wave non-local separable potential in momentum representation with leading order contact interactions C_0 of the form

$$\langle \mathbf{p}|V_{\rm eff}|\mathbf{p}'\rangle \overset{\rm S-wave}{\longrightarrow} \chi(p)\, C_0\, \chi(p')\,, \tag{6.49}$$

where $\mathbf{p}/\mathbf{p}'$ is the two-body incoming/outgoing relative momentum, and the $\chi(p)$'s are functions, so-called *form factors*, related to the factorized residues at the poles of the corresponding T-matrix/propagator. Thus, the formalism is quite pertinent to the treatment of halo systems where also the binary subsystems are likely to exhibit universality with distinct separation of scales. Besides, owing to the separable nature of the T-matrix, the LS equation is analytically solvable allowing us to directly fix the coupling constant C_0 from the two-body bound state pole of a given subsystem. In the absence of sub-threshold decay channels,[8] the form factors become real and may be used as regulators to suppress high-momentum modes beyond a certain hard/cut-off scale, i.e, for $p, p' \geq \Lambda_H$, where the effective potential breaks down. In this way, one can directly relate to a low-energy EFT description with zero-range contact interactions. In particular, for the purpose of numerical evaluations it is customary to introduce Gaussian regulators of the form [35–38, 46]

$$\chi(p) = \exp\left(-\frac{p^2}{\Lambda_{\rm reg}^2}\right), \tag{6.50}$$

although the low-energy observables are expected to be regulator independent as $\Lambda_{\rm reg} \to \infty$, consistent with RG invariance. Since we eventually wish to correlate the results of the effective potential approach to those obtained in Ref. [109] using pionless EFT, a natural choice of the UV regulator cut-off can be $\Lambda_{\rm reg} \sim \Lambda_H \sim m_\pi$.

The kernel matrix elements associated with the Faddeev equations, Eqs. (6.47) and (6.48), corresponding to a putative bound D^0nn system with three-body binding energy $z = E = -B_3 < 0$, can be represented as:

$${}_i\langle pq\,\mathbb{Q}|\,G_0(z)t_i(z)\,|p'q'\,\mathbb{Q}'\rangle_i = -\mathcal{G}_0^{(i)}(p,q;B_3)\;{}_i\langle pq\,\mathbb{Q}|\,t_i(z)\,|p'q'\,\mathbb{Q}'\rangle_i\,,$$

[7] Since the two-particle T-matrix operator $t_i(z)$ acts only in the binary subsystem i, henceforth $t_i(z)$ is to be understood as an operator embedded in the three-body space, as evident from Eq. (6.52). Thus, the T-matrices t_n and t_D enter into the Faddeev equations (6.47) and (6.48) off-shell at the "shifted" three-body energies $z_n = z - \frac{q_n'^2}{2\mu_{n(nD)}}$ and $z_D = z - \frac{q_D'^2}{2\mu_{D(nn)}}$, respectively, because the evaluations of the operator products $G_0(z)t_n(z)$ and $G_0(z)t_D(z)$ imply an integration over all possible intermediate states $|p'q'\mathbb{Q}'\rangle_n$ and $|p'q'\mathbb{Q}'\rangle_D$, respectively. These shifted energies are obviously the binary subsystem energies obtained by subtracting the kinetic energy of the spectator particle from the three-body energy.

[8] Recall that we invoke ZCL model idealization in the treatment of the D^0n system. For details of the ZCL model approach, see Ref. [109].

where

$$\mathscr{G}_0^{(n)}(p,q;B_3) = \left[B_3+\frac{p^2}{2\mu_{nD}}+\frac{q^2}{2\mu_{n(nD)}}\right]^{-1} = \left[B_3+\frac{y+1}{2yM_n}p^2+\frac{y+2}{2(y+1)M_n}q^2\right]^{-1},$$
$$\mathscr{G}_0^{(D)}(p,q;B_3) = \left[B_3+\frac{p^2}{M_n}+\frac{q^2}{2\mu_{D(nn)}}\right]^{-1} = \left[B_3+\frac{p^2}{M_n}+\frac{y+2}{4yM_n}q^2\right]^{-1}. \quad (6.51)$$

depending on the choice of the spectator particle $i = n, D$. The T-matrix $t_i(z)$ being associated with the two-body subsystem i must be diagonal with respect to the spectator particle quantum numbers and should be evaluated at the shifted energy $z_i = z - \frac{q_i'^2}{2\mu_{i(jk)}}$, namely,

$$ {}_i\langle pq\,\mathbb{Q}|\,t_i(z_i)\,|p'q'\,\mathbb{Q}'\rangle_i = \delta_{JJ'}\,\delta_{M_JM_J'}\,\delta_{LL'}\,\delta_{SS'}\,\delta_{TT'}\,\delta_{M_TM_T'}\,\delta_{\mathfrak{J}\mathfrak{J}'}\,\delta_{\lambda\lambda'}\,\delta_{\sigma\sigma'}\,\delta_{\tau\tau'} \times\frac{\delta(q-q')}{qq'}\;{}_i\langle p(ls)\mathfrak{j}t|\,\widehat{t}_i(z_i)\,|p'(l's')\mathfrak{j}'t'\rangle_i \quad (6.52)$$

Now it is easy to show (see the following proof) that the partial wave projected T-matrix ${}_i\langle p(ls)\mathfrak{j}t|\,\widehat{t}_i(z_i)\,|p'(l's')\mathfrak{j}'t'\rangle_i$ is related to LO S-wave scattering amplitude $T_i(p,p';z_i)$ by the simple relation:

$${}_i\langle p|\,\widehat{t}_i(z_i)\,|p'\rangle_i = 4\pi\,T_i(p,p';z_i)\,. \quad (6.53)$$

Proof: In order to show this, we assumed that the interactions in the binary subsystems conserve the total spin ($\mathfrak{j}$), intrinsic spin (s) and isospin (t), with the obvious exception of Coulomb interactions which we excluded in our formalism. Using the completeness relation we find

$${}_i\langle p(ls)\mathfrak{j}t|\,t_i(z_i)\,|p'(l's)\mathfrak{j}'t\rangle_i = \sum_{m_l,m_l'}\mathscr{C}(lm_l,sm_s;\mathfrak{j})\mathscr{C}(l'm_l',sm_s;\mathfrak{j}')\int \mathrm{d}^3\mathbf{p}''\int \mathrm{d}^3\mathbf{p}''' \times {}_i\langle plm_l|\mathbf{p}''\rangle_i\;{}_i\langle\mathbf{p}''|\,\widehat{t}_i(z_i)\,|\mathbf{p}'''\rangle_i\;{}_i\langle\mathbf{p}'''|p'l'm_l'\rangle_i\,,$$

where $\mathscr{C}$'s represent the *Clebsch-Gordan coefficients*. Next, using the relation, Eq. (6.32), we obtain

$${}_i\langle p(ls)\mathfrak{j}t|\,t_i(z_i)\,|p'(l's)\mathfrak{j}t\rangle_i = \sum_{m_l,m_l'}\mathscr{C}(lm_l,sm_s;\mathfrak{j})\mathscr{C}(l'm_l',sm_s;\mathfrak{j}') \times\int \mathrm{d}\Omega_{\hat{p}}\int \mathrm{d}\Omega_{\hat{p}'}\,Y_l^{m_l*}(\hat{\mathbf{p}})Y_{l'}^{m_l'}(\hat{\mathbf{p}}')\,T_i(\mathbf{p},\mathbf{p}';z_i)$$

Since we shall eventually deal with an S-wave D^0nn system, it makes sense to consider the S-wave projections of the above expression using Legendre polynomial $P_0(\hat{\mathbf{p}}\cdot\hat{\mathbf{p}}')$ with $l,l'=0$, to obtain the desired result:

$${}_i\langle p(l=0)|\,\widehat{t}_i(z_i)\,|p'(l'=0)\rangle_i = \frac{1}{4\pi}\int \mathrm{d}\Omega_{\hat{p}}\int \mathrm{d}\Omega_{\hat{p}'}\,T_i(\mathbf{p},\mathbf{p}';z_i)\,P_0(\hat{\mathbf{p}}\cdot\hat{\mathbf{p}}') = 4\pi\,T_i(p,p';z_i)\,.$$

As we wish to explore the plausibility of a halo-bound D^0nn system where the binary subsystems are also bound/anti-bound, it is of interest to evaluate the T-matrices at the two-body energies $z_i = \mathscr{E}_i + i0$ expressed in terms of the three-body bound state energy B_3. Thus, for the binary subsystems we define the following functions:

$$\gamma_n(q;B_3) \equiv \sqrt{-2\mu_{nD}\mathscr{E}_n(q)} = \sqrt{\frac{y}{y+1}\left(2M_nB_3 + \frac{y+2}{y+1}q^2\right)}\,,$$
$$\gamma_D(q;B_3) \equiv -\sqrt{-2\mu_{nn}\mathscr{E}_D(q)} = -\sqrt{M_nB_3 + \frac{y+2}{4y}q^2}\,. \tag{6.54}$$

Thus, we obtain the following forms for the kernel matrix elements after S-wave projection:

$${}_i\langle pq(\mathcal{I}\mathcal{J})JM_JTM_T|\,G_0(z)t_i(z)\,|p'q'(\mathcal{I}\mathcal{J})JM_JTM_T\rangle_i = -4\pi\mathcal{G}_0^{(i)}(p,q;B_3)\frac{\delta(q-q')}{qq'}T_i(p,p';z_i)\,, \tag{6.55}$$

where $z = E = -B_3$, $\mathcal{G}_0^{(i)}$'s are defined in Eq. (6.51), and the LO S-wave two-body T-matrices are expressed in the separable form:

$$T_i(p,p';\mathscr{E}_i) = -\frac{1}{4\pi}\chi(p)\,\chi(p')\,\tau_i(q';B_3)\,, \tag{6.56}$$

with the terms containing information regarding the short-range effective interactions, given by

$$\tau_n(q;B_3) = \frac{y+1}{\pi y M_n}\Bigg[-\frac{1}{a_{nD}}\exp\left(\frac{2}{a_{nD}^2\Lambda_{\rm reg}^2}\right)\,\mathrm{erfc}\left(\frac{\sqrt{2}}{|a_{nD}|\Lambda_{\rm reg}}\right)$$
$$+\gamma_n(q;B_3)\exp\left(\frac{2\gamma_n^2(q;B_3)}{\Lambda_{\rm reg}^2}\right)\mathrm{erfc}\left(\frac{\sqrt{2}\gamma_n(q;B_3)}{\Lambda_{\rm reg}}\right)\Bigg]^{-1} \quad \text{and}$$
$$\tau_D(q;B_3) = \frac{2}{\pi M_n}\Bigg[-\frac{1}{a_{nn}}\exp\left(\frac{2}{a_{nn}^2\Lambda_{\rm reg}^2}\right)\,\mathrm{erfc}\left(\frac{\sqrt{2}}{|a_{nn}|\Lambda_{\rm reg}}\right)$$
$$-\gamma_D(q;B_3)\exp\left(\frac{2\gamma_D^2(q;B_3)}{\Lambda_{\rm reg}^2}\right)\mathrm{erfc}\left(\frac{-\sqrt{2}\gamma_D(q;B_3)}{\Lambda_{\rm reg}}\right)\Bigg]^{-1}, \tag{6.57}$$

where the the well-known *complementary error function* defined by the integral

$$\mathrm{erfc}(z) = 1 - \frac{2}{\sqrt{\pi}}\int_0^z \mathrm{d}t\,\exp(-t^2)\,, \tag{6.58}$$

and a_{nn} and a_{nD} are the S-wave n-n and n-D scattering lengths, respectively. Notice that when $q = 0$ the two-body bound states correspond to the respective poles in the above

T-matrices which at LO correspond to binding momenta

$$\gamma_n(q=0;B_3=B_{nD}) = \sqrt{2\mu_{nD}B_{nD}} = \frac{1}{a_{nD}} > 0 \quad \text{and}$$
$$\gamma_D(q=0;B_3=B_{nn}) = -\sqrt{2\mu_{nn}B_{nn}} = \frac{1}{a_{nn}} < 0\,, \tag{6.59}$$

with the three-body binding energy B_3 coinciding with the two-body binding energy $B_2 = B_{nn}$ and $B_2 = B_{nD}$, respectively.[9] We finally, note here that analogous expressions for the T-matrices were previously obtained in Refs. [35–38, 46] in the context of universality based studies of bosonic systems, and in the investigation of ^{20}C as a $2n$-halo nucleus.

6.4.2 Overlap-matrix elements : ${}_i\langle pq\,\mathbb{Q}|p'q'\,\mathbb{Q}'\rangle_j$

Next, we discuss the evaluation of the overlap-matrix elements ${}_i\langle pq\,\mathbb{Q}|p'q'\,\mathbb{Q}\rangle_j$ (where $i,j = n, D$) of the Faddeev equations, Eqs. (6.47) and (6.48), which yields the transition amplitudes between different re-arrangements of the three-body system. These are obtained *via* evaluation of the re-coupling coefficient between different Jacobi momentum state representation. For details of the general method of derivation, we refer the reader to the book by W. Glöckle [50]. Here we only quote the end result for the S-wave projected generic overlap-matrix element relevant to the D^0nn system, namely,

$${}_i\langle pq\,\mathbb{Q}|p'q'\,\mathbb{Q}'\rangle_j \equiv {}_i\langle p_iq_i\,\mathbb{Q}|p_i'q_i'\,\mathbb{Q}'\rangle_j = \int_{-1}^{1} \mathrm{d}x\, \frac{\delta(p-\pi_{ij})}{p\pi_{ij}} \frac{\delta(p'-\pi'_{ij})}{p'\pi'_{ij}}\, \mathscr{G}^{(ij)}_{\mathbb{Q}\mathbb{Q}'}\,, \tag{6.60}$$

where $x \equiv \hat{\mathbf{q}}\cdot\hat{\mathbf{q}}'$ is the cosine of the angle between the initial and final spectator relative momenta with respect to the binary subsystem j-k, such that

$$\pi_{ij}(q,q';x) = \sqrt{\left(\frac{\mu_{jk}}{m_k}\right)^2 q^2 + q'^2 + 2\left(\frac{\mu_{jk}}{m_k}\right) qq'x} \quad \text{and}$$
$$\pi'_{ij}(q,q';x) = \sqrt{q^2 + \left(\frac{\mu_{ki}}{m_k}\right)^2 q'^2 + 2\left(\frac{\mu_{ki}}{m_k}\right) qq'x}\,, \tag{6.61}$$

are the magnitudes of the shifted momenta. The quantity

$$\mathscr{G}^{(ij)}_{\mathbb{Q}\mathbb{Q}'} = \frac{1}{2}\sqrt{\hat{s}\,\hat{\jmath}\,\hat{t}\,\hat{\mathcal{J}}\,\hat{s}'\,\hat{\jmath}'\,\hat{t}'\,\hat{\mathcal{J}}'}\,(-1)^{t_i+2t_j+t_k+t'}\,(-1)^{s_i+2s_j+s_k+s'}$$
$$\times \begin{Bmatrix} t_j & t_k & t \\ t_i & T & t' \end{Bmatrix} \begin{Bmatrix} s_j & s_k & s \\ s_i & S & s' \end{Bmatrix} \sum_S \hat{S} \begin{Bmatrix} 0 & s & \jmath \\ 0 & \sigma & \mathcal{J} \end{Bmatrix} \begin{Bmatrix} 0 & s' & \jmath' \\ 0 & \sigma' & \mathcal{J}' \end{Bmatrix} \begin{Bmatrix} 0 & S & J \end{Bmatrix}, \tag{6.62}$$

[9] Here we re-emphasize that the di-neutron (n-n) form an virtual/anti-bound subsystem with negative binding momenta and S-wave scattering length of $a_{nn} = -18.63$ fm [30], whereas the n-D^0 subsystem is assumed to form a real bound state with positive binding momenta and S-wave scattering length of $a_{nD} = 4.141$ fm. The latter value is extracted from the dynamical coupled-channel model analysis of Ref. [109] in an idealized limit of vanishing couplings to sub-threshold DN ($T=1$) decay channels.

is a simple geometrical constant arising due to re-coupling of the Jacobi momentum between two different spectator representations with indices i and j. Each overlap-matrix has four momenta, of which any two of them can be eliminated in favor of the other two upon integration over the two delta-functions in Eq. (6.60). Here, we prefer to eliminate p and p' in favor of q and q'. Now we consider the following three cases of the overlap-matrix relevant to the Faddeev equations of the D^0nn system:

- **Case I:** Due to swapping of the two spectator neutrons:

$$ {}_{n_1}\langle pq\,\mathbb{Q}|\,\mathcal{P}|p'q'\,\mathbb{Q}'\rangle_{n_1} = {}_{n_1}\langle pq\,\mathbb{Q}|p'q'\,\mathbb{Q}'\rangle_{n_2} \equiv {}_{n_1}\langle pq|p'q'\rangle_{n_2}\delta_{\mathbb{Q}\mathbb{Q}'}\,. \tag{6.63} $$

  In this case, since the states $|pq\,\mathbb{Q}\rangle_{n_1}$ and $|p'q'\,\mathbb{Q}'\rangle_{n_2}$ correspond to identical binary subsystem n-D^0, the particle re-arrangement leads to the same set of discrete quantum numbers, i.e., $\mathbb{Q}' = \mathbb{Q}$, as displayed in Table. 6.1. In particular, the Pauli principle demands that the halo-neutrons must have an opposite intrinsic spin for an S-wave three-body system. Consequently, the total spin of the system should be the same as the spin of the core D^0-meson which is obviously 0. By using these quantum numbers in

$l=0$	$s=1/2$	$\mathcal{j}=1/2$	$t=1$
$\lambda=0$	$\sigma=1/2$	$\mathcal{J}=1/2$	$\tau=1/2$
$L=0$	$S=0$	$J=0$	$T=3/2$

TABLE 6.1: Various discrete quantum numbers corresponding to the state $|pq\,\mathbb{Q}\rangle_n$.

  Eq. (6.62) the value of the geometrical re-coupling constant is obtained as $\mathscr{G}^{(nn)}_{\mathbb{Q}\mathbb{Q}} = -1/2$, which leads to the result:

$$ {}_{n_1}\langle pq\,\mathbb{Q}|p'q'\,\mathbb{Q}\rangle_{n_2} \equiv {}_{n_1}\langle p_{n_1}q_{n_1}\,\mathbb{Q}|p'_{n_1}q'_{n_1}\,\mathbb{Q}\rangle_{n_2} = -\frac{1}{2}\int_{-1}^{1}\mathrm{d}x\frac{\delta(p-\pi_{nn})}{p\pi_{nn}}\frac{(p'-\pi'_{nn})}{p'\pi'_{nn}}\,, \tag{6.64} $$

  with the shifted momenta given as

$$ \begin{aligned} \pi_{nn}(q,q';x) &= \sqrt{\left(\frac{1}{y+1}\right)^2 q^2 + q'^2 + 2\left(\frac{1}{y+1}\right)qq'x} \quad \text{and} \\ \pi'_{nn}(q,q';x) \equiv \pi_{nn}(q',q;x) &= \sqrt{q^2 + \left(\frac{1}{y+1}\right)^2 q'^2 + 2\left(\frac{1}{y+1}\right)qq'x}\,. \end{aligned} \tag{6.65} $$

- **Case II:** Due to interchange of a spectator neutron with the core D^0-meson as a spectator:

$$ {}_{n}\langle pq\,\mathbb{Q}|p'q'\,\mathbb{Q}'\rangle_{D}\,. $$

  In this case, since the state $|pq\,\mathbb{Q}\rangle_n$ corresponds to the n-D^0 binary subsystem, the unprimed quantum numbers are identical to those in Table 6.1. Whereas, the state

$|p'q'\,\mathbb{Q}'\rangle_D$ corresponds to the n-n binary subsystem with the core D^0-meson as the spectator. The set of discrete quantum numbers for the latter state is displayed in Table 6.2. By using in Eq. (6.62) the unprimed and primed set of quantum numbers from Tables 6.1

$l'=0$	$s'=0$	$\mathcal{J}'=0$	$t'=1$
$\lambda'=0$	$\sigma'=0$	$\mathcal{F}'=0$	$\tau'=1/2$
$L=0$	$S=0$	$J=0$	$T=3/2$

TABLE 6.2: Various discrete quantum numbers corresponding to the state $|p'q'\,\mathbb{Q}'\rangle_D$.

and 6.2, respectively, we obtain the value of the re-coupling constant as $\mathscr{G}^{(nD)}_{\mathbb{Q}\mathbb{Q}'}=1/2$, leading to the result:

$$ {}_n\langle p_n q_n\,\mathbb{Q}|p'_n q'_n\,\mathbb{Q}'\rangle_D \equiv {}_n\langle pq\,\mathbb{Q}|p'q'\,\mathbb{Q}'\rangle_D = \frac{1}{2}\int_{-1}^{1}\mathrm{d}x\frac{\delta(p-\pi_{nD})}{p\pi_{nD}}\frac{\delta(p'-\pi'_{nD})}{p'\pi'_{nD}} \tag{6.66} $$

with the shifted momenta given as

$$ \pi_{nD}(q,q';x)=\sqrt{\left(\frac{y}{y+1}\right)^2 q^2+q'^2+2\left(\frac{y}{y+1}\right)qq'x} \qquad \text{and} $$

$$ \pi'_{nD}(q,q';x)=\sqrt{q^2+\frac{q'^2}{4}+qq'x}\,. \tag{6.67} $$

- **Case III:** Due to the interchange of the spectator core D^0-meson with any one of the halo-neutron as the spectator:

$$ {}_D\langle pq\,\mathbb{Q}|p'q'\,\mathbb{Q}'\rangle_n\,. $$

In this case with the unprimed and primed set of discrete quantum numbers swapped with respect to Case II leaving the re-coupling constant unchanged, namely, $\mathscr{G}^{(Dn)}_{\mathbb{Q}\mathbb{Q}'}=1/2$. The corresponding result is obtained as

$$ \begin{aligned} {}_D\langle p_n q_n\,\mathbb{Q}|p'_n q'_n\,\mathbb{Q}'\rangle_n \equiv {}_D\langle pq\,\mathbb{Q}|p'q'\,\mathbb{Q}'\rangle_n &= \frac{1}{2}\int_{-1}^{1}\mathrm{d}x\frac{\delta(p-\pi_{Dn})}{p\pi_{Dn}}\frac{\delta(p'-\pi'_{Dn})}{p'\pi'_{Dn}} \\ &= \frac{1}{2}\int_{-1}^{1}\mathrm{d}x\frac{\delta(p-\pi'_{nD})}{p\pi'_{nD}}\frac{\delta(p'-\pi_{nD})}{p'\pi_{nD}}\,, \end{aligned} \tag{6.68} $$

with the shifted momenta given as

$$ \begin{aligned} \pi_{Dn}(q,q';x) \equiv \pi'_{nD}(q',q;x) &= \sqrt{\frac{q^2}{4}+q'^2+qq'x} \quad \text{and} \\ \pi'_{Dn}(q,q') \equiv \pi_{nD}(q',q;x) &= \sqrt{q^2+\left(\frac{y}{y+1}\right)^2 q'^2+2\left(\frac{y}{y+1}\right)qq'x}\,. \end{aligned} \tag{6.69} $$

6.4.3 Faddeev Equations for an S-wave $2n$-halo D^0nn system at LO

Having all the necessary ingredients (namely, the various LO kernel and overlap-matrix elements), we can spell out the explicit form of the Faddeev equations for a $2n$-halo D^0nn system at LO. We use the results, Eqs. (6.55), (6.56), (6.57), (6.64), (6.65), (6.66), (6.67), (6.68) and (6.69), obtained in the previous two subsections in Eqs. (6.47) and (6.48), and then integrate over the delta functions to obtain the following set of homogeneous integral equations [35–38, 46]:

$$\psi_n(p,q) = \frac{1}{2}\mathcal{G}_0^{(n)}(p,q;B_3)\,\chi(p)\,\tau_n(q;B_3)\int_0^\infty \mathrm{d}q''q''^2\int_{-1}^{1}\mathrm{d}x \times\Big[\chi\left(\pi_{nn}(q,q'';x)\right)\psi_n\left(\pi_{nn}(q'',q;x),q''\right)+\chi\left(\pi_{nD}(q,q'';x)\right)\psi_D\left(\pi'_{nD}(q,q'';x),q''\right)\Big], \tag{6.70}$$

and

$$\psi_D(p,q) = \mathcal{G}_0^{(D)}(p,q;B_3)\,\chi(p)\,\tau_D(q;B_3)\int_0^\infty \mathrm{d}q''q''^2\int_{-1}^{1}\mathrm{d}x\,\chi\left(\pi'_{nD}(q'',q;x)\right)\psi_n\left(\pi_{nD}(q'',q;x),q''\right), \tag{6.71}$$

where for convenience we have defined $\psi_i(p,q) \equiv {}_i\langle pq\,\mathbb{Q}|\psi_i\rangle$.

For the sake of simplicity of the numerical solutions, it is advantageous to simplify the integral equations by introducing the so-called *spectator functions* $F_i(q)$ [223], corresponding to each of the two Faddeev components:

$$\psi_i(p,q) = \mathcal{G}_0^{(i)}(p,q;B_3)\,\chi(p)\,\tau_i(q;B_3)\,F_i(q)\,;\quad i=n,D\,. \tag{6.72}$$

Thus, we end up with the following set of single-variable coupled integral equations instead of two variables which is obviously easier to solve numerically:[10]

$$F_n(q) = \frac{1}{2}\int_0^\infty \mathrm{d}q'q'^2\int_{-1}^{1}\mathrm{d}x\Big[\chi\left(\pi_{nn}(q,q';x)\right)\,\chi\left(\pi_{nn}(q',q;x)\right) \times\mathcal{G}_0^{(n)}(\pi_{nn}(q',q;x),q';B_3)\,\tau_n(q';B_3)\,F_n(q') +\chi\left(\pi_{nD}(q,q';x)\right)\,\chi\left(\pi'_{nD}(q,q';x)\right) \times\mathcal{G}_0^{(D)}(\pi'_{nD}(q,q';x),q';B_3)\,\tau_D(q';B_3)\,F_D(q')\Big], \tag{6.73}$$

[10] Here for brevity we have preferred to replace the integration variable q'' by q'.

and

$$F_D(q) = \int_0^\infty \mathrm{d}q' q'^2 \int_{-1}^{1} \mathrm{d}x \Big[\chi\left(\pi_{nD}(q',q;x)\right) \chi\left(\pi'_{nD}(q',q;x)\right) \times \mathscr{G}_0^{(n)}(\pi_{nD}(q',q;x),q';B_3)\, \tau_n(q';B_3)\, F_n(q') \Big] . \tag{6.74}$$

The above coupled integral equations essentially describe the LO three-body dynamics of multiple scattering between the core D^0-meson and the two spectator neutrons as diagrammatically represented using Feynman diagrams in Fig. 6.4. In effect, they are completely analogous to the homogeneous parts of the corresponding set of two coupled STM equations for the D^0nn system derived in Ref. [109] in the context of LO $\not\pi$EFT [2–6, 12] with sharp momentum cut-off regularization instead.[11] Analogously, they yield the three-body binding energy B_3 for which they have a nontrivial solution. Written in the following matrix form:

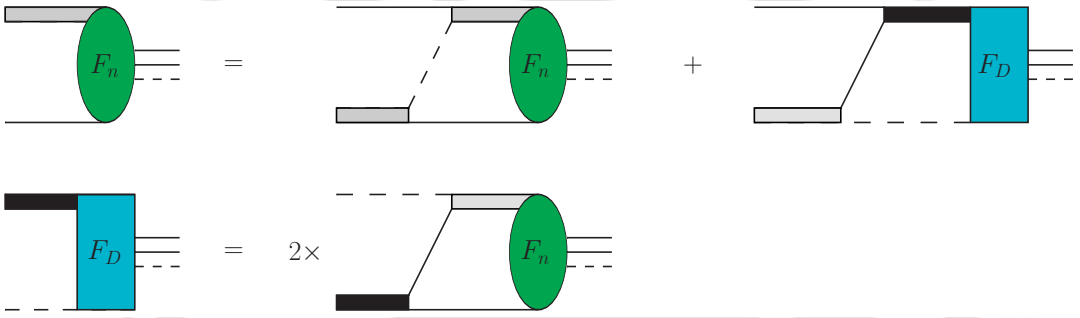

FIGURE 6.4: Feynman diagrams for the leading order coupled-channel homogeneous integral equations for the spectator functions $F_i(q)$ (where $i = n, D$) of an S-wave $2n$-halo D^0nn system. The solid/dashed lines represent the neutron (n)/D^0-meson fields. The gray/black thick shaded thick lines represent the iterated n-D^0/n-n two-body S-wave T-matrices τ_i, which in pionless EFT are interpreted as renormalized dressed propagators for the corresponding dimer fields. The elliptical/rectangular blobs represent, e.g., the elastic/inelastic channel $n + d_{nD} \to n + d_{nD}$ / $D^0 + s_{(nn)} \to n + d_{nD}$ transition amplitudes, which are proportional to the spectator functions in the vicinity of trimer pole energies.

$$\begin{bmatrix} F_n \\ F_D \end{bmatrix} = \begin{bmatrix} \mathscr{K}_{nn} & \mathscr{K}_{nD} \\ \mathscr{K}_{Dn} & 0 \end{bmatrix} \begin{bmatrix} F_n \\ F_D \end{bmatrix} , \tag{6.75}$$

with discretized incoming q and outgoing q' relative momenta, the binding energy B_3 corresponds to the eigenvalue of the kernel matrix $\mathscr{K}_{ij}$ [constructed from Eqs. (6.73) and (6.74)] of unity. In the next section we shall demonstrate how the eigen-solutions to the spectator functions F_n and F_D are used to determine the various one- and two-body matter density form factors, that subsequently yield information on the structural characteristic of a plausible halo-bound D^0nn system. In the following subsection, we shall dwell upon establishing

[11] In the analogous EFT scenario the integral equations are described by *half-off-shell* transition amplitudes instead of the spectator functions F_i, which connect the spectator and the interacting pair to form the three-body bound states. Furthermore, to describe the two-body bound state dynamics the iterated interaction T-matrices τ_i are replaced in EFT by renormalized quasiparticle or *dimeron* propagators [1, 8, 12, 52–55, 224, 225] in the STM equations.

some of the connections between the current effective quantum mechanical framework and the standard LO ♯EFT approach in the analysis of the D^0nn system [109].

6.4.4 Faddeev Equations with Sharp Momentum Cut-off: An EFT connection

In Ref. [109], the S-wave D^0nn system was investigated for the manifestation of Efimov effects under idealized zero coupling limit ansatz that eliminated sub-threshold DN ($T = 1$) decay channels in the charm sector, e.g., $\pi^-\Lambda_c$, $\pi^0\Sigma_c^0$ and $\pi^-\Sigma_c^+$. In this scenario, the D^0nn system forms a three-particle $2n$-halo cluster, with the so-called *Samba* configuration [24], having two real bound n-D^0 subsystems and the virtual bound n-n subsystem. The fact that both types of binary subsystems develop large real-valued scattering lengths make the D^0nn system a good Efimovian candidate. Using the framework of ♯EFT [2–6, 12] at LO the qualitative features of three-body universality were explored. The non-relativistic effective Lagrangian at LO, consistent with low-energy symmetries (P, C, T, and Galilean invariances) can be constructed as the sum of one-, two- and three-body parts [109]:

$$\mathscr{L} = \left[\mathscr{L}_n + \mathscr{L}_D\right]_{1-\text{body}} + \left[\mathscr{L}_{s(nn)} + \mathscr{L}_{d(nD)}\right]_{2-\text{body}} + \mathscr{L}_{3-\text{body}}\,, \tag{6.76}$$

with

$$\mathscr{L}_n(x) = n^\dagger(x)\left[i\partial_t + \frac{\nabla^2}{2M_n}\right] n(x) + \cdots\,, \tag{6.77}$$

$$\mathscr{L}_D(x) = D^\dagger(x)\left[i\partial_t + \frac{\nabla^2}{2yM_n}\right] D(x) + \cdots\,, \tag{6.78}$$

$$\begin{aligned}\mathscr{L}_{s(nn)}(x) = &- s^\dagger_{(nn)}(x)\left[i\partial_t + \frac{\nabla^2}{4M_n} - \Delta_{s(nn)}\right] s_{(nn)}(x) \\ &- g_{2s}\left[s^\dagger_{(nn)}(x)\left(n^T(x)\,\hat{P}^{(^1S_0)}_{(nn)}\,n(x)\right) + \text{h.c.}\right] + \cdots\,,\end{aligned} \tag{6.79}$$

$$\begin{aligned}\mathscr{L}_{d(nD)}(x) = &- d^\dagger_{(nD)}(x)\left[i\partial_t + \frac{\nabla^2}{2M_n(1+y)} - \Delta_{d(nD)}\right] d_{(nD)}(x) \\ &- g_{2d}\left[d^\dagger_{(nD)}(x)\,n(x)\,D(x) + \text{h.c.}\right] + \cdots\,,\end{aligned} \tag{6.80}$$

and

$$\begin{aligned}\mathscr{L}_{3-body}(x) = -\frac{M_n g_3(\Lambda_{\text{reg}})}{\Lambda^2_{\text{reg}}}\Bigg[&y g^2_{2d}\left\{d^T_{(nD)}(x)\,\hat{P}^{(^1S_0)}_{(nd)}\,n(x)\right\}^\dagger\left\{d^T_{(nD)}(x)\,\hat{P}^{(^1S_0)}_{(nd)}\,n(x)\right\} \\ &+ 2g_{2s}g_{2d}\left\{d^T_{(nD)}(x)\,\hat{P}^{(^1S_0)}_{(nd)}\,n(x)\right\}^\dagger\left\{s_{(nn)}(x)\,D(x)\right\} + \text{h.c.}\Bigg] + \cdots\end{aligned} \tag{6.81}$$

where the ellipses are used to denote two- and three-body derivative interactions which by power counting contribute at subleading orders. For details on the ${}^{\not\pi}$EFT power counting, we refer the reader to Refs. [2–6, 12]. In the above expressions as explicit degrees of freedom one includes the neutron field $n(x)$ and the D^0-meson field $D(x)$ as the elementary fields of the theory, whose kinetic parts constitute the one-body terms of the effective Lagrangian. Here we again expressed the mass of the D^0-mesons in terms of the neutron mass, such that $M_D = yM_n$. In view of the bound/anti-bound binary subsystems, it is convenient in the EFT to introduce the unitarized auxiliary/composite dimeron fields [1, 8, 12, 52–55, 224, 225], namely, the spin singlet n-n di-neutron field $s_{(nn)}(x)$ and the spin-doublet n-D^0 dihadron field $d_{(nD)}(x)$.[12] The corresponding renormalized dressed propagators (cf. Fig. 6.5) are given as

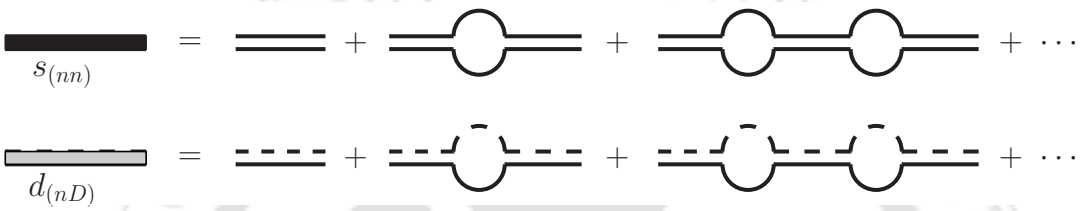

FIGURE 6.5: Renormalized dressed dimeron propagators associated with the n-n and n-D^0 subsystems.

$$iS_d^R(l_0,\mathbf{l}) = i\left[\frac{1}{a_{nD}} - \sqrt{\frac{y}{y+1}\left(-2M_n l_0 + \frac{\mathbf{l}^2}{y+1} - i\epsilon\right)} - i\epsilon\right]^{-1} \quad \text{and}$$
$$iS_s^R(l_0,\mathbf{l}) = i\left[\frac{1}{a_{nn}} - \sqrt{-M_n l_0 + \frac{\mathbf{l}^2}{4} - i\epsilon} - i\epsilon\right]^{-1}, \tag{6.82}$$

where $l \equiv (l_0,\mathbf{l})$ is the *lab*-frame four-momentum of the dimeron fields. Equivalently, in the three-body center-of-mass frame, the above propagators can be re-expressed in terms of the total three-body energy $z = E + i\epsilon$ and the Jacobi momentum $q = |\mathbf{q}|$ by subtracting the respective kinetic energies of the spectator particle:

$$iS_d^R\left(z - \frac{q^2}{2M_n}, \mathbf{q}\right) = i\left[\frac{1}{a_{nD}} - \sqrt{\frac{y}{y+1}\left(-2M_n z + \frac{y+2}{y+1}q^2\right)} - i\epsilon\right]^{-1} \quad \text{and}$$
$$iS_s^R\left(z - \frac{q^2}{2yM_n}, \mathbf{q}\right) = i\left[\frac{1}{a_{nn}} - \sqrt{-M_n z + \frac{y+2}{4y}q^2} - i\epsilon\right]^{-1}. \tag{6.83}$$

[12]The inclusion of the auxiliary field formalism within the ${}^{\not\pi}$EFT framework is known to yield better convergence in the two-body sector, especially in the vicinity of threshold bound states [8, 224, 225]. Besides, that, the construction of *genuine* three-body interaction operators in the effective Lagrangian becomes quite straightforward using such auxiliary fields. In contrast, the general methodology of including three-body interaction in a quantum mechanical framework is rather involved [35, 226].

The ${}^1S_0$ projection operators in the respective spin channels are given in terms of the Pauli matrix σ_2:

$$\hat{P}^{({}^1S_0)}_{(nn)} = -i\frac{1}{2}\sigma_2 \qquad \text{and} \qquad \hat{P}^{({}^1S_0)}_{(nd)} = -i\frac{1}{\sqrt{2}}\sigma_2\,. \tag{6.84}$$

The $\Delta_{s(nn)}$ and $\Delta_{d(nK)}$ are the respective mass differences between the corresponding dimeron fields and their constituent bound particles, and g_{2s} and g_{2d} are the LO two-body contact interaction couplings in the spin-singlet and spin-doublet channels, respectively. These four quantities constitute the S-wave parameters of the LO two-body Lagrangian which can be fixed as follows:

$$\begin{aligned} g^2_{2s} &= \frac{4\pi}{M_n}\,, \quad g^2_{2d} = \frac{2\pi}{\mu_{nD}}\,, \\ \Delta_{s(nn)} + \frac{M_n g^2_{2s}}{2\pi^2} &= \frac{1}{a_{nn}}\,, \quad \text{and} \quad \Delta_{d(nD)} = \frac{1}{a_{nD}}\,, \end{aligned} \tag{6.85}$$

where $a_{nn} = -18.63$ fm [30] is the phenomenologically extracted spin-singlet nn S-wave scattering length, and $a_{nD} = 4.141$ fm is the spin-doublet D^0n S-wave scattering length obtained in the idealized ZCL scenario [109]. The latter value was extracted from the dynamical coupled-channel model analysis with vanishing couplings to sub-threshold decay channels. It is worth noting that the "wrong signs" in front of the kinetic operators for the composite dimeron fields suggest the quasi-particle nature of these fields. Besides, these signs also ensure that corresponding effective ranges remain positive. The LO three-body Lagrangian (also regarded as the *three-body force* (3BF) term) with the sharp momentum cut-off ($\Lambda_{\rm reg}$) dependent contact coupling $g_3 = g_3(\Lambda_{\rm reg})$ is introduced primarily for renormalization of the two-body STM equations.[13] The value of g_3 which is *a priori* unknown is fixed *via* a three-body datum, e.g., one of the D^0nn binding energies B_3 or the corresponding S-wave three-body scattering length a_3. But unfortunately, there is no consensus whether D^0nn forms any bound state with neither of B_3 or a_3 known currently. Therefore, the predictability of the theory at present rests solely upon guesstimating these quantities based on plausibility arguments. Once g_3 is fixed, other low-energy observables, such as the matter density form factors and their corresponding mean square radii, can readily be predicted.

With the above-mentioned components of $\not\pi$EFT, it is straightforward to use Feynman diagram techniques to obtain a set of two inhomogeneous coupled STM integral equation for the D^0nn system. These represent the multiple scattering series in the elastic ($n + d_{nD} \to n + d_{nD}$) and inelastic ($D^0 + s_{(nn)} \to n + d_{nD}$) scattering channels (denoted by a and b) as described

[13] In Ref. [109] it was observed that the STM integral equations for the D^0nn system with only the two-body interaction g_{2s} and g_{2d} included become ill-defined in UV limit of the loop integrations. Thus, a regulator, say, in the form of a sharp momentum cut-off was needed to be included as the finite UV limit of the integrals [61]. Concomitantly, scale-dependent *non-derivatively coupled* 3BF terms are also needed as a part of the LO Lagrangian. This guaranteed that the calculated low-energy observables were regularization invariant.

in terms of the respective half-off-shell transition amplitudes [109]:

$$\mathcal{T}_n(p,q;E) \equiv t_a(p,q;E) \quad \text{and} \quad \mathcal{T}_D(p,q;E) \equiv \sqrt{2}t_b(p,q;E)\,.$$

However, to look for Efimov trimers, the corresponding homogeneous equations are needed to be solved for non-trivial solutions $E = -B_3$ with a given UV cut-off $\Lambda_{\rm reg}$.[14] The solutions correspond to the poles of the scattering amplitudes in the location of which their residues factorize into *dimensionless* spectator functions of the Jacobi momenta p and q:

$$\mathcal{T}_n(p,q;E) \overset{E\to -B_3}{\approx} \frac{F_n(p)F_n(q)}{E+B_3} \quad \text{and} \quad \mathcal{T}_D(p,q;E) \overset{E\to -B_3}{\approx} \frac{F_D(p)F_D(q)}{E+B_3}\,. \tag{6.86}$$

Invoking the above separable ansatz, we can reduce the two-variable STM equations into a single-variable (in Jacobi momentum q) coupled integral equations described by the spectator functions.

Next, to understand the equivalence between the Faddeev and the STM equations, we note that in EFT the effective potentials [cf. Eq. (6.49)] simply correspond to zero-range contact interactions which vanish for momenta larger than the cut-off scale $\Lambda_{\rm reg}$. With the Gaussian regulator function $\chi(p)$, Eq. (6.50), set to 1, the two-body interaction T-matrix element is similarly evaluated, except that the UV limit of the loop integration is replaced by the finite cut-off $\Lambda_{\rm reg} < \infty$. The expression of the T-matrix elements in this case is obtained with the substitution

$$\exp(X^2)\,\mathrm{erfc}(X) \to \frac{2}{\pi}\arctan\left(\frac{\sqrt{2}}{X}\right)$$

in the generic expression for the two-body T-matrix, Eq (2.52), presented in Chapter 2 with Gaussian regulators. To that effect, the corresponding LO S-wave T-matrix elements in the sharp cut-off scheme are given as follows:

$$\tau_n(q;B_3) = \frac{y+1}{\pi y M_n}\left[-\frac{1}{a_{nD}}\frac{2}{\pi}\arctan\left(|a_{nD}|\Lambda_{\rm reg}\right) + \gamma_n(q;B_3)\frac{2}{\pi}\arctan\left(\frac{\Lambda_{\rm reg}}{\gamma_n(q;B_3)}\right)\right]^{-1} \quad \text{and}$$

$$\tau_D(q;B_3) = \frac{2}{\pi M_n}\left[-\frac{1}{a_{nn}}\frac{2}{\pi}\arctan\left(|a_{nn}|\Lambda_{\rm reg}\right) - \gamma_D(q;B_3)\frac{2}{\pi}\arctan\left(\frac{\Lambda_{\rm reg}}{-\gamma_D(q;B_3)}\right)\right]^{-1} \tag{6.87}$$

where the functions γ_n and γ_D are defined in Eq. (6.54), such that their magnitudes at $q = 0$ yield the binding momenta of the respective bound and anti-bound two-body systems. Now, it is easy to check that for large values of the cut-off, $\Lambda_{\rm reg} \to \infty$, both the inverse tangent functions approach $\pi/2$. Thus, the above expressions for the two-body T-matrix elements reduce to the renormalized two-body scattering amplitudes which are also proportional to the

[14] A $\not\pi$EFT using a Gaussian regularization scheme is somewhat non-trivial due to the intricate nature of renormalization associated with the inclusion of the LO 3BF [35]. The sharp momentum cut-off scheme happens to be a more convenient choice for regularization.

renormalized dressed dimeron propagators:

$$\tau_n(q;B_3) = \frac{y+1}{\pi y M_n}\left[-\frac{1}{a_{nD}} + \gamma_n(q;B_3)\right]^{-1} \equiv -\frac{y+1}{\pi y M_n} S_d^R\left(-B_3 - \frac{q^2}{2M_n}, \mathbf{q}\right) \quad \text{and}$$

$$\tau_D(q;B_3) = \frac{2}{\pi M_n}\left[-\frac{1}{a_{nn}} - \gamma_D(q;B_3)\right]^{-1} \equiv -\frac{2}{\pi M_n} S_s^R\left(-B_3 - \frac{q^2}{2yM_n}, \mathbf{q}\right). \tag{6.88}$$

Next, focusing on the coupled integral Faddeev equation for the spectator functions [cf. Eqs. (6.73) and (6.74)], we replace their upper limit of infinite loop integration by the finite cut-off $\Lambda_{\rm reg}$, as well as replace the Gaussian regulator function $\chi(\pi_{ni}) \to 1$ (where $i = n, D$). With the Gaussian functions excluded, the only $x \equiv \hat{\mathbf{q}}\cdot\hat{\mathbf{q}}'$ dependence arises from the free three-body propagator functions $\mathscr{G}_0^{(i)}$. In this case, the integration over x can be analytically performed to obtain a form analogous to the *homogeneous* part of the STM equation (without a 3BF) for the D^0nn system obtained in the context of $\not\pi$EFT [109]:

$$F_n(q) = -\frac{1}{\pi}\int_0^{\Lambda_{\rm reg}} \mathrm{d}q' q'^2 \left[(y+1)\mathscr{K}_{(D)}(q,q';B_3)\, S_d^R\left(-B_3 - \frac{q'^2}{2M_n}, \mathbf{q}'\right) F_n(q') \right.$$
$$\left. + 2\mathscr{K}_{(n)}(q,q';B_3)\, S_s^R\left(-B_3 - \frac{q'^2}{2yM_n}, \mathbf{q}'\right) F_D(q')\right],$$

and

$$F_D(q) = -\frac{2(y+1)}{\pi y}\int_0^{\Lambda_{\rm reg}} dq' q'^2 \left[\mathscr{K}_{(n)}(q',q;B_3)\, S_d^R\left(-B_3 - \frac{q'^2}{2M_n}, \mathbf{q}'\right) F_n(q')\right], \tag{6.89}$$

where the kernel functions are given as

$$\mathscr{K}_{(D)}(q,q';B_3) = \frac{1}{2qq'}\ln\left(\frac{ayM_nB_3 + q^2 + q'^2 + aqq'}{ayM_nB_3 + q^2 + q'^2 - aqq'}\right); \quad a = \frac{2}{y+1}$$

and

$$\mathscr{K}_{(n)}(q,q';B_3) = \frac{1}{2qq'}\ln\left(\frac{M_nB_3 + q^2 + bq'^2 + qq'}{M_nB_3 + q^2 + bq'^2 - qq'}\right); \quad b = \frac{y+1}{2y}. \tag{6.90}$$

Note that the notation used above is different from the spectator representation of the three-particle Green's function $\mathscr{G}_0^{(i)}$, where $i = n, D$. Here instead $\mathscr{K}_{(\gamma)}$ represents the free propagation of the exchanged particle $\gamma = n, D$ between dimers in two different rearrangement channels.

Now, it becomes straightforward to include the LO 3BF term as we discussed in Chapters 3 and 4 of this thesis for the study of $\Lambda\Lambda{}^3$H, $\Lambda\Lambda{}^3$He and the $nn\Xi^-$ three-body systems (also see Refs. [63, 64]). This 3BF converts the single D^0-meson and n exchange interaction kernel functions $\mathscr{K}_{(D)}$ and $\mathscr{K}_{(n)}$, respectively, into their renormalized counterparts $\mathbb{K}^R_{(D)}$ and $\mathbb{K}^R_{(n)}$ [cf.

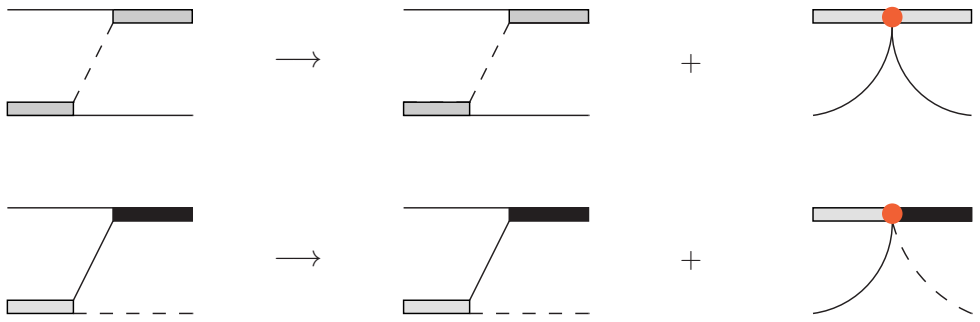

FIGURE 6.6: Feynman diagrams for the modification of a single D^0-meson and n exchange kernel functions $\mathcal{K}_{(D)}$ and $\mathcal{K}_{(n)}$, respectively, into their renormalized versions $\mathbb{K}^R_{(D)}$ and $\mathbb{K}^R_{(n)}$, contributing to the STM3 integral equations. The red-filled circles represent insertions of the regulator ($\Lambda_{\rm reg}$) dependent three-body contact interactions with coupling $g_3 = g_3(\Lambda_{\rm reg})$.

Fig. 6.6], namely,[15]

$$\mathcal{K}_{(\gamma)}(q,q';B_3) \longrightarrow \mathbb{K}^R_{(\gamma)}(q,q',\Lambda_{\rm reg};B_3) = \mathcal{K}_{(\gamma)}(q,q';B_3) - \frac{g_3(\Lambda_{\rm reg})}{\Lambda^2_{\rm reg}}\,; \quad \gamma = n, D\,, \tag{6.91}$$

such that the final forms of coupled STM integral equations renormalized by the 3BF terms, so-called the *STM3 equations* [12], for the D^0nn system become

$$\begin{aligned} F_n(q) = -\frac{1}{\pi}\int_0^{\Lambda_{\rm reg}} {\rm d}q' q'^2 \Bigg[& (y+1)\,\mathbb{K}^R_{(D)}(q,q',\Lambda_{\rm reg};B_3)\, S^R_d\left(-B_3 - \frac{q'^2}{2M_n}, \mathbf{q}'\right) F_n(q') \\ & + 2\,\mathbb{K}^R_{(n)}(q,q',\Lambda_{\rm reg};B_3)\, S^R_s\left(-B_3 - \frac{q'^2}{2yM_n}, \mathbf{q}'\right) F_D(q')\Bigg]\,, \end{aligned}$$

and

$$F_D(q) = -\frac{2(y+1)}{\pi y}\int_0^{\Lambda_{\rm reg}} dq' q'^2 \left[\mathbb{K}^R_{(n)}(q,q',\Lambda_{\rm reg};B_3)\, S^R_d\left(-B_3 - \frac{q'^2}{2M_n}, \mathbf{q}'\right) F_n(q')\right] \tag{6.92}$$

In the asymptotic limit of the above equations, i.e., for $q, q' \sim \Lambda_{\rm reg} \to \infty$, the 3BF term does not contribute, in which case we find

$$\begin{aligned} F_n(q) = {} & \frac{(1+y)^2}{2\pi\sqrt{y(2+y)}}\int_0^\infty \frac{{\rm d}q'}{q} \ln\left(\frac{q^2+q'^2+aqq'}{q^2+q'^2-aqq'}\right) F_n(q') \\ & + \frac{1}{\pi}\sqrt{\frac{4y}{(2+y)}}\int_0^\infty \frac{{\rm d}q'}{q} \ln\left(\frac{q^2+bq'^2+qq'}{q^2+bq'^2-qq'}\right) F_D(q')\,, \\ F_D(q) = {} & \frac{(1+y)^2}{\pi y\sqrt{y(2+y)}}\int_0^\infty \frac{{\rm d}q'}{q} \ln\left(\frac{q'^2+bq^2+qq'}{q'^2+bq^2-qq'}\right) F_n(q')\,, \end{aligned} \tag{6.93}$$

[15]Note here that the sign convention for the dimensionless three-body coupling g_3 is taken opposite to the corresponding coupling for the three-boson system, as followed in Chapter 3 [cf. Eq. (3.55)], accounting for the negative sign in front of g_3 in the above expressions for $\mathcal{K}_{(\gamma)}$.

Because the above asymptotic integrals are scale-free, the spectator functions must exhibit a power-law scaling behavior of the form $F_i(q) \propto q^{s-1}$. With this ansatz, the two coupled integral equations can be reduced into a single *transcendental* equation which must be numerically solved for determining the unknown exponent s:

$$1 = C_1 I_0(s;a) + C_2 I_1(s;b) I_2(s;b)\,, \tag{6.94}$$

with constants $C_{1,2}$ given by

$$C_1 = \frac{(1+y)^2}{2\pi\sqrt{y(2+y)}} \quad \text{and} \quad C_2 = \frac{2(1+y)^2}{\pi^2 y(2+y)}\,, \tag{6.95}$$

and the asymptotic integrals $I_{0,1,2}$ given by

$$I_0(s;a) = \int_0^\infty dx x^{s-1} \ln\left(\frac{1+x^2+ax}{1+x^2-ax}\right) = \frac{2\pi}{s}\frac{\sin\left[s\sin^{-1}\left(\frac{1}{2}a\right)\right]}{\cos\left(\frac{\pi}{2}s\right)}\,, \tag{6.96}$$

$$I_1(s;b) = \int_0^\infty dx x^{s-1} \ln\left(\frac{1+bx^2+x}{1+bx^2-x}\right) = \frac{2\pi}{s}\frac{1}{b^{s/2}}\frac{\sin\left[s\cot^{-1}\left(\sqrt{4b-1}\right)\right]}{\cos\left(\frac{\pi}{2}s\right)}\,, \tag{6.97}$$

$$I_2(s;b) = \int_0^\infty dx x^{s-1} \ln\left(\frac{b+x^2+x}{b+x^2-x}\right) = \frac{2\pi}{s} b^{s/2}\frac{\sin\left[s\cot^{-1}\left(\sqrt{4b-1}\right)\right]}{\cos\left(\frac{\pi}{2}s\right)}\,. \tag{6.98}$$

Solving the transcendental equation yields imaginary values of the parameter s, i.e., $s = \pm i s_0^\infty$, with $s_0^\infty = 1.02387...$ being a transcendental number. Thus, we infer that the D^0nn system exhibits an RG limit cycle in the UV regime which ideally suggests the Efimovian nature of the system. The characteristic behavior stems from the discrete scale invariance of the system which is reflected in the asymptotic log-periodic running with periodicity $\lambda_0^\infty = \exp(\pi/s_0^\infty) = 21.5064...$ of the 3BF coupling $g_3 = g_3(\Lambda_{\rm reg})$ with cyclic singularities well described by the analytical expression [52–55]

$$g_3(\Lambda_{\rm reg}) \sim \aleph\,\frac{\sin\left[s_0^\infty \log(\Lambda_{\rm reg}/\Lambda_*) - \arctan(1/s_0^\infty)\right]}{\sin\left[s_0^\infty \log(\Lambda_{\rm reg}/\Lambda_*) + \arctan(1/s_0^\infty)\right]}\,, \tag{6.99}$$

where Λ_* is a three-body parameter determined by a single low-energy observable, e.g., B_3. The numerical pre-factor $\aleph = 0.870$ is introduced to improve the overall fit to the non-asymptotic data points. However, due to the paucity of information on whether the D^0nn system is bound, the very best we can do is to presume some reasonable values of the (relative) three-body binding energy for a shallow $2n$ halo-bound system, say, $B_T = B_3 - B_{nD} = 0.1$ MeV and 1.0 MeV (i.e., measured with respect to the 2+1 nD^0-dimer-particle break-up threshold energy of $B_{nD} = 1.82$ MeV). This information is enough to determine the corresponding RG limit cycles for the three-body coupling g_3 by solving the STM3 equations in the non-asymptotic kinematical regime. Figure 6.7 displays the cyclic singularities associated with the formation of successive three-body bound states, e.g., the ground D^0nn state along with its first two excites states. The limit cycle nature of the 3BF thus obtained at the LO clearly indicates the flexibility to choose the cut-off scale in a suitable way that the 3BF term

effectively vanishes. Hence, we simply drop the 3BF terms and continue working with the STM integral equations with the finite value of the cut-off. This cut-off may be identified with the interaction range which sets the scale for the ground state or the deepest possible three-body binding energy of the system. Beyond this scale, all other level states are decoupled from the spectrum. In the following section, we revert back to the effective quantum mechanical formulation of the Faddeev equations, dropping all possible 3BFs, to demonstrate how the theoretical framework can be employed to assess the structural features for a plausible D^0nn halo-bound system.

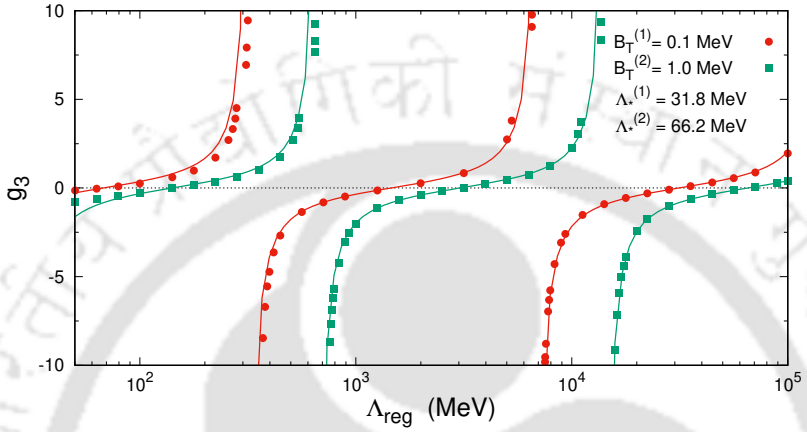

FIGURE 6.7: RG limit cycle for the three-body coupling g_3 of D^0nn system for two choices of the timer (relative) binding energy, $B_T^{(1)} = 0.1$ MeV and $B_T^{(2)} = 1.0$ MeV (i.e., measured with respect to the n-D^0 dimer binding energy $B_{nD} = 1.82$ MeV). The dotted and star data points correspond to the respective numerical solutions to the non-asymptotic STM3 integral equations, while the solid lines denote the corresponding two fitting curves using the asymptotic expression Eq. (6.99) with the three-body fit parameter obtained in each case, namely, $\Lambda_*^{(1)} = 31.8$ MeV and $\Lambda_*^{(2)} = 66.2$ MeV.

6.5 Matter Density Form Factors and Radii

We now revisit the Faddeev techniques which in conjunction with the effective potential formalism can also be used to determine other low-energy observables, such as the various one- and two-body matter density form factors and their corresponding mean square radii, in view of a plausible halo-bound D^0nn system. These observables can help unravel various universal structural features to assess the Efimov nature of the bound system. For this purpose, we need information on the full three-body wavefunction. Following the general methodology outlined in Refs. [38, 46], we now demonstrate in the ensuing subsections, the reconstruction of the full D^0nn wavefunction from the solutions to the spectator function F_n and F_D from Eq. (6.75).

6.5.1 Reconstruction of Three-body S-wave Wavefunction at LO

The full three-body wavefunction is represented by the state which is the sum of the Faddeev partitions for the D^0nn system:

$$|\Psi\rangle = |\psi_{n_1}\rangle + |\psi_{n_2}\rangle + |\psi_D\rangle = (1 - \mathcal{P})|\psi_n\rangle + |\psi_D\rangle\,. \tag{6.100}$$

The form of the wavefunction depends not only on the choice of the binary subsystem but also on the corresponding spectator basis to represent the Jacobi momenta. Let us represent the S-wave projected part as[16]

$$_i\langle pq|\Psi\rangle \equiv \Psi_i(p,q)\,, \tag{6.101}$$

where index $i = n, D$ indicates the actual spectator particle. In other words, the same three-body wavefunction can be represented in two equivalent ways with respect to the two distinct fragmentation channels labeled by n or D. With $p \equiv p_{n_2}$ and $q \equiv q_{n_2}$ as the preferred choice of the Jacobi momentum representation with n_2 neutron as the spectator (cf. *Channel-3* in Fig. 6.3), the full wavefunction can be written as

$$\begin{aligned}\Psi_{n_2}(p,q) &= {}_{n_2}\langle pq|1 - \mathcal{P}|\psi_{n_2}\rangle + {}_{n_2}\langle pq|\psi_D\rangle \\ &= \psi_{n_2}(p,q) - \int \mathrm{d}p'p'^2\mathrm{d}q'q'^2\, {}_{n_1}\langle pq|p'q'\rangle_{n_2}\ \psi_{n_2}(p',q') \\ &\quad + \int \mathrm{d}p'p'^2\mathrm{d}q'q'^2\, {}_{n_2}\langle pq|p'q'\rangle_D\ \psi_D(p',q')\,.\end{aligned} \tag{6.102}$$

In the above equation, we again need to evaluate the overlap-matrix elements as we have done in the previous section using the re-coupling constants $\mathscr{G}^{(nn)} = -1/2$ and $\mathscr{G}^{(nD)} = 1/2$. The only difference with the previous case is that here we need to re-define/shift the n_2 neutron spectator Jacobi relative momenta $p' \equiv p'_{n_2}$ and $q' \equiv q'_{n_2}$ either into the basis of the n_1 neutron as the spectator, or into the basis of the D^0 as the spectator [227]. The results for the S-wave overlap-matrix elements associated with Eq. (6.102) are

$${}_{n_1}\langle pq|p'q'\rangle_{n_2} \equiv {}_{n_1}\langle p_{n_2}q_{n_2}|p'_{n_2}q'_{n_2}\rangle_{n_2} = -\frac{1}{2}\int_{-1}^{1}\mathrm{d}x\frac{\delta(p' - \Pi_{nn})}{p'\Pi_{nn}}\frac{\delta(q' - \Pi'_{nn})}{q'\Pi'_{nn}}\,, \tag{6.103}$$

and

$$\begin{aligned}{}_{n_2}\langle pq|p'q'\rangle_D &\equiv {}_{n_2}\langle p_{n_2}q_{n_2}|p'_{n_2}q'_{n_2}\rangle_D \\ &= {}_D\langle p_Dq_D|p'_{n_2}q'_{n_2}\rangle_D = \frac{1}{2}\int_{-1}^{1}\mathrm{d}x\frac{\delta(p' - \Pi_{nD})}{p'\Pi_{nD}}\frac{\delta(q' - \Pi'_{nD})}{q'\Pi'_{nD}}\,,\end{aligned} \tag{6.104}$$

[16]Here we focus on S-wave halo systems with $l = \lambda = L = 0$, so that the values of the total spins (total angular momenta) are equal to their corresponding intrinsic spins (i.e., $\jmath = s$ and $\jmath = \sigma$). Henceforth, for brevity we shall drop the symbols $\mathbb{Q} \equiv \{(s\sigma)0(t\tau)\frac{3}{2}\}$ and $\mathbb{Q}' \equiv \{(s'\sigma')0(t'\tau')\frac{3}{2}\}$ which stand for the respective sets of discrete quantum numbers.

where the shifted momenta are given by

$$\Pi_{nn}(p,q;x) = \sqrt{\left(\frac{1}{y+1}\right)^2 p^2 + \frac{y^2(y+2)^2}{(y+1)^4} q^2 + 2\frac{y(y+2)}{(y+1)^3}\, pqx}\,,$$
$$\Pi'_{nn}(p,q;x) = \sqrt{p^2 + \left(\frac{1}{y+1}\right)^2 q^2 - 2\left(\frac{1}{y+1}\right) pqx}\,, \tag{6.105}$$

and

$$\Pi_{nD}(p,q;x) = \sqrt{\frac{p^2}{4} + \frac{(y+2)^2}{4(y+1)^2} q^2 + \frac{y+2}{2(y+1)}\, pqx}\,,$$

$$\Pi'_{nD}(p,q;x) = \sqrt{p^2 + \left(\frac{y}{y+1}\right)^2 q^2 - 2\left(\frac{y}{y+1}\right) pqx}\,. \tag{6.106}$$

Using the above results, as well as the relations between the Faddeev components and the spectator functions, Eq. (6.72), yields the following expression for the full S-wave three-body wavefunction in the $i = n$ Jacobi channel after integrating the delta functions:

$$\begin{aligned}
\Psi_n(p,q) &= \psi_n(p,q) + \frac{1}{2}\int_{-1}^{1} \mathrm{d}x \left[\psi_n(\Pi_{nn},\Pi'_{nn}) + \psi_D(\Pi_{nD},\Pi'_{nD})\right] \\
&= \mathscr{G}_0^{(n)}(p,q;B_3)\,\chi(p)\,\tau_n(q;B_3)\,F_n(q) \\
&\quad + \frac{1}{2}\int_{-1}^{1} \mathrm{d}x\, \mathscr{G}_0^{(n)}(\Pi_{nn},\Pi'_{nn};B_3)\,\chi\left(\Pi_{nn}\right)\,\tau_n(\Pi'_{nn};B_3)\,F_n(\Pi'_{nn}) \\
&\quad + \frac{1}{2}\int_{-1}^{1} \mathrm{d}x\, \mathscr{G}_0^{(D)}(\Pi_{nD},\Pi'_{nD};B_3)\,\chi\left(\Pi_{nD}\right)\,\tau_D(\Pi'_{nD};B_3)\,F_D(\Pi'_{nD}) \\
&= \mathscr{G}_0^{(n)}(p,q;B_3)\Bigg[\chi(p)\,\tau_n(q;B_3)\,F_n(q) + \frac{1}{2}\int_{-1}^{1} \mathrm{d}x\,\chi\left(\Pi_{nn}\right)\,\tau_n(\Pi'_{nn};B_3)\,F_n(\Pi'_{nn}) \\
&\qquad + \frac{1}{2}\int_{-1}^{1} \mathrm{d}x\,\chi\left(\Pi_{nD}\right)\,\tau_D(\Pi'_{nD};B_3)\,F_D(\Pi'_{nD})\Bigg]\,.
\end{aligned} \tag{6.107}$$

where we have utilized the fact that $\mathscr{G}_0^{(n)}(\Pi_{nn},\Pi'_{nn};B_3) = \mathscr{G}_0^{(D)}(\Pi_{nD},\Pi'_{nD};B_3) = \mathscr{G}_0^{(n)}(p,q;B_3)$.

Next, with $p \equiv p_D$ and $q \equiv q_D$ as the preferred choice of the Jacobi momentum representation with D^0-meson as the spectator (cf. *Channel-1* in Fig. 6.3), the full wavefunction can be written as

$$\begin{aligned}
\Psi_D(p,q) &= {}_D\langle pq|\psi_D\rangle + {}_D\langle pq|1-\mathscr{P}|\psi_{n_1}\rangle \\
&= \psi_D(p,q) + 2\int \mathrm{d}p\, p'^2 \mathrm{d}q'\, q'^2\, {}_D\langle pq|p'q'\rangle_{n_1}\,\psi_{n_1}(p',q')\,.
\end{aligned} \tag{6.108}$$

In the above equation, we need to evaluate the overlap-matrix elements using the re-coupling factor $\mathscr{G}^{(Dn)} = 1/2$. Here we need to re-define/shift the D^0 spectator Jacobi relative momenta $p' \equiv p'_D$ and $q' \equiv q'_D$ into the basis of the n_1 neutron as the spectator [227]. The result for

the S-wave overlap-matrix element associated with Eq. (6.108) is

$$\begin{aligned} {}_D\langle pq|p'q'\rangle_{n_1} &= {}_D\langle p_D q_D|p'_D q'_D\rangle_{n_1} \\ &= {}_{n_1}\langle p_{n_1} q_{n_1}|p'_D q'_D\rangle_{n_1} = \frac{1}{2}\int_{-1}^{1} \mathrm{d}x \frac{\delta(p'-\Pi_{Dn})}{p'\Pi_{Dn}} \frac{\delta(q'-\Pi'_{Dn})}{q'\Pi'_{Dn}}\,, \end{aligned} \tag{6.109}$$

where the shifted momenta are given by

$$\Pi_{Dn}(p,q;x) = \sqrt{\left(\frac{y}{y+1}\right)^2 p^2 + \frac{(y+2)^2}{4(y+1)^2} q^2 + \frac{y(y+2)}{(y+1)^2} pqx} \qquad \text{and}$$

$$\Pi'_{Dn}(p,q;x) = \sqrt{p^2 + \frac{q^2}{4} - pqx}\,. \tag{6.110}$$

Substituting the above result for the overlap-matrix element ${}_D\langle pq|p'q'\rangle_n$ in Eq. (6.108), then inserting the relations between Faddeev components and spectator functions, and finally performing the delta function integrations, we obtain the following expression for the full S-wave three-body wavefunction in the $i = D$ Jacobi channel:

$$\begin{aligned} \Psi_D(p,q) &= \mathcal{G}_0^{(D)}(p,q;B_3)\,\chi(p)\,\tau_D(q;B_3)\,F_D(q) \\ &\quad + \int_{-1}^{1} \mathrm{d}x\, \mathcal{G}_0^{(n)}(\Pi_{Dn},\Pi'_{Dn};B_3)\,\chi\left(\Pi_{Dn}\right)\,\tau_n(\Pi'_{Dn};B_3)\,F_n(\Pi'_{Dn}) \\ &= \mathcal{G}_0^{(D)}(p,q;B_3)\left[\chi(p)\,\tau_D(q;B_3)\,F_D(q) + \int_{-1}^{1} \mathrm{d}x\,\chi\left(\Pi_{Dn}\right)\,\tau_n(\Pi'_{Dn};B_3)\,F_n(\Pi'_{Dn})\right] \end{aligned} \tag{6.111}$$

where we have utilized the fact that $\mathcal{G}_0^{(n)}(\Pi_{Dn},\Pi'_{Dn};B_3) = \mathcal{G}_0^{(D)}(p,q;B_3)$. In Eqs. (6.107) and (6.111), we obtain the Gaussian regulator function χ from Eq. (6.50), the two-body T-matrices τ_n and τ_D from Eq. (6.57), the free three-body propagator functions $\mathcal{G}_0^{(n)}$ and $\mathcal{G}_0^{(D)}$ from Eq. (6.51), and finally, the spectator functions F_n and F_D as the nontrivial solutions of the matrix equation, Eq. (6.75), subsequently evaluated at a shifted relative momentum $q = \Pi$. The full reconstructed three-body wavefunctions Ψ_n and Ψ_D with respect to the two fragmentation channels $i = n, D$ are illustrated *via* the Feynman diagrams in Fig. 6.8.

6.5.2 Numerical implementation

In this subsection, we elaborate on the numerical procedure of solving the Faddeev equations, Eq. (6.75), namely,

$$\begin{aligned} F_n &= \mathcal{K}_{nn}F_n + \mathcal{K}_{nD}F_D\,, \\ F_D &= \mathcal{K}_{Dn}F_n\,, \end{aligned} \tag{6.112}$$

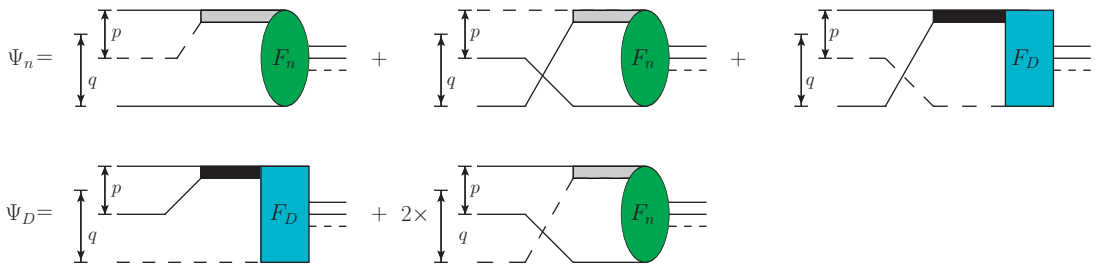

FIGURE 6.8: Reconstruction of the D^0nn three-body S-wave Jacobi wavefunctions $\Psi_i(p,q)$ with respect to the $i = n, D$ channels in Jacobi momentum representation. The solid/dashed lines denote the neutron/D^0-meson propagators. The rectangular/oval blobs represent the three-body scattering kernels associated with the spectator functions $F_i(q)$. The gray/black thick shaded thick lines represent the iterated n-D^0/n-n two-body S-wave T-matrices τ_i, which in pionless EFT are interpreted as renormalized dressed propagators for the corresponding dimer fields.

with the spectator functions F_i evaluated at a shifted momenta Π. The coupled-channel equations can be reduced to a single algebraic equation with two unknown quantities F_n and F_D, and hence, do not yield a unique solution. So, as a convenient choice, we may take $F_n = 1$ and $F_D = \mathscr{K}_{Dn} F_n$.

Since, we perform the numerical integrations using Gaussian quadratures, the integration measure $\mathrm{d}q'$ replaced by a summation over N Gaussian weights w_i, with $q = q_i$ and $q' = q'_j$ being the corresponding discrete Gaussian points between 0 and the UV momentum cut-off limit, say, Λ_{UV}. This upper limit of the integration should ideally be ∞, but for the purpose of numerical implementation we choose a suitably large finite value, say, $\Lambda_{UV} = 10 \times \Lambda_{\mathrm{reg}}$, beyond which numerical instabilities arise from the product of the complementary error and Gaussian functions $\exp(x^2/\Lambda^2_{\mathrm{reg}}) \times \mathrm{erfc}(x/\Lambda_{\mathrm{reg}})$. With the numerical integration defined over N Gaussian quadrature points, the spectator function $F_n = F_n(q')$ becomes a N-dimensional array with all elements equal to 1, while the kernel function $\mathscr{K}_{Dn} = \mathscr{K}_{Dn}(q,q')$ [cf. Eq. (6.73)] becomes an $N \times N$-dimensional matrix defined over the mesh points (q_i, q'_j), namely,

$$\mathscr{K}_{Dn}(q_i,q'_j) = W_j q'^2_j \sum_{m=1}^{N_x} \Big[w_m \chi\left(\pi_{nD}(q'_j,q_i;x_m)\right) \chi\left(\pi'_{nD}(q'_j,q_i;x_m)\right) \times \mathscr{G}_0^{(n)}(\pi_{nD}(q'_j,q_i;x_m),q'_j;B_3)\,\tau_n(q'_j;B_3)\Big], \tag{6.113}$$

where $W_j = W(q'_j)$ is the *weight factor* associated with a given quadrature point q'_j. Notice that the integration of the variable x has also been performed over N_x Gaussian points in the interval $[-1,1]$, with $w_m = w(x_m)$ being the weight associated with a given quadrature point x_m. Finally, the matrix multiplication of $\mathscr{K}_{Dn}$ with the vector F_n yields F_D as an N-dimensional vector:

$$F_D(q_i) = \sum_{j=1}^{N} \mathscr{K}_{Dn}(q_i,q'_j)\, F_n(q'_j)\,. \tag{6.114}$$

Moreover, it is required that the obtained solutions to the spectator functions F_i must be

evaluated at some shifted value of the relative momentum q. For this purpose, we use interpolated values of these functions which are easily obtained *via* a *Cubic Spline* interpolation algorithm of the form:

$$F_i(\Pi) \approx \sum_j \mathcal{S}_j(\Pi) F_i(q_j)\,; \quad i = n, D\,, \tag{6.115}$$

where $\mathcal{S}_j$ are the spline elements evaluated at the desired value $q = \Pi$. Likewise, we also need the spline interpolator for evaluation of the matter density from factors at shifted values of the momentum transfer $p \to |\mathbf{p} - \mathbf{k}|$ or $q \to |\mathbf{q} - \mathbf{k}|$, as discussed in the next subsections.

6.5.3 Matter Density Form Factors

Using the reconstructed three-body wavefunction from the previous subsection, Eqs. (6.107) and (6.111), other low-energy observables like the one- and two-body matter density form factor and the corresponding mean square radii of the S-wave three-body system can be determined. With Jacobi momentum representation, the S-wave matter density form factors are obtained by calculating the S-wave projected Fourier transforms of the respective matter densities with respect to the squares of the three-momentum transfer $\mathbf{k}$. They are symbolized by the normalized functions $\mathcal{F}_i(k^2 = 0) = 1$ and $\mathcal{F}_{ni}(k^2 = 0) = 1$, where $i = n, D$ depending on the choice of the Jacobi channel. The expressions for the S-wave one-body matter form factors are given by

$$\mathcal{F}_i(k^2) = \int \mathrm{d}p\, p^2 \int \mathrm{d}q\, q^2 \int_{-1}^{1} \mathrm{d}\xi\, \widetilde{\Psi}_i(p,q)\, \widetilde{\Psi}_i(p, \sqrt{q^2 + k^2 - 2qk\xi})\,, \quad i = n, D\,, \tag{6.116}$$

where $\xi \equiv \hat{\mathbf{k}} \cdot \hat{\mathbf{q}}$, and $\widetilde{\Psi}_i(p,q)$ represents the S-wave projected part of the complete three-body *normalized* wavefunction $\Psi_i(\mathbf{p}, \mathbf{q})$ in three-dimension, namely,

$$\widetilde{\Psi}_i(p,q) = \frac{1}{4\pi} \int \mathrm{d}\Omega_{\hat{p}} \int \mathrm{d}\Omega_{\hat{q}}\, \widetilde{\Psi}_i(\mathbf{p}, \mathbf{q})\, P_0(\hat{\mathbf{p}} \cdot \hat{\mathbf{q}})\,, \quad i = n, D\,, \tag{6.117}$$

with

$$\widetilde{\Psi}_i(\mathbf{p}, \mathbf{q}) = \frac{\Psi_i(\mathbf{p}, \mathbf{q})}{\sqrt{\int \mathrm{d}^3\mathbf{p} \int \mathrm{d}^3\mathbf{q}\, \Psi_i^2(\mathbf{p}, \mathbf{q})}}\,, \quad i = n, D\,. \tag{6.118}$$

Also for the purpose of illustration, we display the corresponding momentum-space radial probability densities in Fig. 6.9 as functions of the Jacobi momenta p and q, where the normalized probability densities are defined as

$$P_i(p,q) = \frac{p^2 q^2\, \Psi_i^2(p,q)}{\int \mathrm{d}p\, p^2 \int \mathrm{d}q\, q^2\, \Psi_i^2(p,q)}\,, \quad i = n, D\,. \tag{6.119}$$

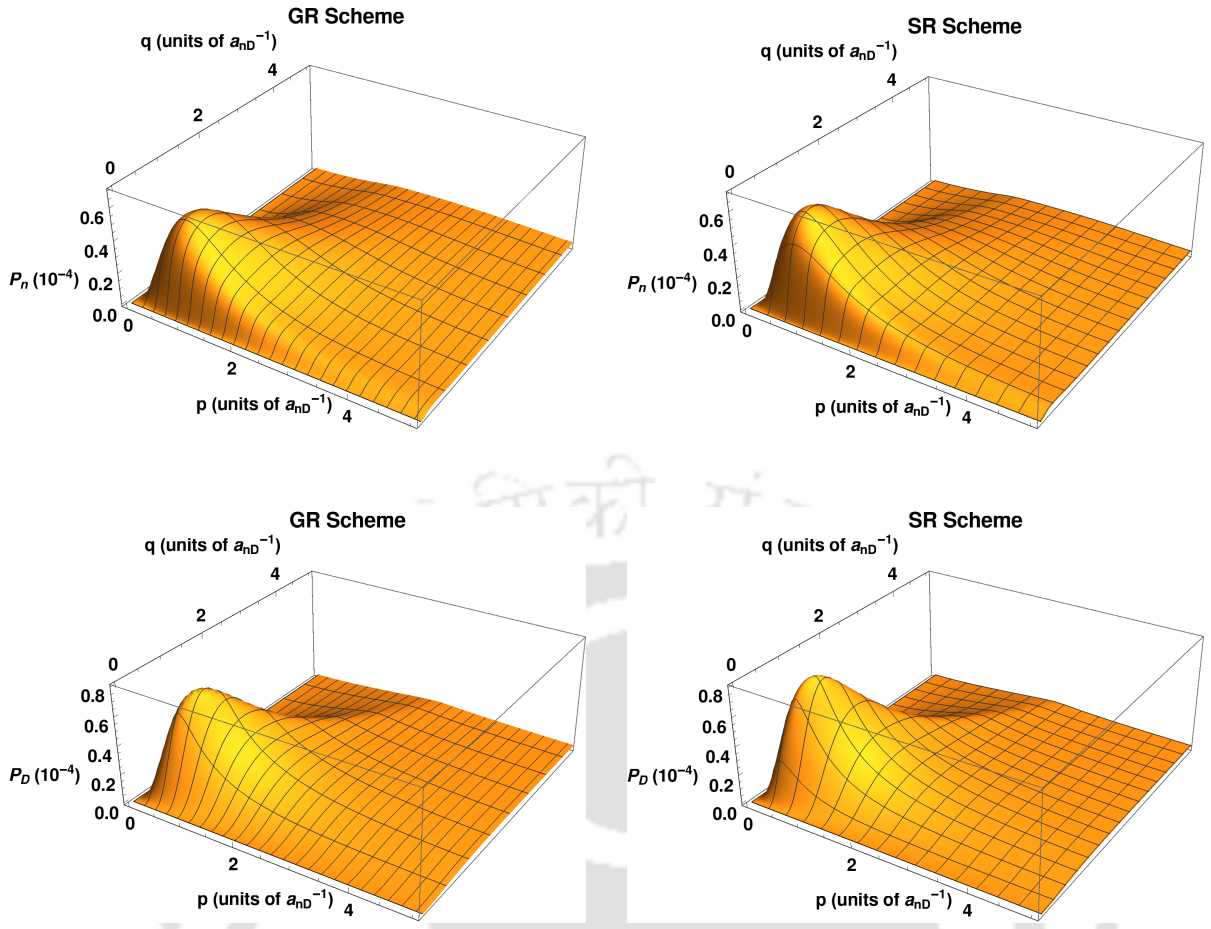

FIGURE 6.9: Normalized momentum-space radial probability densities corresponding the reconstructed D^0nn three-body S-wave Jacobi wavefunctions $\Psi_n(p,q)$ and $\Psi_D(p,q)$ employing Gaussian and sharp cut-off regularization schemes. The Jacobi momentum (p,q) are expressed in units of the inverse S-wave n-D^0 scattering length or nD^0-dimer binding momentum, i.e., $\gamma_{nD} \sim a_{nD}^{-1} = 47.65$ MeV.

Next, the expressions for the S-wave two-body matter form factors are given by

$$\mathcal{F}_{nD}(k^2) = \int \mathrm{d}p\, p^2 \int \mathrm{d}q\, q^2 \int_{-1}^{1} \mathrm{d}\zeta\, \widetilde{\Psi}_n(p,q)\, \widetilde{\Psi}_n(\sqrt{p^2+k^2-2pk\zeta}, q)\,, \tag{6.120}$$

and

$$\mathcal{F}_{nn}(k^2) = \int \mathrm{d}p\, p^2 \int \mathrm{d}q\, q^2 \int_{-1}^{1} \mathrm{d}\zeta\, \widetilde{\Psi}_D(p,q)\, \widetilde{\Psi}_D(\sqrt{p^2+k^2-2pk\zeta}, q)\,, \tag{6.121}$$

where $\zeta \equiv \hat{\mathbf{k}} \cdot \hat{\mathbf{q}}$. The one- and two-body form factors defined above constitute the basis for estimating the universal structural characteristics of Efimov-bound systems.

6.5.4 Mean Square Radii and Geometrical structure of D^0nn

These matter density form factors discussed in the previous subsection can now be used to determine the geometrical structure of the putative S-wave $2n$ halo-bound D^0nn system. In particular, we shall extract the mean square two-particle distances between pairs of individual particles, namely, $\langle r_{nn}^2 \rangle$ and $\langle r_{Dn}^2 \rangle$, as well as the and the mean square distances between a

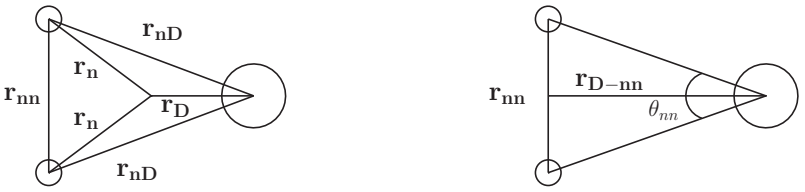

FIGURE 6.10: Various matter radii defining the geometrical structure of a D^0nn halo-bound system.

spectator particle and the binary subsystem center-of-mass, namely, $\langle r^2_{n-nD}\rangle$ and $\langle r^2_{D-nn}\rangle$. These radii are obtained by evaluating the slope of the corresponding one- or two-body form factors at $k^2 = 0$:[17] The three different types of matter radii in the D^0nn system, depending upon the one- and two-body form factors, are illustrated in Fig. 6.10. The slope of $\mathscr{F}_{ni}(k^2)$ gives the information regarding the mean square two-particle distances $\langle r^2_{nn}\rangle$ and $\langle r^2_{nD}\rangle$ for the n-n and n-D^0 binary subsystems, respectively. Whereas, the slope of $\mathscr{F}_i(k^2)$ gives the information regarding the mean square distances $\langle r^2_{D-nn}\rangle$ and $\langle r^2_{n-nD}\rangle$ between the spectator particle $i = n, D$ and the center-of-mass of the n-n and n-D^0 binary subsystems, respectively. Using this information on the mean square distances one can further determine the mean square distances $\langle r^2_i\rangle$ of the individual particles from the center-of-mass of the bound three-body system using the relation [38]:

$$\langle r^2_i\rangle = -6\left(\frac{\mathrm{d}\mathscr{F}_i(k^2)}{\mathrm{d}k^2}\right)_{k^2=0}\left[1-\frac{M_i}{2M_n+M_D}\right]^2, \qquad i = n, D \tag{6.123}$$

where M_i refers to the mass of the bound particle in question whose mean square distance is needed to be determined, and M_n and M_D are masses of neutron and D^0-meson respectively. Similarly, one can define an effective/mean geometrical matter radius for the D^0nn halo-bound

[17] We recall here that the form factor $\mathscr{F}(k^2)$ by definition is the Fourier transform of the density function $\varrho(\mathbf{r})$:

$$\mathscr{F}(k^2) = \int \mathrm{d}^3\mathbf{r}\, e^{i\mathbf{k}\cdot\mathbf{r}}\, \varrho(\mathbf{r})\,,$$

having the normalization $\mathscr{F}(k^2 = 0) = 1$. For an isotropic matter distribution, i.e., $\varrho(\mathbf{r}) = \varrho(r)$, the exponential factor can be expanded for small momentum transfer $|\mathbf{k}| \to 0$ as follows:

$$\mathscr{F}(k^2) \;=\; \int \mathrm{d}^3\mathbf{r}\, \varrho(r)\left(1 + i\mathbf{k}\cdot\mathbf{r} - \frac{(\mathbf{k}\cdot\mathbf{r})^2}{2} + \cdots\right) = 1 - \frac{1}{6}k^2\langle r^2\rangle + \mathcal{O}(k^4)\,,$$

where $\langle r^2\rangle$ is the mean square radius. On the other hand, since the low-energy form factor can be expanded in a Taylor series:

$$\mathscr{F}(k^2) = \mathscr{F}(k^2 = 0) + k^2\left(\frac{\mathrm{d}\mathscr{F}(k^2)}{\mathrm{d}k^2}\right)_{k^2=0} + \mathcal{O}(k^4)\,,$$

it immediately follows that the mean square radius is related to the slope of the form factor at zero momentum transfer:

$$\langle r^2\rangle = -6\left(\frac{\mathrm{d}\mathscr{F}(k^2)}{\mathrm{d}k^2}\right)_{k^2=0} > 0\,. \tag{6.122}$$

system with a *point-like* core [32]:

$$\langle r^2_{\text{eff}}\rangle_{2\text{n}-\text{halo}} = \frac{2(y+1)^2}{(y+1)^3}\langle r^2_{n-Dn}\rangle + \frac{4y}{(y+1)^3}\langle r^2_{D-nn}\rangle\,. \tag{6.124}$$

Finally, it is a matter of simple geometry to determine the $n-D^0-n$ opening angle obtained using the relation [38, 228]:

$$\theta_{nn} = 2\arctan\sqrt{\frac{\langle r^2_{nn}\rangle}{4\langle r^2_{D-nn}\rangle}}\,. \tag{6.125}$$

The estimation of all the aforementioned observables helps to reconstruct a two-dimensional geometrical model of a bound D^0nn system.

6.6 Results and Discussion

In this section, we will display the results of our preliminary LO analysis of S-wave $2n$-halo D^0nn system. Here, we mainly focus on the estimation of the universal geometrical features for a plausible trimer state under an idealized ZCL scenario [109]. Given the close correspondence between the effective potential formalism and $\not\pi$EFT approach pertaining to a LO analysis, merely boils down to the choice of the regularization that distinguishes between the two approaches, namely, the Gaussian regularization (GR) and the sharp cut-off regularization (SR) schemes. In that context, we present a numerical comparison of the structural features obtained in the two schemes to assess the robustness of the LO predictions. For the sake of numerical calculations, we use masses of D^0-meson and neutron as displayed in Table 6.3. Furthermore, as already mentioned earlier, the sole two-body inputs parameters in the effective theory are the S-wave scattering lengths $a_{nD} = 4.141$ fm [109] and $a_{nn} = -18.63$ [30]. In Fig. 6.11 (left panel) we display the sequence of geometrically spaced Efimov states which progressively emerge above the D^0n-dimer-particle break-up threshold energy $B_{nD} = 1.82$ MeV on increasing the regulator cut-off Λ_{reg}. The binding energies represent non-trivial solutions to homogeneous coupled-channel integral equations, Eqs. (6.73) and (6.74) in the GR scheme and Eqs. (6.89) and (6.89) in the SR scheme, respectively, excluding the 3BF terms. For the SR scheme results, the values of the critical cut-offs $\Lambda_{\text{reg}} = \Lambda^{(m)}_{\text{crit}}$ for which the three shallowest Efimov levels appear are $\Lambda^{(m=0)}_{\text{crit}} \approx 48$ MeV, $\Lambda^{(m=1)}_{\text{crit}} \approx 1122$ MeV and $\Lambda^{(m=2)}_{\text{crit}} \approx 23932$ MeV, being consistent with the $\not\pi$EFT analysis of Ref. [109]. The rather small value of the critical cut-off for the ground state relative to the $\not\pi$EFT breakdown scale (m_π) is suggestive of a feasible Efimovian D^0nn system which may either survive as realistic exotic bound nuclei or evolve into a quasi-bound system upon relaxation of the idealized ZCL scenario. Whereas, the other deep states emerging at scales substantially larger than m_π are naturally excluded from the purview of a low-energy EFT description. As with the GR scheme, the excited Efimov states are found to emerge at significantly lower values of the critical cut-off than in the SR scheme, for instance, $\Lambda^{(m=1)}_{\text{crit}} \approx 793$ MeV and $\Lambda^{(m=2)}_{\text{crit}} \approx 20515$ MeV. Whereas the ground state solution

Particle	Mass Symbol	Numerical Value (MeV)
D^0-Meson	M_D	1864.3
Neutron (n)	M_n	939.565

TABLE 6.3: PDG [191] values of masses of the D^0-meson and neutron used in the numerical calculations.

develops numerical convergence issues at low regulator values below $\Lambda_{\rm reg} \lesssim 100$ MeV which typically becomes same as the order of the three-body binding momenta. Nevertheless, only the $m = 0$ trimer solution in the GR scheme is amenable to a low-energy quantum description. The sensitive dependence of the three-body binding energy on the regulator scale, as seen in

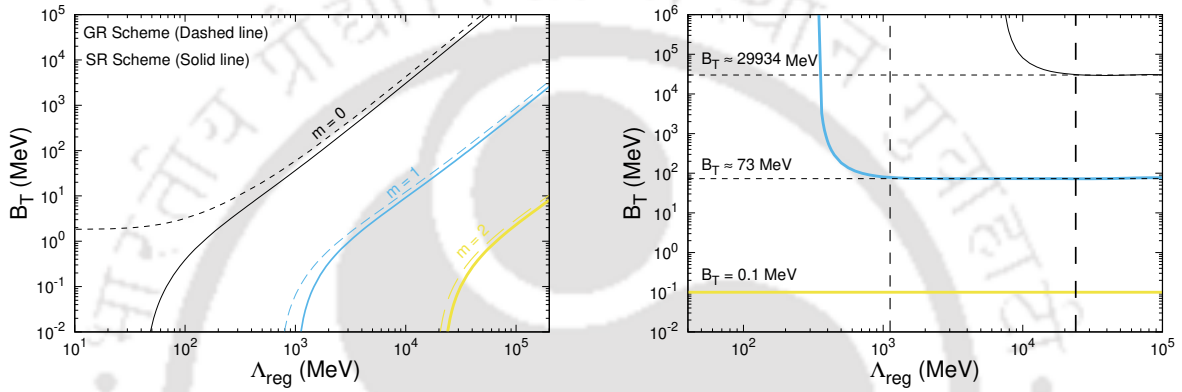

FIGURE 6.11: Cut-off scale ($\Lambda_{\rm reg}$) dependence for a plausible D^0nn trimer (relative) binding energy $B_T = B_3 - B_{nD}$, (where the $B_{nD} = 1.82$ MeV is D^0n-dimer-particle threshold energy) obtained as a nontrivial solution to the Faddeev integral equations at leading order. Here we display three sets of curves corresponding to the ground ($m = 0$) and the first two excited trimer ($m = 1, 2$) states. **Left panel:** In this case the solutions are obtained excluding 3BF terms. The dashed lines correspond to the Gaussian regularization (GR) scheme and the solid lines correspond to the sharp cut-off regularization (SR) scheme. The rather atypical nature of the ground state trimer in the GR scheme is an artifact of low cut-off dependent effects. **Right panel:** In this case the solutions obtained in the SR scheme are only displayed. The integral equations are renormalized by including the 3BF terms with coupling $g_3 = g_3(\Lambda_{\rm reg})$ fixed using the limit cycle [cf. Fig. 6.7]. Upon fixing the trimer binding energy $B_T = 0.1$ MeV for the shallowest Efimov level, the regulator independent eigenenergies $B_T = 73$ MeV and $B_T = 29934$ MeV are yielded as predictions of the effective theory.

Fig. 6.11 (right panel), can nonetheless be renormalized by introducing the 3BF terms. The corresponding coupling requires one piece of three-body datum to uniquely determine its RG running $g_3 = g_3(\Lambda_{\rm reg})$. For instance, in the SR scheme, by fixing the binding energy of the shallowest (most excited) Efimov level, say, $B_3 = 1.92$ MeV (i.e., $B_T = B_3 - B_{nD} = 0.1$ MeV, where the $B_{nD} = 1.82$ MeV is D^0n-dimer-particle threshold energy), the limit cycle nature of g_3 can first be predicted by the integral equations [cf. Fig. 6.7]. Subsequently, the regulator independent values of all other deeper trimer level energies are then readily predictable by the renormalized integral equation including the 3BF terms determined by the limit cycle. This result is illustrated in the right panel of the above figure, where the two deepest-level energies

$B_T \approx 73$ MeV and $B_T \approx 29934$ MeV are yielded as predictions of the theory. Moreover, analogous results renormalized using the GR scheme can in principle be obtained.

As regards to whether there exists a limit cycle in the GR scheme when the SR scheme is explicitly known to exhibit a limit cycle, can be well verified indirectly by investigating the quasi-cyclic periodicity of the regulator $\Lambda_{\rm reg}$ corresponding to the different Efimov states obtained using the GR scheme (cf. left plot in Fig. 6.11) having the same unrenormalized three-body binding energy B_3. Figure 6.12 depicts the convergence of the cut-off dependent non-asymptotic discrete scaling parameter s_0, approaching the same limiting value $s_0^\infty = 1.02387$ as $\Lambda_{\rm reg} \to \infty$, as obtained from the SR scheme, i.e.,

$$s_0 = \pi / \ln\left[\Lambda_{\rm reg}^{(n+1)} / \Lambda_{\rm reg}^{(n)}\right] \longrightarrow s_0^\infty \text{ as } \quad n \to \infty\,.$$

Here, $\Lambda_{\rm reg}^{(n)}$ represents the regulator value for the $n^{\rm th}$ zero of the three-body coupling $g_3 = g_3(\Lambda_{\rm reg}^{(n)})$ for a given B_3. The $s_0 = s_0(\Lambda_{\rm reg}^{(n)})$ dependence of $\Lambda_{\rm reg}^{(n)}$ stems from Eq. (3.61) of Chapter 3. It may be noted that in Fig. 6.12 the solid (red) line corresponding to the three-body binding energy $B_3 = 1.83$ MeV (i.e., $B_T = 0.01$ MeV) in the GR scheme starts from $2^{\rm nd}$ ratio of the commensurate regulator values (i.e., $\Lambda_{\rm reg}^{(2)}/\Lambda_{\rm reg}^{(1)}$) onward, since their $1^{\rm st}$ ratio (i.e., $\Lambda_{\rm reg}^{(1)}/\Lambda_{\rm reg}^{(0)}$) does not exist (due to non-existence of $\Lambda_{\rm reg}^{(0)}$ value for $B_3 = 1.83$ MeV in the GR scheme). Although a comparison with the SR scheme results for the same binding energy shows the same asymptotic limit of the GR scheme integral equations, Eqs. (6.73) and (6.74), the respective pattern of convergence is not the same. This could imply a difference in the respective limit cycle behavior of the 3BFs in each scheme. In other words, choosing $g_3 = 0$ in both the schemes yield different $\Lambda_{\rm reg} \equiv \Lambda_{\rm reg}^{(n)}$ values, and hence, somewhat different values in the predicted observables are expected for a given B_3, as seen in our ensuing results. Therefore, unless the exact functional nature of the limit cycle in the GR scheme is *a priori* determined, such ambiguities in the comparison of results are expected and may lead to an apparent conclusion that the SR and GR scheme results correspond to different three-body physics. This is a shortcoming that is inherent to the methodology we currently adopt in this work. Owing to the rather intricate methodology of including Gaussian regulator-dependent

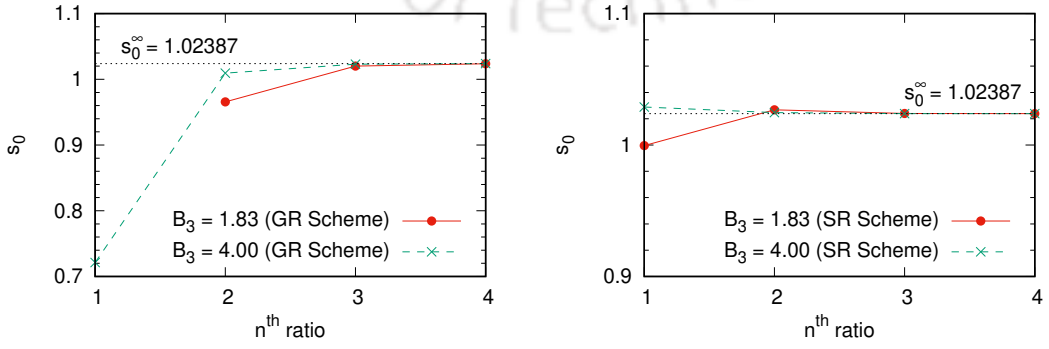

FIGURE 6.12: Convergence of non-asymptotic discrete scaling parameter s_0 as $\Lambda_{\rm reg} \to \infty$ in GR scheme (left panel) and SR scheme (right panel) for the D^0nn system. The asymptotic limit cycle parameter corresponds to the value $s_0^\infty = 1.02387$.

3BF functions in the effective quantum mechanical framework [36], we refrain from explicitly demonstrating the limit cycle behavior of the 3BF in the GR scheme, but nevertheless, rely implicitly on the existence of such a limit cycle and tune the cut-off accordingly to obtain vanishing 3BF.

Next, we present our results pertaining to the *Samba* structure [24] of a putative S-wave halo-bound D^0nn system. For this purpose, we employ both types of regularization (Gaussian and sharp cut-off schemes) and present a comparative study of their results. In Fig. 6.13, we plot the various LO one- and two-body matter density form factors for the ground ($m = 0$) and the first two excited trimer ($m = 1, 2$) states for the D^0nn halo-bound system using both regularization schemes. Here, we demonstrate our numerical results for an arbitrary choice of the three-body binding energy, say, $B_3 = 2.0$ MeV (i.e., $B_T = 0.18$ MeV) for the first two ($m = 1, 2$) excited states (despite the fact that they evidently do not qualify as physically realizable Efimov states in the context of a low-energy effective theory), that correspond to the regulator scale $\Lambda_{\rm reg} \approx 1.3$ GeV (1.7 GeV) for the first ($m = 1$) excited state and $\Lambda_{\rm reg} \approx 31$ GeV (36 GeV) for the second ($m = 2$) excited state in the GR (SR) scheme. As for the ground state ($m = 0$), we are able to demonstrate our results only for a somewhat larger value of the three-body binding energy, say, $B_3 = 3.82$ MeV (i.e., $B_T = 2.0$ MeV), such that it facilitates a comparison between the two schemes. Otherwise, our GR scheme results for the ground state do not converge below a certain minimal value of the three-body binding energy $B_T \lesssim 1.83$ MeV [cf. Fig. 6.13]. The corresponding regulator value for the ground state with $B_T = 2.0$ MeV is $\Lambda_{\rm reg} = 34$ MeV (204 MeV) for the GR (SR) scheme. The non-linear nature of the form factors are evident over a substantial range of low-momentum transfer, say, up to the pion mass ($k^2 \equiv |\mathbf{k}|^2 \lesssim m_\pi^2$). However, in the $k^2 \sim 0$ region they may be considered approximately linear with constant slopes, which in turn determine the corresponding mean squared radii. We find that the ground state form factors look significantly different from those of the excited states. These differences in the unrenormalized results (i.e., without introducing the 3BF terms) are naturally anticipated given the fact that only very shallow (threshold) trimer states with $B_T \to 0$ (however, for substantially large cut-offs) occur within the region of universality of the Efimov spectrum. With the binding energy and cut-off values of comparable size, our ground state results are generally plagued with artifacts of poor numerical convergence in the small cut-off region. Consequently, the evaluated form factors are rendered either unreliable (SR scheme) or indeterminable (GR scheme) below $B_T \lesssim 1.83$ MeV.

With the three lowest D^0nn trimer ($m = 0, 1, 2$) form factors evaluated for various input B_3 (B_T) values (i.e., at specific $\Lambda_{\rm reg}$), we are now in a position to determine the various *root mean squared* (rms) distances defining the geometrical structure of the bound systems. We employ Eqs. (6.122) and (6.123) for this purpose and the corresponding results are summarized in Table 6.4. The inter-particle rms distance between the (ij)-pair is defined as $r_{ij} \equiv \sqrt{\langle r_{ij}^2 \rangle}$. The rms distance of the spectator particle i from the center-of-mass of the binary subsystem j-k is defined as $r_{i-jk} \equiv \sqrt{\langle r_{i-jk}^2 \rangle}$. Finally, the rms distance of the particles i from the

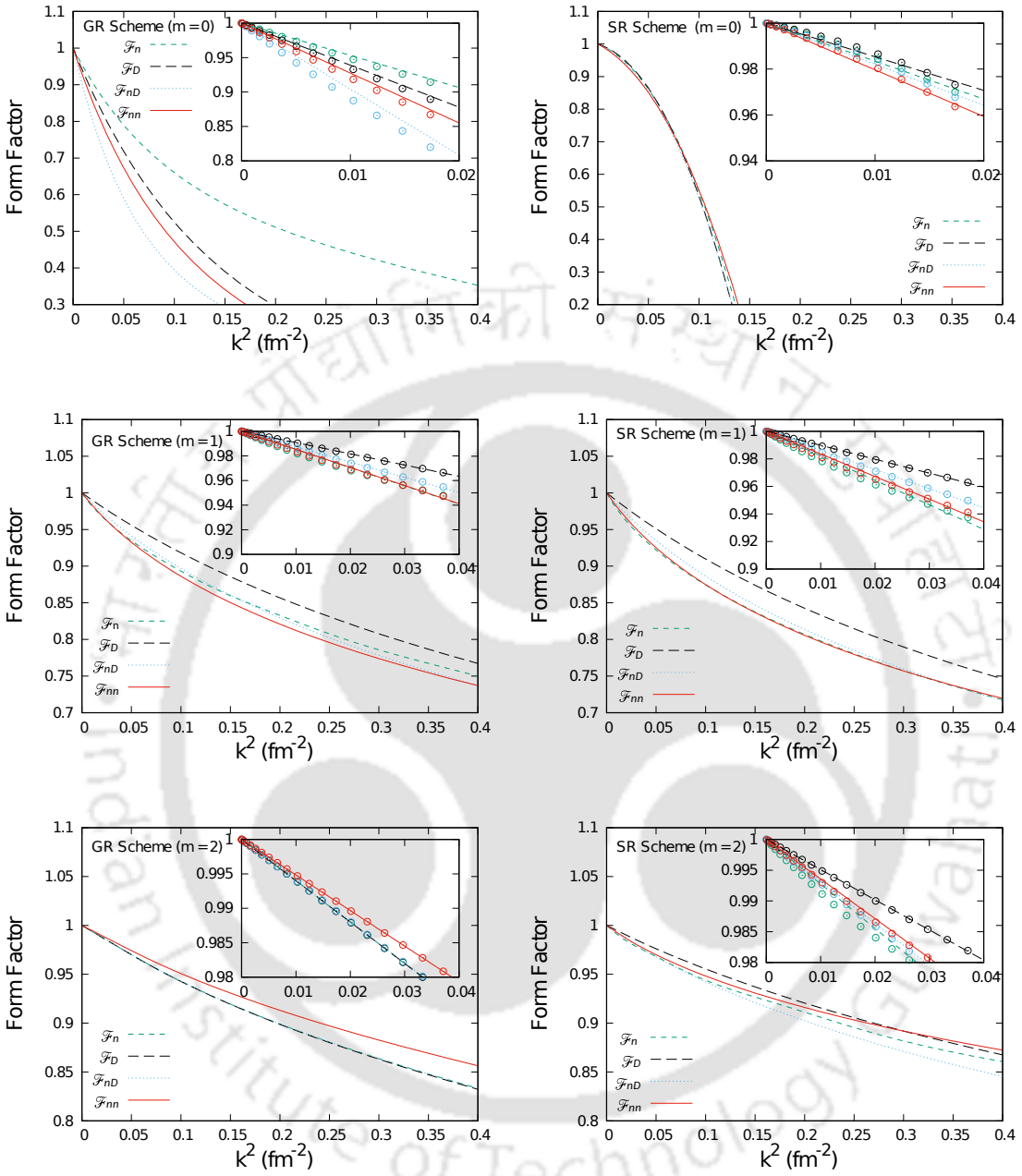

FIGURE 6.13: Leading order S-wave one- and two-body matter density form factors for the D^0nn system as a function of squared three-momentum transfer k^2 for the ground state ($m = 0$) trimer with a (relative) three-body binding energy $B_T = 2.0$ MeV (upper panel), and for the first two excited ($m = 1, 2$) trimer states, each separately corresponding to binding energy $B_T = 0.18$ MeV (middle and lower panel). Results are displayed using Gaussian regularization scheme (GR) in the left panel plots and the sharp cut-off regularization scheme (SR) in the right panel plots. All form factors are normalized to unity at $k^2 = 0$. The inset plots depict the linear fits to our numerical data points for a very low range of momentum transfers. All results correspond to two-body inputs in the ZCL scenario.

Scheme (m^{th} level)	B_3	Λ_{reg}	r_{nn}	r_{nD}	r_n	r_D	r_{n-nD}	r_{D-nn}	θ_{nn} (Degrees)
Sharp cut-off ($m = 0$)	1.92	67.9	13.2	12.6	6.9	3.1	12.7	11.5	59.58
	2.00	78.6	10.6	10.0	5.5	2.7	10.1	9.3	59.51
	2.50	123.8	5.9	5.5	3.3	1.8	5.4	5.1	60.72
	3.00	157.7	4.4	4.1	2.6	1.5	4.0	3.7	62.22
	3.82	204.1	3.3	3.1	2.2	1.3	3.0	2.7	63.03
	4.00	213.1	3.2	2.9	2.0	1.2	2.8	2.6	63.08
Gaussian cut-off ($m = 0$)	1.92	-	-	-	-	-	-	-	-
	2.00	-	-	-	-	-	-	-	-
	2.50	-	-	-	-	-	-	-	-
	3.00	-	-	-	-	-	-	-	-
	3.82	34.0	6.6	7.6	4.3	3.2	5.3	6.1	57.18
	4.00	47.9	5.5	5.9	3.6	2.5	4.5	4.9	59.17
Sharp cut-off ($m = 1$)	1.92	1473	3.5	3.1	3.7	1.4	3.9	2.7	66.58
	2.00	1681	3.1	2.8	2.7	1.3	3.2	2.4	64.72
	2.50	2608	2.1	2.1	1.5	0.9	2.0	1.8	59.46
	3.00	3327	1.7	1.8	1.2	0.8	1.6	1.6	57.33
	3.82	4320	1.4	1.5	1.0	0.7	1.3	1.3	55.50
	4.00	4519	1.4	1.4	1.0	0.7	1.3	1.3	55.23
Gaussian cut-off ($m = 1$)	1.92	1095	3.3	3.0	3.4	1.3	3.5	2.5	66.36
	2.00	1274	2.9	2.7	2.5	1.2	2.9	2.3	64.52
	2.50	2076	2.0	2.0	1.4	0.9	1.9	1.7	59.44
	3.00	2698	1.6	1.7	1.1	0.7	1.5	1.4	57.37
	3.82	3560	1.3	1.4	0.9	0.6	1.2	1.3	55.56
	4.00	3732	1.3	1.3	0.9	0.6	1.2	1.2	55.29
Sharp cut-off ($m = 2$)	1.92	31467	2.2	2.2	2.5	0.9	2.4	1.9	61.43
	2.00	35935	2.0	2.0	1.9	0.9	2.1	1.7	59.59
	2.50	55878	1.4	1.5	1.1	0.7	1.4	1.4	55.11
	3.00	71328	1.2	1.3	0.9	0.6	1.2	1.2	53.40
	3.82	92700	1.0	1.1	0.7	0.5	1.0	1.0	52.02
	4.00	96961	1.0	1.1	0.7	0.5	1.0	1.0	51.82
Gaussian cut-off ($m = 2$)	1.92	27050	1.9	2.0	1.6	1.0	2.1	2.0	50.18
	2.00	30926	1.8	1.9	1.4	1.0	1.9	1.9	49.76
	2.50	48232	1.3	1.4	1.1	0.7	1.4	1.4	49.05
	3.00	61641	1.1	1.2	0.9	0.6	1.2	1.2	48.91
	3.82	81849	0.9	0.9	0.7	0.5	0.9	0.9	48.83
	4.00	83890	0.8	0.9	0.7	0.5	0.9	0.9	48.81

TABLE 6.4: Various leading order root mean squared (rms) distances for a halo-bound D^0nn system. The results are displayed for the ground ($m = 0$) and the first two excited trimer ($m = 1, 2$) states. The results are obtained using both Gaussian and sharp cut-off regularization schemes. The blank entries correspond to unavailable data points in the Gaussian regularization scheme for $B_3 \lesssim 3.65$ MeV, where the form factors could not be numerically evaluated due to cut-off artifacts (see text). The units of B_3 and Λ_{reg} are in MeV, while the units of the rms distances are in Fermi (fm).

center-of-mass of the three-body center-of-mass is defined as $r_i \equiv \sqrt{\langle r_i^2 \rangle}$. Notably, due to the aforementioned pathologies affecting our GR scheme results for the ground state with $B_3 \lesssim 3.65$ MeV, the radii evaluations are unfeasible, and hence the blank entries in the table. As evident from the table, with the increase of the binding energy B_3 for each trimer level, the magnitude of all the rms radii decreases in both schemes. In other words, the stronger is the binding of a given D^0nn trimer level, the more compact it gets. Especially, for small values of the D^0nn ground state ($m = 0$) three-body binding energy near the D^0n-dimer-particle break-up threshold value $B_3 \sim B_{nD} = 1.82$ MeV, the system assumes a characteristic halo structure with large radii with one of the halo-neutrons orbiting at some distance, while the other neutron forms a compact bound D^0n subsystem with the core D^0-meson. This is reflected in the predominantly larger magnitudes of r_{nn}, r_n and r_{n-nD} compared to r_{nD}, r_D and r_{D-nn}, respectively, noting, however, some exceptions in the GR scheme results which are strongly affected by the low cut-off dependent artifacts. In contrast, the rather compact geometries associated with the excited states preclude a halo-like description. We also find that the magnitudes of the SR scheme radii are larger than those in the GR scheme for given $\Lambda_{\rm reg}$. This is understandable given the corresponding smaller values of B_3 obtained in the SR scheme than in GR scheme [cf. Fig. 6.11]. The results for the mean squared radii are then used to obtain the $n - D^0 - n$ opening angle θ_{nn} using Eq. (6.125). For both the schemes, it is mostly observed that θ_{nn} marginally increases ($\sim 4^\circ$) with the increase in B_3 for the ground state, while decreasing more rapidly ($\sim 10^\circ$) for the excited states for the same increase in B_3. This is perhaps indicative of the fact that the strongly attractive ${}^1S_0$ nn (di-neutron) state interactions tend to bring the two neutrons closer, thereby favoring a more symmetrical equilateral triangular Samba structure of the halo-bound D^0nn system rather than the typically elongated halos. Furthermore, our results displayed in Fig. 6.14 for the variation of the effective/mean geometrical matter radius $r_{\rm eff} = \sqrt{\langle r_{\rm eff}^2 \rangle_{\rm 2n-halo}}$ [see Eq. (6.124)] with the three-body binding energy B_3 also corroborates our halo-bound attribution for the ground state, provided of course that the uncertainties caused by the cut-off dependent artifacts do not falsify our inference.

Finally, we turn to the issue of remnant structural universality, if any, exhibited by the D^0nn halo-bound system. We know that on approaching the unitary limit with $a_{nn}, a_{nD} \to \pm\infty$, the square root of the ratio of relative three-body binding energy of two successive Efimov states is expected to approach the universal number λ_∞ characterizing the discrete scaling invariance of the system due to the asymptotic RG limit cycle signature:

$$\sqrt{\frac{B_3^{(m)}}{B_3^{(m+1)}}} \to \sqrt{\frac{B_T^{(m)}}{B_T^{(m+1)}}} \to \lambda_0^\infty = e^{\pi/s_0^\infty} = 21.5064\,, \tag{6.126}$$

where $B_T = B_3 - B_{nD} \to B_3$, and so do the corresponding inverse ratios of the generic rms radii $r \equiv \sqrt{\langle r^2 \rangle}$, namely,

$$\frac{r^{(m+1)}}{r^{(m)}} \to \lambda_0^\infty = 21.5064\,. \tag{6.127}$$

However, at the physical point of the system (i.e., with finite $a_{nn}, a_{nD}, \Lambda_{\rm reg} < \infty$), only the ratio $\sqrt{B_T^{(m)}/B_T^{(m+1)}}$ is obtained somewhat close to asymptotic factor λ_0^∞, which rapidly converges to the same limit on approaching the unitary limit. In contrast, the ratio $\sqrt{B_3^{(m)}/B_3^{(m+1)}}$ is found to be substantially different for the asymptotic scaling factor, especially for a small choice of the cut-off $\Lambda_{\rm reg}$, with a rather slow asymptotic convergence. In fact, we find that the characteristic convergence exhibited by the ratios of the generic rms radii of the successive levels can be reconciled better with the convergence pattern of the ratios of $1/\sqrt{B_3}$ rather than those of $1/\sqrt{B_T}$, corroborating with the similar findings of Refs. [38, 46], i.e.,

$$\frac{r^{(m+1)}}{r^{(m)}} \sim \sqrt{\frac{B_3^{(m)}}{B_3^{(m+1)}}} \nsim \sqrt{\frac{B_T^{(m)}}{B_T^{(m+1)}}} \,. \tag{6.128}$$

To see this, we re-visit our results for the cut-off dependence of the three-body binding energies for the ground ($m = 0$) and first ($m = 1$) excited states of the D^0nn system [cf. Fig. 6.11, left plot]. For instance, with the choice of the cut-off as $\Lambda_{\rm reg} = 1473$ MeV (1095 MeV) in the SR (GR) scheme, the binding energy for the first excited state is obtained as $B_3^{(1)} = 1.92$ MeV ($B_T^{(1)} = 0.1$ MeV), while that of the ground state is obtained as $B_3^{(0)} = 76.63$ MeV ($B_T^{(0)} = 74.81$ MeV) and $B_3^{(0)} = 70.88$ MeV ($B_T^{(0)} = 69.06$ MeV) for the SR and GR schemes, respectively. Thus, we can expect the ratios of the rms radii to roughly follow the non-asymptotic correspondence

$$\frac{r^{(1)}}{r^{(0)}} \sim \sqrt{B_3^{(0)}/B_3^{(1)}} = 6.32\,(6.07)\,, \quad \text{for SR (GR) scheme}\,, \tag{6.129}$$

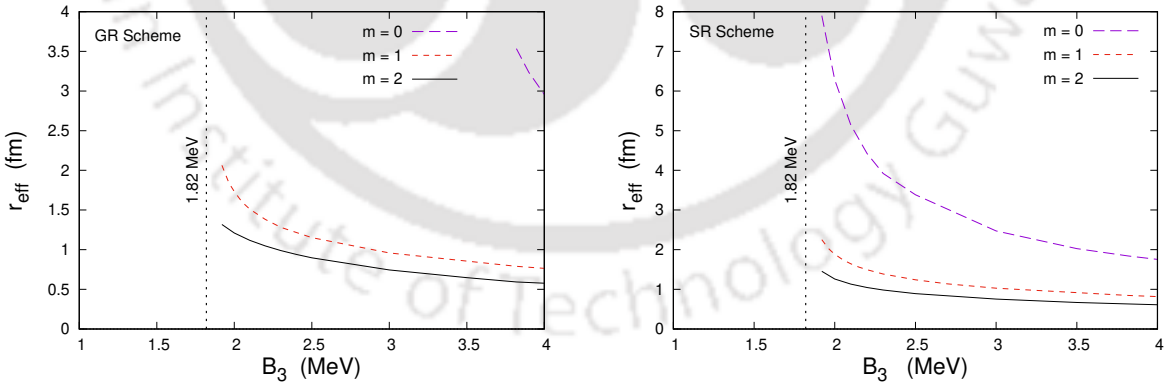

FIGURE 6.14: The variation of the effective/mean geometrical matter radius $r_{\rm eff} = \langle r_{\rm eff}^2 \rangle_{\rm 2n-halo}^{1/2}$ [see Eq. (6.124)] of the D^0nn $2n$-halo system for various input values of the three-body binding energy B_3 for the lowest three trimer states ($m = 0, 1, 2$). The results are obtained using the Gaussian (GR) and sharp cut-off (SR) regularization schemes. The vertical dashed line in each plot denotes the D^0n-dimer-particle break-up threshold energy $B_{nD} = 1.82$ MeV, corresponding to the spin-doublet S-wave scattering length $a_{nD} = 4.141$ fm, extracted in the idealized ZCL model analysis of Ref. [109].

RMS Radius	m^{th} level	r_{nn}	r_{nD}	r_n	r_D	r_{n-nD}	r_{D-nn}	r_{eff}
Sharp cut-off Scheme	0	0.49	0.48	0.32	0.22	0.43	0.43	0.28
Λ_{reg} =1473 MeV	1	3.49	3.12	3.67	1.39	3.81	2.67	2.23
Radius ratio	$\frac{r^{(m=1)}}{r^{(m=0)}}$	7.12	6.50	11.47	6.32	8.86	6.21	7.96
Gaussian cut-off Scheme	0	0.55	0.53	0.35	0.23	0.47	0.46	0.30
Λ_{reg} =1095 MeV	1	3.31	2.97	3.36	1.30	3.46	2.54	2.04
Radius ratio	$\frac{r^{(m=1)}}{r^{(m=0)}}$	6.02	5.60	9.60	5.65	7.36	5.52	6.80

TABLE 6.5: Various leading order root mean squared (rms) radii and their ratios between the ground ($m = 0$) and first ($m = 1$) excited state trimers for a halo-bound D^0nn system. All results correspond to two-body inputs in the idealized ZCL model scenario of Ref. [109].

as compared to the ratio

$$\sqrt{B_T^{(0)}/B_T^{(1)}} = 27.35\,(26.28)\,, \quad \text{for SR (GR) scheme}\,, \tag{6.130}$$

which quickly approaches the limit 21.5064 for larger choices of Λ_{reg} with greater number of excited states. As displayed in Table 6.5, the radius ratios are by and large of the order of the above non-asymptotic inverse square root of the $\sqrt{B_3}$ ratios, and are expected to follow similar convergence pattern as $\Lambda_{\text{reg}} \to \infty$. Nonetheless, the ground state binding energies simultaneously become so anomalously large that it precludes an unambiguous assessment of the D^0nn halo-bound ground state as a manifestation of Efimov universality in the context of our low-energy EFT.

6.7 Summary and Conclusion

In this chapter, we have reviewed the effective quantum mechanical formulation of constructing the Faddeev equations in the momentum representation at leading order. Such a formalism was originally developed in Refs. [35–37] for investigation of a resonant system of three and four bosons, and was later extended to the study of $2n$-halo nuclei such as ^{20}C in Refs [38, 46]. Here, we demonstrated the equivalence of the leading order formalism to the standard leading order pionless EFT approach *via* the STM integral equations [13, 14] to investigate the universal features of the putative S-wave $2n$ halo-bound D^0nn system, *assuming* an idealized ZCL scenario [109] with resonant S-wave interactions between the neutrons and the core D^0-meson. Using Jacobi coordinate system in momenta representation we construct a complete set of partial-wave basis states into which we project the set of coupled integral equations describing the dynamics of the coupled spin and isospin channels for the D^0nn system. In constructing the Faddeev equations we encountered two essential sets of components, namely, the two-body Lippmann-Schwinger kernels, represented by the matrix

elements ${}_i\langle pq\,\mathbb{Q}|G_0 t_i|p'q'\,\mathbb{Q}'\rangle_i$, and the re-couplings between the Jacobi momentum representations of the different re-arrangement channels, represented by the overlap-matrix elements ${}_i\langle pq\,\mathbb{Q}|p'q'\,\mathbb{Q}\rangle_j$ (where $i,j = n, D$). Especially, in view of the three-body description in the presence of shallow-bound S-wave real-bound bound D^0-n and virtual-bound n-n subsystems, following the approach of Refs [38, 46] it becomes advantageous to use separable potentials for the S-wave short-distance two-body interactions, thereby allowing us to compute such two-body kernels exactly. While, for the calculation of the overlap-matrix elements, we follow the prescription detailed in Ref. [50].

In this work we presented a qualitative comparison of our results for solving the Faddeev and STM integral equations obtained using the Gaussian and sharp cut-off regularization schemes, respectively. Investigating the asymptotic behavior of the integral equations (without the three-body force terms) in the both schemes revealed an RG limit cycle behavior of the D^0nn system with an inherent discrete scaling symmetry characterized by the universal number $\lambda_0^\infty = 21.5064....$ This formally indicates the manifestation of Efimov bound states below the D^0n-dimer-particle break-up threshold energy of $B_{nD} = 1.82$ MeV. In particular, for the sharp cut-off scheme, by fixing the relative three-body binding energy of the shallowest (most excited) Efimov level as $B_T = B_3 - B_{nD} = 0.1$ MeV, the two deepest level energies of $B_T \approx 73$ MeV and $B_T \approx 29934$ MeV were yielded as predictions of the theory (i.e., in principle only, although the relevance of such large binding energies lie certainly beyond the realm of our low-energy EFT). However, since the Gaussian scheme is known to become rather technical in the context of inclusion of three-body forces, we have restricted our renormalized binding energy results only for the sharp cut-off scheme where the inclusion of the three-body contact interaction is rather straightforward *via* the so-called STM3 equations, Eqs. (6.92).

We further investigated the remnant structural universality by studying the geometrical aspects of the halo-bound D^0nn system. For this purpose we reconstructed the full momentum space S-wave three-body wavefunctions $\Psi_n(p,q)$, Eq. (6.107), and $\Psi_D(p,q)$, Eq. (6.111), at leading order following the methodology outlined in Refs. [38, 46]. The wavefunctions were then used to determine the one- and two-body matter density form factor, and hence extract the two-particle mean square distances of a chosen two-body subsystem, as well as the mean square distance of the spectator particle from the two-body center-of-mass of the chosen subsystem. Furthermore, using our results for the mean square distances, we also calculated the two-neutron opening angle θ_{nn} and the effective/mean geometrical matter radius for the D^0nn system. Since the results are obtained without renormalization using the three-body force, they exhibit a strong cut-off ($\Lambda_{\rm reg}$) dependence, with especially the Gaussian scheme results beset with numerical convergence problems in the small $\Lambda_{\rm reg}$ region. In this regard, the strong cut-off scheme results are ostensibly more reliable. Thus, based on our latter results for the rms radii, we may conclude that a larger choice of the binding energy of a given trimer state leads to a more compact geometrical structure. In particular, we found that the rms radii for the $m = 0$ ground state trimer are substantially more sensitive to the variation of the binding energy than the excites states, and become quite large for small

values of the binding energy, say, below $B_T \lesssim 0.5$ MeV, favouring a halo-like structure. But this sensitivity on the input binding energy sharply diminishes for the excited states which are seemingly much more compact. Moreover, the marginal increase of θ_{nn} with increasing binding energy seems to indicate that the strongly attractive n-n interaction favours a shallow-bound ground state trimer with a near equilateral three-particle configuration. In contrast, the excited states turn out to be more sensitive to the θ_{nn} variations. Finally, in our quest for possible remnant signature of structural universality, we indeed found that the successive generic rms radius ratios are commensurate with the corresponding inverse binding energy ratios $r^{(m+1)}/r^{(m)} \sim \sqrt{B_3^{(m)}/B_3^{(m+1)}}$. However, at small $\Lambda_{\rm reg}$ these ratios differ significantly from their asymptotic value $\lambda_0^{\infty} = 21.5064$ in the unitary limit. Only for a much larger choice of $\Lambda_{\rm reg}$, do the ratios eventually approach the asymptotic value. But given that the ground state simultaneously becomes unphysically deep, its implications become irrelevant in the low-energy EFT picture.

In conclusion, more investigations on the D^0nn system, particularly on the experimental front, are necessary to throw more light on the possible existence of a $2n$-halo bound or quasi-bound resonance state state. Due to the intrinsic cut-off dependent problems, as well as realistic effects of decay and coupled-channel dynamics, it might be an extremely challenging task to extract the Efimovian signatures of the ground state reliably. Nevertheless, it is far more conceivable that near future experiments at facilities such as J-PARC, KEK and FAIR (GSI) should be able to probe any signature of haloing or clustering phenomena to manifest in the D^0nn system.

Chapter 7

Summary and Outlook

In this thesis we investigated various qualitative aspect of two- and three-body universality inherent to exotic possibilities of three-particle bound nuclear systems in strange and the charm sectors. In particular we looked at the putative bound hypernuclei in the strange sectors, such as the double-lambda systems ${}^{5}_{\Lambda\Lambda}\mathrm{H}$ and ${}^{5}_{\Lambda\Lambda}\mathrm{He}$, as well as the single-$\Xi$ nucleus $\Xi^{-}nn$, and an analogous presumably bound charm nuclei, the $D^{0}nn$ system. A systematic model-independent framework of pionless or halo/cluster EFT at the leading was used to perform qualitative analysis of each of the above systems to assay the role of Efimov physics in the underlying bound state mechanism. A momentum-space Faddeev-like integral equation using cut-off regularization was used to assess the plausible existence of these bound system, and hence to predict their three-body spectrum and low-energy observables thereof. However, the general paucity of the currently available phenomenological information to constrain the various low-energy parameters for all these systems a major hurdle in our approach which precludes definitive predictions. Below we highlight our basic findings in each of the three major works reported in this thesis, as detailed in the Chapters 4, 5 and 6.

In Chapter 4, we studied the doubly strange ($S = -2$) double-Λ-hypernuclear mirror/isospin partners (${}^{5}_{\Lambda\Lambda}\mathrm{H}$, ${}^{5}_{\Lambda\Lambda}\mathrm{He}$) in the ($J = 1/2$, $T = 1/2$) channel. Each mirror partner is identified as a system of three-particle 2Λ-halo cluster constituting the iso-doublet pair ($\Lambda\Lambda t$, $\Lambda\Lambda h$), where t and h stand for the triton and helion, respectively. The following were the highlights of that investigation:

- Their formal character found to be manifestly Efimovian that exhibits an RG limit cycle, characterized by the discrete scaling parameter $\lambda_0^{\infty} = 20.7980...$ and $20.7986...$ for ${}^{5}_{\Lambda\Lambda}\mathrm{H}$ and ${}^{5}_{\Lambda\Lambda}\mathrm{He}$ systems, respectively.

- For values of the cut-off regulator $\Lambda_{\mathrm{reg}} \sim 200$ MeV, our low-energy halo/cluster EFT predicted the double-Λ separation energy versus the Λ-Λ scattering length ($B_{\Lambda\Lambda}$ - $a_{\Lambda\Lambda}$) correlations to exhibit a fairly good agreement with existing potential model findings,

with $B_{\Lambda\Lambda}$ values re-evaluated using recent updated experimental inputs (instead of using the old model predictions of $B_{\Lambda\Lambda}$).

- The renormalized spin-averaged $\Lambda\Lambda T$ (with $T \equiv t, h$) three-body scattering length $a_{\Lambda\Lambda T}$ converged asymptotically for $\Lambda_{\rm reg} \geq 500$ MeV which is well beyond the hard scale $\Lambda_H \sim m_\pi$ of standard $\not\pi$EFT. This may be indicative of the fact that the underlying binding mechanisms may be fairly insensitive to the low-energy Λ-Λ two-body interactions, unless the hard-scale could be sufficiently augmented without potentially invalidating the EFT.

- The effective (spin-averaged) Phillips-line universal curves for the $\Lambda\Lambda t$ and $\Lambda\Lambda h$ systems are predicted.

- Our overall findings in the three-body sector reveal good isospin symmetry between the double-Λ hypernuclear mirror partners despite the substantially large isopin breaking effects in the two-body sector consisting of the single-Λ hypernuclear mirror partners ($^{4}_{\Lambda}$H, $^{4}_{\Lambda}$He).

- For input S-wave double-Λ scattering length $a_{\Lambda\Lambda} = -0.80$ fm, the Λ-separation energy of the $^{5}_{\Lambda\Lambda}$H and $^{5}_{\Lambda\Lambda}$He systems were predicted as $\mathcal{B}_\Lambda = 2.295$ and 2.212 MeV, respectively.

The results of the above investigation were published in *Physical Review C* ***103****, 014001 (2021).*

In Chapter 5, we studied one of the most basic three-body Ξ-hypernucleus, the $\Xi^- nn$ system in maximal isospin channel, i.e., ($J = 1/2$, $T = 3/2$) channel, excluding the predominantly repulsive $^1S_0$ $\Xi^- n$ subsystem channel that generates deeply-bound states causing the EFT to breakdown. The following were the highlights of that investigation:

- The formal character of the $\Xi^- nn$ system is manifestly Efimovian that exhibits an RG limit cycle, characterized by the discrete scaling parameter $\lambda_0^\infty = 49.9197....$ This differs from the expected asymptotic value of 22.432... that follows from the universality of three-particle mass ratios [12]. The decoupling of the $^1S_0$ $\Xi^- n$ channel accounts for this difference.

- In regard to the input values of the $^3S_1$ $\Xi^- n$ scattering length $a^{(1)}_{\Xi n}$ used in the work, two contrasting scenarios arise. In one scenario, inputs corresponding to two contemporary SU(3) chiral EFT analyses, namely, $a^{(1)}_{\Xi n} = -0.09$ fm [179] and $a^{(1)}_{\Xi n} = -1.17$ fm [180], which are known to yield a moderately attractive $(\Xi^- n)_t$ subsystem, hinted at a predominantly unbound $\Xi^- nn$ system. In the second scenario, the input from the Nijmegen model prediction $a^{(1)}_{\Xi n} = 4.911$ fm [183, 184], that correspond to a most-likely bound $(\Xi^- n)_t$ subsystem, indicated favourable prospects for a physically realizable $\Xi^- nn$ Efimov-like ground state. The resulting three-body binding energy was found to lie

within the range $B_3 \sim 2.886$ - 4.06 MeV corresponding to the cut variation of $\Lambda_{\rm reg} \sim 334$ - 465 MeV.

- The three-body S-wave $n - (\Xi^- n)_t$ renormalized scattering length is predicted within the range, $a_3^\infty \sim 2.6$ - 4.9 fm corresponding to the input range of the three-body binding energy $B_3 \sim 2.886$ - 4.06 MeV.
- The Phillips-line universal curve is predicted for the $\Xi^- nn$ system.
- The results of the analysis suggested the extension of the "canonical" hard-scale $\Lambda_H \sim m_\pi$ of pionless EFT to slightly higher values, say, $\Lambda_H \sim 500$ MeV. A rationale for such an extension could be attributed to possible underlying binding mechanisms driven by two-pion or σ-meson exchange.

The results of the above investigation were published in *Euro Physics Journal (Special Topics)* ***230****, 579 (2021).*

Chapter 6 can be considered as an extension of the earlier work of *Raha et al.* [109], concerning the investigation of Efimov universality of the putative $2n$ halo-bound D^0nn system in the $(J = 0, T = 3/2)$ channel using an idealized ZCL anasatz (excluding the effects of decay and coupled channels). Especially, in this work we explored the issue of structural universality using an effective quantum mechanical framework *via* Faddeev techniques developed in a momentum-space representation. The following were the highlights of that investigation:

- At leading order there is an exact one-to-one correspondence of the S-wave Faddeev integral equations in the effective quantum mechanical framework with the standard STM integral equations in pionless EFT.
- The formal character of the D^0nn system is manifestly Efimovian that exhibits an RG limit cycle, characterized by the discrete scaling parameter $\lambda_0^\infty = 21.5064...$.
- For small values of the regulator cut-off, typically of the order of the three-body binding momenta, the Gaussian cut-off regularization scheme is largely affected by numerical convergence problems. In contrast, the sharp momentum cut-off regularization scheme is presumable more stable.
- The ground state exhibits a halo-like equilateral *Samba* structure with large inter-particle rms distances for small (near-threshold) values of the three-body binding energy.
- The generic rms radius of the system varies inversely as the square root of the three-body binding energy $\sqrt{B_3}$, reflecting the remnant structural universality in successive ratios of the trimer states, namely, $\sqrt{B_3^{(m)}/B_3^{(m+1)}} \sim r^{(m+1)}/r^{(m)}$.

The above results shall be reported in the near-future publication currently under preparation.

Outlook:

Finally, we mention some of the future prospects of the works carried out in this thesis:

- As a trivial extension of the work in Chapter 6, the structural information of ${}^{5}_{\Lambda\Lambda}\mathrm{H}$, ${}^{5}_{\Lambda\Lambda}\mathrm{He}$ and $\Xi^{-}nn$ hypernuclear system, where the cores have non-zero spin, should be investigated in the same context of the effective quantum mechanical framework.

- A more rigorous analysis (without approximations) of the $\Xi^{-}nn$ system should be undertaken by including both $\Xi^{-}n$ spin channels. This however requires a modification of power counting to circumvent the effects of the unphysical deep-dimer state in the repulsive ${}^{1}S_{0}$ $\Xi^{-}n$ channel.

- All the results presented in the thesis corresponds to leading order EFT analysis only, which by all means are to be considered preliminary as well as qualitative. In order to utilize the predictive power of the EFT in assessing a reliable error estimate, next-to-leading order (NLO) analyses including effective range corrections should be undertaken in the future, as and when relevant phenomenological information becomes available.

- In all our three-body systems discussed in this thesis, possible momentum-dependent three-body forces may appear either at NLO or next-to-next-to-leading order (NNLO), as it happens in the case of the triton at NNLO [7]. Such investigations lie beyond the scope of this thesis but should be pursued as a future endeavor.

- A consideration must be given to the extension of the pionless EFT analysis to address the kind of remnant universality features that could manifest in kaonic systems, such as the $\bar{K}NN$, where the $\bar{K}N$ scattering lengths are complex. For this purpose, one needs to explore the possibility of using powerful techniques such as the *Method of Complex Scaling* [229] to systematically investigate the effects of resonances in the *Riemann sheet* with complex energy eigenstates based on non-Hermitian quantum mechanics. Besides, such methods naturally open up new avenues of investigation in the domain of Efimov resonances, rather than bound states.

Appendix A

Derivation of Eq. (2.118) in Chapter 2

The hyper-radial solution in the region $R \ll |a_0|$ as given by Eq. (2.117) in Chapter 2 is

$$f_0(R) \approx C_1(\kappa) R^{1/2+is_0} + C_2(\kappa) R^{1/2-is_0}\,, \quad R \ll |a_0|, 1/\kappa\,, \tag{A.1}$$

where $C_{1,2} = C_{1,2}(\kappa)$ are complex-valued constants (i.e., independent of the hyper-radius), such that in the absence of deeply-bound states, $|C_1| = |C_2|$. Let us now write $C_{1,2}$ by introducing the phases α and β, namely,

$$C_1(\kappa) = |C| e^{i\alpha} \kappa^{is_0}\,, \qquad C_2(\kappa) = |C| e^{i(\beta+\pi)} \kappa^{-is_0}\,, \tag{A.2}$$

where $\kappa = \sqrt{m|E|/\hbar^2}$ in above equation. Inserting $C_{1,2}$ in the Eq. A.1, we get

$$\begin{aligned} f_0(R) &\approx |C| R^{1/2} \left[e^{i\alpha} (\kappa R)^{is_0} + e^{i(\beta+\pi)} (\kappa R)^{-is_0} \right] \\ &= |C| R^{1/2} \left[e^{\ln(\kappa R)^{is_0} + i\alpha} - e^{\ln(\kappa R)^{-is_0} + i\beta} \right] \\ &= 2i|C| R^{1/2} \left[\frac{e^{\ln(\kappa R)^{is_0} + i\alpha} - e^{\ln(\kappa R)^{-is_0} + i\beta}}{2i} \right]. \end{aligned} \tag{A.3}$$

Next, introducing the phases θ and δ such that $\alpha = \delta + \theta$ and $\beta = \delta - \theta$, we have

$$\begin{aligned} f_0(R) &\approx 2i|C| R^{1/2} \left[\frac{e^{\ln(\kappa R)^{is_0} + i\theta + i\delta} - e^{\ln(\kappa R)^{-is_0} - i\theta + i\delta}}{2i} \right] \\ &= e^{i\delta} 2i|C| R^{1/2} \left[\frac{e^{is_0 \ln(\kappa R) + i\theta} - e^{-is_0 \ln(\kappa R) - i\theta}}{2i} \right]. \end{aligned} \tag{A.4}$$

Finally, we can express the hyper-radial solution in the following form:

$$f_0(R) \approx A\sqrt{R} \sin\left[s_0 \ln(\kappa R) + \theta\right]\,, \tag{A.5}$$

where $A = e^{i\delta} 2i|C|$, which yields Eq. (2.118) in Chapter 2.

Appendix B

One- and Two-body non-relativistic Propagators For $\Lambda\Lambda T$ system

Here we summarize the one- and two-body nonrelativistic propagators specific to the $\Lambda\Lambda T$ three-body systems in pionless effective theory ($\not\pi$EFT). In this framework, at sufficiently low-energies below the respective breakup scales, we may consider the triton (^{3}H or t) and the helion (^{3}He or h) as being fundamental particles. Thus, as the fundamental one-body components of the theory, the Λ and T propagators are given as

$$iS_{\Lambda,T}(p_0,\mathbf{p}) \;=\; \frac{i}{p_0-\frac{\mathbf{p}^2}{2M_{\Lambda,T}}+i\eta}\,, \tag{B.1}$$

where p_0 and $\mathbf{p}$ are the generic off-shell energy and three-momentum. In our analysis we only consider the S-waves contributions from the two-body interactions at LO. We have incorporated a power counting scheme [3, 4] for the ^{1}S$_0$ Λ-T, ^{3}S$_1$ Λ-T and the ^{1}S$_0$ Λ-Λ interactions in the two-body sector, in which the unitarized two-body amplitudes are conveniently expressed in terms of the auxiliary fields, namely, the spin-singlet and spin-triplet ΛT-dimer fields $u_{0,1}$, and the spin-singlet $\Lambda\Lambda$-dibaryon field u_s. The leading order renormalized dressed dimer

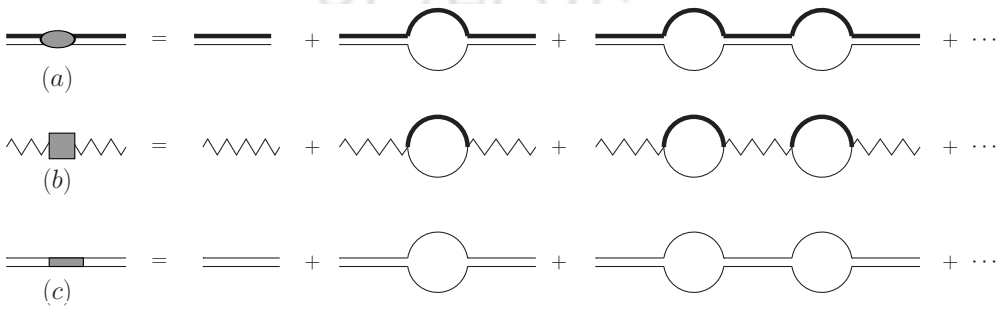

FIGURE B.1: Diagrams for the renormalized dressed dimer propagators: (a) $i\Delta_0$ for the spin-singlet auxiliary field u_0, (b) $i\Delta_1$ for the spin-triplet auxiliary field u_1, and (c) $i\Delta_s$ for the spin-singlet auxiliary field u_s. Thick (thin) lines denote the Λ-hyperon (core $T \equiv t, h$) field propagators.

propagators [52–54] are given by the expressions (see Fig. B.1)

$$\mathscr{D}_{0,1}(p_0,\mathbf{p}) \;=\; \frac{1}{\gamma_{0,1}-\sqrt{-2\mu_{\Lambda T}(p_0-\frac{\mathbf{p}^2}{2(M_T+M_\Lambda)})-i\eta}-i\eta}\,, \tag{B.2}$$

and,

$$\mathscr{D}_{s}(p_0,\mathbf{p}) \;=\; \frac{1}{\frac{1}{a_{\Lambda\Lambda}}-\sqrt{-M_\Lambda(p_0-\frac{\mathbf{p}^2}{4M_\Lambda})-i\eta}-i\eta}\,, \tag{B.3}$$

respectively, with the LO two-body contact interactions y_0, y_1, and y_s fixed as in Eq. 4.8 in the text. In the above expressions, γ_0 and γ_1 are the binding momenta of spin-singlet and spin-triplet states of the ΛT subsystem, and $a_{\Lambda\Lambda}$ is S-wave double-Λ scattering length.

Appendix C

Integral equation for $\Xi^- nn$ $(T = 3/2, J^P = 1/2^+)$ system

The Faddeev-like three-body coupled integral equation for the $n+(\Xi^- n)_t \to n+(\Xi^- n)_t$ elastic scattering amplitude t_A (cf. Fig. 5.2) (excluding the $(\Xi^- n)_s$ singlet subsystem channel) can be easily obtained *via* Feynman rules from the non-relativistic effective Lagrangian, and is given as

$$
\begin{aligned}
t_A\left(\mathbf{p},\mathbf{k};E\right) \;=\; & (-y_1^2)\left[\mathscr{C}_2^{(11)} S_\Xi\left(E-\frac{\mathbf{p}^2}{2M_n}-\frac{\mathbf{k}^2}{2M_n},\mathbf{p}+\mathbf{k}\right)+\mathscr{C}_3^{(11)}\frac{M_\Xi}{2}\frac{g_3(\Lambda_{\rm reg})}{\Lambda_{\rm reg}^2}\right] \\
& -\mathscr{C}_2^{(11)}(-y_1^2)\int^{\Lambda_{\rm reg}}\frac{\mathrm{d}^3\mathbf{q}}{(2\pi)^3}\,t_A\left(\mathbf{q},\mathbf{k};E\right)\,S_\Xi\left(E-\frac{\mathbf{p}^2}{2M_n}-\frac{\mathbf{q}^2}{2M_n},\mathbf{p}+\mathbf{q}\right) \\
& \qquad\qquad \times\mathscr{D}_1\left(E-\frac{\mathbf{q}^2}{2M_n},\mathbf{q}\right) \\
& -\mathscr{C}_3^{(11)}(-y_1^2)\frac{M_\Xi}{2}\int^{\Lambda_{\rm reg}}\frac{\mathrm{d}^3\mathbf{q}}{(2\pi)^3}t_A\left(\mathbf{q},\mathbf{k};E\right)\mathscr{D}_1\left(E-\frac{\mathbf{q}^2}{2M_n},\mathbf{q}\right)\frac{g_3(\Lambda_{\rm reg})}{\Lambda_{\rm reg}^2} \\
& -\mathscr{C}_2^{(10)}(-y_0y_1)\int^{\Lambda_{\rm reg}}\frac{\mathrm{d}^3\mathbf{q}}{(2\pi)^3}\,t_B\left(\mathbf{q},\mathbf{k};E\right)S_n\left(E-\frac{\mathbf{p}^2}{2M_n}-\frac{\mathbf{q}^2}{2M_\Xi},\mathbf{p}+\mathbf{q}\right) \\
& \qquad\qquad \times\mathscr{D}_0\left(E-\frac{\mathbf{q}^2}{2M_\Xi},\mathbf{q}\right) \\
& +\mathscr{C}_3^{(10)}(-y_0y_1)\sqrt{\frac{3}{2}}M_n\int^{\Lambda_{\rm reg}}\frac{\mathrm{d}^3\mathbf{q}}{(2\pi)^3}\,t_B\left(\mathbf{q},\mathbf{k};E\right)\frac{g_3(\Lambda_{\rm reg})}{\Lambda_{\rm reg}^2} \\
& \qquad\qquad \times\mathscr{D}_0\left(E-\frac{\mathbf{q}^2}{2M_\Xi},\mathbf{q}\right)\,, \qquad\qquad \text{(C.1)}
\end{aligned}
$$

and

$$
\begin{aligned}
t_B\left(\mathbf{p},\mathbf{k};E\right) \;=\; & (-y_0 y_1)\left[\mathscr{C}_2^{(10)} S_n\left(E-\frac{\mathbf{k}^2}{2M_n}-\frac{\mathbf{p}^2}{2M_\Xi},\mathbf{p}+\mathbf{k}\right)-\mathscr{C}_3^{(10)}\sqrt{\frac{3}{2}}M_n\frac{g_3(\Lambda_{\rm reg})}{\Lambda_{\rm reg}^2}\right] \\
& -\mathscr{C}_2^{(10)}(-y_0 y_1)\int^{\Lambda_{\rm reg}}\frac{\mathrm{d}^3\mathbf{q}}{(2\pi)^3}t_A\left(\mathbf{q},\mathbf{k};E\right)S_n\left(E-\frac{\mathbf{p}^2}{2M_\Xi}-\frac{\mathbf{q}^2}{2M_n},\mathbf{p}+\mathbf{q}\right) \\
& \qquad\qquad \times\mathscr{D}_1\left(E-\frac{\mathbf{q}^2}{2M_n},\mathbf{q}\right) \\
& +\mathscr{C}_3^{(10)}(-y_0 y_1)\sqrt{\frac{3}{2}}M_n\int^{\Lambda_{\rm reg}}\frac{\mathrm{d}^3\mathbf{q}}{(2\pi)^3}\,t_A\left(\mathbf{q},\mathbf{k};E\right)\frac{g_3(\Lambda_{\rm reg})}{\Lambda_{\rm reg}^2} \\
& \qquad\qquad \times\mathscr{D}_1\left(E-\frac{\mathbf{q}^2}{2M_n},\mathbf{q}\right)\,. \qquad\qquad \text{(C.2)}
\end{aligned}
$$

Here, $\mathscr{C}_2^{(11)}=1/2$, $\mathscr{C}_2^{(10)}=-\sqrt{3/2}$ are spin-isospin re-coupling coefficients for diagrams with two-body interaction only, and $\mathscr{C}_3^{(11)}=\mathscr{C}_3^{(10)}=1$ are those with the three-body contact interaction. Upon renormalization using the wavefunction renormalization constant $\mathscr{Z}_{\Xi n}$ (cf. Eq. 5.18), and projecting on to the S-wave, the above amplitudes lead to Eqn. 5.13 and 5.14.

Bibliography

[1] D. B. Kaplan, "More effective field theory for nonrelativistic scattering", Nucl. Phys. B **494**, 471 (1997).

[2] D. B. Kaplan, M. J. Savage and M. B. Wise, "Nucleon - nucleon scattering from effective field theory", Nucl. Phys. B **478**, 629 (1996).

[3] D. B. Kaplan, M. J. Savage and M. B. Wise, "A New expansion for nucleon-nucleon interactions", Phys. Lett. B **424**, 390-396 (1998).

[4] D. B. Kaplan, M. J. Savage and M. B. Wise, "Two nucleon systems from effective field theory", Nucl. Phys. B **534**, 329-355 (1998).

[5] D. B. Kaplan, M. J. Savage and M. B. Wise, "A Perturbative calculation of the electromagnetic form-factors of the deuteron", Phys. Rev. C **59**, 617 (1999).

[6] U. van Kolck, "Effective field theory of short range forces", Nucl. Phys. A **645**, 273 (1999).

[7] P. F. Bedaque, G. Rupak, H. W. Griesshammer and H. W. Hammer, "Low-energy expansion in the three-body system to all orders and the triton channel", Nucl. Phys. A **714**, 589-610 (2003)

[8] M. C. Birse, J. A. McGovern and K. G. Richardson, "A Renormalization group treatment of two-body scattering", Phys. Lett. B **464**, 169 (1999).

[9] V. Efimov, "Energy levels arising form the resonant two-body forces in a three-body system", Phys. Lett. B **33**, 563 (1970).

[10] V. N. Efimov, "Weakly-bound states of 3 resonantly-interacting particle",, Yad. Fiz. **12**, 1080 (1970) [Sov. J. Nucl. Phys. **12**, 589 (1971)].

[11] V. Efimov, "Energy levels of three resonantly interacting particles", Nucl. Phys. A **210**, 157 (1973).

[12] E. Braaten and H. W. Hammer, "Universality in few-body systems with large scattering length", Phys. Rept. **428**, 259-390 (2006).

[13] G. V. Skornyakov and K. A. Ter-Martirosyan, "Three body problem for short range forces. I. Scattering of low energy neutrons by deuterons", Sov. Phys. JETP **4**, 648 (1957) [Zh. Eksp. Teor. Fiz. 31, 775 (1956)].

[14] G. V. Skornyakov and K. A. Ter-Martirosyan, Sov. Phys. JETP **31**, 775 (1956).

[15] P. Naidon and S. Endo, "Efimov Physics: a review", Rept. Prog. Phys. **80**, no.5, 056001 (2017).

[16] L. H. Thomas, "The Interaction Between a Neutron and a Proton and the Structure of H**3", Phys. Rev. **47**, 903-909 (1935).

[17] K. G. Wilson, "The Renormalization Group and Strong Interactions", Phys. Rev. D **3**, 1818 (1971).

[18] S. D. Glazek and K. G. Wilson, "Limit cycles in quantum theories", Phys. Rev. Lett. **89**, 230401 (2002) [Erratum-ibid. **92**, 139901 (2004)].

[19] S. D. Glazek and K. G. Wilson, "Universality, marginal operators, and limit cycles", Phys. Rev. B **69**, 094304 (2004).

[20] A. LeClair, J. M. Roman and G. Sierra, "Russian doll renormalization group and superconductivity", Phys. Rev. B **69**, 020505 (2004).

[21] A. LeClair, J. M. Roman and G. Sierra, "Russian doll renormalization group, Kosterlitz-Thouless flows, and the cyclic sine-Gordon model", Nucl. Phys. B **675**, 584-606 (2003).

[22] A. LeClair, J. M. Roman and G. Sierra, "Log periodic behavior of finite size effects in field theories with RG limit cycles", Nucl. Phys. B **700**, 407 (2004).

[23] D. Sornette, "Discrete scale invariance and complex dimensions", Phys. Rept. **297**, 239 (1998).

[24] M. T. Yamashita, L. Tomio and T. Frederico, "Radii in weakly bound light halo nuclei", Nucl. Phys. A **735**, 40 (2004).

[25] K. Riisager, "Nuclear halo states", Rev. Mod. Phys. **66**, 1105-1116 (1994).

[26] M. V. Zhukov *et al.*, "Bound state properties of Borromean Halo nuclei: He-6 and Li-11", Phys. Rept. **231**, 151-199 (1993).

[27] P. G. Hansen, A. S. Jensen and B. Jonson, "Nuclear halos", Ann. Rev. Nucl. Part. Sci. **45**, 591-634 (1995).

[28] I. Tanihata, "Neutron halo nuclei", J. Phys. G **22**, 157 (1996).

[29] A. S. Jensen, K. Riisager, D. V. Fedorov and E. Garrido, "Structure and reactions of quantum halos", Rev. Mod. Phys. **76**, 215-261 (2004).

[30] Q. Chen *et al.*, "Measurement of the neutron-neutron scattering length using the pi-d capture reaction", Phys. Rev. C **77**, 054002 (2008).

[31] C. A. Bertulani, H. W. Hammer and U. Van Kolck, "Effective field theory for halo nuclei", Nucl. Phys. A **712**, 37-58 (2002).

[32] H. W. Hammer, C. Ji and D. R. Phillips, "Effective field theory description of halo nuclei", J. Phys. G **44**, no.10, 103002 (2017).

[33] A. Gal, E. V. Hungerford and D. J. Millener, "Strangeness in nuclear physics", Rev. Mod. Phys. **88**, 035004 (2016).

[34] L. D. Faddeev, "Scattering theory for a three particle system", Sov. Phys. JETP **12**, 1014 (1961) [Zh. Eksp. Teor. Fiz **39**, 1459 (1960)].

[35] L. Platter, H. W. Hammer and U. G. Meissner, "The Four boson system with short range interactions", Phys. Rev. A **70**, 052101 (2004).

[36] L. Platter, H. W. Hammer and U. G. Meissner, "Universal properties of the four boson system in two dimensions", Few Body Syst. **35**, 169-174 (2004).

[37] L. Platter, H. W. Hammer and U. G. Meissner, "On the correlation between the binding energies of the triton and the alpha-particle", Phys. Lett. B **607**, 254-258 (2005).

[38] D. L. Canham and H. W. Hammer, "Universal properties and structure of halo nuclei", Eur. Phys. J. A **37**, 367-380 (2008).

[39] A. W. Thomas, "Modern Three Hadron Physics", Top. Curr. Phys. **2**, pp. 1-250 (1977).

[40] J. J. Sakurai, "*Modern Quantum Mechanics*.", Addison-Wesley Publisher.

[41] S. A. Coon and B. R. Holstein, "Anomalies in Quantum Mechanics: the $1/r^2$ Potential", Am. J. Phys. **70**, 513-519 (2002).

[42] H. Bethe, "Theory of the effective range in nuclear scattering", Phys. Rev. **76**, 38-50 (1949).

[43] H. Bethe and C. Longmire "The effective range of nuclear forces II. Photo-disintegration of the deuteron", Phys. Rev. **77**, 647 (1950).

[44] H. W. Hammer and D. Lee, "Causality and the effective range expansion", Annals Phys. **325**, 2212-2233 (2010)

[45] D. R. Phillips, G. Rupak and M. J. Savage, "Improving the convergence of N N effective field theory", Phys. Lett. B **473**, 209-218 (2000)

[46] D. L. Canham, Ph.D. Thesis, *Three-Body Halo Nuclei in an Effective Theory Framework*.

[47] E. Nielsen, D. V. Fedorov, A. S. Jensen and E. Garrido, "The three-body problem with short-range interactions", Phys. Rep. **347**, 373 (2001).

[48] J. Macek, "Properties of autoionizing states of He", J. Phys. B **1**, 831 (1968).

[49] D. V. Fedorov and A. S. Jensen, "Efimov effect in coordinate space Faddeev equations", Phys. Rev. Lett. **71**, 4103 (1993).

[50] W. Glöckle, *The Quantum Mechanical Few-Body Problem*, Springer Verlag Publication, December 2012.

[51] P. F. Bedaque, H. W. Hammer and U. van Kolck, "Narrow resonances in effective field theory", Phys. Lett. B **569**, 159-167 (2003).

[52] P. F. Bedaque, H. W. Hammer, and U. Van Kolck, "Renormalization of the three-body system with short range interactions", Phys. Rev. Lett. **82**, 463 (1999).

[53] P. F. Bedaque, H. W. Hammer, and U. Van Kolck, "Effective theory of the triton", Nucl. Phys. A **676**, 357 (2000).

[54] P. F. Bedaque, H. W. Hammer and U. van Kolck, "The Three boson system with short range interactions", Nucl. Phys. A **646**, 444 (1999).

[55] P. F. Bedaque, H. W. Hammer and U. van Kolck, "Effective theory for neutron deuteron scattering: Energy dependence", Phys. Rev. C **58**, 641 (1998).

[56] S. R. Beane, P. F. Bedaque, W. C. Haxton, D. R. Phillips and M. J. Savage, "*From hadrons to nuclei: Crossing the border*", [arXiv:nucl-th/0008064 [nucl-th]].

[57] H. W. Hammer, S. König and U. van Kolck, "Nuclear effective field theory: status and perspectives", Rev. Mod. Phys. **92**, 025004 (2020).

[58] D. B. Kaplan, "Five lectures on effective field theory", [arXiv:nucl-th/0510023 [nucl-th]].

[59] M. Hjorth-Jensen, M. P. Lombardo and U. van Kolck, "An Advanced Course in Computational Nuclear Physics", Lect. Notes Phys. **936**, pp. (2017).

[60] S. Weinberg, "Effective chiral Lagrangians for nucleon - pion interactions and nuclear forces", Nucl. Phys. B **363**, 3-18 (1991).

[61] G. S. Danilov, "On the three-body problem with short-range forces", Zh. Eksp. Teor. Fiz. **40**, 498 (1961) [Sov. Phys. JETP **13**, 349 (1961)].

[62] R. A. Minlos and L. D. Faddeev, "Comment on the problem of three particles with point interactions", Dokl. Akad. Nauk SSSR **141** 1335 (1961) [Sov. Phys. Doklady **6**, 1072 (1962)].

[63] G. Meher and U. Raha, "Investigation of $\Xi^- nn$ ($S = -2$) Hypernucleus in Low-energy Pionless Halo Effective Theory", Eur. Phys. J. ST **230**, no.2, 579-601 (2021).

[64] G. Meher and U. Raha, "${}^{5}_{\Lambda\Lambda}$H and ${}^{5}_{\Lambda\Lambda}$He Hypernuclei reexamined in Halo/Cluster Effective Theory", Phys. Rev. C **103**, no.1, 014001 (2021).

[65] H. Takahashi *et al.*, "Observation of a (Lambda Lambda)He-6 double hypernucleus," Phys. Rev. Lett. **87**, 212502 (2001).

[66] J. K. Ahn *et al.*, "Production of (Lambda Lambda)H-4 hypernuclei," Phys. Rev. Lett. **87**, 132504 (2001).

[67] D. H. Davis, "50 years of hypernuclear physics. I. The early experiments," Nucl. Phys. A **754**, 3-13 (2005).

[68] C. J. Yoon *et al.* [E522 (KEK-PS) Collaboration], "Search for the H-dibaryon resonance in C-12 (K-, K+ Lambda Lambda X)," Phys. Rev. C **75**, 022201(R) (2007).

[69] J. K. Ahn *et al.* [E373 (KEK-PS) Collaboration], "Double-Λ hypernuclei observed in a hybrid emulsion experiment," Phys. Rev. C **88**, no. 1, 014003 (2013).

[70] H. Tamura *et al.*, "Gamma-ray spectroscopy of hypernuclei - present and future", Nucl. Phys. A **914**, 99 (2013).

[71] L. Adamczyk *et al.* [STAR Collaboration], "ΛΛ Correlation Function in Au+Au collisions at $\sqrt{s_{NN}} = 200$ GeV", Phys. Rev. Lett. **114**, 022301 (2015).

[72] T. Yamamoto *et al.* [J-PARC E13 Collaboration], "Observation of Spin-Dependent Charge Symmetry Breaking in ΛN Interaction: Gamma-Ray Spectroscopy of ${}^{4}_{\Lambda}$He", Phys. Rev. Lett. **115**, 222501 (2015).

[73] A. Esser *et al.* [A1 Collaboration], "Observation of ${}^{4}_{\Lambda}$H Hyperhydrogen by Decay-Pion Spectroscopy in Electron Scattering", Phys. Rev. Lett. **114**, 232501 (2015).

[74] F. Schulz *et al.* [A1 Collaboration], "Ground-state binding energy of ${}^{4}_{s}$H from high-resolution decay-pion spectroscopy", Nucl. Phys. A **954**, 149-160 (2016).

[75] T. Koike *et al.* [J-PARC E13 Collaboration], "Gamma-ray spectroscopy of single Λ-hypernuclei at J-PARC: results and perspective", AIP Conf. Proc. **2130**, No.1, 020011 (2019).

[76] S. Achariya *et al.* [ALICE Collaboration], "p-p, p-Λ and Λ-Λ correlations studied via femtoscopy in pp reactions at $\sqrt{s} = 7$ TeV", Phys. Rev. C **99**, 024001 (2019).

[77] S. Achariya *et al.* [ALICE Collaboration], "Study of the Λ-Λ interaction with femtoscopy correlations in pp and p-Pb collisions at the LHC", Phys. Lett. B **797**, 134822 (2019).

[78] R. L. Jaffe, "Perhaps a Stable Dihyperon", Phys. Rev. Lett. **38**, 195 (1977).

[79] H. W. Hammer, "The Hypertriton in effective field theory", Nucl. Phys. A **705**, 173 (2002).

[80] I. N. Filikhin and A. Gal, "Faddeev-Yakubovsky calculations for light lambda lambda hypernuclei", Nucl. Phys. A **707**, 491 (2002).

[81] I. N. Filikhin, A. Gal and V. M. Suslov, "Faddeev calculations for the A = 5,6 Lambda Lambda hypernuclei", Phys. Rev. C **68**, 024002 (2003).

[82] H. Nemura, Y. Akaishi and K. S. Myint, "Stochastic variational search for H-4(Lambda Lambda)", Phys. Rev. C **67**, 051001 (2003).

[83] K. S. Myint, S. Shinmura and Y. Akaishi, "Lambda Lambda - Xi N coupling effects in light hypernuclei", Eur. Phys. J. A **16**, 21 (2003).

[84] D. E. Lanskoy and Y. Yamamoto, "Hyperonic mixing in five baryon double strangeness hypernuclei in a two channel treatment", Phys. Rev. C **69**, 014303 (2004).

[85] M. Shoeb, "Variational Monte Carlo calculation of he-6 and other s-shell hypernuclei", Phys. Rev. C **69**, 054003 (2004).

[86] H. Nemura, S. Shinmura, Y. Akaishi and K. S. Myint, "Full-coupled channel approach to doubly strange (s)-shell hypernuclei", Phys. Rev. Lett. **94**, 202502 (2005).

[87] H. Nemura, S. Shinmura, Y. Akaishi and K. S. Myint, "Full-coupled channel approach to S=-2 s-shell hypernuclear systems", Nucl. Phys. A **754**, 110 (2005).

[88] S.-I. Ando, G.-S.Yang and Y. Oh, "${}^{4}_{\Lambda\Lambda}$H in halo effective field theory", Phys. Rev. C **89**, 014318 (2014).

[89] S.-I. Ando and Y. Oh, "${}^{6}_{\Lambda\Lambda}$He in cluster effective field theory", Phys. Rev. C **90**, 037301 (2014).

[90] L. Contessi *et al.*, "The onset of ΛΛ hypernuclear binding", Phys. Lett. B **797**, 134893 (2019).

[91] A. M. Gasparyan, J. Haidenbauer and C. Hanhart, "Scattering lengths of strangeness S=-2 baryon-baryon interactions", Phys. Rev. C **85**, 015204 (2012).

[92] S. R. Beane *et al.* [NPLQCD Collaboration], "Evidence for a Bound H-dibaryon from Lattice QCD", Phys. Rev. Lett. **106**, 162001 (2011).

[93] S. R. Beane *et al.* [NPLQCD Collaboration], "Present Constraints on the H-dibaryon at the Physical Point from Lattice QCD", Mod. Phys. Lett. A **26** 2587 (2011).

[94] S. R. Beane *et al.* [NPLQCD Collaboration], "The Deuteron and Exotic Two-Body Bound States from Lattice QCD", Phys. Rev. D **85**, 054511 (2011).

[95] T. Inoue *et al.* [HAL QCD Collaboration], "Bound H-dibaryon in Flavor SU(3) Limit of Lattice QCD", Phys. Rev. Lett. **106**, 162002 (2011).

[96] T. Inoue *et al.* [HAL QCD Collaboration], "Bound H-dibaryon in the Flavor SU(3) Limit from a Full QCD Simulation on the Lattice", AIP Conference Proceedings 1441, 335 (2012).

[97] P. E. Shanahan, A. W. Thomas and R. D. Young, "Mass of the H-dibaryon", Phys. Rev. Lett. **107**, 092004 (2011).

[98] J. Haidenbauer and Ulf.-G. Meissner, "To bind or not to bind: The H-dibaryon in light of chiral effective field theory", Phys. Lett. B **708**, 100 (2011).

[99] K. Sasaki *et al.* [HAL QCD Collaboration], "ΛΛ and NΞ interactions from lattice QCD near the physical point", Nucl. Phys. A **998**, 121737 (2020).

[100] K. Morita, T. Furumoto and A. Ohnishi, "ΛΛ interaction from relativistic heavy-ion collisions", Phys. Rev. C **91**, 024916 (2015).

[101] A. Ohnishi, K. Morita and T. Furumoto, "Lambda-Lambda interaction from two-particle intensity correlation in relativistic heavy-ion collisions", JPS Conf. Proc. **17**, 031003 (2017).

[102] A. Ohnishi, K. Morita, K. Miyahara, and T. Hyodo, "Hadron–hadron correlation and interaction from heavy–ion collisions", Nucl. Phys. A **954**, 294 (2016).

[103] N. Barnea *et al.*, "Effective Field Theory for Lattice Nuclei", Phys. Rev. Lett. **114**, 052501 (2015).

[104] A. Kirscher *et al.*, "Spectra and Scattering of Light Lattice Nuclei from Effective Field Theory", Phys. Rev. C **92**, 054002 (2015).

[105] A. Kirscher *et al.*, "Electromagnetic characteristics of $A \leq 3$ physical and lattice nuclei", Phys. Rev. C **96**, 024001 (2017).

[106] L. Contessi, N. Barnea and A. Gal, "Resolving the Λ Hypernuclear Overbinding Problem in Pionless Effective Field Theory", Phys. Rev. Lett. **121**, 102502 (2018).

[107] M. Juric *et al.*, "A new determination of the binding-energy values of the light hypernuclei (15>=a)", Nucl. Phys. B **52**, 1 (1973).

[108] S. I. Ando, U. Raha and Y. Oh, "Investigation of the $nn\Lambda$ bound state in pionless effective theory", Phys. Rev. C **92**, no. 2, 024325 (2015).

[109] U. Raha, Y. Kamiya, S. I. Ando, and T. Hyodo, "Universal physics of the few-body system of two neutrons and one flavored meson", Phys. Rev. C **98**, no. 3, 034002 (2018).

[110] F. Hildenbrand and H.-W. Hammer, "Three-Body Hypernuclei in Pionless Effective Field Theory", Phys. Rev. C **100**, 034002 (2019).

[111] M. .M. Nagels, T. A. Rijken, and J. J. de Swart, "Baryon Baryon Scattering in a One Boson Exchange Potential Approach. 3. A Nucleon-Nucleon and Hyperon - Nucleon Analysis Including Contributions of a Nonet of Scalar Mesons", Phys. Rev. D **15**, 2547 (1977); D **20**, 1633 (1979).

[112] T. A. Rijken, V. G. J. Stoks, and Y. Yamamoto, "Soft core hyperon - nucleon potentials", Phys. Rev. C **59**, 21 (1999).

[113] V. G. J. Stoks and Th. A. Rijken, "Soft core baryon baryon potentials for the complete baryon octet", Phys. Rev. C **59**, 3009 (1999).

[114] D. Gazda and A. Gal, "Charge symmetry breaking in the A = 4 hypernuclei", Nucl. Phys. A **954**, 161-175 (2016).

[115] A. C. Phillips, "Consistency of the low-energy three-nucleon observables and the separable interaction model", Nucl. Phys. A **107**, 209-216 (1968).

[116] S. R. Beane and M. J. Savage, "Rearranging pionless effective field theory", Nucl. Phys. A **694**, 511 (2001).

[117] S.-I. Ando and C. H. Hyun, "Effective field theory on the deuteron with dibaryon field", Phys. Rev. C **72**, 014008 (2005).

[118] S. I. Ando and M. C. Birse, "Effective field theory of 3He", J. Phys. G **37**, 105108 (2010).

[119] F. Gabbiani, P. F. Bedaque and H. W. Griesshammer, "Higher partial waves in an effective field theory approach to nd scattering", Nucl. Phys. A **675**, 601-620 (2000).

[120] H. W. Griesshammer, "Improved convergence in the three-nucleon system at very low energies", Nucl. Phys. A **744**, 192 (2004).

[121] H. W. Griesshammer, "Naive dimensional analysis for three-body forces without pions", Nucl. Phys. A **760**, 110-138 (2005)

[122] K. G. Wilson, "The Renormalization Group and Strong Interactions", Phys. Rev. D **3**, 1818 (1971).

[123] G. S. Danilov, "A model of local field theory with finite charge renormalization", Zh. Eksp. Teor. **40**, 498 (1961) [Sov. Phys. JETP **13**, 349 (1961)].

[124] G. S. Danilov and V. I. Lebedev, "Calculation of the doublet neutron–deuteron scattering length in the theory of zero range forces", Sov. Phys. JETP **17**, 1015 (1963).

[125] P. J. Mohr, D. B. Newell and B. N. Taylor, "CODATA Recommended Values of the Fundamental Physical Constants: 2014", Rev. Mod. Phys. 88, no.3, 035009 (2016).

[126] K. L. Kowalski, "Off-Shell Equations for Two-Particle Scattering", Phys. Rev. Lett. **15**, 798 (1965).

[127] H. P. Noyes, "A New Nonsingular Integral Equation for Two Particle Scattering", Phys. Rev. Lett. **15**, 538 (1965).

[128] A. Gal, "Charge symmetry breaking in Λ hypernuclei revisited", Phys. Lett. B **744**, 352 (2015).

[129] J. Pochodzalla *et al.* [PANDA Collaboration], "Roadmap for double hypernuclei spectroscopy at PANDA", EPJ Web of Conferences 3, 07008 (2010).

[130] G. Boca *et al.* [PANDA Collaboration], "The experiment PANDA: physics with antiprotons at FAIR", EPJ Web of Conferences 95, 01001 (2015).

[131] I. Vassiliev *et al.* [CBM Collaboration], "Hypernuclei Program at the CBM Experiment", JPS Conf. Proc. **17**, 092001 (2017).

[132] H. Fujioka *et al.* [JPARC Collaboration], "${}^{5}_{\Lambda\Lambda}H$ production experiment by use of ${}^{7}_{\Xi}H$ production and decay at J-PARC", AIP Conference Proceedings 2130, 040002 (2019).

[133] S. Petschauer *et al.*, "Hyperon-nuclear interactions from SU(3) chiral effective field theory", Front. in Phys. **8**, 12 (2020).

[134] E. Hiyama and K. Nakazawa, "Structure of $S = -2$ Hypernuclei and Hyperon- Hyperon Interactions", Ann. Rev. Nucl. Part. Sci. **68**, 131-159 (2018).

[135] A. Gal, "Progress Report on Few-Body Hypernuclei", AIP Conf. Proc. **2249**, 030001 (2020).

[136] H. Garcilazo, A. Valcarce and J. Vijande, "Neutral baryonic systems with strangeness", Int. J. Mod. Phys. E **29**, 1930009 (2020).

[137] L. Tolos and L. Fabbietti, "Strangeness in Nuclei and Neutron Stars", Prog. Part. Nucl. Phys. **112**, 103770 (2020).

[138] A. L. Watts *et al.*, "Colloquium : Measuring the neutron star equation of state using x-ray timing", Rev. Mod. Phys. **88**, 021001 (2016).

[139] J. Schaffner-Bielich and A. Gal, "Properties of strange hadronic matter in bulk and in finite systems", Phys. Rev. C **62**, 034311 (2000).

[140] P. Demorest *et al.*, "Shapiro Delay Measurement of A Two Solar Mass Neutron Star", Nature **467**, 1081-1083 (2010).

[141] J. Antoniadis *et al.*, "A Massive Pulsar in a Compact Relativistic Binary", Science **340**, 6131 (2013).

[142] M. Oka, K. Shimizu and K. Yazaki, "The Dihyperon State in the Quark Cluster Model", Phys. Lett. B **130**, 365 (1983).

[143] B. Silvestre-Brac, J. Carbonell and C. Gignoux, "H Particle Stability in the Nonrelativistic Quark Model", Phys. Rev. D **36**, 2083 (1987).

[144] U. Straub *et al.*, "Binding Energy of the Dihyperon in the Quark Cluster Model", Phys. Lett. B **200**, 241 (1988).

[145] C. Nakamoto, Y. Suzuki and Y. Fujiwara, "Central force of baryon baryon interactions with S = -2 in the SU(6) quark model", Prog. Theor. Phys. **97**, 761 (1997).

[146] T. Inoue *et al.* [HAL QCD Collaboration], "Two-Baryon Potentials and H-Dibaryon from 3-flavor Lattice QCD Simulations", Nucl. Phys. A **881**, 28 (2012).

[147] K. Sasaki *et al.* [HAL QCD Collaboration], "Lattice QCD studies on baryon interactions in the strangeness -2 sector with physical quark masses", EPJ Web Conf. **175**, 05010 (2018).

[148] Y. Yamaguchi and T. Hyodo, "Quark-mass dependence of the H dibaryon in ΛΛ scattering", Phys. Rev. C **94**, 065207 (2016).

[149] A. Francis *et al.*, "Lattice QCD study of the H dibaryon using hexaquark and two-baryon interpolators", Phys. Rev. D **99**, 074505 (2019).

[150] H. Garcilazo and A. Valcarce, "ΛΛN-ΞNN S wave resonance", Chin. Phys. C **44**, 104104 (2020).

[151] J. K. Ahn *et al.* [KEK-PS E224 Collaboration], "Enhanced Lambda Lambda production near threshold in the C-12(K-,K+) reaction", Phys. Lett. B **444**, 267 (1998).

[152] B. H. Kim *et al.*, "Search for an H-dibaryon with mass near $2m_\Lambda$ in $\Upsilon(1S)$ and $\Upsilon(2S)$ decays", Phys. Rev. Lett. 110, 222002 (2013).

[153] J. M. Lattimer, "Neutron star equation of state", New Astr Rev. **54**, 101 (2010).

[154] D. Lonardoni, F. Pederiva and S. Gandolfi, "Accurate determination of the interaction between Λ hyperons and nucleons from auxiliary field diffusion Monte Carlo calculations", Phys. Rev. C **89**, 014314 (2014).

[155] D. Lonardoni *et al.*, "Hyperon Puzzle: Hints from Quantum Monte Carlo Calculations", Phys. Rev. Lett. **114**, 092301 (2015).

[156] B. P. Abbott *et al.* [LIGO Scientific and Virgo Collaboration], "GW170817: Observation of Gravitational Waves from a Binary Neutron Star Inspiral", Phys. Rev. Lett. **119**, 161101 (2017).

[157] P. Khaustov *et al.* [AGS E885], "Evidence of Xi hypernuclear production in the C-12(K-,K+)(Xi)Be-12 reaction", Phys. Rev. C **61**, 054603 (2000).

[158] S. Aoki *et al.* [KEK E176 Collaboration], "Nuclear capture at rest of Ξ hyperons", Nucl. Phys. A **828**, 191 (2009).

[159] K. Nakazawa *et al.*, "The first evidence of a deeply bound state of Xi^{-}–^{14}N system", PTEP **2015**, no.3, 033D02 (2015).

[160] E. Hiyama *et al.*, "Light Xi hypernuclei in four-body cluster models", Phys. Rev. C **78**, 054316 (2008).

[161] T. F. Carames and A. Valcarce, "Examination of the H dibaryon within a chiral constituent quark model", Phys. Rev. C **85**, 045202 (2012).

[162] H. Garcilazo and A. Valcarce, "Light Ξ hypernuclei", Phys. Rev. C **92**, 014004 (2015).

[163] T. T. Sun *et al.*, "Mean field approaches for Ξ^- hypernuclei and current experimental data", Phys. Rev. C **94**, 064319 (2016).

[164] H. Garcilazo and A. Valcarce, "Deeply bound Ξ tribaryon", Phys. Rev. C **93**, 034001 (2016).

[165] H. Garcilazo, A. Valcarce and J. Vijande, "Maximal isospin few-body systems of nucleons and Ξ hyperons", Phys. Rev. C **94**, 024002 (2016).

[166] I. Filikhin, V. M. Suslov and B. Vlahovic, "Faddeev calculations for light Ξ-hypernuclei", Math. Model. Geom. **5**, 1-11 (2017).

[167] E. Hiyama *et al.*, "Possible lightest Ξ Hypernucleus with Modern Ξ*N* Interactions", Phys. Rev. Lett. **124**, 092501 (2020).

[168] Y. Jin *et al.*, "Study of Ξ hypernuclei in the Skyrme-Hartree-Fock approach", Eur. Phys. J. A **56**, 135 (2020).

[169] D. H. Wilkinson *et al.*, "Double-Hyperfragment Event", Phys. Rev. Lett. **3**, 397 (1959).

[170] L. Fabbietti, "*The 13th International Conference on Hypernuclear and Strange Particle Physics, Portsmouth USA, June 2018*", https://www.jlab.org/conferences/hyp2018/program.html.

[171] A. Sanchez Lorente [PANDA Collaboration], "Hypernuclear physics studies of the PANDA experiment at FAIR", Hyperfine Interact. **229**, 45 (2014).

[172] S. Aoki *et al.*, "Quasifree p(K-,K+)Xi- reaction in nuclear emulsion", Nucl. Phys. A **644**, 365 (1998).

[173] T. Tamagawa *et al.*, "The Xi N interaction in quasifree Xi- production", Nucl. Phys. A **691**, 234 (2001).

[174] J. K. Ahn *et al.*, "Measurement of the Xi-p scattering cross sections at low energy", Phys. Lett. B **633**, 214 (2006).

[175] M. Yamaguchi *et al.*, "Xi N and Xi Xi OBEP and Xi- nucleus bound states", Prog. Theor. Phys. **105**, 627 (2001).

[176] E. Friedman and A. Gal, "In-medium nuclear interactions of low-energy hadrons", Phys. Rept. **452**, 89 (2007).

[177] E. Hiyama *et al.*, "S = -2 hypernuclear structure", Prog. Theor. Phys. Suppl. **185**, 152 (2010).

[178] J. Haidenbauer, U.-G. Meißner and S. Petschauer, "Strangeness S=-2 baryon-baryon interaction at next-to-leading order in chiral effective field theory", Nucl. Phys. A **954**, 273 (2016).

[179] K. W. Li, T. Hyodo and L. S. Geng, "Strangeness $S = -2$ baryon-baryon interactions in relativistic chiral effective field theory", Phys. Rev. C **98**, 065203 (2018).

[180] J. Haidenbauer and U.-G. Meißner, "In-medium properties of a ΞN interaction derived from chiral effective field theory", Eur. Phys. J. A **55**, 23 (2019).

[181] M. Kohno and S. Hashimoto, "Xi-nucleus potential and (K-,K+) inclusive spectrum at Xi- production threshold region", Prog. Theor. Phys. **123**, 157 (2010).

[182] Krishichayan *et al.*, "Elastic and inelastic scattering to low-lying states of Ni-58 and Zr-90 using 240-MeV Li-6", Phys. Rev. C **81**, 014603 (2010).

[183] M. M. Nagels, T. A. Rijken and Y. Yamamoto, "Extended-soft-core Baryon-Baryon ESC08 model III. S=-2 Hyperon-hyperon/nucleon Interaction", [arXiv:1504.02634 [nucl-th]].

[184] T. A. Rijken and H. J. Schulze, "Hyperon-hyperon interactions with the Nijmegen ESC08 model", Eur. Phys. J. A **52**, 21 (2016).

[185] M. M. Nagels, T. A. Rijken and Y. Yamamoto, "Extended-soft-core baryon-baryon model ES^{16}C. III. $S = -2$ hyperon-hyperon/nucleon interactions", Phys. Rev. C **102**, no.5, 054003 (2020).

[186] H. Garcilazo and A. Valcarce, "Strangeness -2 Hypertriton", Phys. Rev. Lett. **110**, 012503 (2013).

[187] H. Garcilazo, A. Valcarce and T. F. Carames, "The $N\Lambda\Lambda - \Xi NN$ bound state problem", J. Phys. G **41**, 095103 (2014).

[188] H. Garcilazo, A. Valcarce and T. F. Carames, "The $N\Lambda\Lambda - \Xi NN$ bound state problem with $N\Lambda\Sigma$ and $N\Sigma\Sigma$ channels", J. Phys. G **42**, 025103 (2015).

[189] T. Hyodo, T. Hatsuda, and Y. Nishida, "Universal physics of three bosons with isospin", Phys. Rev. C **89**, 032201 (2014).

[190] V. Bernard, N. Kaiser and U.-G. Meissner, "Chiral dynamics in nucleons and nuclei", Int. J. Mod. Phys. E **4**, 193 (1995).

[191] P. A. Zyla *et al.* [Particle Data Group], "Review of Particle Physics", PTEP **2020**, No.8, 083C01 (2020).

[192] E. Wilbring, Ph.D Dissertation, *Efimov Effect in Pionless Effective Field Theory and its Application to Hadronic Molecules*, Univ. of Bonn (2016).

[193] S. I. Ando and Y. Oh, "${}^{6}_{\Lambda\Lambda}$He in cluster effective field theory", Phys. Rev. C **90**, 037301 (2014).

[194] E. Braaten and M. Kusunoki, "Low-energy universality and the new charmonium resonance at 3870-MeV", Phys. Rev. D **69**, 074005 (2004).

[195] U. Raha, "Universality of Two Neutrons and One Flavored Meson in Low-Energy Effective Theory", Springer Proc. Phys. **238**, 995-999 (2020).

[196] R. H. Dalitz and S. F. Tuan, "A possible resonant state in pion-hyperon scattering", Phys. Rev. Lett. **2**, 425-428 (1959).

[197] R. H. Dalitz and S. F. Tuan, "The energy dependence of low energy K- -proton processes", Annals Phys. **8**, 100-118 (1959).

[198] R. H. Dalitz and S. F. Tuan, "The phenomenological description of -K -nucleon reaction processes", Annals Phys. **10**, 307-351 (1960).

[199] R. H. Dalitz, "On the strong interactions of the strange particles", Rev. Mod. Phys. **33**, 471-492 (1961).

[200] R. H. Dalitz, "-K -nucleon bound-state interpretation of the 1385-Mev pi-lambda resonance", Phys. Rev. Lett. **6**, 239-241 (1961).

[201] Y. Nogami, "Possible existence of $\bar{K}$NN bound states", Phys. Lett. **7**, no.4, 288-289 (1963).

[202] Y. Akaishi and T. Yamazaki, "Nuclear anti-K bound states in light nuclei", Phys. Rev. C **65**, 044005 (2002).

[203] N. V. Shevchenko, A. Gal and J. Mares, "Faddeev calculation of a K- p p quasi-bound state", Phys. Rev. Lett. **98**, 082301 (2007).

[204] N. V. Shevchenko, A. Gal, J. Mares and J. Revai, "anti-K NN quasi-bound state and the anti-K N interaction: Coupled-channel Faddeev calculations of the anti-K NN - pi Sigma N system", Phys. Rev. C **76**, 044004 (2007).

[205] Y. Ikeda and T. Sato, "Strange dibaryon resonance in the anti-K NN - pi Sigma N system", Phys. Rev. C **76**, 035203 (2007).

[206] Y. Ikeda and T. Sato, "On the resonance energy of the anti-K NN - pi YN system", Phys. Rev. C **79**, 035201 (2009).

[207] T. Yamazaki and Y. Akaishi, "The Basic $\bar{K}$ nuclear cluster K^-pp and its enhanced formation in the $p+p \to K^+ + X$ reaction", Phys. Rev. C **76**, 045201 (2007).

[208] A. Dote, T. Hyodo and W. Weise, "K- pp system with chiral SU(3) effective interaction", Nucl. Phys. A **804**, 197-206 (2008).

[209] A. Dote, T. Hyodo and W. Weise, "Variational calculation of the ppK- system based on chiral SU(3) dynamics", Phys. Rev. C **79**, 014003 (2009).

[210] S. Wycech and A. M. Green, "Variational calculations for K-few-nucleon systems", Phys. Rev. C **79**, 014001 (2009).

[211] Y. Ikeda, H. Kamano and T. Sato, "Energy dependence of barKN interactions and resonance pole of strange dibaryons", Prog. Theor. Phys. **124**, 533-539 (2010).

[212] N. Barnea, A. Gal and E. Z. Liverts, "Realistic calculations of $\bar{K}NN$, $\bar{K}NNN$, and $\bar{K}\bar{K}NN$ quasibound states", Phys. Lett. B **712**, 132-137 (2012).

[213] S. Ohnishi, W. Horiuchi, T. Hoshino, K. Miyahara and T. Hyodo, "Few-body approach to structure of $\bar{K}$-nuclear quasi-bound states", Phys. Rev. C **95**, no.6, 065202 (2017).

[214] T. Hyodo and D. Jido, "The nature of the Lambda(1405) resonance in chiral dynamics", Prog. Part. Nucl. Phys. **67**, 55-98 (2012).

[215] J. Hofmann and M. F. M. Lutz, "Coupled-channel study of crypto-exotic baryons with charm", Nucl. Phys. A **763**, 90-139 (2005).

[216] T. Mizutani and A. Ramos, "D mesons in nuclear matter: A DN coupled-channel equations approach", Phys. Rev. C **74**, 065201 (2006).

[217] M. Bayar, C. W. Xiao, T. Hyodo, A. Dote, M. Oka and E. Oset, "Energy and width of a narrow $I = 1/2$ DNN quasibound state", Phys. Rev. C **86**, 044004 (2012).

[218] S. Yasui and K. Sudoh, "Exotic nuclei with charm and bottom flavors", Prog. Theor. Phys. Suppl. **186**, 199-204 (2010).

[219] J. R. Taylor, "*Scattering Theory: The Quantum Theory of Nonrelativistic Collisions*", Dover Publication, May 2006.

[220] A. E. A. Amorim, T. Frederico and L. Tomio, "Universal aspects of Efimov states and light halo nuclei", Phys. Rev. C **56**, R2378(R).

[221] I. Mazumdar, V. Arora and V. S. Bhasin, "Three body analysis of the occurrence of Efimov states in 2n halo nuclei such as B-19, C-22 and C20", Phys. Rev. C **61**, 051303 (2000).

[222] V. S. Bhasin, I. Mazumdar, V. S. Bhasin and I. Mazumdar, "*Few Body Dynamics, Efimov Effect and Halo Nuclei*", SpringerBriefs in Physics, December 2020.

[223] A. N. Mitra, "The nuclear three-body problem", Adv. Nucl. Phys. **3**, 1 (1969).

[224] S. R. Beane and M. J. Savage, "Rearranging pionless effective field theory," Nucl. Phys. A **694**, 511-524 (2001).

[225] S. i. Ando and C. H. Hyun, "Effective field theory on the deuteron with dibaryon field", Phys. Rev. C **72**, 014008 (2005).

[226] W. Meier and W. Gloeckle, "Need of repulsion in form factors for separable two-nucleon forces in conjunction with the two-pion-exchange three-nucleon force", Phys. Rev. C **28**, 1807-1811 (1983).

[227] A. Nogga, Ph.D. Thesis, *Ruhr-Universität Bochum,Bochum, 2001.*

[228] B. Acharya, C. Ji and D. R. Phillips, "Implications of a matter-radius measurement for the structure of Carbon-22", Phys. Lett. B **723**, 196-200 (2013).

[229] T. Myo, Y. Kikuchi, H. Masui and K. Katō, "Recent development of complex scaling method for many-body resonances and continua in light nuclei", Prog. Part. Nucl. Phys. **79**, 1-56 (2014).

List of publications

Journal publications included in the Thesis:

1. Ghanashyam Meher and Udit Raha, " ${}^{5}_{\Lambda\Lambda}$H and ${}^{5}_{\Lambda\Lambda}$He Hypernuclei reexamined in Halo/Cluster Effective Theory", Phys. Rev. C 103, no.1, 014001 (2021).

2. Ghanashyam Meher and Udit Raha, "Investigation of $\Xi^{-}nn$ ($S = -2$) hypernucleus in low-energy pionless halo effective theory", Eur. Phys. J. ST 230, no.2, 579-601 (2021).

3. Ghanashyam Meher, Sourav Mondal, and Udit Raha, "Universal Characteristics of Efimovian $D^{0}nn$ System *via* Faddeev Techniques", (In preparation).

Outside of the Thesis:

1. P. Talukdar, F. Myhrer, G. Meher and U. Raha, "Low-Energy Lepton-Proton Bremsstrahlung via Effective Field Theory", Eur. Phys. J. A 54, no.11, 195 (2018).

Conferences attended

1. Attended a school on strangeness nuclear physics and delivered a talk on the topic " Antikaon deutron universality in low-energy EFT" at J-PARC, Tokai, Japan (2017).

2. Attended CNT workshop on effective field theory of hadrons : vacuum to medium at Variable Energy Cyclotron Center, Kolkata, India (2018).

Curriculum vitae

Education

2014 - 2022 Ph.D in Physics, IIT Guwahati.
Advisor: Dr. Udit Raha
Thesis title: Efimov Universality in Exotic Strange and Charm Nuclei: A Low-energy Effective Theory Framework.

2011 - 2013 M.Sc. in Department of Physics, IIT Kharagpur.
CGPI: 7.12

2007 - 2010 B.Sc. in Department of Physics, Gangadhar Meher (auto.) College, Sambalpur.
Percentage: 74.75% (Sambalpur University)

2005 - 2007 Higher secondary, Rajendra Jr. College, Bolangir.
Percentage: 57.78% (Orissa state board)

2005 High school, Panchayat High School, Chadaipank.
Percentage: 71.20% (Orissa state board)

Academic achievements

2015 CSIR NET (LS) in Physics.
All India Rank: 54.

2013 GATE in Physics.
All India Rank: 129.

2011 IIT JAM in Physics.
All India Rank: 163.

Skills

While working on the Ph.D. research problems I have developed certain expertise on

- Programming with FORTRAN

- Analytical calculations using MATHEMATICA, FeynCalc
- Usages of LaTeX

भारतीय प्रौद्योगिकी संस्थान गुवाहाटी
Indian Institute of Technology Guwahati